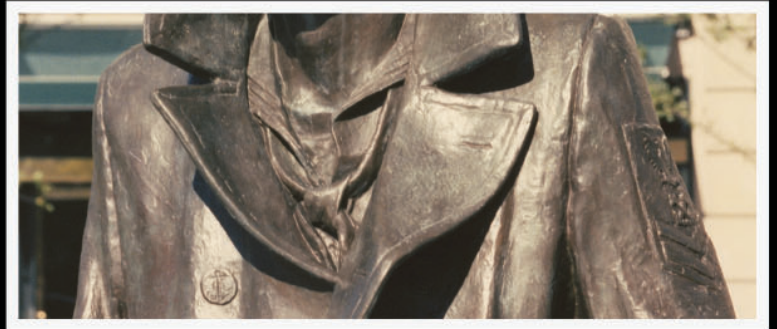


nrl review

2003



the Navy's Corporate Laboratory



naval research laboratory
washington dc 20375

Report Documentation Page

Report Date 00062003	Report Type N/A	Dates Covered (from... to) -
Title and Subtitle NRL 2003 Review	Contract Number	
	Grant Number	
	Program Element Number	
Author(s)	Project Number	
	Task Number	
	Work Unit Number	
Performing Organization Name(s) and Address(es) U.S. Naval Observatory, Washington, DC 20392	Performing Organization Report Number	
Sponsoring/Monitoring Agency Name(s) and Address(es)	Sponsor/Monitor's Acronym(s)	
	Sponsor/Monitor's Report Number(s)	
Distribution/Availability Statement Approved for public release, distribution unlimited		
Supplementary Notes The original document contains color images.		
Abstract		
Subject Terms		
Report Classification unclassified	Classification of this page unclassified	
Classification of Abstract unclassified	Limitation of Abstract UU	
Number of Pages 264		

On the cover ...

The Lone Sailor

The Lone Sailor statue represents all who have ever served, are serving now, or are yet to serve in the military service of our country. The Lone Sailor is a composite of the U.S. Navy blue-jacket, past, present, and future. He's called The Lone Sailor, yet he is hardly ever alone. The statue stands on a broad granite plaza that forms the amphitheater of the U.S. Navy Memorial in downtown Washington, DC.



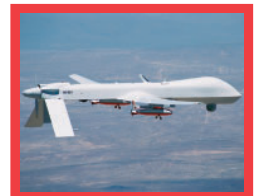
©Stanley Bleifield

More than a physical presence, however, his spirit is always with researchers at the Naval Research Laboratory. Indeed, "he" is the very reason for our existence. In May 1915, Thomas Edison proposed that "The Government should maintain a great research laboratory...In this could be developed...all the technique of military and naval progression without any vast expense." We exist to support "him"; he is never truly alone...researchers at the Naval Research Laboratory are constantly at work, constantly supporting "him" with the best that our diverse multidisciplinary efforts can provide.

The bronze statue is the creation of Stanley Bleifield, U.S. Navy Memorial's official sculptor. It was unveiled at the formal dedication of the Memorial on October 13, 1987. As part of the casting process, the bronze for The Lone Sailor was mixed with artifacts from eight U.S. Navy ships. One last addition was a personal decoration from today's Navy—one given to sailors in war and peace—the National Defense Service Medal. These bits of material are now part of The Lone Sailor.

Since time immemorial, statues have been society's way of honoring heroic endeavors. In this NRL Review, statues and monuments that honor our military heroes are highlighted on section divider pages.

Two FINDER unmanned air vehicles (UAVs) are being carried to the test area by a U.S. Air Force Predator UAV in a successful test of the world's first deployment of a UAV from a UAV.

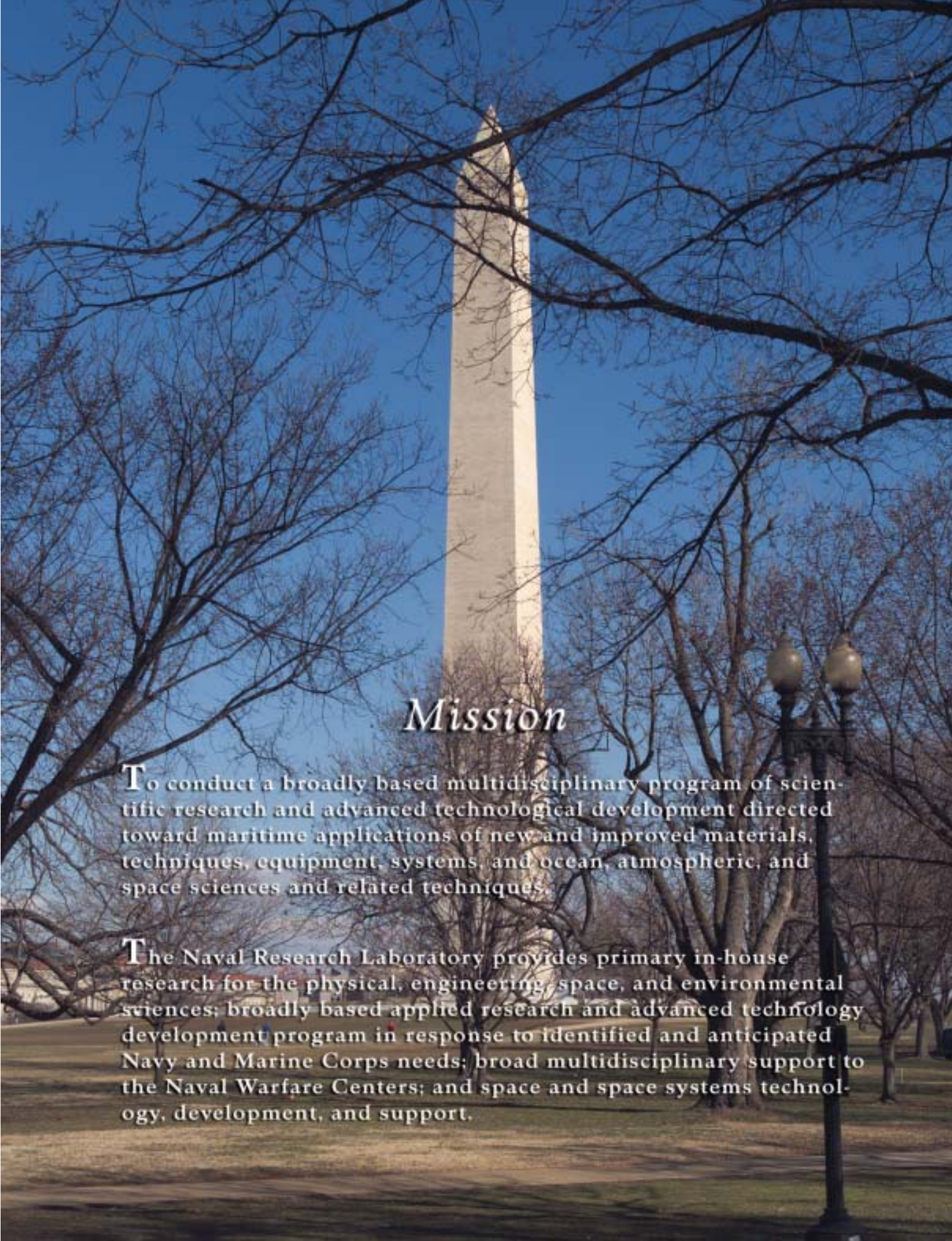


The *Clementine* satellite, an NRL project jointly sponsored by NASA and the Ballistic Missile Defense Organization, was launched in early 1994. *Clementine* took 1.8 million images of the moon's surface and was significant in finding evidence of water ice on the lunar surface. It is now on display at the Smithsonian's National Air and Space Museum.



Emission from a small size series of colloidal β -HgS quantum dots under ultraviolet irradiation.





Mission

To conduct a broadly based multidisciplinary program of scientific research and advanced technological development directed toward maritime applications of new and improved materials, techniques, equipment, systems, and ocean, atmospheric, and space sciences and related techniques.

The Naval Research Laboratory provides primary in-house research for the physical, engineering, space, and environmental sciences; broadly based applied research and advanced technology development program in response to identified and anticipated Navy and Marine Corps needs; broad multidisciplinary support to the Naval Warfare Centers; and space and space systems technology, development, and support.

features

View from the Top

NRL's Involved!

- 3** Our People Are Making a Difference
- 7** Infralynx
- 8** Scientists Helping America Conference
- 10** NRL's New Nanoscience Laboratory — Under Construction
- 12** WINDSAT — Satellite-based Multifrequency Polarimetric Microwave Radiometer
- 14** CT-Analyst™ — Dispersion Prediction with Zero Delay and High Fidelity for Urban Settings
- 16** Technology Transfer at NRL

The Naval Research Laboratory

- 21** NRL — Our Heritage
- 22** 2002 In Review
- 24** NRL Today
- 44** Looking Ahead

articles

Featured Research

- 51** Unified Approach to Fatigue Damage Evaluation
K. Sadananda, R.L. Holtz, and A.K. Vasudevan
- 59** Filamentation and Propagation of Ultra-Short, Intense Laser Pulses in Air
A.C. Ting, D.F. Gordon, C.K. Manka, R.F. Hubbard, J.R. Peñano, and P. Sprangle
- 69** Satellite Surveillance of Desert Dust Storms
S.D. Miller
- 79** Timing Studies of X-ray Binary Objects
P.S. Ray, M.T. Wolff, K.S. Wood, and P. Hertz

Acoustics

- 91** Through-The-Sensors Concepts to Refresh the Environmental Picture
W.E. Avera, M.M. Harris, D.J. Walter, L.D. Bibee, and D.N. Lambert
- 93** Simultaneous Inversion of Bio- and Geo-Acoustic Parameters in the Yellow Sea
O.I. Diachok and S.C. Wales
- 95** Simulations of Low-Frequency Bubble Pulsations Generated by Impacting Cylindrical Water Jets
W.G. Szymczak and S.L. Means

Atmospheric Science and Technology

- 101** High-Resolution Modeling of Tropical Cyclones Using Moving Grids
C.-S. Liou and T.R. Holt
- 103** A "Satellite Focus" for the War on Terror
S.D. Miller
- 105** NRLMSISE-00: A New Empirical Model of the Atmosphere
J.M. Picone, D.P. Drob, R.R. Meier, and A.E. Hedin
- 108** Free-Space High-Speed Laser Communication Link Across the Chesapeake Bay
C.I. Moore, H.R. Burris, M.R. Suite, M.F. Stell, M.J. Vilcheck, M.A. Davis, R.T. Smith, R. Mahon, W.S. Rabinovich, J.P. Koplrow, S.W. Moore, W.J. Scharpf, and A.E. Reed

Chemical/Biochemical Research

- 113** Protein Crystal Surfaces at Molecular Resolution
J.H. Konnert and S. Gorti
- 114** Orientation, Manipulation, and Assembly of Carbon Nanotubes
P.E. Pehrsson and J.W. Baldwin
- 117** Creating Chemical and Biological Diamond Interfaces
J.N. Russell, Jr., J.E. Butler, R.J. Hamers, L.M. Smith, and S.F. Bent
- 120** An Improved Method for TNT Analysis in Ground Water, Seawater, and Soil
E.R. Goldman, G.P. Anderson, and J.M. Mauro
- 122** An Automated, Portable Array Biosensor
F.S. Ligler, J.P. Golden, Y.S. Shubin, L.C. Shriver-Lake, J.B. Delehanty, K.E. Sapsford, and C.R. Taitt

Electronics and Electromagnetics

- 127** EMI and EM Energy Transport in the Near Field
D.J. Taylor, M.G. Parent, and S. Samaddar
- 128** Detection and Imaging of Buried Objects
K.M. Scheff and J.P. Hansen
- 130** Imaging Stacking Fault Growth in SiC Diodes
R.E. Stahlbush, M.E. Twigg, and M. Fatemi
- 133** Long Spin Coherence Lengths for Quantum Devices
M.J. Yang, C.H. Yang, and Y.B. Lyanda-Geller

Energetic Particles, Plasmas, and Beams

- 139** Tactical Aircraft Directed Infrared Countermeasures System Overview
K.A. Sarkady, H.A. Romero, D.M. Cordray, J.G. Lynn, R.M. Mabe, K. Strothers, J.A. Schlupf, and R.C. Cellucci
- 141** Nested Multi-Wire Array Implosions for KeV X-ray Generation
J. Davis, A.L. Velikovich, and V.I. Oreshkin
- 143** Dusty Plasma Dynamics in the NRL Space Physics Simulation Chamber Laboratory
W.E. Amatucci, D.N. Walker, and G.I. Ganguli

Information Technology and Communications

- 149** Multimodal Interactions with Dynamically Autonomous Robots
D.J. Perzanowski, A.C. Schultz, W.L. Adams, M. Bugajska, M.S. Skubic, G. Trafton, D.P. Brock, E. Marsh, and M. Abramson
- 151** Demonstration of a High-Rate Tactical Reconnaissance System with Real-Time Airborne Image Exploitation
J.N. Lee, D.C. Linne von Berg, M.R. Kruer, and M.D. Duncan
- 153** Real-Time Tactics Planning Aid for Weapons of Mass Destruction Defense
G.E. Layman
- 156** Better Codes—Better Communication
R.A. Echard and S.C. Chang
- 159** Programmable Embeddable INFOSEC Product
S.J. Chincheck

Materials Science and Technology

- 163** Image-Based Modeling of Naval Steels
A.B. Geltmacher, G. Spanos, and J.F. Bingert
- 165** Molecular Beam Epitaxial Growth of AlGa_N/Ga_N High Electron Mobility Transistors
S.C. Binari, D.S. Katzer, D.F. Storm, B.V. Shanabrook, E.R. Glaser, and J.A. Roussos
- 167** A New Ferromagnetic Semiconductor: Mn_xGe_{1-x}
A.T. Hanbicki, Y.D. Park, B.T. Jonker, S.C. Erwin, J.M. Sullivan, C.S. Hellberg, A. Wilson, and G. Spanos

Ocean Science and Technology

- 173** Roughness-Induced Ocean Bottom Scattering
R.J. Soukup and R.F. Gragg
- 175** Global Ocean Nowcasts and Forecasts with the Navy Coastal Ocean Model (NCOM)
C.N. Barron, R.C. Rhodes, L.F. Smedstad, C.D. Rowley, P.J. Martin, and A.B. Kara
- 178** The Influence of Microbial Fe(III) Reduction on Clayey Sediment Flocculation
J.-W. Kim, Y. Furukawa, T. Daulton, S.E. O'Reilly, and S. Newell
- 181** Dissociation of Sub-Seafloor Gas Hydrates and Seafloor Stability: What Thermobaric Models Show
P.R. Vogt and W.-Y. Jung

Optical Sciences

- 189** Fiber-Optic Bottom Mounted Array
C.K. Kirkendall and G.A. Cranch
- 191** Athermal Solid-State Lasers
S.R. Bowman

Remote Sensing

- 195** Synthetic Aperture Ladar
R.L. Lucke, L.J. Rickard, M. Bashkansky, J.F. Reintjes, and E.E. Funk
- 197** Dynamic Ocean Fronts
A.L. Cooper, R.P. Mied, G.L. Lindemann, and M.A. Sletten
- 199** Coastal Transport of Organic and Inorganic Matter
R.W. Gould, Jr. and R.A. Arnone

Simulation, Computing, and Modeling

- 205** NRL's Finder UAV: A Counterproliferation Asset
A. Cross
- 207** Networked Specific Emitter Identification in Fleet Battle Experiment Juliet
I. Terry
- 209** Flapping Flight in Insects and Fish: 3-D Unsteady Computations
W.C. Sandberg and R. Ramamurti
- 212** RAM to Navy Standard Parabolic Equation: Transition from Research to Fleet Acoustic Model
R.A. Zingarelli and D.B. King

Space Research and Satellite Technology

- 217** Inter-Spacecraft Optical Communication and Navigation Using Multiple Quantum Well Modulating Retroreflectors
N.G. Creamer, T.J. Meehan, M.J. Vilcheck, J.A. Vasquez, G.C. Gilbreath, W.S. Rabinovich, and R. Mahon
- 220** Modeling Single-Event Transients in Complex Digital Devices
K.A. Clark
- 222** Full-Sky Astrometric Mapping Explorer Solar Precession
T.W. Lim and P.G. DeLaHunt

awards

Special Awards and Recognition

- 229** Special Awards and Recognition
- 242** Alan Berman Research Publication and Edison Patent Awards

programs

Programs for Professional Development

- 249** Programs for NRL Employees — Graduate Programs, Continuing Education, Professional Development, Equal Employment Opportunity (EEO) Programs, and Other Activities
- 252** Programs for Non-NRL Employees — Recent Ph.D., Faculty Member, and College Graduate Programs, Professional Appointments, College Student Programs, and High School Student Programs

general information

General Information

- 257** Technical Output
- 258** Key Personnel
- 259** Contributions by Divisions, Laboratories, and Departments
- 262** Subject Index
- 265** Author Index
- 266** Employment Opportunities

VIEW FROM THE TOP

a message from the Captain and the Director of Research



CAPT David M. Schubert, USN



Dr. John A. Montgomery, Director of Research

We are very privileged to have the opportunity to lead the Naval Research Laboratory into the 21st century. Since assuming our duties as Commanding Officer and Director of Research last May, we have been given ample opportunity to see the outstanding work being produced at the Laboratory, and to represent the fine work of our scientists and engineers to senior Department of Defense and Navy leadership.

Given the uncertainty of today's world situation, it is an understatement to say that we are in a period of dramatic change. Threats of new terrorist attacks and the specter of war

with Iraq make ever more urgent the need for new technologies for our Armed Forces. We are proud of the impact that NRL has made and see many opportunities in the years ahead.

For 80 years, the Naval Research Laboratory has served as the cornerstone of science and technological invention and innovation for the Navy and Marine Corps team. NRL has literally tipped the balance of power in favor of our Armed Forces a number of times. Examples include NRL's invention and development of the first U.S. radar prior to World War II; NRL's development and launching of the world's first intelligence

satellite, GRAB I; and NRL's TIMATION concept in the 1960s that led to the Laboratory's invention and development of the first satellite prototypes of the NAVSTAR Global Positioning System (GPS) in the 1970s. GPS technology is the cornerstone for today's precision guided munitions. Each of these NRL discoveries transformed how our Navy operates.

Today's NRL researchers and engineers continue the legacy of timely and transformational science and technology excellence. In response to the war on terrorism, the Naval Research Laboratory accelerated development of the Dragon

Eye unmanned aerial vehicle, a small and inexpensive unit that can be carried by a Marine in a backpack. Dragon Eye can be configured with various day and night vision cameras, chemical and biological sensors, and other payloads. Other promising research programs have been accelerated, including the InfraLynx mobile crisis communications response system; the CT-Analyst chemical, biological, and radiological dispersion prediction system; and the nuclear quadrupole resonance explosives detector.

We are constantly evaluating our program balance to ensure that we stay at the cutting edge of new scientific fields. We have

established NRL's Institute of Nanoscience; its new state-of-the-art facility will open later this year. The Nanoscience center will be available to all our divisions as a resource that crosses many traditional disciplines.

As our recently retired Director of Research, Dr. Timothy Coffey, stated "The true mission of NRL is to ensure, in concert with many other organizations, that this nation is never surprised nor defeated by a technologically

superior foe. That is the business of defense research and engineering." We are proud to continue his legacy, ensuring that the Naval Research Laboratory remains vital as the Department of the Navy's

Corporate Laboratory – providing research solutions to tomorrow's problems and ensuring that our Navy of the future is the most technologically superior in the world.

"For 80 years, the Naval Research Laboratory has served as the cornerstone of science and technological invention and innovation for the Navy and Marine Corps team."

Timothy Coffey
John A. Matzinger



NRL'S INVOLVED!



JOHN ERICSSON MONUMENT.

John Ericsson perfected the screw propeller, thus revolutionizing propulsion. He designed the ironclad Union ship, the *Monitor*, that engaged in the famous Civil War naval battle with the *Merrimac* in 1862 and changed naval warfare for all time.

- 3** Our People Are Making a Difference
- 7** Infraclynx
- 8** Scientists Helping America Conference
- 10** NRL's New Nanoscience Laboratory — Under Construction
- 12** WINDSAT — Satellite-Based Multifrequency Polarimetric Microwave Radiometer
- 14** CT-Analyst™ — Dispersion Prediction with Zero Delay and High Fidelity for Urban Settings
- 16** Technology Transfer at NRL

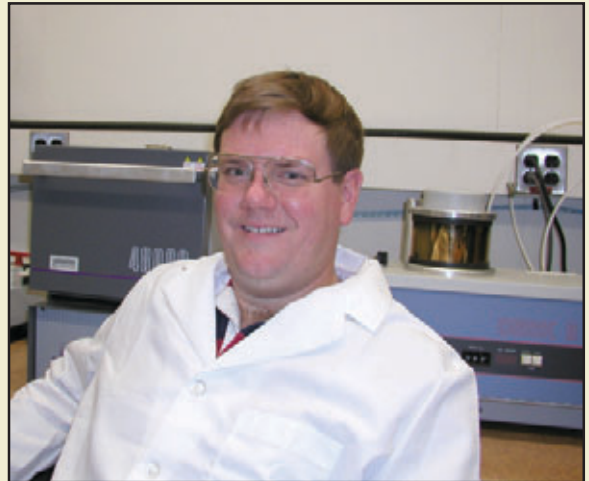
[BACK TO CONTENTS](#)

OUR PEOPLE ARE MAKING A DIFFERENCE

This publication dramatically illustrates the range of research capabilities that have been and are being developed to provide the Naval Research Laboratory with the world-class technologies for which we are known. However, these capabilities, no matter how expensive and complex, are of no value without the highly motivated people who work here. It is these people who make the Laboratory the great institution that it is, who provide the ideas and sustained efforts to make these great research capabilities "come to life." In this section, we highlight some of these special people.

DR. JEFFREY CALAME

Dr. Jeffrey Calame is an electronics engineer in the Vacuum Electronics Branch of the Electronics Science and Technology Division. In the five years that he has been at NRL, he has been responsible for interdisciplinary research in electronic materials science, high average power microwave and millimeter-wave amplifiers, and high heat flux cooling technologies. He has pioneered the creation and use of tailored-microstructure, composite-ceramic materials to eliminate electromagnetic instabilities and broaden the bandwidth of the power amplifiers for microwave and millimeter-wave radars. Such materials are also of great importance for improved passive components used in electronic warfare, communications, and multifunctional RF systems and antennas. Dr. Calame is also developing novel types of nonmetallic microchannel and porous-channel cooling technologies for removing steady-state heat fluxes of several kilowatts per square centimeter. Such cooling techniques are a critical technology for the next generation of radar transmit/receive modules, millimeter-wave electronics warfare sources, and power electronics. "NRL provides a wonderful environment for creative thinking and interdisciplinary research, and at the same time, the means to rapidly transition the new technologies to the Navy and the nation. I consider it a great honor to be a member of this diverse and vibrant institution."



MRS. SUSAN HERRIN



Mrs. Susan Herrin joined NRL in 1988 as a program analysis officer and Head of the Program Administration Staff in the Office of Program Administration and Policy Development. While her primary function is program manager for the NRL 6.1/6.2 Base Program, her Staff Office is also responsible for a variety of programs that include the Research Problem Acceptance database; RDT&E Activities reports and management briefs; yearly NRL R&D Accomplishments; and coordinating the annual Alan Berman Research Publications Awards Program, which is the Laboratory's most important awards program in honor of its technical work. "The Laboratory is an exciting place to work. I especially enjoy dealing with our researchers—to watch their ideas and research formulate at

the proposal level and then to see the development and progress of the research through the many accomplishments and recognitions they've achieved is a very rewarding experience. I am proud to be a team member of the Navy's Corporate Laboratory."

MR. JEFFREY HAWKINS



Mr. Jeffrey Hawkins is Head of the Satellite Meteorological Applications Section in the Marine Meteorology Division. His section is engaged in a wide variety of space-based weather research, ranging from an improved micro-physical understanding of clouds and rain to transitioning new weather applications to Naval operations both ashore and afloat. The section routinely acquires and processes near real-time data from 5 geostationary and 13 polar orbiter satellite sensors. "NRL permits a creative mix of basic and applied science in concert with meeting real-world Navy problems. My job enables me to work directly with Navy personnel around the world and understand first hand their unique requirements and satellite assets available. My group then determines the best satellite

products that meet the user's needs, often including multiple satellite sensors and merging with numerical weather model analyses and forecasts. We strongly interact with our U.S. and international colleagues at universities and laboratories who are working with the latest R&D satellite sensors. Our tropical cyclone monitoring research has been especially rewarding since the results are routinely used internationally and represent a longtime personal interest."

DR. JOHN MCLEAN

Dr. John McLean is NRL's Senior Scientist for Information Assurance and Acting Superintendent of the Information Technology Division. The Division's research program in computer science and telecommunication ranges from basic theory to advanced technology demonstrations and covers a wide range of topics in the areas of information collection, transmission, processing, and presentation.

"When I started at NRL, my primary interest was in basic research in a very specialized niche. NRL fully supported my interests, giving me an ideal environment to pursue my own research and the opportunity to interact with other researchers throughout the world. NRL also offered me opportunities to expand my theoretical interests to other research areas and to learn about real-world systems. Real-world problems drive basic research and serve as the transition vehicles for that research. NRL's commitment to basic research and the opportunities NRL provides to learn about potential applications made it an ideal place for me to start my career. Once I started here, I was hooked."



MS. ANNE REED



Ms. Anne Reed is Head of the Electro-Optics Technology Section in the Space Systems Development Department. Her section supports a diverse set of sponsors, focusing their efforts in the areas of laser communications, satellite laser ranging, and spaceborne imaging. They have recently completed the integration of a new optical test facility located at the Midway Research Center in Quantico, Virginia. The centerpiece of the facility is a one-meter telescope that is available for collaborative research programs with scientists and engineers throughout NRL and the DOD. “When I came to NRL as a co-op student, I never envisioned being here 18 years later. What I most enjoy is the freedom to pursue a diverse set of projects while building and maintaining my technical skills. Our

management rewards a strong sense of entrepreneurial spirit – a spirit that has encouraged me to pursue and lead activities ranging from basic research to applied engineering to operational support.

Opportunities abound in the Naval Center for Space Technology, where government engineers and scientists are integral to every aspect of the development of experimental space systems. We explore concepts, build payloads, integrate satellites and ground support systems, and provide overall system engineering. While I feel extremely lucky with the depth and breadth of projects available, it is my colleagues at the Lab, especially in my section, who have inspired such a rewarding career at NRL.”

MR. DAVID SPENCER

Mr. David Spencer works for the Spacecraft Engineering Department within NRL’s Naval Center for Space Technology (NCST). He is currently the program manager for NRL’s WindSat meteorological remote sensing payload. By developing WindSat, NRL is supporting not only the Navy, but also the nation’s new, merged operational weather satellite system, NPOESS. This allows NRL to continue to be a player in the fields of remote sensing and space applications. Mr. Spencer has spent his entire career at NRL supporting NCST. “The field of spacecraft engineering is an exciting profession, with large challenges and big pay-offs. There’s never a dull moment, and each successive program is different from the first. I’ve seen many interesting places and things during my career. I’m always learning. Something that I am most proud of is my support of the *Clementine* Lunar/Asteroid mission. It is a perfect example of the capability of NRL and the NCST, and I am happy to have been a member of that team. To think that something I helped create is now hanging in the National Air and Space Museum with all those legendary pieces of engineering is still difficult to comprehend. It is a pleasure working at NRL. I enjoy the camaraderie of the people I work with. People of all talents and expertise whom I respect and trust have made my career here enjoyable. I hope I provide the same to them.”



DR. LEONARD TENDER



Dr. Leonard Tender is a research chemist in the Center for Bio/Molecular Science and Engineering. This center is composed of chemists, physicists, materials scientists, polymer scientists, molecular biologists, microbiologists, and engineers. It is engaged in the study of relationships between molecular structure and molecular function with the aim of learning from nature's solutions to material, structural, and sensing problems. "Our center is multidisciplinary and very collegial. While trained in electrochemistry, I have learned a tremendous amount of molecular biology through collaborations with my colleagues. This has given me confidence and skills to pursue exciting areas of research in bio-electrochemistry. Currently I am involved in multiple projects spanning laboratory-based biosensor research to development of power supplies for scientific instruments deployed on the seafloor based on microbial oxidation of marine sediment. The center and the Naval Research Laboratory have been very supportive my multidisciplinary interests."

MR. DENNIS THERNING

Mr. Dennis Therning is the Associate Director of Research for Business Operations; he serves as the NRL Comptroller and leads the Business Operations Directorate. This directorate includes the Contracts, Financial Management, Supply, and Research and Development Services Divisions, and the Management Information Systems Office. "While we are not in the direct science and technology mission of NRL, the employees of the Business Operations Directorate provide critical day-to-day support to ensure that NRL scientists and others have the equipment and facilities, and the contract, procurement, travel, financial, and other business-type support necessary for them to accomplish their science and technology efforts. Additionally, we spend a significant amount of time in the Navy, DOD, and government-wide efforts to re-engineer, streamline, consolidate, and standardize government operations and information systems in order to improve efficiency and reduce costs. These types of changes are not easy but often are unavoidable, so we try to ensure that the impacts to NRL are either really beneficial or at least not too disruptive. Fortunately, I have a great team of managers and employees to work with. I think we are all proud to be part, in our own way, of the important work that NRL accomplishes."



InfraLynx

A Transportable Communications Hub for Emergency First Response



InfraLynx support at the Winter Olympics in Salt Lake City, Utah, February 2002.
(L to R: Ivan Corretjer, Chris Herndon, Jeff Westley, Dave Kolesar – NRL; member of the Salt Lake City Police Department.)

After the terrorist attacks of September 11, 2001, the U.S. Navy sent out a request to all commands for assistance to the rescue and recovery effort in New York City. NRL responded immediately with the offer of InfraLynx, a combination of technologies from the Information Technology Division (ITD) and the Tactical Technologies Development Laboratory (TTDL) of the Space Science Division. This collaborative effort combined a transportable satellite networking unit (mounted on a high-mobility, multipurpose, wheeled vehicle (HMMWV)) and a mobile cellular hub developed by the TTDL. The resulting system provided Internet connectivity and interactive cellular communication capabilities, utilizing a satellite network connection back to ITD in Washington, D.C. to link into the internet and local telephone system. Although NRL was not requested to field its solution at this time, the need for such a capability was clearly illustrated.

Before September 11, NRL had been developing modular communications systems for the military, using standardized RF components that work in all kinds of scenarios rather than requiring custom installations for each application. Since 1993, the Satellite and Wireless Networking Section of ITD had been extending local-area and wide-area networks with satellite and line-of-sight radio links. This section had developed a satellite network point-of-presence configuration and installed it on a Marine Corps HMMWV. The resulting system provides an infrastructure reconstruction that uses interoperable radio communications (2 to 800 MHz) combining private cellular and landline telephone networks with microwave and two-way satellite communications for voice, data, and video.

“Our goal was to devise a unit that could roll into a ‘hot zone’ and immediately provide first responders with the connectivity they need,” said Chris Herndon, head of NRL’s Tactical Technologies Development Laboratory. “In particular, now that first responders are faced with the possibility of coordinated terror attacks, we want to make sure that they can talk easily with each other and the outside world.”

InfraLynx is equipped with a rigid shelter having a roof-mounted 1.5-m Ku-band satellite dish, and is fitted with a JPS Communications ACU-1000 modular interconnect system. This system allows as many as 10 two-way radios or handsets into the computer-controlled cross-connect. With its satellite capability, the InfraLynx can remotely provide as many as 96 landline telephones to an emergency command post. All capabilities can be remotely operated up to 100 feet from the vehicle.

For more information, contact Mr. Charles C. Herndon
Space Systems Development Department, NRL-DC • (202) 767-6525



First Annual
**Scientists Helping America
 Conference**

March 11 - 13, 2002

During March 11-13, 2002, the Naval Research Laboratory hosted the first annual Scientists Helping America (SHA) Conference. Sponsors were U.S. Special Operations Command (USSOCOM), Defense Advanced Research Projects Agency (DARPA), and the Naval Research Laboratory. The conference was targeted at universities, small and nontraditional businesses, and companies that did not generally work with the Department of Defense.

A Defense Advanced Research Projects Agency (DARPA) press release described it thus, "DOD is particularly interested in researchers who have never before worked with DOD, and who might have innovative ideas in nine key technical areas: Advanced Training Systems; Batteries and Fuel Cells; Bioengineering and Chemical/Biological Defense; Directed-energy Weapons; Wide-bandwidth Reach-back Communications; Remote Sensing; Signature Reduction; and Underwater Communications and Unmanned Systems...We want to tap new resources to help us in our fight against terrorism. These scientists can bring a lot to the table. They can take us in directions that we might not have thought of in the past."

More than 270 invitees learned about military needs. They learned about the Special Forces and how government technologists interact with DOD. Workshops allowed the scientist to network directly with DOD program managers; special tutorial sessions described working with the government, obtaining security clearances, and understanding the Broad Agency Announcement process.



LTG W.P. Tagny, Deputy CINC USSOCOM, Mr. H.E. Schulte, Deputy for Acquisition, USSOCOM, Mr. Schulte's aide, and Dr. Robert Tulis, DARPA program manager.



Dr. Anthony J. Tether, Director, DARPA



Dr. Joseph Jacobson, MIT, Dr. Jane Alexander, Deputy Director of DARPA, Dr. Robert Tulis, DARPA program manager, and Mr. Walter Wilson, Merlin Technologies, San Carlos, CA.



NRL welcomes SHA participants.



Special Forces A-Team.



The conference begins with a Plenary Session.

It was a jam-packed conference! In addition to the conference itself, which was held at NRL, a reception was held at the Smithsonian National Air and Space Museum. Attendees were lodged at a hotel in Crystal City, Virginia, and brought by bus to NRL every day. Lunch was provided in a large tent on the mall. Also in this tent were displays by various military units who demonstrated their equipment and described its limitations. This provided lots of interaction with all participants, lots of food for thought for the attendees ("How could my company respond to this need?")



Lots of food for thought!

The conference proved to be useful, productive, and interesting to all involved; many good ideas were presented and the results have been outstanding. DARPA is currently funding four New Starts—two in Advanced Training, one in Signature Reduction (jointly with USSOCOM), and one in Chemical/Biological Defense. USSOCOM is currently funding three efforts—two in Batteries/Fuel Cells and one in Signature Reduction (jointly with DARPA). The Navy Warfare Command is also working with one vendor to develop a needed product using the vendor's own funds. This is a good beginning!



Mr. Joseph Peak, NRL (center), and ONR science advisors.

According to Harry Schulte, acquisition lead for USSOCOM, "USSOCOM is looking for nontraditional help from companies and scientists who have not had a role in DOD projects in the past. Twenty-first century warfare requires our agency and others in DOD to think out of the box to come up with solutions. We're looking for the best scientists in America to help develop technology relevant to the mission of USSOCOM." The Scientists Helping America Conference was a big step in this search.



Dr. Alan J. Heeger, 2000 Nobel Prize in Chemistry.



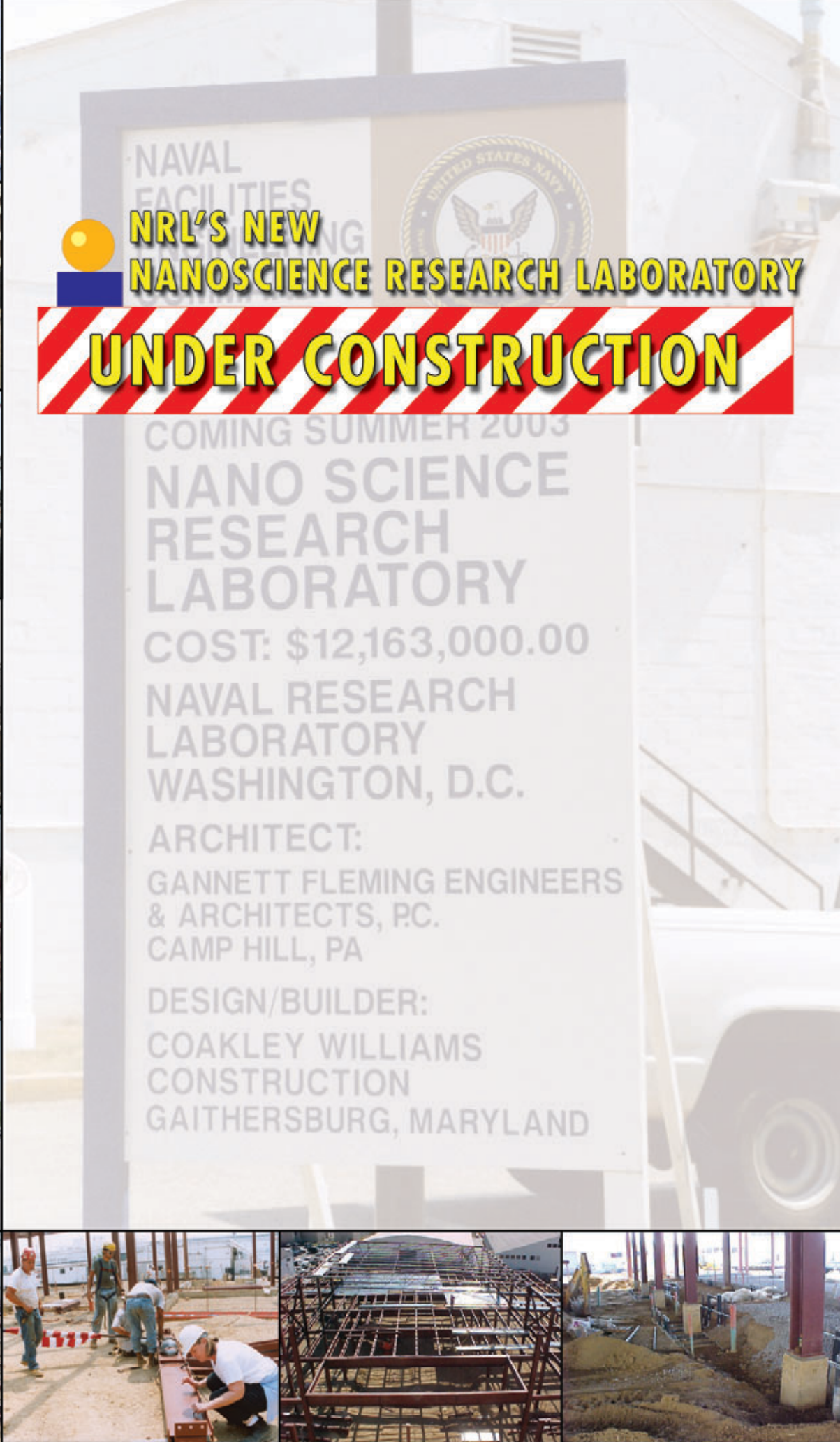
Evening reception at the Smithsonian National Air and Space Museum.



Scientists speak directly with members of Special Forces units to get a better understanding of their needs.



Member of America's Special Forces unit demonstrates the equipment and hardware currently being used in combat.



NAVAL
FACILITIES

ENGINEERING

**NRL'S NEW
NANOSCIENCE RESEARCH LABORATORY**

UNDER CONSTRUCTION

COMING SUMMER 2003

NANO SCIENCE
RESEARCH
LABORATORY

COST: \$12,163,000.00

NAVAL RESEARCH
LABORATORY
WASHINGTON, D.C.

ARCHITECT:

GANNETT FLEMING ENGINEERS
& ARCHITECTS, P.C.

CAMP HILL, PA

DESIGN/BUILDER:

COAKLEY WILLIAMS
CONSTRUCTION

GAITHERSBURG, MARYLAND



Groundbreaking for the new Nanoscience Research Laboratory took place on January 23, 2002. In attendance, with chrome-plated shovels, were Acting Director of Research, Dr. Eric Hartwig; NRL's Commanding Officer, Captain Douglas Rau; Commanding Officer of Facilities Engineering Command EFA-Chesapeake, Captain William Boudra; Vice President of Coakley Williams Construction, Pat Caulfield; Associate Director of Research for Materials Science and Component Technology, Dr. Bhakta Rath; and the Director of the Institute for Nanoscience, Dr. Gary Prinz.

The first task was to clear the site of the earlier construction (prefabricated metal sheds and pre-World War II concrete buildings). Below-ground artifacts (abandoned sewers, water lines, electrical lines, etc.) also had to be removed. The first building components to go into the freshly leveled and compacted ground were deep concrete footers to support the structural steel framework. Next, the steel framing was quickly assembled and defined the space to be enclosed by the new building. The concrete roof was poured and then the concrete floors. The floors of all of the interior rooms are isolated from each other by thick, elastic vibration-isolation barriers. These barriers are easily visible near the bases of the massive steel supporting columns. Finally, the outside walls themselves were attached to the supporting steel framework. They are solid reinforced concrete slabs, prefabricated off-site, delivered by flat-bed trucks, and lifted into place. This wall assembly also proceeded rapidly. Its mass provides the primary thermal and acoustic barrier for the delicate experiments to be conducted within the building.

The completion of this outer shell of floors, walls, and roof was just the beginning of the process. Much more work will be needed to complete the highly sophisticated interior space and install the state-of-the-art research equipment before NRL scientists will be able to move in and begin their research. The schedule anticipates this to begin in the fall of 2003.



WINDSAT

satellite-based multifrequency polarimetric microwave radiometer



WindSat is the primary payload on the Coriolis mission.

WindSat is a satellite-based multifrequency polarimetric microwave radiometer developed by the Naval Research Laboratory for the U.S. Navy and the National Polar-orbiting Operational Environmental Satellite System (NPOESS) Integrated Program Office (IPO). WindSat will be the first demonstration of using polarimetric microwave radiometry to measure the ocean surface wind vector from space. A polarimetric radiometer measures the partially polarized microwave emissions. On the ocean surface, the magnitude and polarization state of this emitted energy is driven by roughness, which is directly correlated to the ocean surface wind speed and direction.

The Naval Center for Space Technology partnered with the Remote Sensing Division to design, develop, and operate the WindSat payload for the Navy and the nation's new merged weather satellite office, NPOESS. The sensor provides risk reduction data that NPOESS will use in the development of its future operational payload, the Conical Microwave Imager Sounder (CMIS).

WindSat is the primary payload on the Coriolis mission, which is sponsored jointly by the Department of Defense Space Test Program (STP) and the Navy (SPAWAR PMW-155). WindSat shares this mission with the Solar Mass Ejection Imager (SMEI) developed by the Air Force Research Laboratory (AFRL). Spectrum-Astro of Gilbert, Arizona, developed the spacecraft that supports both payloads. This mission was launched onboard a Titan II rocket from Vandenberg AFB on January 6, 2003.

The 10-foot tall, 675-pound WindSat radiometer operates in discrete bands at 6.8, 10.7, 18.7, 23.8, and 37.0 GHz. It uses a 1.8-m offset parabolic reflector antenna fed by 11 dual-polarized feed horns. This antenna assembly rotates at 31 rpm.

The WindSat design and ground processing algorithms focus on the primary mission of measuring the sea surface wind vector. However, it will produce a unique data set with numerous environmental remote sensing applications.

For more information, contact Dr. Richard Bevilacqua
Remote Sensing Division, NRL-DC • (202) 767-0768





CT-ANALYST™



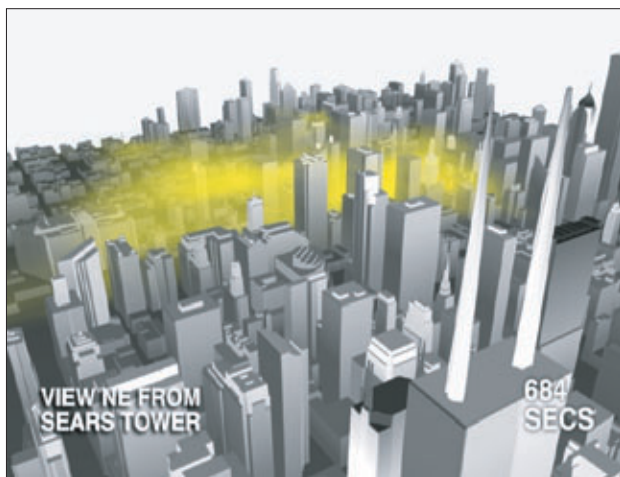
Dispersion Prediction with Zero Delay and High Fidelity for Urban Settings

DESCRIPTION

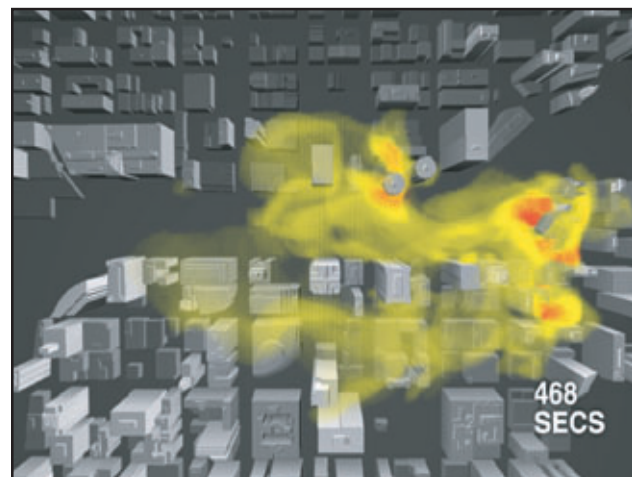
CT-Analyst provides accurate, instantaneous, 3D predictions of CBR agent transport in urban settings. In the past, more accuracy has always meant more computing and more computing means more delay. Waiting even a fraction of a minute for a simplified scenario computation can be far too long for timely situation assessment. Therefore, CT-Analyst uses the best computations possible prepared well ahead of time and captures their salient results in a highly compressed database to be manipulated and displayed instantly. A detailed, citywide model of dynamic urban airflow (called FAST3D-CT) supplies a cutting-edge 3D database of agent airflow to power CT-Analyst. The accuracy of full 3D fluid dynamics simulations with meter-scale resolution is placed at the fingertips of first-responders and emergency managers. In a visual, easy-to-comprehend form with zero time delay. The “transformational” new technology enabling this breakthrough capability is called “Dispersion Nomographs™.”

APPLICATIONS

Versions of CT-Analyst can support emergency response of civilian and military personnel to CBR incidents and can be applied to the control and integration of sensor networks. On site and headquarters staff would use this tool for data fusion to give a minute-by-minute situation assessment including projected evacuation routes. It could also be used for war games, virtual reality training, site defense planning, and sensor placement optimization. Three or four appropriate sensor readings can be backtracked to an unknown source, and the downwind “Footprint” of the expanding plume can be determined in small a fraction of a second. The implementation also has sensor fusion capabilities with a “point-and-click” controller to select, morph, and manipulate user-constructed or sensor-driven CBR scenarios directly. Sources and sensors can be dragged across the screen as the resulting situation shifts instantaneously to follow. CT-Analyst is being incorporated into Mevatec’s PEGEM system under Pentagon Missile Defense Agency sponsorship.



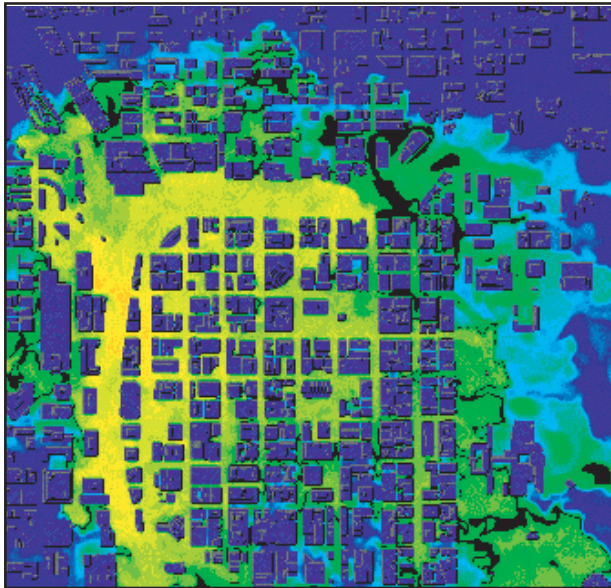
(a) View from the northeast



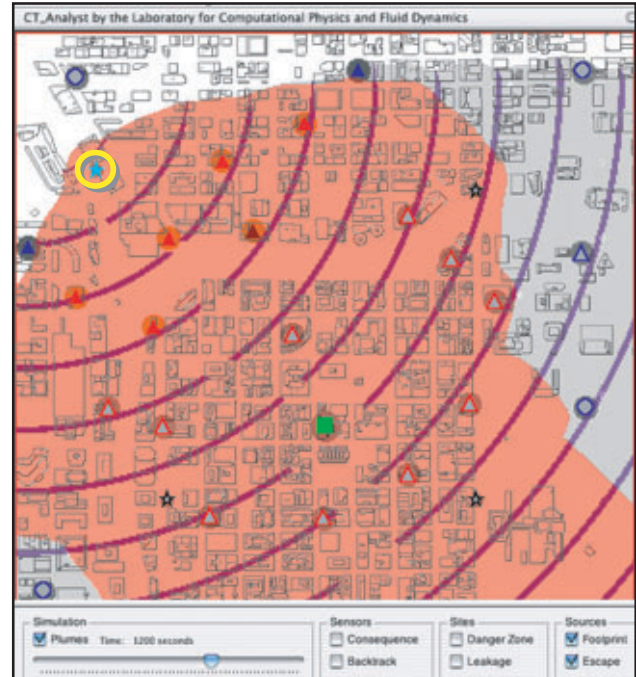
(b) View from above

Frames from a high-resolution video of a FAST3D-CT simulation of downtown Chicago computed using a $360 \times 360 \times 55$ grid (6-m resolution). A 3-m/s wind off the lake from the east blows contaminant across a portion of the detailed FastCity urban geometry required for accurate flow simulations.

COMPARISON OF FAST3D-CT WITH CT-ANALYST (RIGHT) DOWNTOWN CHICAGO



FAST3D-CT simulation of a contaminant cloud in an urban area with the average wind from 320 degrees at 3 m/s. The time after release, source location, and conditions correspond exactly to the CT-Analyst scenario shown in the figure to the right.



CT-Analyst full screen display showing plume envelope (pink), contamination footprint (grey), and evacuation routes (magenta/purple) overlaid on a city map.

REQUIREMENTS CHECKLIST

- IMMEDIATE DATA FUSION USING**
 Anecdotal information, qualitative data and sensor data
- IMMEDIATE CONSEQUENCES**
 Simple, instantaneous computation of exposed and soon-to-be exposed regions based on very limited data
- SITUATION-BASED ESCAPE ROUTES**
 Quickly project optimal evacuation routes based on the current evolving situation assessment and support building defense
- EMERGENCY MANAGEMENT TOOLS**
 - Web broadcast of results, connection to urban Geophysical Information Systems (GIS)
 - Coordinate remotes and backtrack to unknown sources

CT-ANALYST ACHIEVES

ACCURACY

80-90% as accurate as state-of-the-art 3D time-accurate CFD based on a quantitative Figure of Merit

FLEXIBILITY

Unique new features include graphical sensor fusion, forward and reverse plumes, rotate winds, source backtrack, evacuation and building infiltration

SPEED ("zero latency")

- 100 to 10000 × faster than real time
- Instant visual interpretation and comprehension

Contributors:

Graphics and Computations – Mr. Robert Doyle, Prof. John Iselin, Dr. Jay Boris, Dr. Gopal Patnaik, Mr. Theodore Young, Jr., and Mr. Keith Obenschain

Dr. Warren W. Schultz • NRL Code 6101 • (202) 767-2479 • wschultz@ccs.nrl.navy.mil
 Dr. Jay Boris • NRL Code 6400 • (202) 767-3055 • boris@lcp.nrl.navy.mil



TECHNOLOGY TRANSFER

at NRL



<http://techtransfer.nrl.navy.mil>

NRL IS A RECOGNIZED LEADER IN TECHNOLOGY TRANSFER

NRL is committed to transitioning its technologies into products or services for military and civilian use. Many of NRL's technologies have commercial applications in addition to the defense-oriented objectives for which they were originally developed. NRL innovations in areas such as radar, radio, satellite navigation, fiber optics, chemical and biological sensors, and a wide variety of materials and coatings have made significant contributions to the safety and welfare of the military and civilian communities.

The transitioning of NRL's dual use technologies is facilitated by NRL's Technology Transfer Office. This office implements the Technology Transfer Act by which Congress authorized Federal Laboratories such as NRL to participate in Cooperative Research and Development Agreements (CRADAs) and patent licensing agreements. NRL has entered into more than 200 CRADAs with industry, universities, non-profit organizations and other government organizations. In addition, NRL has executed over 60 licenses to its inventions.

Entering into a CRADA is an excellent way for U.S. companies to gain access to commercially important NRL research and development capabilities. As the Navy's corporate laboratory, NRL draws on the powerful resources of an interdisciplinary combination of scientific expertise and modern facilities. NRL's technical staff is recruited from all disciplines of engineering and the physical sciences and is available to work with private companies to solve technical problems in any area of research that is consistent with NRL's mission.

NRL's CRADA partners include small and large companies as well as universities. In some cases, NRL is working under a CRADA to transition technology that the CRADA partner plans to license. In other cases, NRL is contributing expertise in the development of new products and services that will be available to both civilian and government customers.

The topics of new CRADAs signed in 2002 spanned a wide range of technologies. For example, NRL entered into a CRADA with Spatial Integrated Systems directed at improving the simulation of complex systems, such as aircraft and other vehicles. Detailed simulations are an integral part of the development and engineering process, and the enhancements being developed under the CRADA will sub-

stantially reduce the time and cost of developing various commercial and military systems. Under another CRADA, NRL and Broadley-James Corporation are evaluating NRL's nanochannel glass for use as a membrane in reference electrodes for measuring pH. Broadley-James anticipates that the ability to control the size and number of channels uniformly in the NRL glass will significantly improve the performance of its electrodes.

NRL supports an active licensing program and has more than 500 patents available for licensing. A license to a Navy invention authorizes the licensee to manufacture and sell a product based on NRL's technology in exchange for royalty payments that are shared by the Laboratory and the inventors. Examples of technologies licensed in 2002 include software for the compression and analysis of hyperspectral imaging data and technology for the fabrication of optical modulators. NRL also collaborated with the Johns Hopkins University Applied Physics Laboratory (JHUAPL) to license a radio frequency beacon that was invented jointly by



Quantum Magnetics luggage screeners that incorporate NRL's NQR technology for explosives detection were fielded immediately after the September 11th terrorist attacks.

NRL and JHUAPL scientists. NRL is proud of its record of transitioning the results of its research to the operational Navy as well as to the private sector. At last count, over 100 products were on the commercial market for sale under license from NRL, and NRL leads the Navy in both number of licenses and royalty income from licenses.

In addition to providing a return on the government's R&D investments, NRL's CRADA and licensing programs contribute to the country's readiness to respond to threats such as the terrorist attacks on September 11, 2001. Because NRL had licensed its Nuclear Quadrupole Resonance technology for the detection of explosives in 1995, immediately following September 11, the U.S. Government was able to purchase commercial off-the-shelf (COTS) package screening units to be deployed at high-risk government sites. Likewise, NRL's licensee is responding to the government's call for automated explosives screening of airline luggage. NRL's CRADA program has similarly contributed to threat response readiness. NRL's collaborations with several companies under CRADAs led to rapid implementation of NRL's p-CAD chemical sensor in systems to be used for homeland security. Several other NRL CRADAs relate to the development of chemical and biological sensors for homeland defense and public safety. For example, NRL and Thermo Biostar, Incorporated are developing a portable immunoassay system for rapid, easy-to-use, semi-quantitative detection of specific biomolecules. Under another CRADA, NRL and ITT Industries are working toward the development of sensors based on DNA hybridization assay technology for automated, continuous, real-time environmental monitoring of specific biological agents.

Among Federal laboratories, NRL is a recognized leader in the area of Technology Transfer. In FY2002, NRL was the recipient of the Harold G. Bowen Award for the patented invention that had the greatest impact on the operational Navy. Dr. George Kang and Mr. Larry Fransen of NRL's Information Technology Division were awarded the Bowen Award for their development of a Voice Communication Processing system that enhances speech intelligibility on secure telephones and provides direct interoperability between old and new speech parameters. The latter feature allows new secure phones and legacy secure phones to work together, saving the Navy nearly \$600 million to date by obviating the need to replace legacy phones.

NRL was also recognized by the Federal Laboratory Consortium (FLC) with two Awards for Excellence in Technology Transfer. The FLC awards were given for successful transfer of dual use technology under CRADAs and licenses. The NRL technologies so recognized included an antifouling coating for ships and pipelines and an extremely stable fiber-optic pulsed laser. Dr. Joanne Jones-Meehan of the Chemistry Division accepted the award for the antifouling coating technology, and Dr. Thomas Carruthers accepted the award for the laser technology.

Life Point launched their Impact™ saliva-based drug and alcohol testing product in 2002. The Impact™ system is based on the flow immunosensor developed in NRL's Center for BioMolecular Science and Engineering.



NRL TECHNOLOGY TRANSFER OFFICE

Code 1004, 4555 Overlook Ave., S.W., Washington, D.C. 20375-5320
(202) 767-7230

E-mail: techtransfer@nrl.navy.mil
<http://techtransfer.nrl.navy.mil>



THE NAVAL RESEARCH LABORATORY



THOMAS EDISON.

Thomas Edison's remarks in May 1915 to a *New York Times* correspondent were the basis for the establishment of the Naval Research Laboratory – "The Government should maintain a great research laboratory...In this could be developed...all the technique of military and naval progression without any vast expense."

- 21** NRL — Our Heritage
- 22** 2002 In Review
- 24** NRL Today
- 44** Looking Ahead

[BACK TO CONTENTS](#)

NRL — OUR HERITAGE

Today, when government and science seem inextricably linked, when virtually no one questions the dependence of national defense on the excellence of national technical capabilities, it is noteworthy that in-house defense research is relatively new in our Nation's history. The Naval Research Laboratory (NRL), the first modern research institution created within the United States Navy, began operations in 1923.

Thomas Edison's Vision: The first step came in May 1915, a time when Americans were deeply worried about the great European war. Thomas Edison, when asked by a *New York Times* correspondent to comment on the conflict, argued that the Nation should look to science. "The Government," he proposed in a published interview, "should maintain a great research laboratory....In this could be developed...all the technique of military and naval progression without any vast expense." Secretary of the Navy Josephus Daniels seized the opportunity created by Edison's public comments to enlist Edison's support. He agreed to serve as the head of a new body of civilian experts—the Naval Consulting Board—to advise the Navy on science and technology. The Board's most ambitious plan was the creation of a modern research facility for the Navy. Congress allocated \$1.5 million for the institution in 1916, but wartime delays and disagreements within the Naval Consulting Board postponed construction until 1920.

The Laboratory's two original divisions—Radio and Sound—pioneered in the fields of high-frequency radio and underwater sound propagation. They produced communications equipment, direction-finding devices, sonar sets, and perhaps most significant of all, the first practical radar equipment built in this country. They also performed basic research, participating, for example, in the discovery and early exploration of the ionosphere. Moreover, the Laboratory was able to work gradually toward its goal of becoming a broadly based research facility. By the beginning of World War II, five new divisions had been added: Physical Optics, Chemistry, Metallurgy, Mechanics and Electricity, and Internal Communications.

The War Years and Growth: Total employment at the Laboratory jumped from 396 in 1941 to 4400 in 1946, expenditures from \$1.7 million to \$13.7 million, the number of buildings from 23 to 67, and the number of projects from 200 to about 900. During WWII, scientific activities necessarily were concentrated almost entirely on applied research. New electronics equipment—radio, radar, sonar—was developed. Countermeasures were devised. New lubricants were produced, as were antifouling paints, luminous identification tapes, and a sea marker to help save survivors of disasters at sea. A thermal diffusion process was conceived and used to supply some of the ^{235}U isotope needed for one of the first atomic bombs. Also, many new devices that developed from booming wartime industry were type tested and then certified as reliable for the Fleet.

NRL Reorganizes for Peace: Because of the major scientific accomplishments of the war years, the United States emerged into the postwar era determined to consolidate its wartime gains in science and technology and to preserve the working relationship between its armed forces and the scientific community. While the Navy was establishing its Office of Naval Research (ONR) as a liaison with and supporter of basic and applied scientific research, it was also encouraging NRL to broaden its scope and become, in effect, its corporate research laboratory. There was a transfer of NRL to the administrative oversight of ONR and a parallel shift of the Laboratory's research emphasis to one of long-range basic and applied investigation in a broad range of the physical sciences.

However, rapid expansion during the war had left NRL improperly structured to address long-term Navy requirements. One major task—neither easily nor rapidly accomplished—was that of reshaping and coordinating research. This was achieved by transforming a group of largely autonomous scientific divisions into a unified institution with a clear mission and a fully coordinated research program. The first attempt at reorganization vested power in an executive committee composed of all the division superintendents. This committee was impracticably large, so in 1949, a civilian director of

research was named and given full authority over the program. Positions for associate directors were added in 1954.

The Breadth of NRL: During the years since the war, the areas of study at the Laboratory have included basic research concerning the Navy's environments of Earth, sea, sky, and space. Investigations have ranged widely—from monitoring the Sun's behavior, to analyzing marine atmospheric conditions, to measuring parameters of the deep oceans. Detection and communication capabilities have benefitted by research that has exploited new portions of the electromagnetic spectrum, extended ranges to outer space, and provided a means of transferring information reliably and securely, even through massive jamming. Submarine habitability, lubricants, shipbuilding materials, firefighting, and the study of sound in the sea have remained steadfast concerns, to which have been added recent explorations within the fields of virtual reality, superconductivity, and biomolecular science and engineering.

The Laboratory has pioneered naval research into space—from atmospheric probes with captured

V-2 rockets, through direction of the *Vanguard* project (America's first satellite program) to inventing and developing the first satellite prototypes of the Global Positioning System. Today, NRL is the Navy's lead laboratory in space systems research, fire research, tactical electronic warfare, microelectronic devices, and artificial intelligence.

The consolidation in 1992 of NRL and the Naval Oceanographic and Atmospheric Research Laboratory, with centers at Bay St. Louis, Mississippi, and Monterey, California, added critical new strengths to the Laboratory. NRL now is additionally the lead Navy center for research in ocean and atmospheric sciences, with special strengths in physical oceanography, marine geosciences, ocean acoustics, marine meteorology, and remote oceanic and atmospheric sensing. The expanded Laboratory is focusing its research efforts on new Navy strategic interests and needs in the post-Cold War world. Although not abandoning its interests in blue-water operations and research, the Navy is also focusing on defending American interests in the world's littoral regions. NRL scientists and engineers are working to give the Navy the special knowledge and capabilities it needs to operate in these waters.

2002 IN REVIEW

The last year at the Naval Research Laboratory has been a busy one—with a new Commanding Officer and a new Director of Research, plus a busy schedule of research initiatives and records of accomplishments. Additionally, the events of September 11, 2001 have led to an increased commitment by the Laboratory to apply science and technology in the fight against terrorism and on behalf of homeland security.

As a result of the Combating Terrorism Technology Task Force, the Laboratory has produced the *InfraLynx*, a surge communications system. *InfraLynx* is a mobile system that provides a full suite of communications equipment (phone lines, fax, secure voice, networks, and conventional communications (VHF/UHF/800 MHz)) connected to NRL via satellite. Video from cameras inside and outside the system is viewable at the Laboratory. The communications suite is packaged in a specially outfitted truck that can operate on-location. As a test of the system, *InfraLynx* was taken to the Winter Olympic Games in Salt Lake City, Utah, at the invitation of the Office of Domestic Preparedness. The NRL system performed fully up to expectations.

In another application of NRL satellite expertise and technology, the Laboratory's Satellite and Wireless Networking Section provided satellite connectivity to a Navy command vessel at sea, using an inclined-orbit Ku-band satellite. NRL researchers used a 2.4-m satellite terminal installed onboard the USS *Coronado* in support of Fleet Battle Experiment (FBE)-India (2001) and FBE-Juliet (2002). Over three days, a high-data-rate networked full-duplex link was established between the *Coronado* and a mobile lightweight multiband satellite terminal collocated at the Air Force Pacific Air Operations Center, Hickam Air Force Base, Hawaii. The exercise demonstrated Navy-Air Force interservice satellite networking in a simulated combat situation. Inclined-orbit satellites, such as those used in the Joint Service experiment, can generate cost savings of up to 50 percent on satellite bandwidth and increase satellite lifetime.

Researchers within NRL's Optical Sciences Division demonstrated the first autonomous real-time hyperspectral target detection system flown aboard a Predator unmanned air vehicle (UAV). The exercise took place over the Camp Roberts training facility in California. It was performed as part of the Division's DARKHORSE Project, which has been

developing algorithms to detect and classify ground targets in clutter and camouflage, based on the targets' spatial and temperature signatures. Data from a nadir-looking visible hyperspectral sensor were analyzed by an onboard real-time processor. When a target was detected, a high-resolution image was produced from a bore-sighted panchromatic visible sensor. A three-band waterfall display of the data with overlaid target clues, along with high-resolution image chips, was transmitted to a ground station via a digital RS-170 data link. The technology has applicability to several operational Navy systems.

Another NRL system received advanced testing this year. The Laboratory's Navy Technology Center for Safety and Survivability manages the Damage Control-Automated Reduced Manning system (DC-ARM). DC-ARM is a multitiered effort to evaluate and demonstrate incremental reductions in damage-control manning based on increases in automated shipboard sensing and response. The new integrated fire and damage-fighting response system includes water misting, fire sensing, automated smart valves, smoke ejection systems, access closure, compartment video monitoring, and an integrated Supervisory Control System. The goal of DC-ARM is to both rationalize and improve damage control and assessment efforts and to reduce dedicated manning, thus decreasing overall costs. The system was tested on the ex-USS *Shadwell*, NRL's full-scale damage control research, development, test, and evaluation platform moored in Mobile Bay, Alabama.

Researchers from the Laboratory's Radar and the Electronics Science and Technology divisions have developed a new radar system called WARLOC. WARLOC is a high-power, coherent W-band advanced radar operating at 94 GHz (the world's highest). Earlier attempts to develop coherent radars at W-band achieved only very limited success because of limitations in power amplifier technology and the lack of suitable microwave components. The NRL researchers developed novel gyrokystron amplifier technology to overcome power limitations. Over several years, the researchers performed theoretical analyses, developed pilot designs, and carried out prototype experiments on gyrokystrons. This work has led to the development of a high-average-power prototype of the amplifier in collaboration with industry and the University of Maryland. The goal of the NRL research was to develop an advanced coherent mobile radar system, with important Navy applications of millimeter-wave radar. Future applications include noncooperative target recognition, target imaging based on inverse synthetic aperture radar techniques, missile

test range instrumentation, detection of low cross section threats, and very accurate tracking close to the sea surface.

Scientists from NRL's Chemistry and Electronics Science and Technology Divisions have collaborated in work that advances the eventual application of carbon nanotubes for use in electronic devices. The researchers developed a means of growing nanotubes inside arrays of gated apertures on a silicon chip. The new devices consist of many small sets of carbon nanotubes, with an individual metal aperture or gate provided to each set. Application of a voltage to the apertures produces a high electric field at the nanotube tips, causing electrons to be produced by field emission. The fabrication and characterization of these prototype arrays is an important advance that brings carbon nanotubes closer to device application and provides much improved field emitter arrays. Nanotube field emitter arrays fabricated at NRL start to produce measurable current at gate potentials below 20 V and have produced as much as 1 mA at 41 V. The NRL devices are more robust than their predecessors and operate well in the presence of water vapor and other residual gases and at temperatures up to 700 °C. Potential Navy applications include high-voltage, high-temperature, and high-frequency electronics, spacecraft propulsion systems, miniature X-ray sources, cathodoluminescent devices (flat panel displays), and miniature mass spectrometers. Work is currently underway to refine the NRL gated carbon nanotube emitters to provide more reliable fabrication and produce higher currents.

In astronomy, NRL instruments are providing greater and more detailed information and visuals about near and far space. The Lab's new Low-Frequency Array radio telescope (LOFAR), now in the planning stage, will build on advances achieved by NRL in its 74 MHz receiving system installed on the National Science Foundation's Very Large Array radio telescope in New Mexico. The new LOFAR telescope will use advances in computing power and consumer electronics to build a low-frequency radio telescope operating between 10 and 240 MHz. This new telescope will produce dazzling, high-quality images of distant galaxies, rapidly spinning pulsars, and possibly planets in other solar systems. In near space, the Laboratory's Large Angle Spectrometric Coronagraph (LASCO) flying aboard the Solar and Heliospheric Observatory has already borne great fruit in its search for comets in solar orbit. LASCO detected its 500th comet on August 12, 2002. The search for comets is a secondary mission of LASCO, which was built to detect and anticipate the origin of coronal mass ejections. These ejections are the source of space weather and can strongly affect

atmospheric conditions on Earth, thereby disrupting communications and military systems.

NRL's success at transitioning technology to the Fleet was recognized in May 2002 when Rear Admiral Jay Cohen presented the Vice Admiral Harold G. Bowen Award for Patented Inventions to Dr. George Kang and Mr. Larry Fransen. The Bowen Award singles out a patented invention that has had a significant impact on the operation of the Navy as measured by the extent of adoption for Navy use and cost savings, increased military capability, and/or increased quality of life for Navy personnel. Dr. Kang and Mr. Fransen (now retired) of NRL's Information Technology Division were awarded the Bowen Award for their development of a Voice Communication Processing system that enhances speech intelligibility on secure telephones and provides direct interoperability between old and new speech parameters. The interoperability allows new secure phones and legacy secure phones to work together, and has saved the Navy nearly \$600 million to date by obviating the need to replace legacy phones.

NRL's achievements in technology transfer to the private sector were also recognized with awards in 2002. In May 2002, at the Annual Meeting of the Federal Laboratory Consortium (FLC), NRL received two FLC Awards for Excellence in Technology Transfer. The first FLC award was presented to Dr. Joanne Jones-Meehan of NRL's Chemistry Division to recognize her exemplary work that led to the successful transition and licensing of NRL's Fouling Release Coating technology to Smart Surfaces, LLC. Adhesion of marine organisms to



Navy range boat (30-ft, aluminum hull) coated with the NRL Fouling Release Coating System. NRL has licensed this coating system to Smart Surfaces, LLC.

surfaces coated with this technology is so poor that when a vessel so coated moves through the water (or when water moves past the vessel) the organisms are washed away. Smart Surfaces offers this coating for commercial and recreational watercraft as well as pipelines.

The second FLC award was presented to Dr. Thomas Carruthers of NRL's Optical Sciences Division. Dr. Carruthers and his colleagues in the Optical Sciences Division invented an extremely stable fiber-optic pulsed laser that can produce pulses as brief as one picosecond at repetition rates as high as 40 GHz. The ultrashort pulse length, high repetition rates, and extreme stability make this laser capable of processing electronic data and more precisely generating and measuring optical frequencies. The technology has been licensed to two companies, PriTel and Calmar Optcom.

NRL TODAY

ORGANIZATION AND ADMINISTRATION

The Naval Research Laboratory is a field command under the Chief of Naval Research, who reports to the Secretary of the Navy via the Assistant Secretary of the Navy for Research, Development and Acquisition.

Heading the Laboratory with joint responsibilities are CAPT David M. Schubert, USN, Commanding Officer, and Dr. John Montgomery, Director of Research. Line authority passes from the Commanding Officer and the Director of Research to three Associate Directors of Research, the Director of the Naval Center for Space Technology, and the Associate Director for Business Operations. Research

divisions are organized under the following functional directorates:

- Systems
- Materials Science and Component Technology
- Ocean and Atmospheric Science and Technology
- Naval Center for Space Technology.

NRL operates as a Navy Working Capital Fund (NWCF). All costs, including overhead, are charged to various research projects. Funding in FY02 came from the Chief of Naval Research, the Naval Systems Commands, and other Navy sources; government

agencies, such as the U.S. Air Force, the Defense Advanced Research Projects Agency, the Department of Energy, and the National Aeronautics and Space Administration; and several nongovernment activities.

PERSONNEL DEVELOPMENT

At the end of FY02, NRL employed 2950 persons—34 officers, 73 enlisted, and 2843 civilians. In the research staff, there are 731 employees with doctorate degrees, 334 with masters degrees, and 580 with bachelors degrees. The support staff assists the research staff by providing administrative, computer-aided design, machining, fabrication, electronic construction, publication and imaging, personnel development, information retrieval, large mainframe computer support, and contracting and supply management services.

Opportunities for higher education and other professional training for NRL employees are available through several programs offered by the Employee Relations Branch. These programs provide for graduate work leading to advanced degrees, advanced training, college course work, short courses, continuing education, and career counseling. Graduate students, in certain cases, may use their NRL research for thesis material.

For non-NRL employees, several postdoctoral research programs exist. There are also agreements with several universities for student opportunities under the Student Career Experience Program (formerly known as Cooperative Education), as well as summer and part-time employment programs. Summer and interchange programs for college

faculty members, professional consultants, and employees of other government agencies are also available.

NRL has active chapters of Women in Science and Engineering, Sigma Xi, Toastmasters International, and the Federal Executive and Professional Association. Three computer clubs meet regularly—NRL Microcomputer User's Group, NeXT, and Sun NRL Users Group. An amateur radio club, a drama group (the Showboaters), and several sports clubs are also active. NRL has a Recreation Club that provides sports leagues and swim, whirlpool bath, gymnasium, and weight-room facilities. The Recreation Club also offers classes in martial arts, aerobics, swimming, and water walking.

The Community Outreach Program traditionally has used its extensive resources to foster programs that provide benefits to students and other community citizens. Volunteer employees assist with and judge science fairs, give lectures, and serve as tutors, mentors, coaches, and classroom resource teachers. The program also sponsors African American History Month art and essay contests for local schools, student tours of NRL, a student Toastmasters Youth Leadership Program, an annual holiday party for neighborhood children in December, and a book donation program for both students and teachers. Through the Community Outreach Program, NRL has active partnerships with four District of Columbia, three Aberdeen, Maryland, and three Calvert County, Maryland, public schools.

NRL has an active, growing Credit Union. Since its creation in 1946, NRL Federal Credit Union (NRL FCU) has grown to about \$300 million in



In a traditional change-of-command ceremony on May 31, 2002, CAPT David Schubert relieved CAPT Douglas Rau as the 34th naval officer to command the Naval Research Laboratory. The ceremony involves the Reading of Orders, which signifies the transfer of total responsibility, authority, and accountability from one commanding officer to another.

assets and serves about 22,000 NRL employees, contractors, select employee groups, and their families. NRL FCU is a leader in providing innovative financial services such as a dynamic home page and Online Access (Internet home banking) with bill payer. Focusing on the credit union philosophy of *People Helping People*, NRL FCU offers a wide array of no-fee services plus financial education and assistance. NRL FCU is a full-service financial institution providing various mortgage programs and creative lending services. In its inaugural year, NRL FCU Financial Services, LLC (NFFS), a wholly owned subsidiary of NRL Federal Credit Union, has about \$8 million in assets under management. NFFS offers full-service investment and brokerage services. For information about membership or any financial service, call (301) 839-8400 or click on www.nrlfcu.org.

Public transportation to NRL is provided by Metrobus. Metrorail service is three miles away.

For more information, see the *NRL Review* chapter, "Programs for Professional Development."

SCIENTIFIC FACILITIES

In addition to its Washington, D.C., campus of about 130 acres and 102 main buildings, NRL maintains 11 other research sites, including a vessel for fire research and a Flight Support Detachment. The many diverse scientific and technological research and support facilities are described in the following paragraphs.

RESEARCH FACILITIES

Institute for Nanoscience

The revolutionary opportunities available in nanoscience/nanotechnology have led to a National Nanotechnology Initiative. NRL has been a major contributor to the science of nanostructures and is making a commitment to expand that effort. The NRL Institute for Nanoscience has been established with \$10 million in core research funds. The mission of the Institute for Nanoscience is to conduct highly innovative, interdisciplinary research at the intersections of the fields of materials, electronics, and biology in the nanometer-size domain. The Institute will exploit the broad multidisciplinary character of the Naval Research Laboratory to bring together scientists with disparate training and backgrounds to attack common goals at the intersection of their respective fields at this length scale. The objective of the Institute's programs is to provide the Navy and DOD with scientific leadership in this complex,

emerging area and to identify opportunities for advances in future Defense technology.

Its current research program emphasizes multidisciplinary, cross-division efforts in nano-assembly, nanochemistry, nanophotonics, nano-electronics, and nanomechanics.

Radar

NRL has gained worldwide renown as the "birthplace of radar" and, for a half-century, has maintained its reputation as a leading center for radar-related research and development. A number of facilities managed by NRL's Radar Division continue to contribute to this reputation.

A widely used major facility is the Compact Antenna Range (operated jointly with the Space Systems Development Department) for antenna design and development, as well as radar cross section measurements. The range is capable of simulating farfield conditions from 1 to 110 GHz, with a quiet zone of approximately 7 ft in diameter and 8 ft in length. Instrumentation covers from 1 to 95 GHz. Another strong division capability is in the Computational Electromagnetics (CEM) Facility, which has capabilities for complex electromagnetic



The WARLOC radar system is located at NRL's CBD. This site overlooks the Chesapeake Bay, making it ideal for research related to Naval applications. The radar system is housed in two transportable shelters. A larger shelter houses the gyro-klystron amplifier and its power supply and modulator. An integral part of this shelter is the antenna support structure that provides a rigid platform for the precision pedestal and the 6-ft Cassegrain antenna. The smaller shelter contains receivers, waveform generators, the antenna controller, and the real-time signal processing computer.

modeling, including radar target and antenna structures. The Radar Signature Calculation Facility within this group produces detailed computations of radar cross sections of various targets, primarily ships. The CEM facility includes multiple-CPU supercomputers that are also used to design phased array radar antennas. There is tremendous synergism between the CEM group and the Compact Range Facility. This provides the ability to design in the CEM environment, test in the compact range, and have immediate feedback between the theoretical and experimental aspects to shorten the development cycle for new designs.

In connection with airborne radar, the division operates a supercomputer-based Radar Imaging Facility and an inverse synthetic aperture radar (ISAR) deployed either in the air, on the ground, or aboard ship for radar-imaging data collection. A P-3 aircraft equipped with the AN/APS-145 radar and cooperative engagement capability is also available for mounting experiments.

In connection with ship-based radar, the division operates a Radar Test Bed Facility at the Chesapeake Bay Detachment (CBD), Randle Cliffs, Maryland. Represented are radars for long-range air search, point defense, and surface search functions. The point defense radar, with its large (4 ft × 8 ft) X-band phased array antenna, and the AN/SPQ-9B ADM systems are designed to be mobile so that testing is not limited to this specific environment. The CBD facility also features the newly developed WARLOC. This high-power coherent millimeter-wave radar operating at 94 GHz is now fully opera-

tional. The transmitter is capable of producing 10 kW of average power, with a variety of waveforms suitable for precision tracking and imaging of targets at long range. Waveforms with a bandwidth of 600 MHz can be transmitted at full power. A 6-ft Cassegrain antenna is mounted on a precision pedestal and achieves 62 dB of gain.

The division also operates the microwave microscope, a high-resolution (2-cm) capability for investigating backscatter from both surface and volumetric clutter. The division provides direct technical support and has direct access to data from the AN/TPS-71, the Navy's relocatable over-the-horizon radars. Concepts and engineering developments in connection with target identification are explored by using an experimental Cooperative Aircraft Identification system.

Information Technology

The Information Technology Division (ITD) is at the forefront of DOD research and development in artificial intelligence, telecommunications, computer networking, human-computer interaction, information security, parallel computation, and computer science.

The division maintains local-area computer networks to support its research and hosts metropolitan-area testbeds for advanced high-performance fiber-optic network research. These networks make hundreds of high-performance computers across DOD available to local and remote users. The ITD research networks connect to NRL's internal



The 128-processor Silicon Graphics Origin3800 system, currently with 128 Mbytes of RAM, the first production unit in the world with R14000 processors, was brought on-line in mid FY01. The NRL Center for Computational Science, as a Distributed Center of the DOD High Performance Computing Modernization Program, provides such systems (at no cost) for anyone approved by the Program Office.

network via high-speed links ranging from links on the NASA Science Internet (NSI); to OC-12c (622 Mbps) on DREN/S-DREN; to multiple OC-192 (9.6 Gbps) on ATDnet. The ATDnet is a metropolitan ATM network that supports advanced network research on multiple wavelengths, each with 10 Gbps capability; other major partners include the National Security Agency, the Defense Information Systems Agency, the Defense Advanced Research Projects Agency, the Defense Intelligence Agency, and the National Aeronautics and Space Administration. Research on ATDnet includes introduction and testing of new networking protocols; wave division multiplexing to greatly increase network capacity; and the evolution to all-optical networks, with switching at the optical layer. Research on the high-end computational assets and networks results in close association with applications that demand these leading-edge capabilities and has allowed ITD to achieve significant results in a number of areas. These include current efforts in pushing the state of the art in motion imagery with progressive scan in high-definition TV (HDTV) where 1.5 Gbps data streams are needed to handle the raw output. The Motion Imagery Laboratory (MIL) continues at the leading edge of technology to provide the environment for experiments in the convergence of the progressive video, high-performance computing, very large data sets at hundreds of terabytes, and high-speed networking that allows the user to be enveloped in the data presentation with a capability for real-time manipulation. The Defense Research and Engineering Network (DREN) is a high-speed continental United States network that connects the four Major Shared Resource Centers (MSRCs) and 19 Distributed Centers (DCs) of DDR&E's High Performance Computing Modernization Program (HPCMP) as well as a number of user organizations that use the HPCMP resources.

As one of the 19 Distributed Centers in the HPCMP, ITD's Center for Computational Science supports a range of shared resources, including massively parallel computer systems and high-performance networks. Current systems include an SGI Origin3800 with 128 processors and 128 gigabytes of memory. The next generation of Sun Microsystems high-performance computers was installed for beta testing at the end of FY02 and was made available for users in early FY03. Also at the end of FY02, a first-of-a-kind Multi-Threaded Architecture (MTA) from Cray Systems was delivered as part of the NRL Distributed Center's leading-edge work in HPC. The Cray MTA is a 40-processor machine with 160 gigabytes of memory capable of executing across 128 threads for each of its 40 processors. The CCS also has more than 12.5

terabytes of on-line shared rotating disk as well as robotic storage systems for fileserving and archiving that hold 300 terabytes of multimedia data but are scalable to over a Petabyte. The Center manages the NRL local-area network, NICEnet, which has transitioned from the older FDDI and shared Ethernet local-area networks to a fully switched environment based on ATM backbones, and both high-speed mid-Atlantic Crossroads (MAX)/University of Maryland Ethernet and ATM to the users' desktops. The evolutionary goal is to provide digital transparency of resources with security across the information infrastructure—from globally available archives, to the computational engines, to the networks that bring it all together at 10 Gbps directly to the desktops of the most demanding users. NICEnet provides external connections to other networks and to the Internet.

The division facilities include an Information Security Engineering Laboratory, a Robotics Laboratory, immersive simulation and spatial audio laboratories, and a high-data-rate multimedia satellite transmission facility. Laboratories for the development and testing of communication and network protocols both for Internet Protocols (IP) and ATM research are also included. These network testbeds are routinely interfaced to the DOD wide-area research networks for collaboration with other government laboratories. A wireless networking testbed is being used to develop Mobile Ad Hoc Networking (MANET) standards that can meet a wide range of military and commercial needs.

The Virtual Reality (VR) Laboratory provides the facilities and expertise to allow NRL scientists to use virtual reality in a variety of scientific investigations. Research areas include shipboard firefighting; simulation-based design; command and control; and scientific visualization. A number of high-speed graphics workstations, including Onyx Reality Engine 2 and Infinite Reality computers, and a variety of VR peripherals comprise the VR Lab computer equipment inventory.

Current VR technologies available include desktop VR systems, head-mounted displays (HMDs), the Responsive Workbench, and the surround-screen Immersive Room. The Responsive Workbench is an interactive 3-D tabletop environment that displays computer-generated, stereographic images on the workbench surface for use in battlespace situation awareness, simulation-based design, and other applications. The surround-screen Immersive Room is a multiuser, high-resolution 3-D visual and audio environment that projects computer-generated images onto three walls and the floor to create an immersive, large-scale, shared virtual environment. It uses an SGI Onyx RE2 so



NRL's Ship Motion Simulator is located at the Chesapeake Bay Detachment, Randall Cliffs, Maryland.

scientists can interact and control their super-computing calculations in real time.

The NEWAVE facility has been developed as a multiscreen distributed simulation laboratory and viewport. Powered by SGI and Pentium workstations and linked to the NRL parallel computing facilities with ATM/SONET networking, the facility is capable of handling high-performance computing, graphics, and distributed simulation.

NRL has owned and operated a Ship Motion Simulator (SMS) since 1943. This facility is currently located at the NRL Chesapeake Bay Detachment. Originally developed to provide gunnery practice for sailors, the SMS has been used more recently to test radar and satellite receiving systems. A roll motion of up to 28 degrees (14 degrees to port and 14 degrees to starboard) can be applied to the roll axis. The pitch axis has a fixed motion of 10 degrees (5 degrees to stern and 5 degrees to bow). Periods along both the pitch and roll axes are variable—from a slow 20-s to a brisk 8-s per cycle.

A 7-ft × 12-ft operations van (Connex box) was recently mounted on the SMS, following structural modifications to the platform. The van can accommodate four to five experimenters and subjects. A work area provides adequate space for computer monitors and support hardware. Climate control is maintained by a heat pump. The integrated van/SMS system is designed to be a permanent NRL facility for evaluating the impact of shipboard motion on human performance. This research was sponsored by Aviation Medicine, Code 341, and Virtual Environment Technologies, Code 342, at the Office of Naval Research.

Code 5580 is procuring a one-person three degrees-of-freedom motion platform for vestibular research. NRL has also contributed to the design of

a single degree-of-freedom motion simulator being developed with ONR funding. Both degree-of-freedom platforms will be housed and maintained at NRL, DC. The point of contact for the Ship Motion Simulator and the vestibular motion platform is Dr. Roger Hillson, Code 5580, NRL. LT Joseph Cohn, Code 5580, is the point of contact for the one degree-of-freedom simulator.

Optical Sciences

The Optical Sciences Division has a broad program of basic and applied research in optics and electro-optics. Areas of concentration include infrared materials and fibers, organic electro-optics, optical signal and information processing, fiber-optic sensors, surveillance and reconnaissance, integrated optical devices, and laser development.

The division occupies some of the most modern optical facilities in the country. This includes an Ultralow-loss, Fiber-Optic Waveguide Facility using high-temperature infrared glass technology. There is also a Focal-Plane Evaluation Facility to measure the optical and electrical characteristics of infrared focal-plane arrays being developed for advanced Navy sensors. The IR Missile-Seeker Evaluation Facility performs open-loop measurements of the susceptibilities of IR tracking sensors to optical countermeasures. The Large-Optic, High-Precision Tracker system is used for atmospheric transmission and target signature measurements. The Infrared Test Chamber is an ultradry test chamber used to measure the IR signatures of new surface treatments, scale models, and components used for signature control on ships, aircraft, and missiles. A



An organic, green, light-emitting diode (LED) and the advanced UHV controlled atmosphere multichamber deposition apparatus in which it was made.

UHV multichamber deposition apparatus for fabrication of electro-optical devices is interfaced to a surface analysis chamber equipped with UPS, XPS, AFM, and STM. Other scanning probe facilities are equipped with Atomic Force and Magnetic Force Microscopes.

There are several fiber-optic sensor facilities with fiber splicers, an acoustic test cell, a three-axis magnetic sensor test cell, equipment for evaluating optical fiber coatings, and various computers for concept analysis. The Digital Processing Facility is used to collect, process, analyze, and manipulate infrared data and imagery from several sources. The Emittance Measurements Facility performs measurements of directional hemispherical reflectance. An extensive set of laboratories exists to develop and test new laser and nonlinear frequency conversion concepts and to evaluate nondestructive test and evaluation techniques.

Electronic Warfare

The scope of the Tactical Electronic Warfare (TEW) Division's program for electronic warfare (EW) research and development covers the entire electromagnetic spectrum. The program includes basic technology research and advanced developments and their applicability to producing EW products. The range of ongoing activities includes components, techniques, and subsystems development as well as system conceptualization, design,

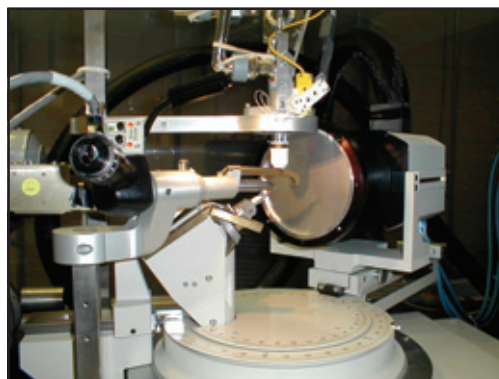


Two FINDER unmanned air vehicles (UAVs) are being carried to the test area by a U.S. Air Force Predator UAV, in a successful test of the world's first deployment of a UAV from a UAV. Standoff sensors aboard Predator allow bomb damage assessment and identification of chemical weapons in the smoke, while FINDER descends to collect samples for positive identification and weather data to allow accurate prediction of the cloud's effects. The FINDERs then follow the Predator toward home, transmitting their data to it for relay to the operators by satellite communications links.

and effectiveness evaluation. The focus of the research activities extends across the entire breadth of the battlespace. These activities emphasize providing the methods and means to counter enemy hostile actions—from the beginning, when enemy forces are being mobilized for an attack, through to the final stages of the engagement. In conducting this program, the TEW Division has an extensive array of special research and development laboratories, anechoic chambers, and modern computer systems for modeling and simulation work. Dedicated field sites and an NP-3D EW flying laboratory allow for the conduct of field experiments and operational trials. This assembly of scientists, engineers, and specialized facilities also supports the innovative use of all Fleet defensive and offensive EW resources now available to operational forces through the Naval Fleet/Force Technology Innovation Office.

Laboratory for Structure of Matter

This laboratory investigates the atomic arrangements in materials to improve them or facilitate the development of new substances. Various diffraction methodologies are used to make these investigations. Subjects of interest include the structural and functional aspects of energy conversion, ion transport, device materials, and physiologically active substances such as drugs, antibiotics, and antiviral agents. Theoretical chemistry calculations are used to complement the structural research. A real-time graphics system aids in modeling and molecular dynamics studies. The facilities include three x-ray diffraction units, two being state-of-the-art facilities, and an atomic force microscope.



SMART 6000 CCD X-ray detector, which detects the x-ray scattering pattern of interest, is shown mounted on a platform goniometer. The scattering patterns are used to determine the geometric arrangements of molecules in their crystallographic form.

Chemistry

NRL has been a major center for chemical research in support of naval operational requirements since the late 1920s. The Chemistry Division continues this tradition with a broad spectrum of basic and applied research programs focusing on controlled energy release (fuels, fire, combustion, countermeasure decoys, explosives), surface chemistry (corrosion, adhesion, tribology, adsorbents, film growth/etch), advanced materials (high-strength/low-weight structures, drag reduction, damping, polymers, thin films, nanostructures), and advanced detection techniques (environment, chemical/biological, surveillance). Facilities for research include:

Chemical analysis facilities, including a wide range of modern photon/electronic, magnetic- and ion-based spectroscopic/microscope techniques for bulk and surface analysis;

Synchrotron Radiation Facility, with intense, monochromatic X-ray photon beams tunable from 10 eV to 12 KeV available from two beam lines developed by NRL at the National Synchrotron Light Source at the Brookhaven National Laboratory. Environmental target chambers span a pressure range from 10^{-12} to 10^5 atm and temperatures from 10 to 1500 K;

Nanometer measurement facility, which includes fabrication and characterization capability based on scanning tunneling microscopy/spectroscopy, atomic force microscopy, and related techniques;

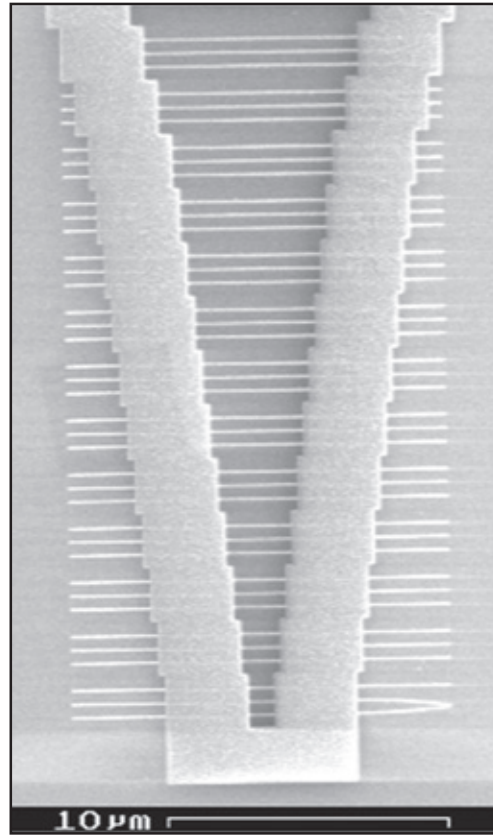
Materials synthesis/property measurement facility, with special emphasis on polymers, surface/film processing, and directed self assembly.

Fire research facilities, ranging from laboratory combustion chemistry to a 10^4 ft³ fire-research chamber (Fire I) and the 475-ft ex-USS *Shadwell* (LSD-15) advanced fire research ship; and

Marine Corrosion Test Facility, located on Fleming Key at Key West, Florida, offers an ocean-air environment and clean, unpolluted, flowing seawater for studies of environmental effects on materials. Equipment is available for experiments involving weathering, general corrosion, fouling, and electrochemical phenomena as well as coatings, cathodic protection devices, and other means to combat environmental degradation.

Materials Science and Technology

NRL has capabilities for X-ray and electron-diffraction analyses and for electron and Auger spectroscopy. Scanning, transmission, and combined scanning-transmission electron microscopes are used to study surface and/or internal microstruc-



Diamond “nano-xylophone”—the superior mechanical properties of diamond enable very high-frequency oscillations of nanometer-sized beams constructed from MEMS fabrication techniques in a collaboration between NRL and Cornell University. A mechanical resonant frequency of 640 MHz has been demonstrated, with even higher frequencies expected. Potential applications include sensing and electronic signal delay.

tures. The division has a secondary ion mass spectrometer for surface analysis that significantly extends the diagnostic capability of the technique. A high-resolution, reverse-geometry mass spectrometer is used to probe reactions between ions and molecules. The Laboratory has a fully equipped fatigue and fracture laboratory and hot isostatic press facilities. The Laboratory’s cryogenic facilities include dilution refrigerators and superconducting magnetic sensors for measuring ultrasmall magnetic fields. Also available are two molecular beam epitaxy devices for growing thin films. In addition, division facilities include:

Molecular Beam Epitaxy: As well as other materials synthesis and processing equipment, an up-to-date fatigue and fracture laboratory, and state-of-the-art diagnostic equipment, including electron microscopes, spectrometers, and electron and X-ray diffraction equipment are being used to fabricate and characterize thin films and other materials.

Trace Element Accelerator Mass Spectrometry (TEAMS) – 3 MV Tandem Pelletron Accelerator Facility: Used for standard materials analysis such as Rutherford backscattering, for MeV-energy ion implantation, and for accelerator mass spectrometry (AMS). AMS measures trace elements in parallel with 3-D imaging at 10- μm lateral resolution (0.01 μm in depth) to 10-ppt sensitivity, and isotopes for sample dating and forensics.

Laser Facilities: Pulses of up to several joules are available from one system, while time resolutions down to 30 femtoseconds are produced by another. Synchronized Q-switched oscillators are configured for pump-probe experiments.

Thin-Film Preparation Facilities: The division has several major capabilities for preparation of thin films of advanced materials, such as high-temperature superconductors and active dielectrics. These include ion-assisted evaporation (which produces dense, adherent films), various dc plasma sources (which can etch as well as deposit films), and pulsed laser deposition (for production of chemically complex films).

Ion Implantation Facility: The facility consists of a 200-keV ion implanter with specialized ultrahigh vacuum chambers and associated in situ specimen analysis instrumentation.

Laboratory for Computational Physics and Fluid Dynamics

The Laboratory for Computational Physics and Fluid Dynamics (LCP & FD) maintains a very powerful collection of computer systems. There are currently a total of 150 parallel SGI processors, 272 clustered x86 processors, 72 clustered Alpha processors, and several other support systems.

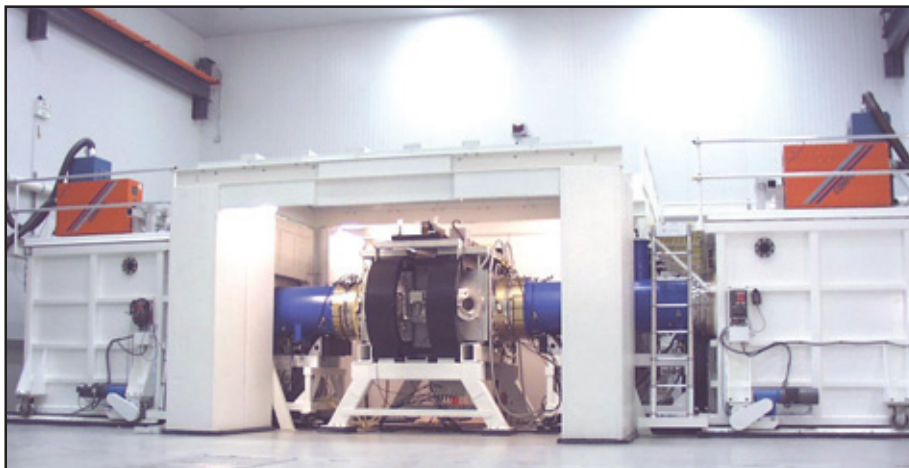
The individual systems are composed of a 64 R12K processor SGI Origin 2000, a 32 R10K processor Origin 2000, an 18 R10K processor Power Challenge, and an 8 R12K processor Origin. There are two x86 clusters, a 16 Athlon processor cluster, and a 256 Pentium 4 processor cluster, both with Myrinet interconnect. The Alpha cluster is a collection of 21264 processor Linux systems well coupled with Myrinet high-speed switched interconnect.

Each system has on the order of 200 gigabytes of disk space for storage during a simulation, and at least 256 megabytes of memory per processor. All unclassified systems share a common disk space for home directories as well as almost 250 gigabytes of AFS space that can be used from any AFS-capable system throughout the allowed Internet.

The AFS capability also allows access to other storage systems including NRL's multiresident AFS (MRAFS) system, which automatically handles archival to a multiterabyte tape archival system.

Plasma Physics

The Plasma Physics Division is the major center for in-house Navy and DOD plasma physics research. The division conducts a broad experimental and theoretical program in basic and applied research in plasma physics, which includes laboratory and space plasmas, pulsed-power sources, plasma discharges, intense electron and ion beams and photon sources, atomic physics, laser physics, advanced spectral diagnostics, plasma processing, nonlinear dynamics and chaos, and numerical simulations. The facilities include an extremely high-power laser—Pharos III—for the laboratory simulation of space plasmas and nuclear weapons effects studies and a short pulse, high-intensity Table-Top



Electra is developing the science and technology for a high-energy, repetitive, electron beam pumped laser for energy and defense applications.



Electron beam nanowriter in use defining geometries as small as 50 Å (approximately 10 atomic layer spacings).

Terawatt (T^3) laser to study intense laser-plasma, laser-electron beam, and laser-matter interactions. The division also has an 11 m³ space chamber capable of reproducing the near-Earth space plasma environment and a Large Area Plasma Processing System (LAPPS) facility to study material modification such as surface polymerization or ion implantation. The division has developed a variety of pulsed-power sources to generate intense electron and ion beams, powerful discharges, and various types of radiation. The largest of these pulsers—GAMBLE II—is used to study the production of megampere electron and ion beams and to produce very hot, high-density plasmas. Other generators are used to produce particle beams that are injected into magnetic fields and/or cavities to generate intense microwave pulses. A large array of high-frequency microwave sources (2.45, 35, and 83 GHz) are available to conduct research on microwave processing of advanced ceramic materials. In particular, the division added a 15-kW, continuous wave, 83 GHz gyrotron to its facility for research on high-frequency microwave processing of materials. The Russian-made gyrotron produces a focused, high-intensity millimeter-wave beam (10^3 - 10^5 W/cm²) that has unique capabilities for rapid, selective heating of a wide range of nonmetallic materials. The new gyrotron-based system will be used to investigate the application of such beams to important areas of material processing, including coating of materials, soldering and brazing, and treatment of ceramics, semiconductors, and polymers.

A major 3 kJ KrF laser facility (Nike) opened in June 1995. This facility is made up of 56 laser beams and is single-pulsed (4-nanosecond pulse). This facility provides intense radiation for studying

inertial confinement fusion (ICF) target heating at short wavelengths (0.25 microns) and high-pressure physics.

Electronics Science and Technology

In addition to specific equipment and facilities to support individual science and technology programs, NRL operates the Nanoelectronics Processing Facility (NPF), the Compound Semiconductor Processing Facility (CSPF), the MOCVD Laboratory, the EPICENTER, the Vacuum Electronics Fabrication Facility (VEFF), the Ultrafast Laser Facility (ULF), and the Space Solar Cell Characterization Facility (SSCCF). The NPF's mission is to provide service to both NRL and external organizations requiring micro- and nanofabrication processing support. Lithography is a particular strength of the NPF, with definition of feature sizes down to 150 angstroms possible with an e-beam nanowriter. The NPF can supply items ranging from individual discrete structures and devices to circuits with very-large-scale integration complexity. The CSPF is dedicated to processing III-V semiconductor devices and circuits in addition to serving the hands-on fabrication needs of individual NRL scientists. The CSPF uses a single-pass air-ventilation system to minimize human risk from potentially hazardous III-V semiconductor processes and associated chemicals, thereby further meeting existing safety standards. The MOCVD Laboratory uses organometallic vapor phase epitaxy to synthesize a wide range of thin films such as InSb, InGaP, InP, and GaN. The EPICENTER (a joint activity of the Electronics Science and Technology, Materials Science and Technology, Optical Sciences, and Chemistry

Divisions) is dedicated to the production of multi-layer microstructures using in situ surface analytical techniques in one of several ultrahigh vacuum, molecular-beam-epitaxy growth and processing chambers—one for growth of conventional III-V semiconductors, one for vacuum processing, one for growth of III-V semiconductor ferromagnetic materials, one for growth of 6.1 angstrom III-V semiconductors, and another for growth of magnetic materials and II-VI semiconductors. The Ultrafast Laser Laboratory is optimized for the characterization of photophysical and photochemical processes in materials on a timescale of tens of femtoseconds and also includes a synchronously pumped dye laser system for simulating the effects of charge deposited in semiconductors characteristic of space radiation. The SSCCF studies the effect of particle irradiation on new and emerging solar cell technologies for space applications. The VEFF provides electrical and mechanical design, fabrication, assembly, modification, and repair, as well as processing services for vacuum electronic devices.

Bio/Molecular Science and Engineering

The Center for Bio/Molecular Science and Engineering conducts research and development using biotechnological approaches to support the Navy, DOD, and the nation at-large. Studies are currently underway to investigate biomaterial development (for electronic and structural applications), environmental quality (including pollution cleanup and control), and chemical/biological warfare defense. Other program areas of interest include optical biosensors, nanoscale manipulations, genomics and proteomics, controlled sustained release, bio/molecular and cellular arrays, surface modification and patterning, energy harvesting and microbatteries, advanced materials from self-assembly, and liquid-crystal-based-electro-optic materials.

The staff of the Center is an interdisciplinary team with expertise in bio- and surface chemistry, biophysics, genetic engineering, cell biology, advanced organic synthesis, solid-state and theoretical physics, and electronics and materials engineering. In addition, the Center has collaborations throughout the Laboratory, with other government laboratories, at universities, and in industry.

The Center occupies laboratories and offices in Buildings 30 and 42. These modern facilities include general laboratories for research in chemistry, biochemistry, molecular biology, and physics. Specialized areas include a 600-ft² Class-1000 clean room; an advanced electron microscope facility; and a scanning probe microscope laboratory. Instrument

rooms provide access to a variety of spectrophotometers and other equipment used in biochemical or physical analyses of biomaterials. Additional laboratories accommodate an X-ray diffraction instrument, a liquid crystal fabrication facility, and equipment for advanced electronics, microarrays, and biosensor programs.

Acoustics

The Acoustics Division has three integrated structural acoustic facilities—two pools, including one with a sandy bottom, and a large in-air, semi-anechoic laboratory—that support research in submarine target characteristics for antisubmarine warfare, submarine acoustic design and quieting, sensors for hull mounted sonars, mine detection and identification, torpedo quieting, and noise control in the interior of air and submarine structures. Scaled submarine targets, real mines, sensors mounted on hull simulators, underwater buried objects, actual torpedoes, small aircraft fuselages, and satellite payload launch fairings can all be examined with advanced nearfield holographic and scanning 3-D laser vibrometer systems to measure and visualize the sound fields near a structure, the vibrations of the structure itself, the resulting farfield and interior sound fields, and the physics of the sound-structure-fluid interactions.

The division operates state-of-the-art laboratories equipped to study the structural dynamics and performance of high-Q oscillators and other micro-mechanical systems. A number of laser Doppler vibrometers permit the spatial mapping of the complex vibratory motion of the micro-oscillators. Nanostructures are probed with a super-resolution nearfield scanning optical microscope, or NSOM, allowing the monitoring of modes with a spatial resolution of 100 nm. These unique databases can be used to identify and analyze the modes of vibration and the various loss mechanisms with a view toward pushing the Q to still higher levels and for designing optimum oscillator coupling for micro- and nano-oscillator array applications. In addition, the viscoelastic properties of thin films can be studied by depositing them on portions of the oscillator. The laboratory includes the ability to measure many of these mechanical and electrical properties down to 370 mK.

The division operates several sound sources for the generation and reception of sound in at-sea experiments. Sound sources include three XF-4 units, one ITC 2077 source that can be operated while being towed by a ship, and two battery-operated organ-pipe sources that can project single tones from offboard moorings. In addition, the



The Bottomed Vertical Line Array (BVLA) provides an autonomous system for collecting 64 channels of acoustic data for a total record time of 80 hours. The system can be controlled remotely from the ship and can telemeter data for shipboard analysis. The system can also be deployed in an L-shaped configuration, using 32-channel vertical and horizontal arrays.

division has several battery-operated rubidium-clock controlled, programmable sound source moorings that can transmit sounds having arbitrary waveforms.

The division has a number of acoustic receiving arrays for at-sea experiments. Receive systems include a moored 32-channel array that RF telemeters data to a recording site at a rate up to 50 kHz/channel, a 16-channel midfrequency array, and a 128-channel autonomously recording receiving system with 2.2 terabyte capacity. These systems acquire data with rubidium-clock sampling accuracy. The division also has unique, self-recording digital acquisition buoy systems (DABS) that are used to obtain multichannel (up to 128) acoustic data in the 10 Hz to 5 kHz regime. These systems provide up to 250 gigabytes of data on a single 15-inch reel of 1-inch tape.

The division has a 32-channel (expandable to a 64-channel) broadband source-receiver array with time-reversal mirror functionality. Projects involving scanning focused acoustic fields and phase conjugation for multistatic sonar will use the new array to test and study time reversal methods. The transducers for the array are 6-inch spheres that operate over a frequency band of 500 to 3500 Hz.

The Acoustics Division has a satellite-linked buoy system with underwater receive arrays designed to collect acoustic and oceanic data, unattended, for periods of up to one month. The system currently can handle 64 channels of acoustic data (distributed on one or two arrays), and can imple-

ment onboard signal processing prior to data transmission. Two-way satellite communication is supported, providing a high-speed data link (up to 1.5 Mbps) for data transfer from the buoy to shore, and a low-speed command and control link to remotely control buoy functions. The system also contains high-speed (up to Mbps) line-of-sight communications using a GPS-linked directional antenna.

The division conducts underwater acoustic communications research using digital, acoustic modems capable of receiving and processing signal from 8 channels at various carrier frequencies and with various bit rates. An Acoustic Communication Laboratory provides environment simulation, pre-experiment testing and preparation, and post-experiment data analysis.

A narrowbeam 200 and 350 kHz backscattering system is used to study internal wave and larger scale turbulent processes. The system is used to estimate the magnitude of the randomization of the sound speed field by a variety of fluid processes. The system consists of a deck-mounted towing assembly, power and signal amplifiers, as well as a real-time display and digital data acquisition system. In addition, a 25-kW narrowbeam radar is used to detect surface manifestations of fluid processes, including internal waves and fronts in conjunction with the acoustic system.

The division operates high-frequency (up to 600 kHz) acoustic measurement systems to obtain scattering, target strength, and propagation data

using bottom-moored instrumentation towers and a high-speed, remotely operated vehicle. These data are used to simulate the performance of weapons and mine countermeasure sonars.

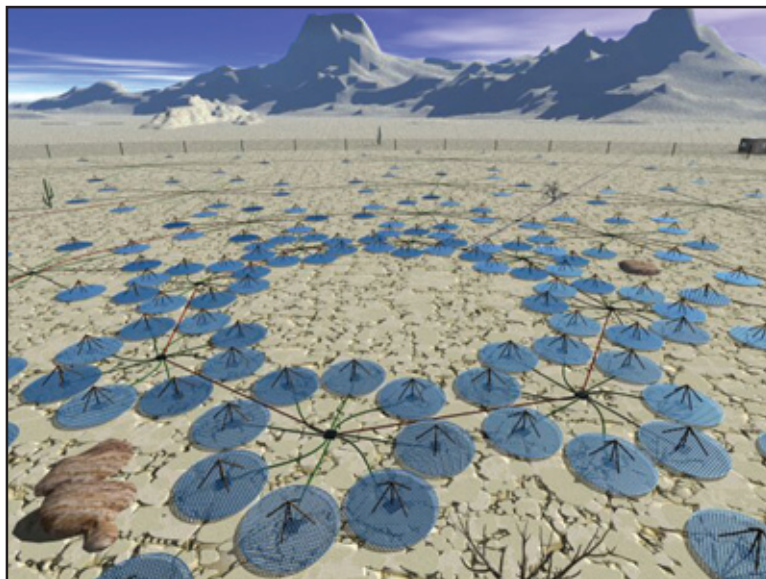
The Tactical Oceanography Simulation Laboratory (TOSL) is a modeling and simulation architecture consisting of a set of tools for processing climatology and real-time environmental data and applying energy propagation models to those data. TOSL features a high-performance computational capability to provide calculations in support of training, war games, operations rehearsal, and other distributed simulation functions. TOSL is coupled via Ethernet and SIPRNET with the Tactical Oceanography Wide Area Network (TOWAN) repository of environmental data, which allows full participation in a distributed simulation environment.

Remote Sensing

The Remote Sensing Division conducts a program of basic research, science, and applications to develop new concepts for sensors and imaging systems for objects and targets on Earth, in the near-Earth environment, and in deep space. The research, both theoretical and experimental, leads to discovery and understanding of the basic physical principles and mechanisms that give rise to background environmental emissions and targets of interest and to absorption and emission mechanisms of the intervening medium. Accomplishing this research requires the development of sensor systems technology. The developmental effort includes active and passive sensor systems used for study and

analysis of the physical characteristics of phenomena that evolve from naturally occurring background radiation, such as that caused by the Earth's atmosphere and oceans, and man-made or induced phenomena, such as ship/submarine hydrodynamic effects. The research includes theory, laboratory, and field experiments leading to ground-based, airborne, or space systems for use in remote sensing, astrometry, astrophysics, surveillance, nonacoustic ASW, meteorological/oceanographic support systems for the operational Navy, and the environmental/global climate change initiatives. Special emphasis is given to developing space-based platforms and exploiting existing space systems.

The Remote Sensing Division conducts airborne hyperspectral data collections for characterization of the environment. Hyperspectral data are series of pictures, taken simultaneously, of a scene at many different wavelengths (colors). The sensors are built and calibrated in-house, although they rely heavily on commercial off-the-shelf elements. The most recent sensor was specifically designed for use over ocean areas. It covers the 400 to 1000 nanometer wavelength range with 128 different wavelengths (channels). The sensor consists of a standard video camera lens, a grating spectrograph, and a 1024×1024 pixel charge-coupled device (CCD). The spectrograph and CCD are specially designed to achieve high sensitivity in the blue end of the spectrum to optimize water-penetrating measurements. This makes possible measurements such as the determination of the ocean bottom type (coral, sea grass, sand, rock, etc.) to water depths of as much as 20 meters (in clear water), and the identification of



Artist concept of the future Low Frequency Radio Array (LOFAR) telescope.



The Navy Prototype Optical Interferometer (NPOI) is used for both operational astrometry and for development of distributed aperture imaging techniques.

material in the water column (phytoplankton, sediments, colored dissolved organic matter, etc.). The sensor is very compact and can be flown at heights of 8000 to 10,000 feet, simply “looking” out of a hole in the bottom of the airplane. At ground speeds of 90 knots, the data can still be collected digitally and stored on computer. They are then processed in a ground system operating on a standard personal computer.

Proper interpretation of the hyperspectral data requires calibration of the sensor. This means both radiometric and spectral calibration. The latter plays a critical role in the successful correction of the data for atmospheric effects. The Remote Sensing Division operates an Optical Calibration Facility to perform these calibrations. NIST radiometric standards are transferred to a large integrating sphere. The integrating sphere has 10 precisely controlled quartz-halogen lamps to enable linearity measurements. A set of gas emission standards provides wavelength calibration. As a result, the complete process of data collection through data analysis can be handled in-house.

In order to validate the results of airborne hyperspectral sensing and to support the interpretation of the physical processes they reveal, the Remote Sensing Division has developed a Profiling Optics Package. This system measures the inherent optical properties of water (absorption, attenuation, and scattering) in the 400 to 700-nanometer range,

and collects water samples for various laboratory measurements. The package was built around a Seabird Rosette frame and includes a WETLabs Histar meter to measure water absorption and attenuation at 103 wavelengths; an unfiltered WETLabs ac9 meter to measure water absorption and attenuation at nine wavelengths; a filtered WETLabs ac9 meter to measure colored dissolved organic matter (CDOM) absorption and attenuation at nine wavelengths; a HOBILabs Hydroscat to measure backscattering of water in six wavelengths; a WETLabs WetStar fluorometer to measure stimulated fluorescence of chlorophyll; a Seabird CTD to measure conductivity (salinity), temperature, and depth; and eight sample bottles to collect up to 20 liters of water. Data from each sensor are collected and archived inside a WETLabs Super MODAPS instrument. They are then transmitted to the surface via an armored sea cable, where they are stored on a computer disk. The package has a maximum depth rating of 300 meters, although it is usually operated in coastal waters of less than 50 meters.

The Navy Prototype Optical Interferometer (NPOI), a major facility of the Remote Sensing Division, is actually two collocated instruments for making high-angular-resolution optical measurements of stars. Light from widely separated individual siderostats is combined simultaneously to synthesize the angular resolution of a telescope tens to hundreds of meters in diameter. Four siderostats are

placed in an array with extremely accurate metrology to enable very-high-precision measurements of stellar positions (wide-angle astrometry). These measurements are used by the U.S. Naval Observatory to refine the celestial reference frame, determine Earth rotation parameters, and thus satisfy Navy requirements for precise time and navigation data. They also provide determinations of basic astrophysical parameters, such as stellar masses and diameters. Additional relocatable siderostats can be placed out to distances of 250 m from the array center and used to construct very-high-resolution images of stars. These images provide fundamental astrophysical information on stellar structure and activity. When complete, the NPOI will be the most advanced high-resolution imaging optical interferometer in the world.

To validate numerical and theoretical efforts ongoing within the Remote Sensing Division, extensive hierarchical-coupled experiments are carried out in the Free-Surface Hydrodynamics Laboratory. This laboratory is used to study free-surface turbulence interactions, wave-generation phenomena, jet-flow phenomena, vorticity dynamics, and free-surface/surfactant interactions. Emphasis is placed on those processes that determine the fluxes of heat, mass, and momentum across the air-sea interface. State-of-the-art diagnostic tools are available, such as Langmuir film balance to measure the properties of surface films, hot-wire and laser-Doppler anemometry, and the new quantitative flow techniques of laser speckle, particle tracking, and particle image velocimetry. The laboratory is also equipped with an IR camera with a 20×10^{-3} K resolution. These experimental diagnostic techniques use high-powered lasers, high-tolerance optical lenses, and extensive ultra-high-resolution video-imaging hardware and PC-based computerized systems. Further computational assets consist of powerful graphical computer work stations, the NRL Connection Machine, and other off-site Cray supercomputer systems.

The Airborne Polarimetric Microwave Imaging Radiometer (APMIR) is a state-of-the-art multichannel microwave radiometer system being designed and built by the Remote Sensing Division. APMIR is being developed in response to the emerging need for extensive airborne calibration and validation of spaceborne remote sensing assets: the SSMIS, WindSat, and CMIS spaceborne microwave imaging systems. APMIR will cover five frequency bands: 5-7, 10.7, 18.7/19.35, 22.23/23.8, and 37.0 GHz. Frequency agility allows for frequency matching to each of the spaceborne systems of interest. The 10.7, 18.7/19.35, and 37.0 GHz channels are fully polarimetric, and will thus measure the ocean surface

wind speed and direction. The 5 to 7 GHz channel simultaneously observes several frequencies, providing sensitivity to sea surface temperature; the means to separate rain effects from surface effects; and protection from radio frequency interference (RFI). The 22.23/23.8 GHz channels respond to the atmospheric water vapor in the column below the aircraft, while the 18.7/19.35 and 37.0 GHz channels are sensitive to both ocean surface and cloud parameters. The APMIR system will be mounted in the bomb bay of the NRL P-3 aircraft and flown at altitudes ranging from 500 to 25,000 feet over the ocean.

Oceanography

The Oceanography Division is the major center for in-house Navy research and development in oceanography. It is known nationally and internationally for its unique combination of theoretical, numerical, experimental, and remote sensing approaches to oceanographic problems. The division numerically models the ocean and coastal areas of the world. This modeling is conducted on the Navy's and DOD's most powerful vector and parallel-processing machines. To study the results of this intense modeling effort, the division operates a number of highly sophisticated graphic systems to visualize ocean and coastal dynamic processes. The seagoing experimental programs of the division range worldwide. Unique measurement systems include a wave measurement system to acquire in situ spatial properties of water waves; a salinity mapper that acquires images of spatial and temporal sea surface salinity variabilities in littoral regions; an integrated absorption cavity, optical profiler system, and towed optical hyperspectral array for studying ocean optical characteristics; and self-contained bottom-mounted upward-looking acoustic Doppler current profilers for measuring ocean variability. In the laboratory, the division operates an environmental scanning electron microscope for detailed studies of biocorrosion in naval materials. The division's remote sensing capabilities include the ability to analyze and process multi/hyperspectral, IR, SAR, and other satellite data sources. The division is a national leader in the development and analysis of Sea WiFS data for oceanographic processes and naval applications in littoral areas.

Marine Geosciences

The Marine Geosciences Division is the major Navy in-house center for research and development in marine geology, geophysics, geodesy, geoacoustics, geotechnology, and geospatial information

and systems. The division has unique suites of instrumentation and facilities to support laboratory and field experimental programs.

The instrumentation used in the field experiments is deployable from ships, remotely operated and unmanned vehicles, and airborne platforms and by divers. Seafloor and subseafloor measurements use the Deep-Towed Acoustic Geophysical System (DTAGS—220 to 1000 Hz); high-resolution sidescan sonars (100 and 500 kHz); the Acoustic Seafloor Characterization System (ASCS-15, 30, and 50 kHz); ocean bottom seismometers and magnetometer; the In Situ Sediment Acoustic Measurement System (ISSAMS); underwater stereo photography; and nearshore video imaging systems. ISSAMS has specialized probes that measure acoustic compressional and shearwave velocities and attenuation, pore water pressure, and electrical conductivity in surficial marine sediments.

Laboratory facilities include sediment physical, geotechnical, and geoacoustic properties and sediment core laboratories. The Electron Microscopy Facility is the focal point for research in microscale biological, chemical, and geological processes. The key instrumentation includes a 300 kVa transmission electron microscope with environmental cell. The environmental cell allows hydrated and gaseous experiments. The Moving Map Composer Facility is used to design and write mission-specific map coverages for F/A-18 and AV-8B tactical aircraft onto militarized optical disks. The National Imagery and Mapping Agency also uses this state-of-the-art computer facility to update the compressed aeronautical chart library on CD for distribution. The Geospatial Information Data Base (GIDB) capability provides Internet access to the Digital Nautical Chart data, mapping data, imagery, and other data types such as video and pictures. This development tool can be used for planning, training, and operations.

Marine Meteorology

The Marine Meteorology Division is located in Monterey, California. NRL-Monterey (NRL-MRY) serves the Navy's needs for basic research in atmospheric sciences. It develops meteorological analysis and prediction systems and other products to support global and tactical operations.

NRL-MRY is collocated with Fleet Numerical Meteorology and Oceanography Center (FNMOC), the Navy's operational center of expertise in numerical weather prediction. This provides NRL-MRY with efficient access to a variety of classified and unclassified computer resources and databases to support development and transition of opera-

tional analysis and prediction systems. In addition, interfaces to the Defense Research and Engineering Network provide access to the DOD High Performance Computing resources. NRL-MRY has established the Daley Supercomputer Resource and Bergen Data Center to support research and development requirements. The Daley Supercomputer is an Origin2000 128-processor supercomputer that contains high-performance graphics workstations, an 8-terabyte (expandable to 24-terabyte) Storage Area Network, and tactical applications systems. It is used to conduct numerical weather prediction experiments, process and analyze satellite data, perform simulation studies, and demonstrate tactical weather products. The Bergen Data Center has a 24-terabyte capacity data center with a hierarchical storage management capability to provide archival and easy retrieval of research data sets. The John B. Hovermale Visualization Laboratory provides state-of-the-art capability for data visualization, which aids the interpretation of both observational and modeled data and the development of weather briefing tools.

State-of-the-art satellite receiving and processing systems allow local collection of real-time geostationary data globally from four different satellites for applications research in support of Navy and Joint Typhoon Warning Center operations. This capability has allowed NRL-MRY to take the lead in developing meteorological applications of satellite data for the FMQ-17, which is installed at the Navy's regional meteorological/oceanographic (METOC) centers.

Space Science

The Space Science Division conducts and supports a number of space experiments in the areas of upper atmospheric, solar, and astronomical research aboard NASA, DOD, and other government-agency space platforms. Division scientists are involved in major research thrusts that include remote sensing of the upper and middle atmospheres, studies of the solar atmosphere, and astronomical radiation ranging from the ultraviolet through gamma rays and high-energy particles. In support of this work, the division maintains facilities to design, construct, assemble, and calibrate space experiments. A network of computers, workstations, image-processing hardware, and special processors is used to analyze and interpret space data. The division's space science data acquisition and analysis efforts include: data analyses of the Oriented Scintillation Spectrometer Experiment (OSSE) for NASA's Compton Observatory; observation of the Sun's interaction with the Earth's upper atmosphere through the Solar Ultraviolet Spectral



Naval Center for Space Technology Optical Test Facility at the Midway Research Center, Stafford County, Virginia. Large dome on the left houses a 1-m telescope with active laser transmit and receive capability. Smaller dome and trailer in background is a self-contained transportable 16-inch telescope that has been used as a passive optical tracker and a laser communications receiver.

Irradiance Monitor (SUSIM) experiment in support of NASA's Upper Atmosphere Research Satellite (UARS); observation and analysis of solar flares using the Bragg Crystal Spectrometer (BCS) on the Japanese Yohkoh space mission; and observation and analysis of the evolution and structure of the solar corona from the disk to 0.14 AU. This latter effort involves acquiring and analyzing data from the Large-Angle Spectrometric Coronagraph (LASCO) and the Extreme Ultraviolet Imaging Telescope (EIT) on the Solar Heliospheric Observatory satellite. In each of these missions, NRL maintains a complete database of spacecraft observations and control over acquisition of data from new observations. These data are available to qualified investigators at DOD and civilian agencies. In addition, the division has a sounding rocket program that affords the possibility of obtaining specific data of high interest and of testing new instrument concepts. These include the general area of high-resolution solar and stellar spectroscopy, extreme ultraviolet imagery of the Sun, and high-resolution, ultraviolet spectral-imaging of the Sun.

In addition, selected celestial and atmospheric targets in the ultraviolet and X-ray bands are observed by three Advanced Research and Global Observation Satellite (ARGOS) experiments—Global Imaging of the Ionosphere (GIMI), High-Resolution Airglow and Auroral Spectroscopy (HIRAAS), and Unconventional Stellar Aspect (USA). ARGOS was successfully launched on February 23, 1999. As part of this program, NRL is establishing collaborative programs to make use of ARGOS data to validate various upper atmosphere models and to study time phenomena in X-ray sources.

Optical calibration facilities, including clean rooms, are maintained to support these activities. These calibration facilities are routinely used by outside groups to support their own calibration requirements.

Space Technology

In its role as a center of excellence for space systems research, the Naval Center for Space Technology (NCST) designs, builds, analyzes, tests, and operates spacecraft as well as identifies and conducts promising research to improve spacecraft and their support systems. NCST facilities that support this work include large and small anechoic radio frequency chambers, clean rooms, shock and vibration facilities, an acoustic reverberation chamber, large and small thermal/vacuum test chambers, a spacecraft robotics engineering and control system interaction laboratory, satellite command and control ground stations, a fuels test facility, and modal analysis test facilities. Also, the Center maintains and operates a number of electrical and electronic development laboratories and fabrication facilities for radio frequency equipment, spacecraft power systems, telemetry, and command and control systems, and includes an electromagnetic interference-electromagnetic compatibility test chamber. NCST has a facility for long-term testing of satellite clock time/frequency standards under thermal/vacuum conditions linked to the Naval Observatory; a 5-m optical bench laser laboratory; and an electro-optical communication research laboratory to conduct research in support of the development of space systems.

RESEARCH SUPPORT FACILITIES

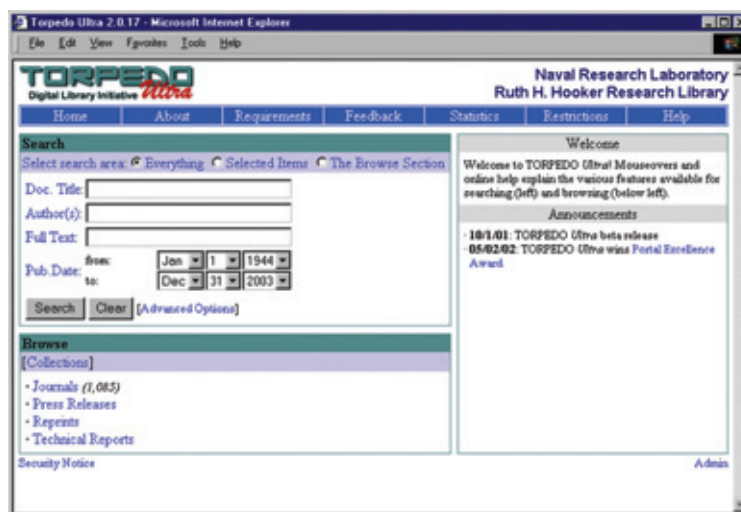
Technical Information Services

The Ruth H. Hooker Research Library offers a full range of traditional library services to support the research program of the Naval Research Laboratory. In addition, it is actively engaged in developing the NRL Digital Library that is available 24-hours-a-day, 7-days-a-week from any of the NRL sites (including ONR headquarters) and through the NRL dial-up facilities. The "portal" to the NRL Digital Library, InfoWeb, is located at <http://infoweb2.nrl.navy.mil>. InfoWeb provides desktop access to more than 2,500 research journals and hundreds of technical databases and reference tools including Science Citation Index (part of Web of Science) and INSPEC. A key InfoWeb service is TORPEDO *Ultra* v.2, which hosts more than a thousand licensed journals and thousands of NRL publications, such as technical reports, press releases, and NRL-authored journal articles/conference proceedings. TORPEDO *Ultra* v.2 is the only known system that permits integrated searching, browsing, display, and printing of scientific journals from multiple publishers along with agency publications. Many of the online services (including the library catalog, Web of Science, the e-mail alerting service called Contents-to-Go, and INSPEC) have been enhanced to link directly from the bibliographic citation to the full-text article, either in TORPEDO or on a publisher's web site.

The Technical Information Services Branch combines publications, graphics, photographic, multimedia, video, and exhibit services into an integrated organization. Publication services include

writing, editing, composition, publications consultation and production, and printing management. Quick turnaround digital black-and-white and color copying/printing services are provided. The primary focus is to use digital publishing technology to produce scientific and technical reports that can be used for either print or Web. Graphic support includes technical and scientific illustrations, computer graphics, design services, photographic composites, display panels, sign making, and framing. The NovaJet Pro 600e printer offers exceptional color print quality up to 600 dpi. It produces large-format posters and signs up to 48 inches wide. Lamination and mounting are available. Photographic services include still-camera coverage for data documentation both at NRL and in the field. Photographic images can also be captured with state-of-the-art digital cameras. Photofinishing services provide custom processing and printing of black-and-white and color films. Quick-service color prints are also available. Video services include producing video reports of scientific and technical programs. Digital video editing equipment is available to support video production and produce QuickTime movies. The NRL Exhibits Program develops and produces displays, audiovisual material, and multimedia programs for presentation at technical meetings, conferences, and symposia. The Multimedia Center uses two complete multimedia systems with Macromedia Director and Adobe Photoshop and a digital video editing system, the AVID Media Composer 1000.

The Administrative Services Branch is responsible for collecting and preserving the documents that comprise NRL's corporate memory. Archival documents include personal papers and correspon-



TORPEDO *Ultra* v.2 interface.

dence, laboratory notebooks, and work project files—documents that are appraised for their historical or informational value and considered to be permanently valuable. The branch provides records management services, training, and support for the maintenance of active records, including electronic records and e-mail, as an important information resource. The Administrative Services Branch is also responsible for NRL's postal mail services and NRL's Forms and Reports management programs (including electronic forms). The Administrative Services Branch also compiles and publishes the NRL Code Directory and Organizational Index and provides NRL Locator service.

FIELD STATIONS

NRL has acquired or made arrangements over the years to use a number of major sites and facilities for research. The largest facility is located at the Stennis Space Center (NRL-SSC), in Bay St. Louis, Mississippi. Others include a facility at the Naval Postgraduate School in Monterey, California (NRL-MRY), and the Chesapeake Bay Detachment (CBD) in Maryland. Additional sites are located in Maryland, Virginia, Alabama, and Florida.

Flight Support Detachment (NRL FSD)

Located at the Naval Air Station Patuxent River, Lexington Park, Maryland, the Flight Support Detachment (NRL FSD) is manned by approximately 9 officers, 80 enlisted personnel, and four civilians. NRL FSD is currently responsible for the maintenance and security of five uniquely configured P-3 Orion turboprop research aircraft. The FSD conducts numerous single-aircraft deployments



The Electra Doppler Radar (ELDORA) located on the tail and a laser mounted to the side of the fuselage of Researcher 587 were used to collect atmospheric data in the skies over Oklahoma from the International H₂O Project (IHOP).

around the world in support of a wide range of scientific research projects.

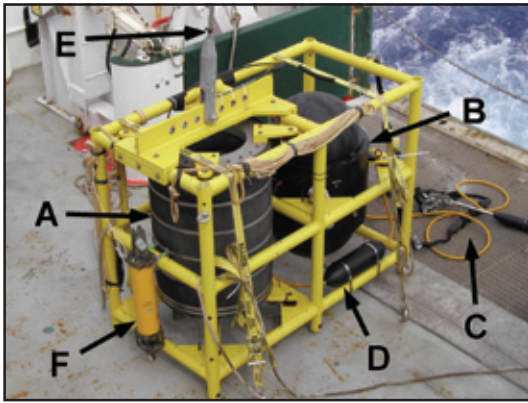
In FY02, NRL FSD provided flight support for diverse research programs including: the International H₂O Project (IHOP) and Crystal Face in conjunction with the National Center for Atmospheric Research and NASA to advance severe storm prediction capabilities; Cooperative Engagement Capability (CEC), an airborne suite to test USN Aegis Cruiser systems; Airborne Geographical Sensor Suite (AGSS), involving data and gravimeter testing to detect variations in the ocean floor; Integrated Electronic Warfare System (IEWS), a system that simulates radar of various surface and airborne platforms; Shared Reconnaissance Pod System (SHARPS), a follow-on upgrade to the TARPS System; and NAVOCEANO Oceanographic Surveillance (OS).

The Flight Support Detachment flew more than 1,300 total hours in FY02. On March 20, 2002, the Chief of Naval Operations awarded the Meritorious Unit Commendation to the FSD for unprecedented levels of mission accomplishment, aircraft availability, and the safe execution of more than 2,900 flight hours while detached to 29 worldwide locations. NRL FSD's flight safety record spans more than 40 years and includes more than 62,000 mishap-free flight hours.

Chesapeake Bay Detachment (CBD)

CBD occupies a 168-acre site near Chesapeake Beach, Maryland, and provides facilities and support services for research in radar, electronic warfare, optical devices, materials, communications, and fire research. A ship-motion simulator (SMS) is used to test and evaluate radar, satellite communications, and line-of-sight RF communications systems under dynamic conditions (various sea states). The SMS can handle up to 12,000 pounds of electronic systems. A roll motion of up to 30 degrees (15 degrees to port and 15 degrees to starboard) can be applied to this axis. The pitch axis has a fixed motion of 10 degrees (5 degrees to stern and 5 degrees to bow). Periods along both axes, pitch and roll, are variable—from a slow 32-s to a brisk 4-s rate. Variable azimuth motion can also be added to the pitch and roll action. Synchronized positioning information ($\times 1$ and $\times 36$) is available for each of the three axes of the SMS.

Because of its location high above the western shore of the Chesapeake Bay, unique experiments can be performed in conjunction with the Tilghman Island site, 16 km across the bay from CBD. Some of these experiments include low clutter and generally



The field-ready DTAGS2 (Deep Towed Acoustic Geophysics System) shown here aboard the R/V *Cape Hatteras* in June 2002. (A) Helmholz resonator, a stack of piezo-ceramic rings designed to emanate 220-1000 Hz at 200 dB. (B) Electronics "egg" pressure-rated to 6000-m water depth holds the towfish computer and capacitor banks. (C) Array harness and neutrally buoyant array cable, shown here in 48-channel configuration. (D) Engineering node containing sensors for depth, magnetic compass heading, roll, pitch, and azimuth. (E) Termination and armored coaxial tow cable. (F) Acoustic transponder with a bottom-deployed transponder constellation used for deep-water acoustic navigation.

low-background radar measurements. By using CBD's support vessels, experiments are performed that involve dispensing chaff over water and radar target characterizations of aircraft and ships. Basic research is also conducted in radar antenna properties, testing of radar remote-sensing concepts, use of radar to sense ocean waves, and laser propagation. CBD also hosts facilities of the Navy Technology Center for Safety and Survivability, which conducts fire research on simulated carrier, surface, and submarine platforms.

Stennis Space Center (NRL-SSC)

The NRL Detachment at Stennis Space Center, Mississippi (NRL-SSC) consists of NRL's Oceanography Division and portions of the Acoustics and Marine Geosciences Division. NRL-SSC, a tenant activity at NASA's John C. Stennis Space Center (SSC), is located in the southwest corner of Mississippi, about 50 miles northeast of New Orleans, Louisiana, and 20 miles from the Mississippi Gulf Coast. Other Navy tenants at SSC include the Commander, Naval Meteorology and Oceanography Command; the Naval Oceanographic Office; the Navy Small Craft Instruction and Training Center; and the Human Resources Service Center South East. The other Federal and State agencies at SSC involved in marine-related science and technology

are the National Coastal Data Development Center; the National Data Buoy Center; the U.S. Geological Survey; the Environmental Protection Agency's Gulf of Mexico Program and Environmental Chemistry Laboratory; the Center for Higher Learning, University of Southern Mississippi, and Mississippi State University.

The Commander, Naval Meteorology and Oceanography Command and the Naval Oceanographic Office are major operational users of the oceanographic, acoustic, and geosciences technology developed by NRL researchers. The Naval Oceanographic Office operates the Major Shared Resource Center (MSRC), one of the nation's High Performance Computing Centers, which provides operational support to the warfighter and access to NRL for ocean and atmospheric science and technology.

The Acoustics, Marine Geosciences, and Oceanography Divisions occupy more than 175,000 ft² of research, computation, laboratory, administrative, and warehouse space. Facilities include the Electron Microscopy Facility, an oceanographic visualization center, numerous large antennas to receive oceanographic and meteorological satellite data, an electrochemistry laboratory, unique oceanographic and geotechnical laboratories, the Map Data Formatting Facility, the Tactical Oceanography Simulation Laboratory with TOWAN databases, and numerous laboratories for acoustic and oceanographic computation, instrumentation, analysis, and testing. Special areas are available for constructing, staging, refurbishing, and storing sea-going equipment.

Marine Meteorology Division (NRL-MRY)

NRL's Marine Meteorology Division (NRL-MRY) is located in Monterey, California, on the grounds of the Naval Postgraduate School (NPS) Annex, which is about a mile from the NPS main campus. The NRL facility is collocated with the Navy's operational Fleet Numerical Meteorology and Oceanography Center (FNMOC) and with a NOAA National Weather Service Forecast Office (NWSFO). The NPS Annex campus, which covers approximately five acres, comprises four primary buildings—one occupied exclusively by NOAA, one that houses both the NRL and FNMOC super-computer/operational facilities, and two large buildings containing office space, computer laboratories, and conference facilities that are shared by FNMOC and NRL-MRY personnel. The site also provides warehouse space and recreational facilities. NRL-MRY occupies approximately 30,000 square

feet in shared buildings. This includes not only office space, but also a small library, the Daley Supercomputer, the John B. Hovermale Visualization Laboratory, the Bergen Data Center, the Geostationary Satellite Processing Facility, and space for the hardware supporting the Navy Integrated Tactical Environmental System (NITES), the Coupled Ocean/Atmosphere Mesoscale Prediction System-On Scene (COAMPS-OS™), and the Master Environmental Laboratory.

NRL-MRY is dedicated to advancing fundamental scientific understanding of the atmosphere, including the air-sea interface, and to applying those scientific discoveries in the development of innovative objective weather prediction systems. FNMOC is the Navy's central site facility for the production and distribution of numerical weather prediction products in support of Navy operations around the globe, as well as to other defense-related activities. Fleet Numerical and the Navy's regional METOC Centers are the primary customers for the numerical weather prediction systems that are developed by NRL-MRY. This collocation of the scientific developer with the operational customer offers advantages for the successful implementation of new systems and system upgrades, and for the rapid infusion of new research results from the community at large. NRL-MRY has efficient access to FNMOC's large classified vector supercomputer and other systems. This allows advanced development to take place using the real-time on-site global atmospheric and oceanographic databases. Collocation also offers the opportunity for FNMOC scientists to team with NRL-MRY scientists during the transition

and implementation process, and NRL-MRY scientists remain readily available for consultation on any future problems that arise.

NRL-MRY benefits from the opportunities provided by NPS for continuing education and collaborative research with the Department of Meteorology and Oceanography.

Midway Research Center

The Midway Research Center (MRC) is located on a 158-acre site in Stafford County, Virginia. Located adjacent to the Quantico Marine Corps' Combat Development Command, the MRC has 10,000 ft² of operations and administration area. Instruments include three precision 18.5-m-diameter parabolic antennas housed in 100-ft radomes, a fast-tracking 1-meter telescope currently used for satellite laser ranging, and a transportable 16-inch telescope capable of passive optical tracking and laser communications. The MRC, under the auspices of the Naval Center for Space Technology, provides NRL with state-of-the-art facilities dedicated solely to space-related applications in naval communications, navigation, and basic research.

Research Platforms

Mobile research platforms contribute greatly to NRL's research. These include six P-3 Orion turboprop aircraft and one ship, the ex-USS *Shadwell* (LSD-15), berthed in Mobile Bay, Alabama. The ex-USS *Shadwell* is used for research on aboard-ship fire-suppression techniques.

LOOKING AHEAD

To provide preeminent research for tomorrow's Navy, NRL must maintain and upgrade its scientific and technological equipment to keep it at the forefront of modern research facilities. The physical plant to house this equipment must also be state of the art. NRL has embarked on a Corporate Facilities Plan to accomplish these goals. This plan and future facility plans are described below.

THE CORPORATE FACILITIES INVESTMENT PLAN (CFIP)

The CFIP is a capital investment plan that uses both Congressionally approved military construction (MILCON) and Laboratory overhead funds to provide modern, up-to-date laboratory facilities for

NRL. Past MILCON projects have included the Electro-Optics Building at NRL-DC and a new Ocean Acoustics Research Laboratory at NRL-SSC. Future MILCON projects include the Nanoscience Research Laboratory now under construction and a proposed Autonomous Vehicles Research Building in the FY05 time frame.

To complement these efforts, overhead funds have been used to renovate and upgrade laboratory and support areas in several existing buildings. Modern laboratory facilities have recently been provided for the Center for Bio/Molecular Science and Engineering, the Materials Science and Technology Division, the Remote Sensing Division, the Acoustics Division, the Information Technology Division, and the Radar Division.

In parallel with efforts to upgrade laboratory buildings to the most modern standards, those buildings that were built during World War II and do not lend themselves to renovation are being demolished. This will provide space for the construction of future MILCON buildings, and it will also reduce the Laboratory's overhead costs.

Institute for Nanoscience

The manipulation and measurement of materials with nanometer dimensions is very difficult. One must be able to reliably and precisely locate structures of nanometer dimensions in much larger areas. Furthermore, the measurement of nanostructure properties is difficult simply because not many atoms/molecules are present. Vibrations and thermal/humidity/pressure fluctuations in the environment can cause major problems in positioning a tool. Good signal-to-noise ratios require electromagnetic and acoustic interference-free environments. Airborne contamination can readily cover a nanostructure. A new nanoscience building is under construction that will control these sources of "noise"; it will become available in the summer of 2003. There will be 5000 ft² of Class 100 cleanroom for device fabrication; 4000 ft² of "quiet" space with temperature controlled to 0.5 °C, acoustic isolation at the NC35 standard (35 dB at 1 kHz), and vibration isolation to <3 m/s rms 10-100 Hz. There will also be 1000 ft² of "ultra-quiet" space with temperature controlled to 0.1 °C and acoustic isolation at the NC25 standard (25 dB at 1 kHz).

Ruth H. Hooker Research Library

The Ruth H. Hooker Research Library has encouraged "Innovation for Research" for many years, exemplified by the first-of-its-kind systems such as InfoNet, InfoWeb, and TORPEDO *Ultra*. These custom systems, combined with the licensing of online resources for all NRL sites, dramatically increase resources available at the researcher's desktop. Plans for FY03 include search enhancements to the TORPEDO *Ultra* system, in addition to the loading of thousands of new journal titles into TORPEDO *Ultra* (including titles from Academic Press, American Meteorological Society, IEEE, IEE, Institute of Physics, Kluwer, Optical Society of America, and Wiley). Cross-database searching (searching multiple databases from various publishers with a single search) is also being investigated, and the NRL Online Bibliography (containing references to scholarly work created by NRL authors over the past decade) will be released in FY03. Finally, the NRL Library is working closely with the

Navy CIO's office and the Librarian of the Navy to extend several NRL Digital Library services across the Navy, including the Warfare Centers, Navy Academic institutions, and Naval Medical facilities. The first step has been the expansion of TORPEDO *Ultra* v.2 to more than a dozen Navy sites, with future steps including the creation of a Navy-wide Journal Information Managements System.

Information Technology

The Information Technology Division's Center for Computational Science (CCS) operates scalable, massively parallel Global Shared Memory (GSM) computer systems, including a 128-processor SGI Origin3800 with cache-coherent Non-Uniform Memory Access (ccNUMA) architecture. Recent additions in FY02 include an experimental multi-threaded architecture (MTA) high-performance computer with 40 or more processors and the replacement of existing Sun HPC Cache-Only Memory Access (COMA) architecture with next-generation SUN machines. These systems comprise the Distributed Center (DC) at NRL whose hardware is funded by the DOD High Performance Computing Modernization Program (HPCMP). The systems are used in the innovative exploration and evaluation of MPP technology for the solution of significant militarily relevant problems relating to computational and information science. The systems allow for leading-edge research in support of heterogeneous parallel processing applications by the Navy and DOD science and technology communities.

Chemistry

Homeland Defense has been a focus of the Chemistry Division since September 11, 2001, especially in the development of improved detection techniques for chemical, biological, and explosive threats. In conjunction with technologies contributed by other divisions, Chemistry Division staff will be major contributors to the definition and development of new technology systems. In a parallel and complementary multidivisional program, the Chemistry Division will be a major contributor to the NRL Nanoscience Institute. Nanoscience complements Homeland Defense in that nanoscience is expected to provide dramatic improvements to chemical/biological detection, protection, and neutralization. Chemistry will approach the nanoscale from the bottom-up—building smaller atoms and molecules into nanostructures with new properties, and developing the directed assembly of nanostructures into

hierarchical systems. The new NRL Nanoscience building is linked directly into the Chemistry building to provide both controlled access and auxiliary space for work not requiring a “low noise” environment.

Plasma Physics

The Plasma Physics Division has set up a Large Area Plasma Processing System (LAPPS) facility to investigate a new technique to produce plasmas for plasma processing. Applications include production of large-area flat-screen displays or elements for phased arrays or materials modification such as surface polymerization or ion implantation. The system is based on low-energy electron beam ionization of a background gas to produce the desired plasma. The system may have advantages over existing techniques for production of large-area (square meter) plasmas, efficiency of plasma production, and control of reactive species.

Electronics Science and Technology

Important division emphasis is focused on the continual upgrading of the Nanoprocessing Facility (NPF) and the Compound Semiconductor Processing Facility (CSPF) and expanding activities in the nanoelectronics, wafer bonding, heterostructures, and vacuum electronics integration programs. The NPF has added a third e-beam writer that provides low-voltage pattern writing capability and an inductively coupled plasma etcher that provides deep etching capability for non-silicon materials. The MOCVD Facility will install an updated custom computer control capability for the growth of complex structures.

Ocean Research Laboratory

NRL's Ocean Research Laboratory is a 52,000 ft² building that houses the Oceanography Division of the Ocean and Atmospheric Science and Technology Directorate. The building contains office space, oceanographic laboratories, staging areas, a small machine shop, electronic and secure laboratories, and visualization and computing facilities for research and development in ocean science and remote sensing.

Acoustics

NRL's Salt Water Tank Facility is designed to provide a controlled environment for studying complex bubble-related processes found in the ocean. It is an experimental pool facility for studies

of underwater acoustics, fluid dynamics, and air-sea interface environmental topics under saline conditions. This facility is currently being used to study the acoustics of bubbly media, including bubble entrainment and ambient noise generation, scattering from bubbly structures, and propagation through bubbly media. Future studies include the interaction of bubbles with turbulent fluid flows, bubble coalescence and dissolution, effects of surfactants and contaminants, and bubble-related gas exchange across the air-sea interface.

Remote Sensing

The Remote Sensing Division has developed and installed 74 MHz receivers on the National Radio Astronomy Observatory's Very Large Array (VLA), thereby producing the world's highest angular resolution and most sensitive astronomical interferometric array operating below 150 MHz. In contrast to the VLA's maximum baseline of 35 km, all previous astronomical interferometers operating below 150 MHz had baselines less than 5 km because ionospheric structure had been thought to impose phase variations that would corrupt the interferometric imaging. Work in the Remote Sensing Division has shown that radio astronomical techniques can now remove the ionospheric phase variations and extend interferometer baselines to arbitrary lengths. In its first year of operation, the NRL/NRAO 74 MHz system has been used for a variety of innovative observations with encouraging initial results in solar system, Galactic, and extragalactic astrophysics. The success of the NRL/NRAO 74 MHz system indicates that it is possible to open a new high-resolution, high-sensitivity astronomical window by going to an even larger, more sensitive system. The Remote Sensing Division, in collaboration with the Netherlands Foundation for Research in Astronomy, is currently designing a follow-on instrument, the Low Frequency Array (LOFAR). LOFAR will be a fully electronic, broadband array operating in the 15 to 150 MHz range, with a collecting area of 1 square km at 15 MHz and a maximum baseline of 500 km resolution and sensitivity over the state of the art.

The Remote Sensing Division is also developing other new facilities-class sensors including the Navy Ultrawideband Synthetic Aperture Radar (NUSAR). NUSAR is a fully capable high-resolution (less than 1 m impulse response) synthetic aperture radar system made to be operated from light aircraft. It is fully polarimetric and can operate as an along-track interferometer. Its frequency range will be expandable, and ultimately it will operate from VHF to X-band.

Marine Geosciences

The Marine Geosciences Division has greatly enhanced the capabilities and quality of seafloor sediment fabric analyses through completion of installation and staff training for its 300-kV transmission electron microscope (TEM) and accompanying environmental cell (EC). The TEM-EC is housed in a specially built facility imparting a null effect on the functioning of the TEM-EC electronics. The new facility will improve transition of developed capabilities and sediment fabric understanding to applied issues of acoustic and shock-wave propagation, mine burial, and mine countermeasures.

Vacuum Ultraviolet Space Instrument Test Facility

The Space Science Division facilities include an ultraclean solar instrument test facility in Building A-13 on the main NRL campus. The facility is designed to satisfy the rigorous contamination requirements of state-of-the-art solar spaceflight instruments. The facility has a 400-ft² Class 10 clean room and a large Solar Coronagraph Optical Test Chamber (SCOTCH). This completely dry-pumped, 550-ft³ vacuum chamber is maintained at synchrotron levels of cleanliness. Solar instrumentation up to 1 m in diameter and 5 m in length can be physically accommodated in the chamber. The instrument's optical performance is probed and calibrated with a variety of visible and XUV sources mounted on the chamber's 11-m beamline. The optical testing and characterization of the Large-Angle Spectrometric Coronagraph (LASCO) instrument for the European Space Agency's Solar Heliospheric Observatory satellite were conducted in this chamber. Coronagraph stray-light characterization was carried out by mounting a set of baffles in the main beamline, illuminating the instrument with a simulated solar beam, and measuring the residual radiation. A stray light background measurement of 10⁻¹² was successfully measured in the LASCO C3 channel. Coronagraph calibration was carried out by installing back-illuminated calibrated opals in front of the instrument entrance aperture. Instrument polarization properties were analyzed by using a variety of polarizers installed in a wheel located between the opal and the instrument. The wheel was remotely controlled from outside the chamber. Instrument Mueller matrices were verified with a 12-in. diameter, two-plate partial polarizer. Calibration and focus of XUV solar instrumentation are accomplished by exposing the instrument to an XUV windowless collimator at the end of the tank. The facility also has a small thermal bake/vacuum

test chamber used for vacuum conditioning and thermal testing of spaceflight components and subassemblies. Both the SCOTCH and the small test chamber are instrumented with temperature-controlled quartz-crystal monitors and residual gas analyzers for real-time, quantitative measurements of volatile contamination.

REHABILITATION OF SCIENTIFIC FACILITIES

Specialized facilities are being installed or upgraded in several of the research and support divisions.

Flight Support Detachment

NRL's Flight Support Detachment (FSD) has continued to improve both capabilities and diversity among its aircraft platforms. Aircraft 153442 has undergone extensive modifications with Lockheed Martin to install a "rotodome" antenna and full AEW radar system. The aircraft is currently supporting the Navy's Theater Air Defense programs and providing a testbed for advanced EW radar research. Additionally, all aircraft have completed extensive bomb-bay design improvements that will allow the aircraft to carry more diverse scientific payloads. The Electra Doppler Radar (ELDORA) and a laser were installed on aircraft 154587 during an extensive modification for the IHOP and Crystal Face projects, and will be used in upcoming atmospheric research projects. These upgrades and modifications will ensure that NRL will have the finest airborne research capabilities well into this century.

Radar

In August 2002, the Radar Division completed its move to renovated facilities in buildings 60 and 42.

Information Technology

The Information Technology Division continues to transition stable technology from high-performance network testbed activities into the NRL local area network. This effort includes support of ATM technology at stream rates of 622 Mbps (OC12c) and 2.5 Gbps (OC48) across the enterprise with demonstrations and technology integration to allow first use of 10 Gbps single streams and higher. The current computing architectures, the SGI Origin3800 and the Sun Ultra, are continuously undergoing upgrade and evaluation of both hardware and software. The NRL CCS works closely with the DOD HPC community and the HPC vendors to

provide insight, balance, and value-added capabilities within the MPP testbed infrastructure.

Plasma Physics

A state-of-the-art short-pulse (0.4 ps), high-intensity Table-Top Terawatt (T^3) laser currently operates at 10 TW and 2×10^{19} W/cm² for a variety of physics studies. The T^3 laser will be upgraded to boost its power to 25 TW and intensities to $>10^{19}$ W/cm². This will provide a facility to do fundamental physics experiments in intense laser-plasma interactions, intense laser-electron beam interactions, and intense laser-matter interactions.

The division is building a repetitively pulsed (5 pps) krypton fluoride (KrF) laser called Electra. Electra will develop the technologies needed for inertial fusion energy (IFE). A laser for a power plant would have to fire five times per second, run for several years, and meet stringent cost and efficiency requirements. Electra will develop the technologies that can meet these requirements. It will have a laser output of around 400 to 700 joules. The size of Electra was chosen to be large enough to be scalable to a power plant size, but small enough to be flexible.

The Plasma Physics Division will be bringing on line the new Mercury pulsed-power generator in

FY03. The facility will be located in renovated space in Building 256. Mercury is an inductively isolated, voltage-adder device that will be capable of producing a 6-MV, 375-kA, 50-ns electrical power pulse for driving electron beam and ion beam diodes. The new facility will support ongoing radiographic source development for the Department of Energy and nuclear weapons effects simulation for the Defense Threat Reduction Agency.

Electronics Science and Technology

The Electronics Science and Technology Division continues to upgrade and expand its capabilities in nanofabrication science, solar cell characterization, and ultrafast lasers. Facilities will be enhanced with new laboratories and an expanded EPICENTER that includes a new vacuum processing chamber and two new epitaxial growth chambers. The Space Solar Cell Characterization Laboratory has moved into Building 208 and is being upgraded. The Laboratory for Proximal Probe Nanofabrication (LPPN) will explore the limits of nanolithography with proximal probes and techniques to exploit carbon nanotube-based devices. The Ultrafast Laser Facility will be moving into Building 208 in FY03.

FEATURED RESEARCH



NAVY AND MARINE MEMORIAL.

This monument, sculpted in aluminum, consists of seven seagulls in flight above the crest of a wave. It stands on a green granite base and was erected in honor of men of the United States who gave their lives or are still offering their lives in the performance of heroic deeds upon the waters of the world.

- 51** Unified Approach to Fatigue Damage Evaluation
K. Sadananda, R.L. Holtz, and A.K. Vasudevan
- 59** Filamentation and Propagation of Ultra-Short, Intense Laser Pulses in Air
A.C. Ting, D.F. Gordon, C.K. Manka, R.F. Hubbard, J.R. Peñano, and P. Sprangle
- 69** Satellite Surveillance of Desert Dust Storms
S.D. Miller
- 79** Timing Studies of X-ray Binary Objects
P.S. Ray, M.T. Wolff, K.S. Wood, and P. Hertz

[BACK TO CONTENTS](#)



UNIFIED APPROACH TO FATIGUE DAMAGE EVALUATION

K. Sadananda and R.L. Holtz

Materials Science and Technology Division

A.K. Vasudevan

Office of Naval Research

Fatigue damage limits the service life of many structural components that are subjected to variable stress. Fatigue is irreversible and usually unavoidable. High-priority objectives for preventing fatigue include containment of the fatigue damage, diagnostic tools to detect the beginnings of fatigue damage, monitoring the damage evolution during service, prognostics for reliable prediction of remnant service life, and fatigue-resistant materials by design. The key to success for mitigating life-cycle costs is the development of fundamental understanding of fatigue damage evolution in engineered materials. NRL has been working in recent years to replace fundamentally unsound empiricism extant in fatigue life prediction with a new systematic interpretative framework derived from basic principles.

INTRODUCTION

Fatigue damage can result from fluctuating stress. At low stress, material behaves elastically and reversibly. However, if stress is greater than the yield point, then irreversible plastic deformation occurs. If a single peak stress is high enough, fracture or other monotonic failures occur. If the stress is variable, such that there is a peak stress and an amplitude, then damage can accumulate with each cycle. After a sufficient number of cycles, failure can occur even if the peak stress is too low to cause fracture.

Fatigue is the principal cause of premature failure of engineering components. Sometimes these failures can be quite catastrophic, leading to severe property damage and loss of life. Fatigue cracks can nucleate at preexisting flaws in materials and tend to occur at stress concentrators in components such as notches or holes. Generally, fatigue damage is unavoidable. Once formed, the propagation rate of a crack is strongly influenced by load history and environmental factors. Thus, the accurate prediction of fatigue life is a complex problem. It is very difficult and rare to predict fatigue life accurately to within a factor of two. Indeed it is not only necessary to improve fatigue life prognostics to avoid catastrophic failures, but methods for optimizing inspection, maintenance, and parts replacement intervals would have a tremendous impact on service life costs and systems readiness. Clearly, new approaches to the problem of fatigue prognostics are needed.

The Fatigue Crack Growth Threshold

It was recognized in the 1960s that the fracture mechanics stress intensity K is an appropriate parameter for describing fatigue phenomena. The actual stress near a crack tip is equal to stress intensity divided by the distance from the tip and multiplied by some angular factors. Peak stress intensity K_{max} is the parameter that determines whether a component fractures. In the case of cyclically varying K , it was found that many fatigue phenomena correlated very well with the stress intensity amplitude $\Delta K = K_{max} - K_{min}$. In particular, ΔK must exceed a threshold value $\Delta K_{threshold}$ for a fatigue crack to grow. However, it also was recognized that a second parameter was necessary to adequately describe empirical fatigue data to account for the variation of ΔK with peak stress intensity. The customary and experimentally expedient choice for this second parameter has been the load ratio $R = K_{min}/K_{max}$, which is the ratio of minimum to maximum stress intensity.

Crack Closure

In the customary approach, ΔK is considered the only fatigue driving force, so that the R effects are considered the results of other phenomenology. In particular, the concept of "crack closure" was proposed to account for observations that ΔK_{th} is low at high values of R and increases with decreasing values of R (Fig. 1). The concept, known as "plasticity-induced

crack closure,” was advanced and generally accepted in the 1970s. In this concept, it is assumed that the plastic deformation at and ahead of the tip of the growing crack leaves a residual stretching of the material. Upon unloading, this results in a buildup of residual compressive stresses at the crack tip. Upon further unloading, the crack faces come into contact (as illustrated in Fig. 2) – in effect, shielding the crack tip from further changes in applied load. Thus if the specimen is completely unloaded ($R = 0$), a higher K_{max} must be applied to open the crack and overcome the residual compressive stresses so that the measured ΔK_{th} necessary for crack advance is increased. At high enough values of R , however, the minimum applied load is high enough to hold the crack open and is higher than the residual compressive stress, thus no change in ΔK_{th} is observed.

Another effect with similar manifestation in the fatigue behavior is if there is an obstruction in the crack. Then, in effect, the crack tip is wedged open. The stress intensity actually acting on the crack tip is then somewhat higher than the applied stress intensity. As a result, the effective stress intensity amplitude $\Delta K_{effective}$ is less than the applied ΔK . Consequently, a

higher $\Delta K_{threshold}$ will be measured than if the crack faces did not interfere. Crack face interference can occur, for example, if an oxide layer forms on the crack surfaces, if debris is in the crack, or if slight misalignments of the crack faces cause surface roughness to interfere on opposing crack faces. Although the true effect of these crack obstruction processes is to wedge a crack open, and this is unrelated to plasticity-induced crack closure, the terminology “crack closure” is generally used to describe all of these effects.

The crack closure concept has been successful in empirical parameterization of a wide range of fatigue data. It has become the default interpretation of load ratio effects and is used in some form or another in fatigue life prediction models. However, well-known ambiguities in its experimental determination make it virtually impossible to predict. In fact, in an ASTM-sponsored round-robin test involving 10 laboratories, each using 3 different methods for the determination of crack closure for the same material, 30 different values spread within a factor of 3 were reported. The practical value of this is that it is little more than an adjustable fitting parameter.

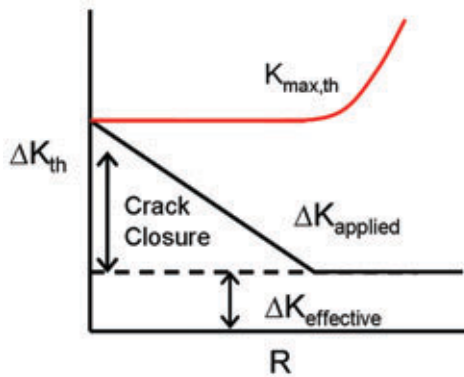
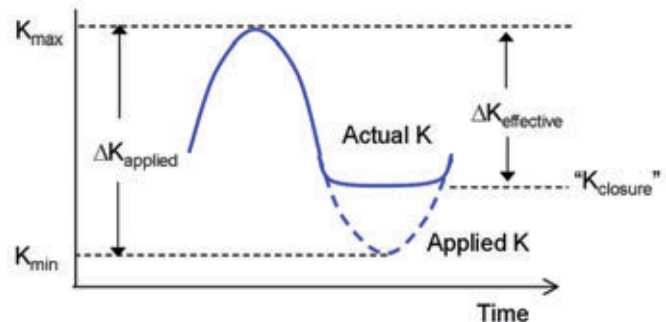
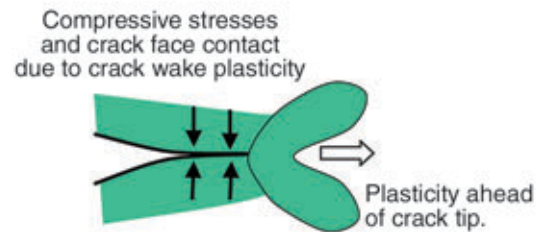


FIGURE 1

Crack closure contribution to the thresholds at low load ratio R . Applied ΔK is greater than effective ΔK due to crack closure. At high R there is no crack closure contribution.

FIGURE 2

Crack closure is assumed to result from plasticity in the crack wake, causing crack surfaces to contact before the applied load is completely removed upon unloading. Crack closure reduces the effective crack tip driving force ΔK_{eff} to a value less than the applied ΔK .



Fundamental Problems with Plasticity-Induced Crack Closure

Plasticity-induced crack closure relies on the assumption that as a crack opens, the material at the crack tip stretches. As the crack subsequently closes, compressive stresses occur at the tip and premature crack face contact occurs in the wake of the crack. However, based on fundamental concepts of dislocation theory, NRL has shown that plasticity either at the crack tip or in the wake does not cause the crack to close. This is shown schematically in Fig. 3. In crystalline materials, plastic deformation occurs by the creation and movement of dislocations, which are each characterized by a Burger's vector related to the orientation and size of the dislocation. A Burger's vector of a dislocation is a conserved quantity. Thus, dislocations are created in pairs with opposite Burger's vector. Every dislocation emitted from the crack to form the plastic zone ahead of a crack tip is accompanied by a dislocation of opposite Burger's vector being absorbed into the crack, creating a ledge. Such a ledge always opens in the wake of the crack. Any closure contribution induced by the dislocation in the plastic zone cannot be greater than the opening contribution induced by the ledge dislocation. This statement is true for each dislocation pair emitted from the crack; therefore, it is true for any aggregate of many dislocations pairs – whatever their distribution.

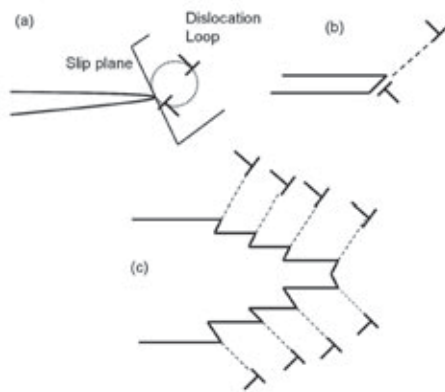


FIGURE 3

(a) Nucleation of a dislocation loop on a slip plane at the crack tip. (b) Dislocation loop expands with negative dislocation forming a ledge at the crack tip, thereby opening the crack, while positive dislocation becomes a part of plastic zone ahead of the crack. (c) As the crack grows, a buildup of plasticity with associated ledges occurs in the wake of the crack. Ledge dislocations always keep the crack open. In effect, matter is removed from the crack and redistributed around it.

A more intuitive way of conceptualizing this is to consider the conservation of mass, which is equivalent to conservation of Burger's vector for a dislocation. In

addition, plasticity occurs with constant volume. Conservative plastic flow of mass from the crack is equivalent to removal of material from the crack and redistributing it into the plastic zone associated with the crack tip. The closure contribution from this redistributed matter cannot be greater than the opening of the crack due to its removal. By using continuum dislocation theory, NRL also has shown that other forms of crack closure are also smaller than generally thought and, in some cases, have negligible effects on crack tip driving force.

The most important consequence of NRL's dislocation analysis of crack closure is that if the various crack closure mechanisms are either nonexistent or small, then some other formulation is needed for the various phenomena that have hitherto been attributed to crack closure. This has led to a complete reformulation of how fatigue crack growth is interpreted and represented.

THE UNIFIED APPROACH TO FATIGUE

To achieve the reformulation of fatigue crack growth behavior, it is only necessary to adopt six seemingly commonsense principles:

1. Fatigue crack growth requires two driving forces, both ΔK and K_{max} . ΔK creates fatigue damage through the irreversible plasticity, but K_{max} is necessary to open and increment the crack. The customary approach recognizes only ΔK as a driving force, and uses the load ratio R to describe how "open" the crack is.

2. Each driving force has a threshold criterion. For a fatigue crack to propagate, two conditions must exist: ΔK must be large enough to create cumulative damage, and K_{max} must be large enough to increment the crack. The corresponding thresholds are termed ΔK_{th} and $K_{max,th}$. In terms of dislocations, the equivalent K_{max} must be large enough to create new dislocations, and ΔK must be large enough to overcome friction in the reverse dislocation flow. The customary approach assumes that only ΔK is important.

3. The correct representation of fatigue is as a three-dimensional map of da/dn , ΔK , and K_{max} (Fig. 4). The preferred two-dimensional representation of fatigue data should be constant da/dn contours projected onto the ΔK vs K_{max} plane. Such a representation reveals clearly the roles of ΔK_{th} and $K_{max,th}$ for threshold behavior as defining a roughly L-shaped curve. In fact, for da/dn greater than zero, similar curves can be defined, and the characteristic parameters ΔK^* and K_{max}^* are defined for constant da/dn contours. In addition, the shapes of the curves fall into a limited number of classifications associated with the type of fatigue mechanism. The mechanism also may

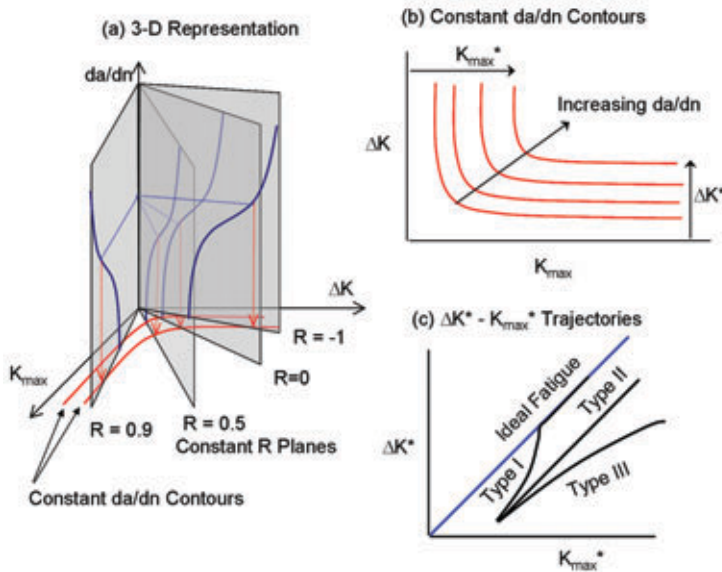


FIGURE 4 (a) Fatigue crack growth rate da/dn is a function of two variables, ΔK and K_{max} , thus requiring a three-dimensional representation. (b) The preferred two-dimensional projection is obtained by projecting constant da/dn contours onto the $\Delta K - K_{max}$ plane. The two limiting values ΔK^* and K_{max}^* for any constant da/dn contour become the two thresholds ΔK_{th} and $K_{max,th}$ when da/dn approaches zero. (c) Plotting ΔK^* vs K_{max}^* for a range of da/dn gives characteristic curves that are associated with material resistance to crack growth. The line $\Delta K^* = K_{max}^*$ represents ideal fatigue behavior. Deviations of $\Delta K - K_{max}$ curves from the ideal fatigue line indicate the degree of environmental effect on the fatigue mechanism.

change with da/dn . Customary representation of fatigue data is plots of da/dn vs ΔK at fixed R and plots of ΔK_{th} vs R . Typically, however, only one or two values of R are used so that the customary description necessarily is incomplete.

4. Fatigue crack growth is driven by the net local stress intensity acting at the crack tip. This idea is more often stated as the principle of similitude, i.e., that for a given stress intensity and given fatigue mechanism, the crack growth rate will be the same, regardless of specimen geometry. This also is equivalent to saying that, for a given fatigue mechanism, if one knows the stress intensity then one can deterministically predict the crack growth rate.

5. Internal stresses must be included in the fatigue driving forces. This is a consequence of the similitude concept. An immediate consequence of accounting for superimposed internal stresses is that if the internal stress is not a function of applied stress, then at first order, internal stress contributes to K_{max} and K_{min} equally. Thus, internal stress produces effects on K_{max} but not on ΔK . Customary interpretation of internal stress effects is that they can be treated as a form of crack closure, such that the effect is to reduce $\Delta K_{effective}$.

6. Environment and fatigue mechanism affect the characteristic parameters ΔK^* and K_{max}^* differently. The simplest way to think about this is to consider that environmental influences such as hydrogen, which can diffuse into the material, can directly affect ΔK^* , but environmental effects acting primarily at the crack tip surfaces, such as oxidation, affect primarily K_{max}^* . The preferred representation of environmental effects is parametric plots of ΔK^* vs K_{max}^* for the full range of da/dn . Ideal behavior in the absence of any environmental effect is manifested as the line $\Delta K^* = K_{max}^*$. The curves on these $\Delta K^* - K_{max}^*$ plots, which we usually

refer to as “trajectories,” reveal certain characteristic behaviors identifiable with the environmental mechanism when they deviate from ideal behavior. Customary treatment, on the other hand, is that environmental effects act as perturbations to da/dn .

We refer to this as a Unified Approach¹ because these six elements provide a unified framework for the representation of all fatigue crack growth phenomena. We examine three key topical areas to demonstrate how the Unified Approach has enabled new understanding and interpretation of certain common fatigue phenomena.

Short Crack Phenomena

Understanding of short crack growth behavior is essential for fatigue life prognostics because most of the life of a fatigue crack, before detection or failure, is spent as a short crack. Fatigue cracks are considered “short” if they are small compared to the important characteristic dimensions in the region in which they are growing (for example, grain size, plastic zone size, or specimen dimensions). The distinction between “short” cracks and “long” cracks has been made because short cracks exhibit a wide range of complex behaviors. These complex behaviors include growth at stress intensities below the long crack growth thresholds, arrest at stress intensities above the threshold, and anomalous acceleration and deceleration of the crack growth rates. Figure 5(a) shows some examples.

Conventional thinking based on crack closure arguments is that nascent short cracks have not yet developed enough plasticity in their wake to support crack closure. Long cracks in this picture, on the other hand, have developed a crack wake plastic zone and exhibit steady-state crack closure. Thus, the underlying

concept is that short cracks represent intrinsic behavior while long cracks are dominated by crack closure.

The Unified Approach interprets this completely differently.² Long crack behavior is considered the fundamental behavior because the long crack thresholds are intrinsic to the material and are independent of crack size. Short crack behavior is simply the result of internal stress variations on the short crack length scale since short cracks invariably form at notches, defects, and other stress concentrations. Internal stresses also arise from thermomechanical stress, phase transformations, residual welding stresses, forging, rolling, machining, and surface treatments, and they can be induced by transient loads in the cyclic loading history. The magnitude of internal stresses may be tensile or compressive, and they decrease rapidly as a short crack propagates away from microscopic stress concentrations. Since crack growth is due to the superimposed effects of internal and applied stresses, deceleration and acceleration can occur if the net stress exhibits a minimum or maximum as a function of distance along the crack path. This is illustrated in Figure 5(b).

It is worth repeating that the primary effect of internal stresses is on the K_{max} , not ΔK . Hence, short-crack growth behavior considered anomalous in the $\Delta K_{effective}$ crack-closure interpretation is actually a manifestation of internal stress effects on K_{max} and the principle of similitude. Practical progress on fatigue

prognostics now focuses on tractable problems of modeling, measuring, and controlling internal stress distributions.

Overload Effects

The importance of proper accounting of internal stress also is crucial to the understanding of transient and spectral load effects. Real load histories of engineering components are, of course, never perfect sine waves. This is most readily apparent for aircraft structures. These structures experience in-flight vibrations interspersed with occasional huge overloads or underloads that correspond to extreme maneuvering, turbulence, takeoffs, and landings. However, there are other examples. Ship hull structures undergo spectrum loading due to variable sea conditions. Motor, generator, turbine rotors, and gears experience cyclic stresses with occasional large transient stresses. Propulsion shafting experiences low-amplitude cyclic bending and torsional and longitudinal fatigue loading with occasional shocks as ships pass through variations in water density.

We have shown that overload effects are quite easily understood in terms of induced compressive residual stresses and the resultant effect on K_{max} . We further have shown that, based on dislocation analysis, a crack tip shielding effect due to dislocations occurs some distance ahead of the crack tip. This accounts for delayed crack growth retardation effects that have

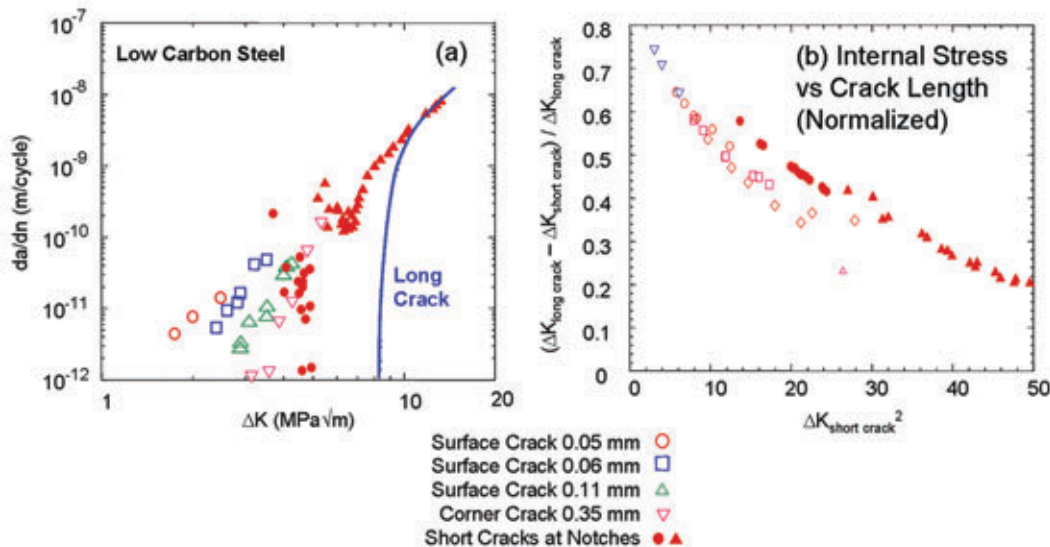


FIGURE 5

(a) Example of short crack growth behavior in a low alloy steel. Note the wide range of crack growth rates for various short cracks compared to the long crack behavior. (b) Internal stresses derived from the same short-crack growth as a function of crack length. The results are expressed in normalized units such that the x-axis is a relative measure of crack length and the y-axis is a relative measure of the internal stress relative to long crack behavior. Note that these are the same data as shown in (a), but they now all fall nearly on the same curve. This shows that the apparent anomalous variations of short-crack growth rates are explained by correctly accounting for internal stresses. (Data taken from K. Tanaka et al., *Eng. Fracture Mech.* **17**, 519-533 (1981)).

heretofore been considered puzzling in the crack closure context. In the Unified Approach, overload retardation effects can be most easily understood without crack closure.

Environmental Effects

The effects of environment on fatigue are unavoidable and almost always detrimental. This is particularly important for the Navy because corrosion due to seawater and humid salt-fog exposure is particularly damaging to many structural steels and aluminum alloys. The environmental effects on fatigue are not only cyclically stress-dependent through the process known as corrosion-fatigue but are also time-dependent and directly K_{max} -dependent via the stress-corrosion-cracking mechanism. Environmental effects on fatigue cannot be properly accounted for unless K_{max} is explicitly recognized as a driving force, hence the Unified Approach provides a natural and superior interpretative framework.

As an interesting example, Fig. 6(a) shows constant da/dn contours for cast iron in air. Except for the threshold curve, the constant da/dn contours are all

composed of two L-shaped curves. One needs some very convoluted mechanisms to explain this in terms of crack closure. However, if we take the K_{max}^* and ΔK^* values for each of the L-shaped curves and plot them on the ΔK^* vs K_{max}^* trajectory map explained earlier and shown in Fig. 6(b), the true nature of this complex behavior is revealed. Two competing fatigue mechanisms are operating. One mechanism, corresponding to the trajectory that approaches the ideal fatigue line, is characteristic of pure environmentally assisted fatigue. The mechanism is that the environmental species (hydrogen) diffuses into the material at a certain rate, embrittling the material for a distance ahead of the crack tip and reducing the ΔK^* . As the crack growth rate increases, the crack tip can outrun the diffusing hydrogen and propagate through mostly unaffected material. The other competing mechanism is the trajectory that diverges from the ideal line with increasing K_{max}^* . This is characteristic of stress-dependent monotonic cracking modes, in particular, stress-corrosion cracking. A more detailed analysis, which cannot be pursued here due to space limitations, shows that the competing mechanisms are the result of competing intergranular vs transgranular mechanisms.

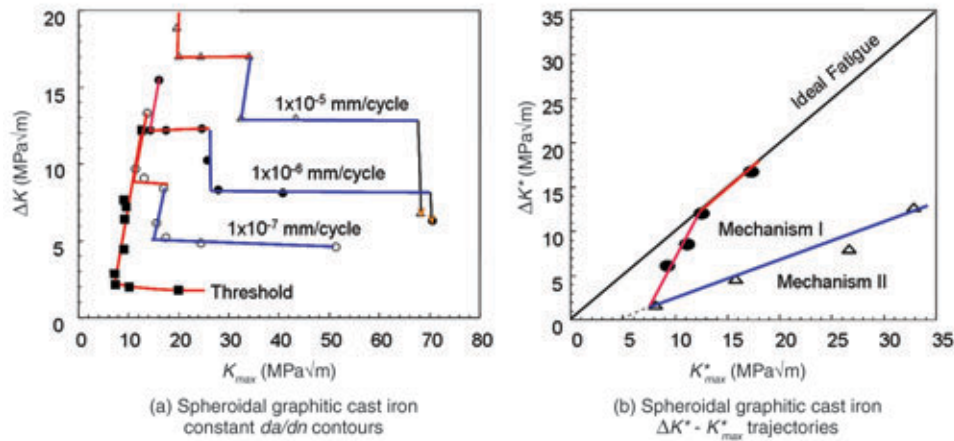


FIGURE 6

(a) Constant da/dn contours for several da/dn data for a spheroidal cast iron. Two fatigue mechanisms are identifiable, Mechanism I and Mechanism II. (b) ΔK^* - K_{max}^* trajectory corresponding to the data shown in (a). Mechanism I approaches then merges with the ideal fatigue line as crack growth rate increases. This is characteristic of environmental species that penetrate into the material (such as hydrogen) at a fixed rate of diffusion. At higher crack growth rates, the crack tip outruns the environmental effect. Mechanism II diverges from the ideal fatigue line, characteristic of stress-dependent environmental effects such as stress-corrosion cracking. In this particular case, the crack growth is intergranular in Mechanism I but transgranular in Mechanism II. (Data taken from J.H. Bulloch, *Theoret. Appl. Fracture Mech.* **17**, 19-45 (1992)).


SUMMARY

The Unified Approach to fatigue crack growth developed at NRL is a departure from the conventional fatigue interpretative framework in that the relative importance of crack closure is reduced and the role of internal stresses is more important. The examples described here illustrate the power of the Unified Approach to fatigue crack growth for provid-

ing clear physical insight into the fundamental mechanisms by using a correct and consistent interpretative framework.

[Sponsored by ONR]

References

- ¹ K.Sadananda and A.K.Vasudevan, "A Unified Framework for Fatigue Damage Analysis," *Nav. Res. Rev.* **50**(4), 56-68 (1998).
- ² A.K.Vasudevan, K.Sadananda, and G.Glinka, "Critical Parameters for Fatigue Damage," *Int. J. Fatigue* **23S**, S39-S53 (2001). 

THE AUTHORS



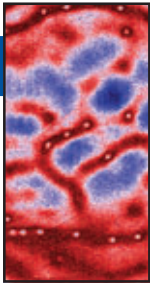
KUNTIMADI SADANANDA is Head of the Deformation and Fracture Section in the Physical Metallurgy Branch, Materials Science and Technology Division. He is responsible for initiating, developing and conducting research programs in the area of deformation and fracture of engineering materials. He is currently involved in reevaluating the entire fatigue area in terms of quantification of the damage using a two-parametric approach. This includes the analysis of crack nucleation, short crack growth, long crack growth and failure, and the role of internal or residual stresses that are either in situ generated or introduced during processing. He is also involved in the study of creep of molybdenum disilicides and SiC-Si₃N₄ composites.



RONALD L. HOLTZ received his B.S. degree in engineering physics from the University of Illinois, Urbana, in 1978, and Ph.D. in experimental solid state physics from Iowa State University in 1985. He first came to NRL in 1985 as an NRC Postdoctoral Associate and performed basic research on percolation properties of phase-separated microwave-absorbing thin films. This work led to some of the first research at NRL on nanostructured materials, for which Dr. Holtz holds two U.S. Patents, as well as basic research on high capacity fine-grained hydrogen storage alloys. Since 1995, Dr. Holtz has been engaged in experimental fatigue damage research, in particular high-vacuum fatigue measurements. Recent research also has included analysis of fatigue properties of high-temperature superconducting tapes for high-power density Navy motors and generators.



ASURI K. VASUDEVAN is a Scientific Officer in the Materials Science and Technology Division, at the Office of Naval Research. In this capacity, he directs materials research relating to bulk nanostructural materials, fatigue damage of structural materials, and fracture/fatigue analysis of piezoelectric materials. Dr. Vasudevan obtained his Ph.D. in metallurgy and materials science. He then joined ALCOA Research Laboratories (1979-1989), Pittsburgh, Pennsylvania, as a staff scientist, where he developed and conducted basic and applied research programs aimed at developing high strength aluminum alloys from aircraft applications. Dr. Vasudevan is best known for his book, *Aluminum Alloys – Contemporary Research and Applications*, published by Academic Press, in 1987. He is a member of ASM International, The Transactions Metals Society, ACS, and MRS. He has been an advisor to NATO in the area of fatigue damage and NASA in the area of lightweight materials.



FILAMENTATION AND PROPAGATION OF ULTRA-SHORT, INTENSE LASER PULSES IN AIR

A.C. Ting, D.F. Gordon, R.F. Hubbard, J.R. Peñano, and P. Sprangle

Plasma Physics Division

C.K. Manka

RSI, Inc.

Ultra-short (femtosecond), high-power laser pulses can exceed the threshold for nonlinear self-focusing in air. This results in an extended propagation from the dynamical balance between the plasma formation and the nonlinear focusing. Experiments were performed using the chirped-pulse-amplification (CPA) lasers in the Plasma Physics Division to study the physics of extended propagation in air and its effects on atmospheric breakdown, laser-induced electrical discharge, and chemical/biological (chem/bio) agent detection. Self-guiding of the laser beams for extended distances and formation of multiple laser and plasma filaments were observed. Time-resolved images of laser-induced electrical discharges showed the initiation and sustention of the discharges by the plasma filaments. Measured optical spectra of the white light generated in the laser propagation revealed the presence of molecular plasmas that are useful for identifying chem/bio agents. Potential applications include directed energy weapons, remote sensing for both chem/bio defense, and environmental air pollutant monitoring.

INTRODUCTION

Ultra-high-power lasers that can deliver intense radiation have traditionally resided in a few, very large national laboratories. This is because more energy is usually required as the power of the laser increases, and thus the size of the laser correspondingly increases. Therefore, research into the physics associated with intense radiation from these ultra-high-power lasers could only be carried out at these large institutions. In addition, the size and cost of the lasers severely limited the range of potential applications. This has all changed during the last decade when a new way of generating high-power lasers was discovered. This simple but effective “trick” to increase laser power starts with the recognition that power is, by definition, energy per unit time. Instead of increasing the energy carried in a laser pulse for a fixed time duration to obtain higher power, one can produce the same laser power if one decreases the pulse duration while maintaining the same amount of energy in it. By utilizing ultra-short laser pulses with durations as short as a few tens of femtoseconds (thousand-trillionth of a second), laser pulses with power as high as tens of terawatts (trillion watt) can now be obtained by using table-top sized laser systems. Research on these lasers can now be performed in reasonably sized laboratories, and many potential applications are envisioned.

Many interesting phenomena are associated with the interactions of these very intense and short laser pulses with various media. In particular, the propagation of a short intense laser pulse in a gas such as air is very different from that of a long or continuous wave (CW) laser pulse. For example, the high intensity of these pulses can produce nonlinear contributions to the index of refraction of the medium. The intensity of the laser pulse could also become so high that the air molecules would ionize and form a plasma. The interplay between the laser pulse and the plasma that it creates can be very complicated and can profoundly affect the evolution of the laser pulse as it propagates through the atmosphere. Experiments using ultra-short (~ 100 fs), high intensity ($> 10^{13}$ W/cm²) laser pulses have demonstrated long-distance self-guided atmospheric propagation,¹ air breakdown, filamentation, and white light generation. Intense, directed white light pulses have been generated and backscattered from atmospheric aerosols. The generation of pulsed THz radiation in plasma channels formed by femtosecond pulses has also been observed and analyzed. Although many of the observations cannot be completely explained, the experimental, theoretical, and numerical results obtained to date indicate potential applications for both passive and active remote sensing and induced electric discharges, among others. In addition, the individual micropulses in a shipboard free electron

laser (FEL) system may exhibit short-pulse propagation characteristics. To achieve these potential applications, it is necessary to have a comprehensive and quantitative understanding of the physical mechanisms that govern the propagation of intense, short laser pulses in air.

The following sections begin with a description of the table-top ultra-high-power lasers in the laboratory. Next, the physics of propagating femtosecond terawatt laser pulses in air is discussed, with experimental demonstration of the novel phenomena of self-guided laser filaments and numerical verification of the experimental results. These filaments and the associated broadband radiation that they generate can be used in the remote sensing of chemical/biological agents in defense or anti-terrorism applications or detecting hazardous air pollutants in environmental monitoring and enforcement. The plasma filaments associated with a self-guided femtosecond intense laser pulse can also be used for triggering high-voltage electrical discharges. This phenomenon is next discussed, with emphasis on the discharge initiation mechanism, by studying the time evolution of the discharge. There is considerable interest worldwide in studying this phenomenon so that it can be applied to areas such as lightning arrest around power plants. The concluding section summarizes research efforts at NRL in studying ultra-short intense laser pulse propagation in air.

NRL T³ AND TFL LASERS

The NRL High Field Physics Laboratory was one of the first laboratories to have a table-top terawatt (TW) laser system soon after the invention of the chirped pulse amplification (CPA) method. The T³ laser was installed in 1992 as the first commercial CPA laser ever built. It has been upgraded several times over the years and is still a state-of-the-art CPA laser. It is a solid state laser involving two lasing media, titanium-doped sapphire (Ti:sapphire) and neodymium-doped glass (Nd:glass). The lasing wavelength is in the infrared at 1054 nanometers (nm). Like most lasers, it consists primarily of a laser oscillator that generates the seed laser pulse and then a series of laser amplifiers to boost the energy in the pulse. The difference is that the seed laser pulse has a pulse length of only 100 femtoseconds (fs). As the laser pulse is amplified, the power and intensity of the pulse continuously increases and eventually will reach the breakdown threshold of the laser glass medium. To avoid such disastrous consequences, the CPA technique stretches the laser pulse after the oscillator with a diffraction grating to ~10,000 times and thus reduces the laser intensity and power by the same factor. The

stretched pulse can now be safely amplified to the desired high energy per pulse. The stretching process is then reversed by re-compressing the amplified pulse with diffraction gratings in air or vacuum to produce a high-power, ultra-short pulse. One interesting observation is that in the stretched pulse, the frequency content of the pulse is arranged such that the high-frequency (pitch) components are moved to the back of the stretched pulse, reminiscent of the chirped tune of a singing robin, and hence the “chirped” pulse amplification technique.

Figure 1 shows the T³ laser. The final amplifier is in the foreground, and the oscillator and preamplifiers are in the back and to the left. It can generate a laser pulse 400 fs long with 5 Joules (J) of laser energy in it. The peak power of the pulse is therefore >10 TW. It has a repetition rate of one shot every 20 minutes. Most experiments on intense laser interactions require both the high power and high energy in the laser pulse. However, a number of interesting behaviors of an ultra-short laser pulse are primarily the consequence of the high power and intensity of the pulse. Since a shorter pulse with less energy could have the same high power, a smaller laser with less energy per pulse could be adequate for some of the high-intensity laser experiments.

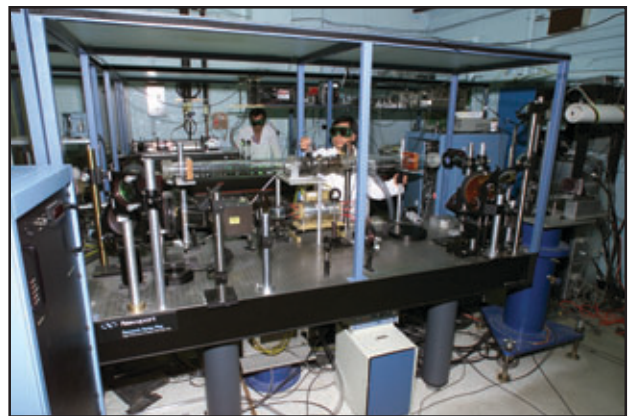


FIGURE 1 The NRL T³ laser is a table-top Ti:sapphire/Nd:glass CPA laser system that produces laser pulses at a wavelength of 1054 nm with 5 J of laser energy in a 400-fs pulse. It is operated at a repetition rate of one shot every 20 minutes. The amplified stretched pulse is compressed with diffraction gratings inside an evacuated chamber (not shown in the picture) to avoid nonlinear propagation effects that would degrade the laser beam quality.

The NRL TFL laser shown in Fig. 2 is a TW laser with a smaller footprint than the T³ laser, and most importantly, it can be rep-rated at 10 times a second (10 Hertz). It is based entirely on Ti:sapphire technology, and it is lasing at the infrared wavelength of 810 nm. The laser pulse width is 50 fs with 50 milli-Joules

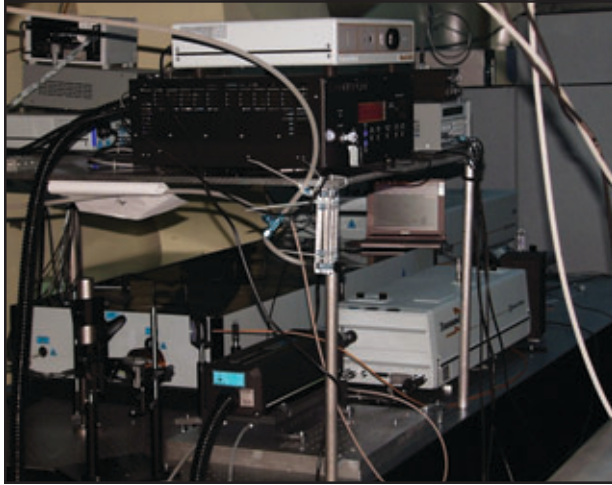


FIGURE 2

The NRL TFL laser is a table-top Ti:sapphire CPA laser system that produces laser pulses at a wavelength of 810 nm with 50 mJ of laser energy in a 50-fs pulse. It is operated at a repetition rate of 10 Hz. The amplified stretched pulse is compressed in a portable compressor (not shown in the picture), which allows optimized positioning of the laser for air propagation experiments.

(mJ) of energy in each pulse. Both lasers are located in our well-equipped laboratory, with extensive optical and electronic diagnostic equipment that can be used to study the effects and mechanisms of these ultra-short intense laser pulses interacting with various media.

PROPAGATION OF INTENSE SHORT LASER PULSES IN AIR

The propagation of intense, short laser pulses in the atmosphere involves a variety of diverse linear and nonlinear optical processes. The nonlinear processes are the consequences of the high intensity of the laser pulse. Processes affecting the laser spot size include diffraction, nonlinear self-focusing, ionization, and plasma defocusing. In addition, self-phase modulation, stimulated Raman scattering, and plasma formation also contribute to considerable spectral broadening and white light generation by the laser pulse. On the other hand, the ultra-shortness of the laser pulse also needs to be taken into consideration. The physics governing the atmospheric propagation of short intense laser pulses can be very different from that of long laser pulses. For example, the Raman instability associated with the excitation of molecular rotational modes, which can disrupt the long-distance propagation of long, e.g., nanosecond (ns) pulses, may not be as disruptive for laser pulses that are shorter than the characteristic picosecond (ps) period of the rotational mode. The implication of this observation is that the

nonlinear refractive index of air could be a function of the laser pulse length. A 100-fs pulse could have an effective nonlinear refractive index several times smaller than that of a picosecond pulse. The inherently large spectral bandwidth of a short pulse also renders it more susceptible to dispersion effects in the atmosphere. Finally, the broad spectrum of the short laser pulse could affect the absorption characteristic of the laser in the atmosphere. In conventional narrow bandwidth, long-pulse lasers that are used in laser radar (LIDAR) applications, the laser line can be positioned between absorption lines to minimize attenuation in the atmosphere. However, the broad spectrum of a short pulse could be overlapping several individual absorption lines, and this could affect the thermal blooming process, which is a sensitive function of the absorption rate. These effects could be important for proposed shipboard FEL systems.

Perhaps the most prominent phenomenon observed when a high-power laser beam propagates in air is the formation of self-guided laser filaments. When no external focusing is provided, the wave nature of the light emitted from a laser will naturally diffract, and the laser beam size will continuously diverge and increase in size. However, the refractive index of air varies with the intensity of the laser in such a way that the higher intensity portion of a laser pulse encounters a higher value of the refractive index. Since the refractive index is a measure of the ratio of the speed of light in vacuum to that in the medium under consideration, a higher index of refraction signifies a slower speed of propagation for that portion of the laser pulse, and the laser pulse will converge (focus) onto this lower velocity portion. This has a very close analog to the propagation of light inside an optical fiber where the core of the fiber has a higher index of refraction. The higher intensity core portion of a laser pulse in air now also encounters a higher index of refraction. Therefore, it will be guided just like the light traveling down an optical fiber.

The condition for which such self-focusing can occur is governed by the initial laser power in the pulse. When the laser power reaches a threshold value, the nonlinear self-focusing effect can overcome the diffractive divergence of the laser beam, and an ideal laser beam will remain at a constant size forever. For air, the conventionally known value for this critical power is about 3 gigawatts (GW). If the laser power is above this critical value, the laser beam will converge instead, and theoretically it will continue to decrease in size until a catastrophic collapse is reached.

Fortunately, at high enough intensities, the air will break down and a plasma is formed. One of the optical properties of plasma is that it has a negative contribution to the index of refraction. Since more

plasma is formed where the laser intensity is high, the refractive index is less near the core of the laser beam. This is exactly the opposite of the nonlinear contribution to the refractive index before the ionization occurs. The two opposing effects can, in certain circumstances, balance each other and result in a long-lived, noncollapsing filament. More filaments can be formed if the laser power is many times higher than the critical power for self-focusing. These filaments can propagate extended distances, much longer than would be allowed if diffraction effect alone is considered. An example is shown in Fig. 3, where a 3.56 TW laser pulse from the 1.054- μm wavelength T^3 laser was propagated for 10 meters in the laboratory. Many tens of filaments are clearly visible. The initial laser beam size is 4 cm in diameter, and the individual filaments have diameters of about 200 μm . At this small size, the propagation distance for which the filament diameter will expand by 41.4% due to diffraction (known as the Rayleigh range) is only ~ 3 cm. The combined effects of nonlinear focusing and plasma formation have kept the filament from diverging for very much longer than was expected. Also, at the small-diameter size of these filaments, the laser intensity are in the range of 10^{13} to 10^{14} W/cm^2 . At such intensities, almost all solid or liquid media will break down and be damaged. The intense field can also generate secondary radiation that can disrupt the operation of many electronic devices. Therefore, these filaments are suitable for applications that involve sensor damage or electronic countermeasure processes.

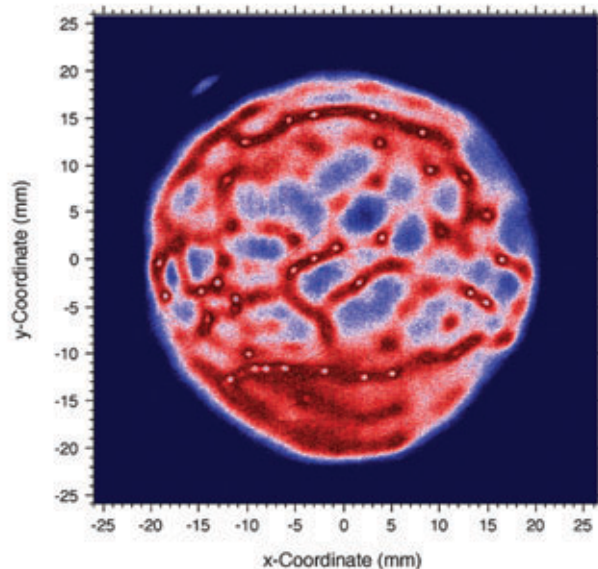


FIGURE 3 False-color image of self-guided filaments in a 3.56 TW laser pulse produced by the T^3 laser after propagating 10 meters in the laboratory. The beam diameter is 4 cm. The pattern of the filament distribution is correlated with the initially nonuniform transverse beam profile.

An interesting observation was that the initial power of the laser pulse was about a thousand times more than the critical self-focusing power. Theory predicts that 1,000 filaments could be formed. The comparatively low number of filaments brought out the question of whether the critical self-focusing power was correctly evaluated in the past. Since the critical power was calculated from the nonlinear refractive index of air, one begins to wonder about the correct value of the index for short, intense laser pulses. A literature search reveals that, indeed, the nonlinear refractive index of air had been measured primarily with optical methods that involved pulses much longer than a picosecond. However, there is strong experimental and theoretical evidence that the standard long pulse value for the nonlinear refractive index for air is not applicable to the self-focusing of femtosecond laser pulses.

An indirect way of obtaining the value of the nonlinear refractive index of air is to compare experimental results of filamentation with numerical results from theoretical models that include all the relevant physics. The NRL air propagation simulation code models atmospheric laser pulse propagation effects with a system of three-dimensional, nonlinear equations. These include diffraction, group velocity, and higher order dispersion, stimulated molecular Raman scattering, photoionization, nonlinear bound electron effects, ionization energy depletion, and propagation in a spatially varying atmosphere.² A coupled set of equations that was derived for the laser amplitude and electron density is used to analyze a number of physical processes, such as optical/plasma filamentation, pulse compression, nonlinear focusing, and white light generation. An experiment was performed using the T^3 laser to generate filaments with a known initial condition that could be simulated with the NRL air propagation code. A circular aperture was imposed on the initial laser beam to create a well-defined “top-hat” transverse profile suitable as an input to the simulation code. As the shaped laser beam propagates through the atmosphere, normal diffraction effects reshape the profile to a donut-looking form. Nonlinear effects enhance the fluctuations in the intensity around this donut shape and filaments are formed. At a distance of 10 m, four distinct filaments are formed, as shown on the left-hand side of Fig. 4. The experimental laser parameters of 400-fs pulse length and 108 GW peak power are imported into the simulation code, and the results are compared to the experiment. The nonlinear refractive index of air is varied in the simulation runs. It was found that in order to match the experimental result for the same number of filaments at the same distance, the simulation had to use a nonlinear refractive index 50% less than the

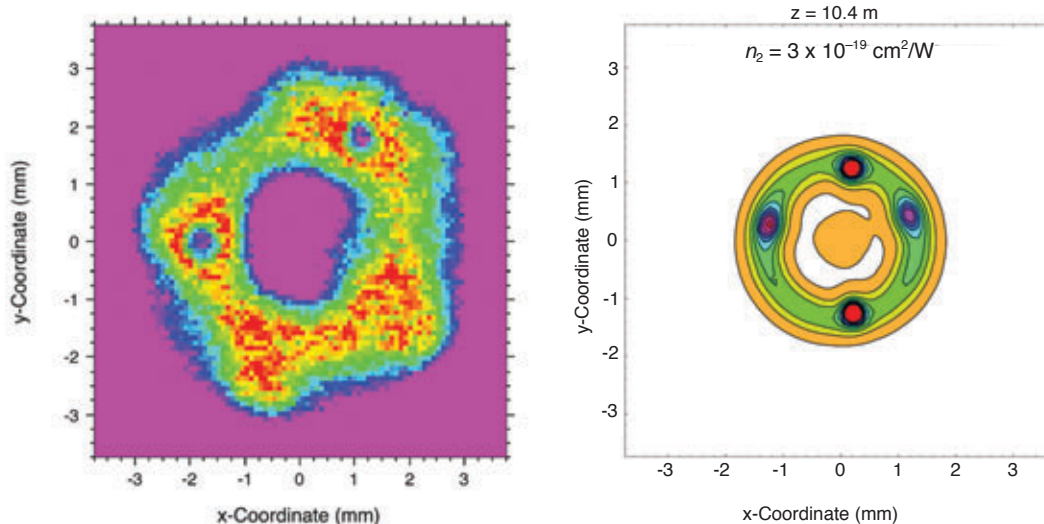


FIGURE 4
The formation of filaments from an apertured 400-fs laser beam with peak power of 108 GW at a distance of 10 meters. The experimental result is shown on the left, with the simulation result on the right. The value of the nonlinear refractive index used in the simulation to obtain the best match with the experiment is found to be 50% of standard value for long pulses.

conventional value. The simulation result is shown on the right-hand side of Fig. 4. This is the first quantitative experimental/numerical verification that the nonlinear refractive index of air has different values when ultra-short intense lasers are involved.

Another interesting phenomenon arising from the propagation of short intense laser pulses in air is the generation of broadband radiation, often referred to as “white light” or “supercontinuum.” This radiation is the result of the nonlinear self-phase modulation and ionization effects that are caused by the rapid variation in the index of refraction from the front to the back of the laser pulse. Nonlinear generation of optical frequencies outside the original laser linewidth can be as broad as 100%. Because the laser wavelength is in the infrared, the broadened spectrum can extend into the ultraviolet (UV) and far infrared. Figure 5 shows a portion of the spectrum of the radiation collected after the laser pulse from the 0.81- μm wavelength TFL laser has propagated for about 7 meters. It shows that radiation was produced in the UV, and many of the spectral features have been identified as those of the neutral or ionic species of the oxygen and nitrogen molecules. These features indicate that the molecules in the air where the laser has traversed can be excited, and it offers the potential application of these ultra-short pulse lasers for identification and detection of chemical and biological molecules from various airborne pollutants or compounds. Substantial spectral broadening is also routinely observed in simulations with the NRL air propagation code.

LASER-INDUCED ELECTRICAL BREAKDOWN

The presence of a plasma column in the filamentation of a femtosecond TW laser pulse in air offers another interesting application for ultra-short intense laser pulses. The plasma column is electrically conducting and can, therefore, support a current between two electrodes that are charged to sufficiently high voltages. Induced high-voltage breakdown has been studied using electron beams or high-power lasers as the trigger mechanism, but the power required is usually quite formidable and the discharge is often erratic. The breakdown is usually caused by an ionization front (streamer) initiated by the laser that progressively links the two electrodes until the circuit is completed for the final discharge. The path of the discharge and the time of discharge after the laser trigger are both quite random. The plasma columns associated with the filaments of a propagating ultra-short pulse could generate a conducting path that will lead to a deterministic discharge time and path for the breakdown. This realization is important to applications such as the arrest of lightning discharges where precise control of the lightning path is required. There are also other applications in which the discharge must be synchronized with other optical and electrical signals so knowledge of the precise discharge time after the laser trigger is crucial.

An experiment has been carried out using the 0.81- μm wavelength TFL laser at peak powers of ~ 100 to 400 GW to initiate electrical breakdown between

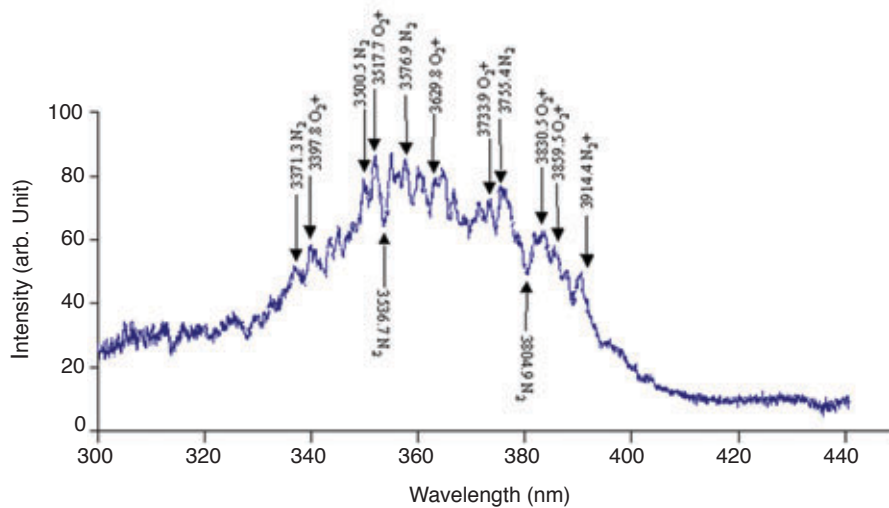


FIGURE 5 Broadband radiation spectrum in the UV region from a 100-fs, 300 GW laser pulse propagating for 7 meters in air. Spectral line structures are identified as electronic transitions of neutral and ionic molecular species in air.

two electrodes maintaining an average electric field of ~1.5 to 2 MV/m. The discharge was monitored with streak cameras that could record its time evolution beginning with the passage of the laser pulse between the two electrodes. Two classes of discharge were observed that would not be distinguishable if it were not for the streak camera catching the discharges in their actions. They are shown in the two pictures in Fig. 6. The pictures are essentially multiple exposures of a discharge, with each image slightly displaced vertically. Images near the bottom of the pictures happen earlier in time, and they move upward as time progresses. The ground electrode is on the left, and the negatively charged high-voltage electrode (cathode) is on the right side of the picture. The picture on

the left in Fig. 6 shows a streamer starting from the bottom left and moving from the ground electrode toward the cathode. Because the images are shifted upward as the streamer moves, it appears to be tracing out a parabolic trajectory but, in reality, it moves directly across the space between the electrodes. From the time scale indicated on the vertical axis of the picture, the speed of the streamer can be estimated to be close to 1% of the speed of light. The effort of this streamer apparently is not enough to cause a breakdown between the electrodes, and one can see that more streamers are involved at later times. Eventually the air between the electrodes breaks down, but at a time much later than could be displayed in this picture.

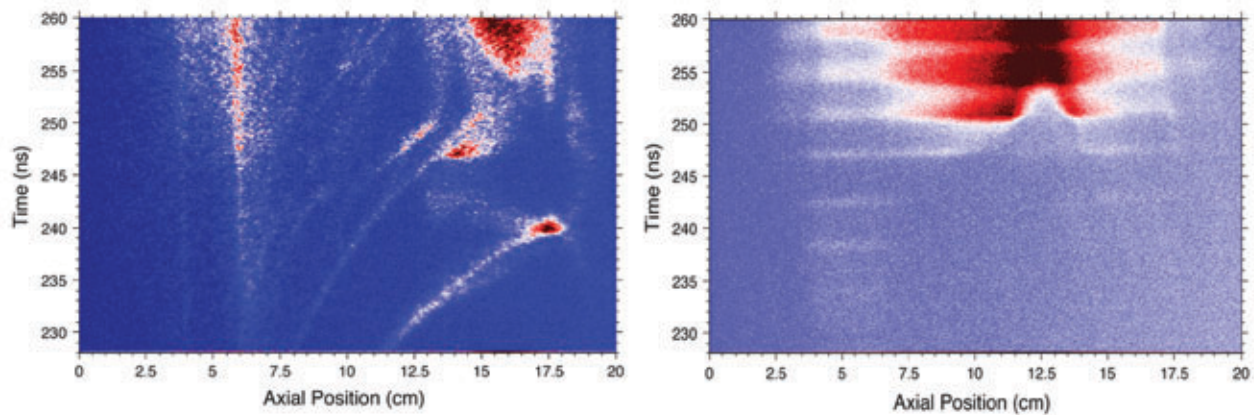


FIGURE 6 Streak camera images of laser-induced electrical discharges. The left-hand picture shows streamer initiated discharges with streamer velocity estimated to be ~1% of light speed. The right-hand picture shows a fully guided discharge occurring at ~255 ns after the laser trigger. The multiple discharges are the consequence of resonant electrical circuit oscillations.

The picture on the right in Fig. 6 shows a totally different behavior in time. There appears to be no indication of any presence of streamers. Instead, there are illuminated horizontal paths that repeat themselves at time intervals of ~ 5 ns as can be measured from the vertical scale. This indicates that a complete conducting path has been formed and a current is flowing between the two electrodes. Since the flow of current occurs at the speed of light, the images are essentially horizontal lines in this picture. The multiple lines represent an oscillation in the flow of current between the two electrodes, with a frequency governed by the circuit inductance and capacitance of the experimental setup. The lowest bright line has a gap in the middle, and it is an indication that the conducting path is not complete at the early stage of the discharge. The width of the gap shortens as time progresses. The speed of approach of the two ends of the gap is found to be around 1% of the speed of light. This is consistent with the motion of an ionization front under these experimental conditions, as seen in the left picture in Fig. 6.

The time delay between the laser and the triggering of the discharge for these fully guided discharges is consistently around 200 ns. This delay is much longer than the expected time for the plasma density to decay due to recombination. Simulations with an NRL air chemistry code that follows a large number of molecular, atomic, and ionic species support the following scenario to explain the long delay time. The applied electric field drives current through the laser-produced plasma filament and produces a sufficiently high electron temperature to maintain the plasma electron density. Eventually, the electron density rises rapidly due to collisional (avalanche) ionization. This leads to a rapid, uniform, fully guided breakdown across the gap. The time for breakdown to occur in the simulations varies with filament size and initial electron density and is consistent with the ~ 200 -ns delay observed in the experiment. This observation and its verification with simulation confirm the utility of an ultra-short intense laser to precisely triggered high-voltage electrical discharges.

CONCLUSIONS

Experimental, theoretical, and numerical studies have been performed on the propagation and interactions of ultra-short intense laser pulses in air. Filamentation of the laser pulse and the formation of plasma columns and the generation of broadband radiation in the UV region were observed. Through the benchmark process between experimental and numerical model calculations, we have gained valuable knowledge of the underlying principles such as the measurement of the nonlinear refractive index of air for fs TW laser pulses and the origin of fully guided and well-defined electric discharges triggered by these laser pulses. There are many applications including the detection of airborne pollutants or chemical/biological compounds and laser-triggered lightning arrests. Further understanding can be achieved with experimental and theoretical/numerical studies of fundamental physics such as the onset of various nonlinear processes as a function of the laser characteristics of the intense laser pulses.

ACKNOWLEDGMENTS

The authors thank Drs. Philip Girardi and Tim Andreadis of the Tactical Electronic Warfare Division, Drs. Andrew Baronavski and Harold Ladouceur of the Chemistry Division, Drs. Steven Slinker, Richard Fernsler, and Mr. Edgar McLean of the Plasma Physics Division, Dr. Christopher Moore of Space Systems Development Department, and Dr. Bahman Hafizi of Icarus, Inc., for useful discussions, and Mr. Eldridge Briscoe from RSI, Inc. for technical support.

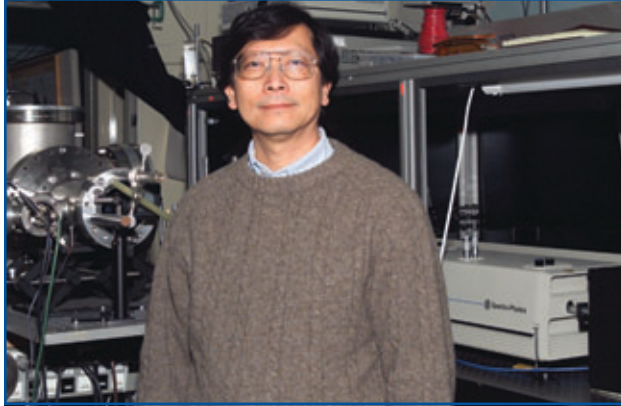
[Sponsored by ONR, JTO, NAVSEA, and U.S. Army SBCCOM]

References

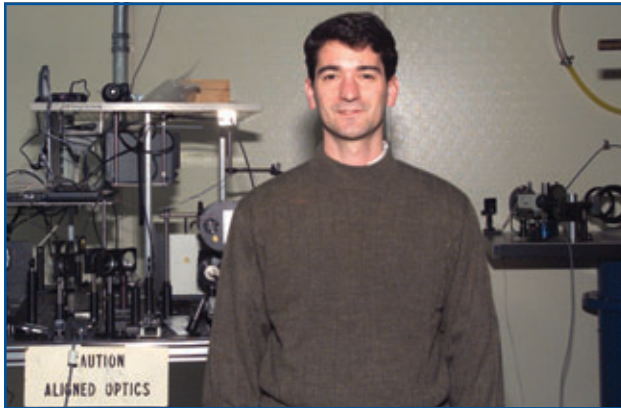
- ¹ A. Braun, G. Korn, X. Liu, D. Du, J. Squier, and G. Mourou, "Self-channeling of High-peak-power Femtosecond Laser Pulses in Air," *Opt. Lett.* **20**, 73–75 (1995).
- ² P. Sprangle, J.R. Penano, B. Hafizi, "Propagation of Intense Short Laser Pulses in the Atmosphere," *Phys. Rev. E* **66**, 046418 (2002).



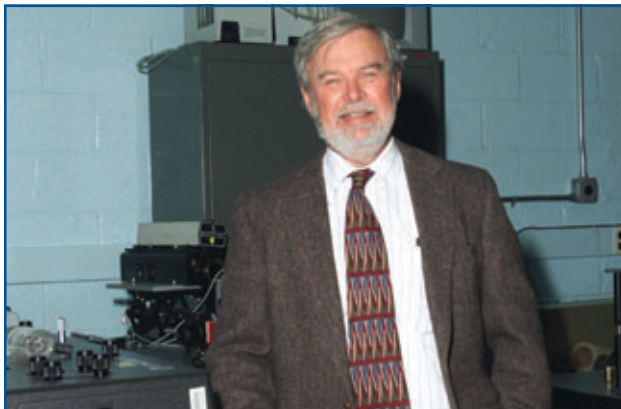
THE AUTHORS



ANTONIO C. TING received his Ph.D. degree in physics from the University of Maryland in 1984 and also holds B.S. and M.S. degrees in physics from the National Taiwan University. He is a senior research physicist in the Beam Physics Branch and is the experimental group leader of the High Field Physics Laboratory of the NRL Table Top Terawatt Lasers. He conducts research in intense ultra-short pulse laser interactions with air, plasmas, and electron beams including extended laser propagation in air for standoff detections and electronic countermeasures, advanced monochromatic X-ray sources and advanced laser-driven particle accelerators. He worked at NRL as a contractor in 1985 and later joined in 1988. Prior to that, he was a research associate at the College of William and Mary and at Dartmouth College. He is a Fellow of the American Physical Society and has twice won the Alan Berman publication award.



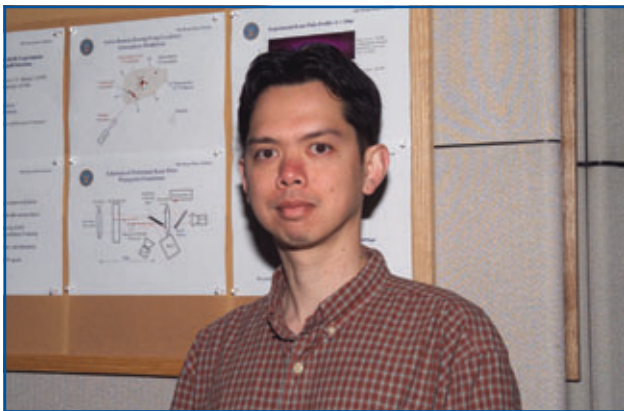
DANIEL F. GORDON received B.S. and Ph.D. degrees in electrical engineering from the University of California, Los Angeles in 1991 and 1999. He joined NRL as a research physicist in the Beam Physics Branch in 2002. He currently conducts research on the propagation of intense femtosecond laser pulses through the atmosphere, nonlinear laser-plasma interactions, plasma-based accelerators, and the dynamics of intense electron beams for advanced accelerator or free electron laser applications. He authored a large-scale parallel particle-in-cell code for simulating laser-plasma interactions, and maintains an active interest in numerical algorithms and high-performance computing. Prior to joining NRL, he conducted research at the Rutherford-Appleton Laboratories in the UK, held a National Research Council postdoctoral fellowship at NRL, and was employed most recently by Icarus Research, Inc.



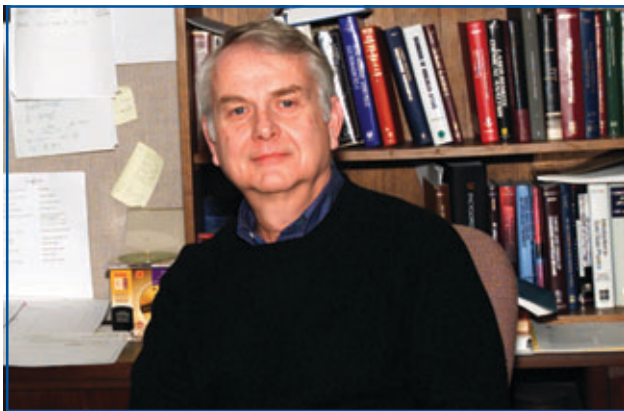
CHARLES K. MANKA received a B.A. degree in physics and mathematics from William Jewell College and M.S. and Ph.D. degrees in plasma physics from the University of Arkansas. He is Principal Research Scientist with Research Support Instruments (RSI) Inc., Lanham, Maryland, and supports research projects in the Beam Physics Branch at NRL. His areas of expertise include ultra-high-speed imaging and spectroscopy, laser-material interaction, shock phenomenon, and plasma diagnostics. He is a member of two professional societies, has more than 40 publications in refereed journals, and holds one U.S. patent. Prior to joining RSI, he was Professor and Chairman in the Department of Physics at Sam Houston State University and research physicist in the Plasma Physics Division, NRL.



RICHARD F. HUBBARD completed his Ph.D. in physics at the University of Iowa in 1975. He also holds M.S. and M.A. degrees in physics and business administration from that university and a B.A. degree from the University of Kansas. He joined NRL in 1985 and is currently a section head in the Beam Physics Branch. His work primarily involves numerical simulation of the propagation of intense pulsed beams through gases and plasmas and has included studies of laser, electron, ion, and microwave beams. His recent work has concentrated on femtosecond lasers, laser-driven accelerators, and novel radiation sources. Prior to joining NRL, he was employed by JAYCOR in Alexandria, Virginia, and held postdoctoral positions at the University of Maryland and NASA's Goddard Space Flight Center. He is a member of four major professional societies and is a four-time winner of NRL Alan Berman Publication Award.



JOSEPH R. PEÑANO received B.S. and Ph.D. degrees in physics from the University of California, Los Angeles in 1991 and 1998. He joined NRL as a research physicist in the Beam Physics Branch in 2001. His present research interests include laser-plasma interactions, laser-driven accelerators, nonlinear optics, radiation sources, and directed-energy countermeasures. His most recent publications have dealt with modulation instabilities in plasma channels, channel-guided laser wakefield accelerators, superluminal propagation of laser pulses, and atmospheric propagation of high-intensity ultra-short laser pulses. He is the chief developer of the NRL atmospheric laser propagation code. Prior to joining NRL, he was employed by LET Corp. He also held a National Research Council (NRC) postdoctoral fellowship at NRL working on modeling of space and ionospheric plasmas. He also received the 2002 Alan Berman publication award.



PHILLIP SPRANGLE received his Ph.D. in applied physics from Cornell University in 1973. He is Chief Scientist and Head of the Beam Physics Branch at NRL. His primary research areas include atmospheric laser propagation, free electron lasers, nonlinear optics, and laser acceleration physics. Dr. Sprangle is a fellow of the American Physical Society and the IEEE. He is winner of the International Free Electron Laser Prize (1991), E.O. Hulburt Science and Engineering Award (1986), Sigma Xi Pure Science Award (1994), as well as numerous publication awards. Dr. Sprangle has published more than 200 refereed scientific articles (28 letters), has presented more than 180 invited lectures, review talks, and keynote addresses at conferences and universities, and holds 12 U.S. invention patents.



SATELLITE SURVEILLANCE OF DESERT DUST STORMS

S.D. Miller

Marine Meteorology Division

The consensus of numerous Navy Meteorology/Oceanography (METOC) post-deployment reports from Operation Enduring Freedom (OEF) holds desert dust accountable for most common and significant adverse impacts to operations. Specifically, these storms impaired visibility, obscured targets, and rendered laser-guided weaponry ineffective. Satellite-based detection of dust is a difficult problem, due in part to observing-system limitations. An unprecedented interagency coordination in support of the War on Terror mitigated this problem by making available a global, near real-time dataset from the Moderate Resolution Imaging Spectroradiometer (MODIS). NRL designed a novel technique for enhancing dust over water and land, leveraging previous capabilities with these new high spectral/spatial resolution MODIS data.

INTRODUCTION

One does not have to dig deeply into the growing compilation of Operation Enduring Freedom (OEF) post-deployment Navy Meteorology/Oceanography (METOC) reports to find strong arguments for the need to better predict and observe dust storms. The following testimony from a METOC Officer supporting aircraft carrier operations in the Northern Arabian Sea (NAS) embodies this theme:

"While operating in the NAS in support of OEF, the primary METOC-related impact to operations was decreased visibility in northwest and southern Afghanistan . . . In one case, the extent of the suspended dust ranged well out into the NAS, with visibility less than one nautical mile."

Such difficult environmental conditions cause any number of undesirable mission outcomes, ranging from diverts/aborts to catastrophic mishaps with potential loss of life.

Long before the OEF-critical demand for improved METOC dust support arose, the general need was well established. Major Naval aviation accident statistics over a nine-year period (1990-1998)¹ find that slightly more than half (54%) of these were associated with visibility problems, representing annual losses of ~\$50 million per year. Moreover, over half (56%) of those visibility-related mishaps were considered avoidable, provided sufficient forecasting and observational tools. Not included in the study are the potential losses during times of conflict from wasted equipment

operations costs, jettisoned ordnance, and off-target laser-guided weaponry due to visibility-impaired conditions at or near the target.

Satellite-based dust detection over the desert terrains characterizing much of the OEF domain requires an observing system capable of extracting as much dust-specific information from the scene as possible. The current approach improves previous methods in this regard through the use of high spatial and spectral information available from the Moderate Resolution Imaging Spectroradiometer (MODIS), a state-of-the-art instrument flown aboard NASA's recently launched Earth Observing System (EOS) Terra and Aqua satellites. This paper begins with an overview of why dust detection is possible, followed by a brief description of MODIS and the algorithm designed to exploit the advantages of this sensor. Presented next are several examples illustrating dust storm enhancement capabilities, with additional applications to smoke and volcanic plume detection. The paper closes with a summary of ongoing efforts to provide this new resource to the warfighter during OEF and beyond.

PHYSICAL BASIS FOR DETECTION

The fundamental principles of dust detection are spatially, spectrally, and temporally based. The idiosyncrasies of dust within these paradigms are what allow for its decoupling from other components of the complex scene. We discuss some of these elements here, placed in the context of previous research done in this area.

Spatial Information

Moderate levels of dust over land cause visual blurring of otherwise sharply definable surface features. This so-called “adjacency effect” has proven useful in detecting dust,² although the method faces inherent challenges over laminar desert backgrounds where the propensity for contrast reduction is reduced. At visible (VIS) wavelengths, highly reflective dust contrasts against darker backgrounds such as vegetation or bodies of water. At infrared (IR) wavelengths, depressed brightness temperatures from elevated (and cooler) dust over hot surfaces yield similar contrast information. Reference 3 demonstrates enhancements based on these VIS/IR spatial contrast principles. Because the corresponding signatures of clouds are similar to dust, an implicit requirement for distinction is recognition of differences between the cloud and dust spatial structures. This inspection is not always straightforward, particularly in the case of thin cirrus clouds that spatially appear very similar to dust.

Spectral Information

An important spectral property allowing for dust detection in the IR is the “split-window” difference (e.g., Ref. 4). The signature arises from the higher spectral absorption of dust sensed at 11.0 micrometers (μm) compared to measurements at 12.0 μm . This spectral behavior contrasts liquid and ice clouds where the opposite absorptive properties hold. The split-window signature is less pronounced for thick dust very close to the surface, where transmission effects are smaller. Additionally, some land surfaces produce ambiguous signatures in the absence of dust.

Mineral dust becomes increasingly absorptive with decreasing VIS wavelength (i.e., progressing from red toward blue light), corresponding to a monotonic increase in the complex part of the imaginary index of refraction (n_i).⁵ These properties result in dust coloration, as illustrated conceptually in Fig. 1. Dust appears as shades of yellow/orange due to its preferential

absorption of blue light, whereas clouds (having small and relatively invariant n_i across the VIS) yield shades of gray to white depending on the strength of illumination. The reasoning behind why the color yellow is the outcome of preferential blue light absorption is explained in the context of red/green/blue composites further along. Exploiting the dust coloration properties for the purpose of enhancement requires a radiometer with spectral resolution sufficient to partition the VIS spectrum into the required components.

These principles have been applied⁶ to the Sea-viewing Wide Field-of-view Sensor (SeaWiFS), which features eight narrowband channels across the VIS spectrum. The technique uses a “normalized dust difference index” (NDDI) between the red (670 nanometer (nm)) and blue (443 nm) channels of SeaWiFS, defined such that dust produces large positive differences while clouds produce relatively smaller differences. Normalization ensures enhancement of weak dust signals over dark backgrounds. The method’s fundamental shortcoming is that land areas are also enhanced since their spectral properties at VIS wavelengths are similar to those of dust. Hence, it is a method limited almost exclusively to overwater applications.

Temporal Information

The ability to observe and track feature motion by looping consecutive satellite images is very useful for dust detection. For this reason, many applications consider only geostationary satellite imagery (typically having 30-minute refresh). Unfortunately, given current instrumentation limitations on the geostationary platform, the trade-off for this high temporal resolution is reduced spatial and spectral information. The featured work concentrates on the superior dust detection capabilities of low-Earth-orbit (LEO) high spatial/spectral resolution sensors, with multiple overpasses from various LEO satellites serving as a possible temporal surrogate.

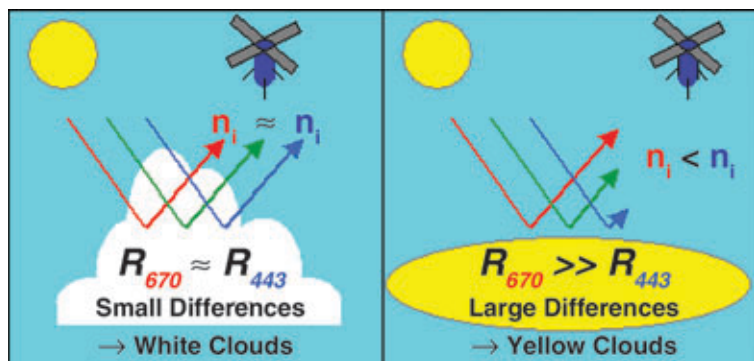


FIGURE 1

Simple conceptual illustration of how spectral differences between clouds and mineral dust translate to observed colorations.

THE MODIS OBSERVING SYSTEM

Instrument Description

MODIS instruments operating aboard the EOS Terra (1030 local equatorial crossing time; descending node) and Aqua (1330; ascending node) satellites offer a 2,330-km cross-track swath with 36 narrowband channels situated between 0.4 and 14.4 μm . All IR channels are available at 1-km subsatellite resolution, and a subset of VIS and near-IR channels exist at 500-m (channels 3-7) or 250-m resolutions (channels 1 and 2). Many of these channels open the door to innovative or entirely new atmospheric sensing applications, including improvements for dust detection.

Data Source and Timeliness

MODIS was never intended to function as an operational instrument – the War on Terrorism scripted this role. The National Oceanographic and Atmospheric Administration (NOAA) and the National Aeronautics and Space Administration (NASA) answered the Department of Defense's (DOD) call for assistance by making the global EOS Terra and Aqua data available in near real-time. Data arrive typically 1.5 to 3.5 hours after collection – timeliness sufficient for including value-added products within the METOC operational decision loops. The proof-of-concept demonstrated by this arrangement played a critical role not only in the immediate benefit to OEF, but also in the lobbying for procurement of sorely needed X-band direct broadcast receiving stations at the Navy Regional Centers in both Rota (Spain) and Bahrain.

THE NEW ENHANCEMENT

The new NRL dust enhancement combines elements of previous methods with the spatial/spectral advantages of MODIS to form a novel, unified product. Because of the very different restrictions between water and land backgrounds, two distinct algorithms operate on their respective backgrounds as determined by a land/sea database. Careful scaling minimizes discontinuities of enhanced dust crossing coastal (algorithmic) zones.

Understanding Color Composites

A prerequisite for understanding the appearance of the dust enhancement is a familiarity with the three-color composite technique. The concept is as follows: three primary colors (red, green, and blue)

form the axes of a “color cube.” In the example of an 8-bit computer display, brightness magnitudes for each primary color range from 0 (black) to 255 (full red, green, or blue saturation). This forms a cube of dimension $256 \times 256 \times 256$ elements whose indices map to a discrete representation of all possible colors, based on varying combinations of the primary color brightness values.

Figure 2 depicts the appearance of the outer surfaces of such a cube, showing how the primaries combine and transition across the three-dimensional color space. This provides a suitable framework for visualizing how the various components of VIS light combine to form all the colors we see. White light is the combination of full red/green/blue saturation, while yellow tonalities arise from high values of green and red with low amounts of blue. Extending this to the real-world example of dust illuminated by a source of white light (the Sun), the removal of blue light (via dust absorption) results in the preferential scattering of yellow light – explaining the observed color of dust.

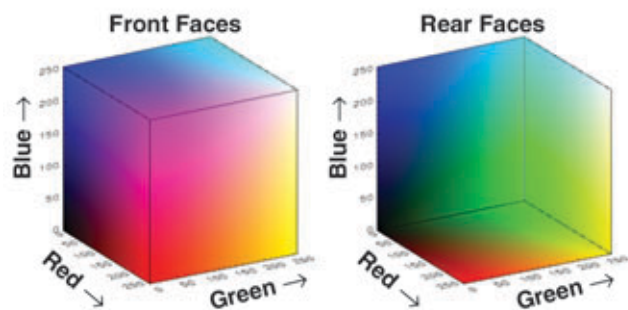


FIGURE 2 The outer surfaces of an 8-bit color cube applicable to three-color composite imagery techniques. Arrows denote directions of increasing primary color saturation.

Creation of a “true color” composite from satellite imagery requires sufficient spectral resolution to separate the red, green, and blue components of VIS light. After applying atmospheric corrections and appropriate scaling, these channels become the respective red, green, and blue indices (sometimes called “color guns”) of the color cube described in Fig. 2. The result is an image with an appearance similar to what we would observe with our own eyes. For the dust enhancement, a multispectral channel combination designed to enhance dust replaces the red gun of the true color product. The effect is for dust to possess relatively brighter red tonality throughout the enhanced imagery. The nondust components appear as red-depleted (e.g., cyan clouds, green land) and generally darker tones to focus attention toward the dust features of interest.

Channel Selection

The current algorithm uses 7 of the 36 available MODIS channels to exploit the spatial and spectral contrast features of dust. Listed in terms of [channel index; central wavelength; native spatial resolution; description] and in order of increasing wavelength, they are as follows: (3; 469 nm; 500 m; blue), (4; 555 nm; 500 m; green), (1; 645 nm; 250 m; red), (2; 853 nm; 250 m; reflective IR), (26; 1.38 μm ; 1 km; short-wave water vapor), (31; 11.0 μm ; 1 km; IR clean window), and (32, 12.0 μm ; 1 km; IR dirty window). The overwater algorithm uses MODIS channels 2, 3, and 4, and the overland algorithm enlists all seven channels listed above.

Overwater Component

The relative ease of dust detection over water (aside from conditions of shallow water or heavy alluvial/biological material suspension) using VIS spatial/spectral contrasts allows for use of a more aggressive method geared toward enhancing fine details of tenuous dust features. Accordingly, the overwater algorithm adopts the NDDI technique described previously.⁶ An important part of this processing is the molecular scatter correction applied to the VIS channels, based on radiative transfer simulations computed offline and stored in look-up tables. The correction reduces limb-brightening effects that would otherwise wash out the imagery on the swath edges.

Overland Component

Detection of dust over bright land backgrounds such as deserts is far more difficult than over water, and requires additional IR information to separate the dust signal from the other components of the scene. The premise for the overland enhancement is threefold: (i) elevated dust, having cooled to its environmental temperature, produces depressed IR brightness temperatures against the hot skin temperature of the land background; (ii) this cool layer of dust is distinguishable from a cloud with the same radiometric temperature using the NDDI technique; and (iii) split-window differencing reveals dust. In the three-color composite dust enhancement, the blue and green color guns contain information from the corresponding blue/green channels of MODIS, and the red gun contains a weighted combination of items (i) to (iii). Statistical composites from many dust storm cases provided the optimal scaling and weighting coefficients. The short-wave water vapor channel (1.38 μm) provides filtering of cirrus clouds whose cold IR temperatures sometimes cause ambiguity.

LIMITATIONS OF ALGORITHM

The daytime-only MODIS dust enhancement is not without its own assortment of interpretive caveats. The overwater component has the undesirable effect of enhancing the region of Sun glint (near-specular reflection of the solar disk off water surfaces) as dust. The current product flags a glint zone based on a prescribed minimum glint angle. High concentrations of sediments suspended in water (e.g., associated with river runoff) occasionally also give rise to false dust enhancements.

Over land, cold surfaces may appear falsely enhanced due to the similar VIS/IR properties of thick dust. The overland algorithm includes a terrain elevation database to filter out a subset of these effects. Depending on surface temperature, an optically thick layer of dust (producing small split-window differences and IR contrast signatures) near the ground may go undetected, a characteristic observed most commonly near strong point-sources of dust. The scaling thresholds and weighting coefficients of the IR enhancement components require seasonal tuning, mainly to reduce false enhancements emerging during the cold winter months.

Because of increased optical paths at higher sensor zenith angles, dust on the edge of the satellite swath exhibits a stronger (brighter) enhancement than the same dust observed near satellite nadir. While brighter pink tonalities do correspond to higher dust opacity over local regions (e.g., of several hundred km), the current product does not quantify this opacity in terms of optical depth, particle size, slant range visibility, or laser attenuation. It is a qualitative dust identifier and a first logical step toward physical retrievals on the subset of pixels thought to be dust. With these limitations in mind, we proceed to highlight the strengths of the enhancement through a series of examples.

DUST ENHANCEMENT EXAMPLES

EgyptAir Accident

On May 7, 2002, an EgyptAir passenger aircraft crashed into a hillside during an emergency landing attempt near Tunis, Tunisia, killing 18 of the 60 people onboard. Local weather at the time of the accident included fog, rain, and blowing sand from the Saharan Desert interior. NRL dust products supported the National Transportation Safety Board during its investigation of this accident.

Near the time of the crash, Terra MODIS collected the imagery shown in Fig. 3. The true color product (left panel) shows the city of Tunis obscured by a squall line. A veil of dust fans into the Mediterranean

Sea, carried northward by strong southerly winds associated with the advancing storm system. Subtle adjacency effects indicate additional inland dust westward of the squall line. The corresponding enhancement (right panel) reveals considerable inland dust throughout the cloud-free regions of the storm. Dust areas appear as shades of pink, clouds are cyan, and land areas free of overlying dust are green. Since the enhancement cannot detect dust obscured by cloud (although dust-over-cloud generally is detectable), only the inference of its presence near the Tunis crash site was possible, based on its observance on either side of the squall line.

False Dust Fronts

Among the many caveats to dust imagery analysis are sudden transitions in vegetation regimes that sometimes masquerade as false dust fronts. The Indus River valley of Pakistan features many such “desert-meets-oasis” discontinuities. The true color image of Fig. 4 notes two possible dust fronts in advance of a storm system crossing central Pakistan. The dust enhancement reveals that front A (yellow dotted line) is in fact a vegetation boundary, while front B (red dotted line) is a true dust front. Also evident in the enhancement are additional fronts not obvious in the true color imagery.

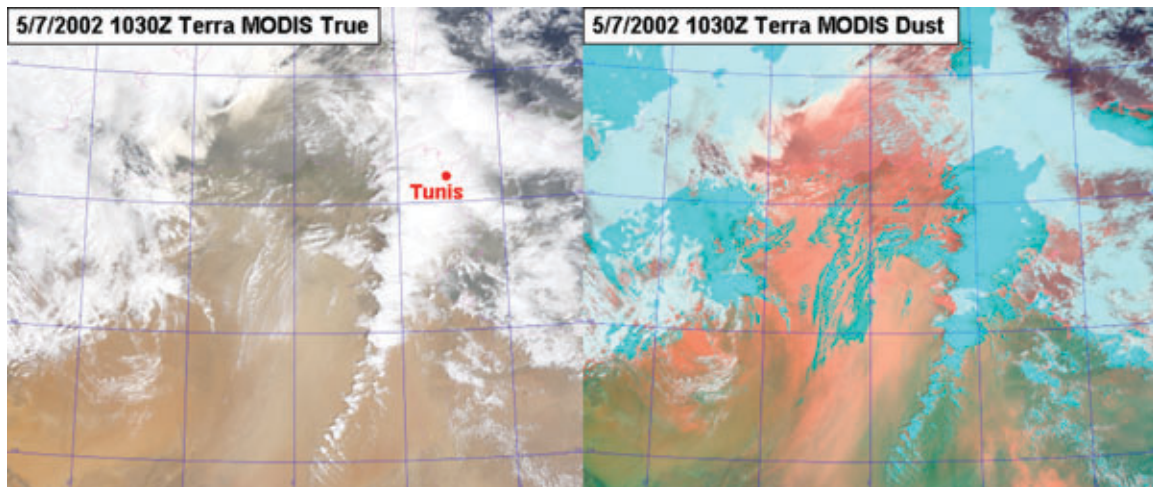


FIGURE 3
Tunisian dust storm captured by MODIS, thought to be a visibility-reducing factor in the crash of a Boeing 737 commercial aircraft.

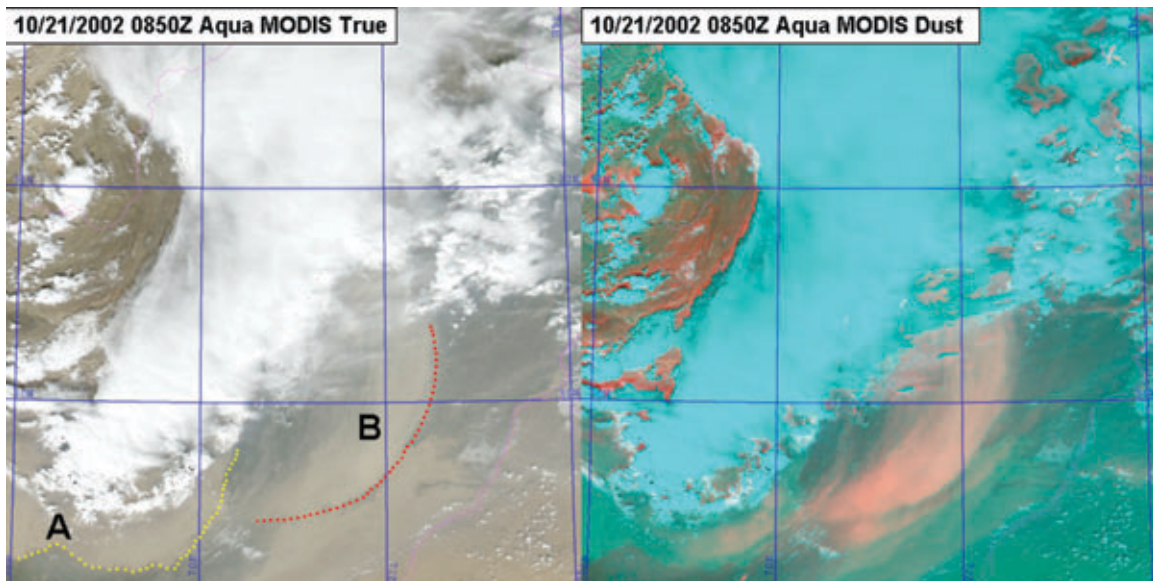


FIGURE 4
Dust in advance of a baroclinic system over central Pakistan, highlighting the enhancement’s ability to distinguish between surface features and actual dust fronts.

Thin Dust Over Bright Land

Figure 5 highlights another OEF-domain application of the dust product. Strong northerly winds in the wake of a passing storm system carry dust from the deserts and dry lakebeds of eastern Iran, southern Afghanistan, and Pakistan. Winds channeled through coastal valleys spawn numerous dense dust plumes, clearly visible in the imagery as they stream into the NAS. The corresponding dust enhancement shows several additional plumes over land, previously washed out by the bright topography. The solid, sharply defined pink object near the inland plumes is a dry lakebed, enhanced for reasons explained later.

ADDITIONAL APPLICATIONS

Analysis of Dust Source Regions

Knowledge of the likely source regions for dust under certain environmental forcing conditions is critical to improving dust-forecasting models. Strong northerly winds channeled into the Margow Desert basin of southwestern Afghanistan produce the recurring dust pattern observed in Fig. 6. Several plumes originate from dry lakebeds noted in the imagery. With high concentrations of fine (and easily lifted) silt deposits, these areas often serve as point sources for dust. The lakebeds are enhanced in the

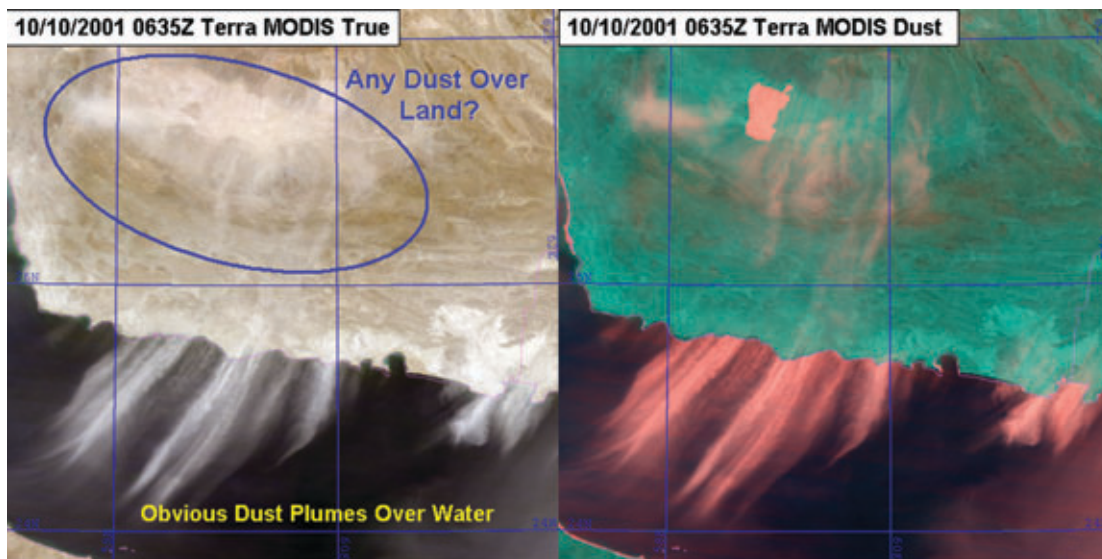


FIGURE 5

Thin dust over land during a strong dust outbreak that affected Naval operations during the preliminary stages of OEF.

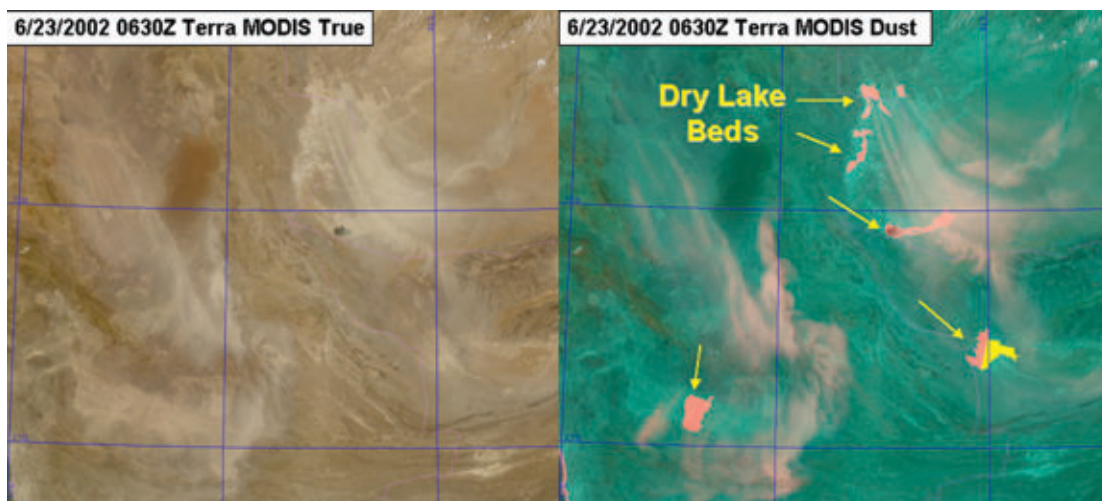


FIGURE 6

Dry lakebeds serve as point sources for dust during a summertime outbreak across the deserts of southern Afghanistan and eastern Iran.

dust product by applying the overwater (NDDI) algorithm to the dry land pixels.

Volcanic Ash Plume Detection

Volcanic aerosol poses an underemphasized and poorly understood hazard to turbine engine-powered aircraft. The danger lies in the very small glass-like particles constituting volcanic ash, which melt readily as they come into contact with certain parts of the hot engine interior. Subsequently they resolidify, clogging air intakes and damaging turbine blades to the point of engine failure. Commercial airline pilot accounts from near-tragic encounters with volcanic ash (steep-dive recoveries from complete engine stalls) noted difficulties in visually discerning the ash haze from the benign cirrus clouds commonly encountered at those same flight levels.

The same physics that allow mineral dust detection in the current product applies to some varieties of volcanic ash plumes. The recent eruptions of Mt. Etna, on the island of Sicily, provided a glimpse into these capabilities. Figure 7 illustrates the detailed structure of Etna's plume as upper-level winds carry it southward across the Mediterranean Sea. The level of detail, combined with the high sensitivity of the NDDI to low concentrations, suggests some utility for the dust enhancement in this regard.

Oil Fire Detection

During the Gulf War, Iraqi troops set fire to numerous oil wells in Kuwait. Pitch-black smoke issuing from these fires cloaked the Arabian Gulf skies, impacting Naval flight operations. The difficulty in satellite monitoring of such plumes over dark (low VIS contrast) water backgrounds warrants examination of the dust enhancement's utility in this capacity. An opportune MODIS overpass captured a small and short-lived plume emerging from an oil fire in southern Kuwait. Pending a detailed analysis, the preliminary results shown in Figure 8 indicate that properties of these plumes are conducive to their enhancement over both land and water under the existing method.

SERVING THE WARFIGHTER

The MODIS dust products are of little use to operations without the proper delivery vehicle in place. In a parallel effort, NRL developed the "Satellite Focus" web page (see "A 'Satellite Focus' for the War on Terrorism," p. 103), designed specifically for hosting satellite imagery in a new and comprehensive way. Cooperation with Fleet Numerical Meteorology and Oceanography Center (FNMOC) made possible the rapid transition of these new products via Secure Internet – the network used by bandwidth-limited

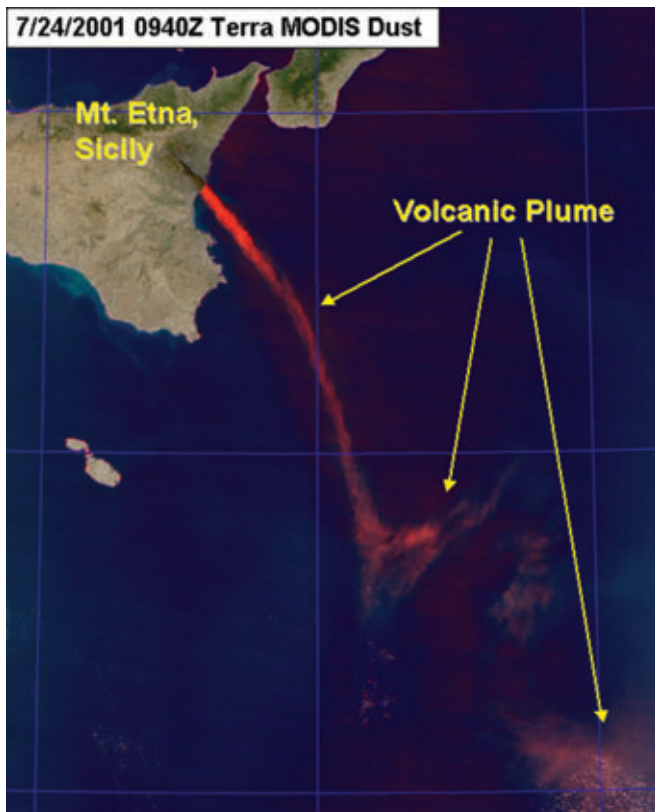


FIGURE 7
Enhanced volcanic ash plume from Mt. Etna streams southward, carrying potentially hazardous implications to any unwary aviators in its path.

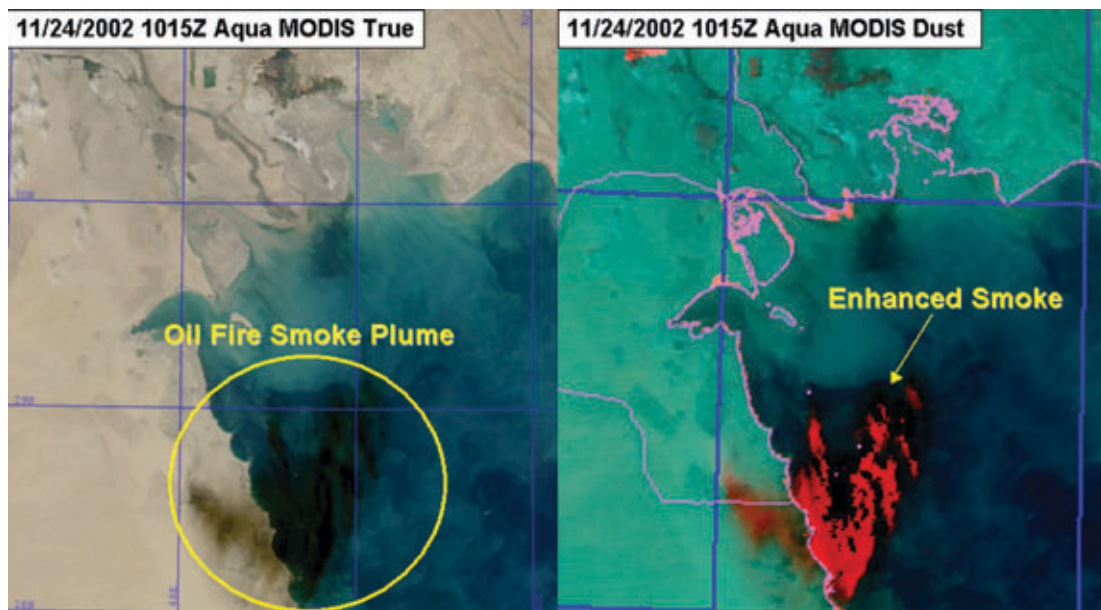


FIGURE 8
Black smoke plume from an oil fire over southern Kuwait suggests an additional potential application of the MODIS dust enhancement.

Navy assets worldwide. Fully automated imagery processing software linked with this dynamic web interface achieves rapid turnaround (on the order of minutes) of near real-time satellite products. Positive and constructive feedback received from a growing base of DOD and coalition users propels the ongoing development of this new resource and refinement of satellite products to better suit warfighter needs.

SUMMARY AND CONCLUSIONS

A satellite technique for identifying dust over water and land using improved spatial and spectral resolution data from MODIS has been designed. The dust enhancement is one of many new and innovative satellite products supporting forecast and strike briefs during OEF. Future refinements include dynamic treatment of the sun glint zone based on surface wind field analysis, overlay of frictional surface wind fields, and creation of a quantitative dust mask. Additional IR channels from MODIS are being explored in the development of a companion nighttime dust enhancement.

Among the many lessons learned in the wake of September 11, perhaps the one bearing most relevance to the DOD research community is the need for a more proactive and forward-focused mindset in terms of both product design and accelerated transition. We must ensure that research topics are based on “need driving technology” principles, and that the fruits of our efforts extend beyond the annals of literature to

reach and truly impact the end users situated at the “pointy end of the spear.” NRL embraces this new philosophy, and continues to push the envelope of satellite remote sensing technology to benefit those who willingly put themselves in harm’s way to protect our freedom.

ACKNOWLEDGMENTS

The ongoing efforts of NOAA/NASA colleagues (Jim O’Neal, Joy Henegar, Paul Haggerty, et al.) in support of near real-time MODIS data are gratefully acknowledged.

[Sponsored by ONR and SPAWAR]

References

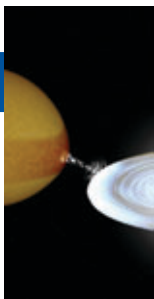
- ¹ R. Cantu, “The Role of Weather in Major Naval Aviation Mishaps FY90-98,” M.S. thesis, Naval Postgraduate School, Monterey, CA., 2002.
- ² D. Tanré and M. Legrand, “On the Satellite Retrieval of Saharan Dust Optical Thickness Over Land: Two Different Approaches,” *J. Geophys. Res.* **96**, 5221-5227 (1991).
- ³ W.E. Shenk and R.J. Curran, “The Detection of Dust Storms Over Land and Water with Satellite Visible and Infrared Measurements,” *Mon. Weather Rev.* **102**, 830-837 (1974).
- ⁴ S.A. Ackerman, “Remote Sensing Aerosols Using Satellite Infrared Observations,” *J. Geophys. Res.* **102**, 17,069-17,079 (1997).
- ⁵ E.M. Patterson, D.A. Gillette, and B.H. Stockton, “Complex Index of Refraction Between 300 and 700 nm for Saharan Aerosols,” *J. Geophys. Res.* **82**, 3153-3160 (1977).
- ⁶ S.D. Miller, “SeaWiFS True Color, Vegetation, and Dust Enhancement Processing at NRL Monterey,” NRL FR/7540/02-0002, March 2002.



THE AUTHOR



STEVEN D. MILLER earned his B.S. degree in electrical and computer engineering from the University of California at San Diego in 1995, and his M.S. and Ph.D. degrees from Colorado State University in 1997 and 2000, respectively, in atmospheric science with an emphasis on radiative transfer theory and remote sensing. He joined the Satellite Meteorological Applications Section of the Naval Research Laboratory's Marine Meteorology Division in 2000, where he has worked to develop new multisensor techniques for the sensing of clouds and dust. His current interests include general satellite meteorology with an emphasis on cloud radiative processes, microphysics, and remote sensing methods. He contributed to the design and execution of the NRL Satellite Focus Web Page, and heads a research work unit to examine key parameters of clouds and precipitation from next-generation passive/active environmental satellite instruments.



TIMING STUDIES OF X-RAY BINARY ORBITS

P.S. Ray, M.T. Wolff, and K.S. Wood
E.O. Hulburt Center for Space Research

P. Hertz
NASA Headquarters

X-ray astronomy, by necessity, involves the study of highly variable stars, nearly all of them in binary systems where one member is a compact object such as a neutron star or black hole. These systems allow us to probe physical effects in regions of extreme gravity, high temperatures, and intense magnetic fields that are characteristic of compact objects and are unattainable in laboratory experiments. By studying the brightness variations and eclipses using space-based X-ray telescopes, we can determine the binary system orbital parameters and characteristics of the mass transfer that powers these variations. This, in turn, allows us ultimately to understand better the evolution of these exotic binary systems. Here we describe two such studies carried out at NRL: the discovery of the orbit of a neutron star orbiting a hot supergiant star, and the surprising orbital period evolution observed in a low-mass X-ray binary.

INTRODUCTION

The night sky viewed with your eyes is a peaceful place, with thousands of point-like stars shining at the same brightness night after night, year after year. Each star is powered by nuclear reactions at its core. These keep the surface hot for millions or billions of years, with nearly all of the energy being emitted at visible wavelengths. Viewing the sky in X-rays is a completely different experience. Nearly all X-ray sources are highly variable, changing brightness and color by large amounts on timescales ranging from milliseconds to millennia. The fundamental reason for this dramatic behavior is that the power source of these celestial X-ray sources is the accretion of matter onto a compact object (a white dwarf, neutron star, or black hole). The compact object in an X-ray binary *in isolation* would emit very little radiation because it has no internal source of heat and, in the case of a black hole, doesn't even have a surface from which to emit! However, if the object is in a binary system with a more normal star it can accrete matter captured either from the stellar wind of the companion or from matter overflowing the equipotential surface called the Roche lobe (Fig. 1). This material typically has a relatively large angular momentum and thus forms an accretion disk around the compact object as it loses energy via viscosity. As this matter falls into the deep potential well of the compact object, it releases an enormous

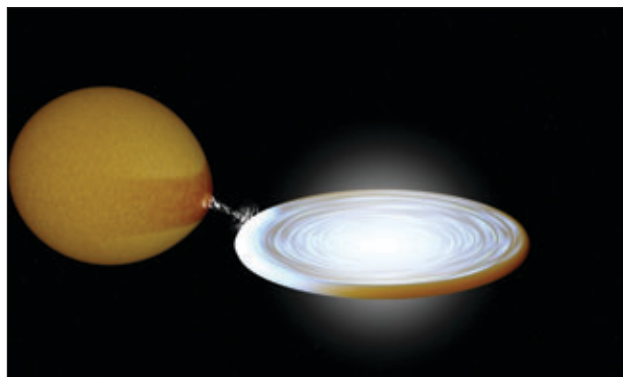


FIGURE 1
Artist's conception of an X-ray binary system. The large star is dumping matter into the accretion disk, and that matter is spiraling inward toward the compact object and heating up. In the central regions of the disk, the temperatures are millions of degrees and the orbital timescales are milliseconds. The thin fuzz above the disk represents an optically thin corona of very hot plasma, which can radiate high-energy X-rays and gamma-rays via the inverse-Compton process. (Illustration created with the binary visualization tool BinSim 0.8 by R. Hynes.)

amount of energy and is heated to extreme temperatures ($\sim 10^7$ K) where X-rays are the dominant radiation emitted.

These X-ray binary systems make wonderful laboratories for studying the physics of matter in extreme conditions and for understanding complex stellar and binary evolution. They also have several

potential applications of relevance to the Navy. These systems exhibit numerous properties that are of great interest and are difficult or impossible to recreate in a laboratory, including magnetic field strengths of up to 10^{14} gauss, matter at super-nuclear densities, rotational periods as short as 1.5 ms, strong gravity effects predicted by Einstein's general theory of relativity, magneto-hydrodynamic effects, relativistic jet acceleration, and more. However, since X-rays cannot penetrate the Earth's atmosphere, we must study them from instruments flown on rockets or satellites.

NRL was among the early pioneers of X-ray astronomy, beginning with Dr. Herbert Friedman's experiments flown on V-2 rockets captured during World War II. NRL has been highly active in the field ever since, flying numerous sounding rockets and serving as principal investigator institution for several satellite instruments, including HEAO A-1, Spartan 1, and the USA Experiment. The Navy initially contributed to the exploration of the X-ray sky to understand natural backgrounds relevant to any possible DOD systems operating in space. As understanding of these unusual celestial sources improved, their value as physics laboratories was appreciated. They can be used, for example, to test hydrodynamics codes in regimes of high temperature, density, and magnetic field strength well beyond laboratory conditions. By now, other kinds of applications are under study, such as the use of celestial X-ray sources to support autonomous satellite operations and navigation in what amounts to a passive GPS-like system.

X-ray binaries are typically classified by the type of compact object they contain and the mass of the companion star. Compact objects are the final stage in the lifecycle of stars. When their nuclear fuel is exhausted, the core of a star collapses until it is supported by some pressure force. Stars similar to our Sun collapse into *white dwarfs* that compress the mass of the Sun into an object the size of the Earth and are supported by electron degeneracy pressure. This pressure is the result of the fact that electrons are fermions and are thus subject to the Pauli Exclusion Principle, which prevents more than two fermions from occupying the same volume. More massive stars can overcome this pressure and collapse into neutron stars that reach densities far above those found in an atomic nucleus and are supported by neutron degeneracy pressure. Neutron stars have a mass of 1.4 times the mass of our Sun and a radius of only 10 km! The collapse of the most massive stars cannot even be stopped by neutron degeneracy pressure and thus they continue collapsing all the way to a *black hole*, an object so compact and massive that even light cannot escape. When one of these stars is orbiting a massive normal star (often about 10 times the mass of our

Sun), the system is referred to as a High-Mass X-ray Binary (HMXB). When the companion is a low-mass star (typically a fraction of the mass of our Sun), the system is called a Low-Mass X-ray Binary (LMXB). The two types of systems are the result of different paths of stellar evolution and, in general, the HMXB systems tend to be younger and contain slowly spinning, highly magnetized neutron stars, while the LMXBs are extremely old and are the progenitors of the millisecond radio pulsars.

The two instruments used in the work described here are NASA's Rossi X-ray Timing Explorer (RXTE) and the Unconventional Stellar Aspect (USA) Experiment. RXTE was launched in December 1995 and carries three instruments, the primary being the Proportional Counter Array (PCA), an array of five xenon proportional counters sensitive to X-rays in the 2 to 60 keV energy range. The USA Experiment aboard the Advanced Research and Global Observation Satellite (ARGOS) was launched in February 1999 and operated until November 2000. USA was built by NRL in collaboration with Stanford University for the dual purposes of doing X-ray astrophysics and exploring several applications of Navy interest. USA consisted of two argon/methane proportional counters sensitive to X-rays in the 1 to 15 keV energy range. During its operating lifetime, USA acquired substantial observing time on about 60 bright X-ray sources, including transient black hole systems, X-ray pulsars, active galactic nuclei, and a variety of bright LMXBs. USA was also designed to conduct experiments in the application of X-ray sources to satellite autonomy, as described above.

In this article, we review two projects whose results were published this year. First, we describe the discovery of the orbit of an accreting pulsar with a supergiant companion, and then we describe the detailed study of the orbital evolution of a nonpulsing neutron star that is eclipsed by its companion.

DISCOVERY OF THE ORBIT OF A SUPERGIANT X-RAY BINARY

Accreting X-ray pulsars are X-ray binary systems (most often high-mass X-ray binaries) where the compact object is a highly magnetized neutron star. The surface magnetic field can be 10^{12} G or higher (for comparison, the magnetic field at the surface of the Earth is about 0.5 G). This strong magnetic field channels the accretion flow inside of a radius where the magnetic pressure overwhelms the ram pressure of the flow (called the Alfvén radius). This channeled flow accretes in columns onto the neutron star surface at the polar caps. As these hot polar cap regions rotate with the spin of the neutron star (assuming that the

magnetic axis is not perfectly aligned with the rotational axis), we view them with periodically varying geometry. This causes the observed X-ray flux to be modulated at the spin period. These pulsations allow us to determine the spin rate of the neutron star to very high precision. This, in turn, allows precise determinations of the torque exerted on the neutron star by the accreting matter. It allows determination of the orbital parameters because of the Doppler shift of the pulse frequency as the pulsar travels in its orbit. In this section, we describe how a study of the X-ray pulsations in one particular system resulted in the discovery of the orbit of that system. This work was done in collaboration with Prof. Deepto Chakrabarty of the Massachusetts Institute of Technology.¹

It is a remarkable coincidence that there are two unrelated X-ray pulsars in Centaurus with nearly identical spin periods separated by only 15 arcminutes on the sky. One of the sources is the 292-s transient X-ray pulsar 2S1145–619, which is associated with the main sequence Be-type companion Hen 715 and is about 5,000 light-years distant. The pulsar exhibits periodic outbursts at 186.5 d intervals, which are believed to occur during periastron passage in the neutron star's eccentric orbit. The X-ray flux in quiescence is typically about 3 mcrab, but the flares near periastron can reach a flux of several hundred mcrab. (A millicrab (mcrab) is a commonly used unit of X-ray flux equal to 1/1000th of the flux of the Crab Nebula, the brightest steady X-ray source in the sky.)

The second source, which is the subject of this study, is a 297-s X-ray pulsar designated 1E1145.1–6141 that is associated with a B-type supergiant companion (V830 Centaurus). Until our study, this source had a rather sparse observational history and an unknown orbital period, despite being a persistent X-ray pulsar and one of only 10 X-ray pulsars with massive supergiant companions. Studies of the companion star with ground-based optical telescopes suggested orbital periods ranging from 5.6 to 12.1 days, but these studies had not produced a definitive result. A binary period of at least 6 days is required for the neutron star's orbit to be outside the surface of the companion star so a measurement of the orbital parameters of the system was of considerable interest. In addition, a supergiant-neutron star binary with an orbital period less than 20 days has a significant a priori probability of exhibiting an X-ray eclipse. Eclipsing pulsars provide important constraints on the masses of accreting neutron stars, and only eight such systems are currently known. Thus motivated, we observed 1E1145.1–6141 with RXTE in an effort to determine the pulsar's orbital period and search for X-ray eclipses.

Observations

We observed the 1E1145.1–6141 system 80 times at four different epochs between June 1997 and February 2000 using the Proportional Counter Array (PCA) on RXTE. The PCA collects X-ray photons in the 2 to 60 keV range and records the arrival time (1- μ s resolution) and energy (129-channel resolution) of every detected photon. Because the PCA has a 1° field of view and no imaging capability, each of the observations was scheduled to occur far from periastron passages of the 2S1145–619 system so that its flares would not contaminate the measurement. It is important to note that nonimaging observations can only resolve the coherent pulsations of 1E1145.1–6141 (297 seconds) and 2S1145–619 (292 seconds) into separate Fourier bins for observation lengths greater than 20,000 s. A few of our observations were this long and we were able to determine that when 2S1145–619 was not flaring, it did not interfere significantly with observations of 1E1145.1–6141.

Timing Analysis

To measure the pulse period of 1E1145.1–6141 precisely and search for delays caused by the pulsar moving in its orbit, we performed a pulse time-of-arrival (TOA) analysis. For each short observation, we selected all of the photons in the 2 to 10 keV energy range, converted them to an inertial reference frame at the solar system center of mass (this process, known as barycentering, removes the effects of the motion of the spacecraft and the Earth from the data), and folded them into an average pulse profile by calculating their phase with respect to a nominal pulse period of 296.65 s. Figure 2 shows a typical pulse profile. From each profile, a TOA is measured by cross-correlation with a high signal-to-noise template profile that defines phase zero.

If a pulsar is pulsing at a constant period and not moving in an orbit, each pulse will arrive an integer number of pulse periods after the first. So, to search for effects of an orbit, we compare the measured arrival times to a simple model with a constant pulse period at each epoch: $T_n = T_0 + P \times n$, where T_n is the arrival time (TOA) of the n th pulse and P is the pulsar period. Figure 3 shows the results of this comparison for each of the four observing epochs. Astronomical times are often reported using the Julian Day (JD) system, which measures days since noon on January 1, 4713 BC. Modified Julian Day (MJD) is defined as $JD - 2,400,000.5$, which shortens dates near the present to five digits and subtracts an extra half day so that the day begins at midnight as it does in civil time. As an example, MJD 51544 is January 1, 2000.)

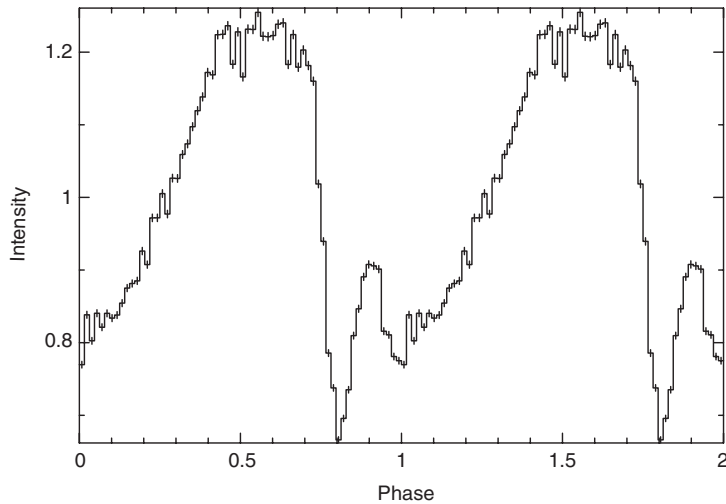


FIGURE 2

A folded light curve (pulse profile) of 1E1145.1–6141 with 64 bins across the 296.65-s period. For clarity, two cycles are shown. The intensity is the 2–10 keV X-ray flux relative to the average flux, indicating that about 20% of the emission is pulsed.

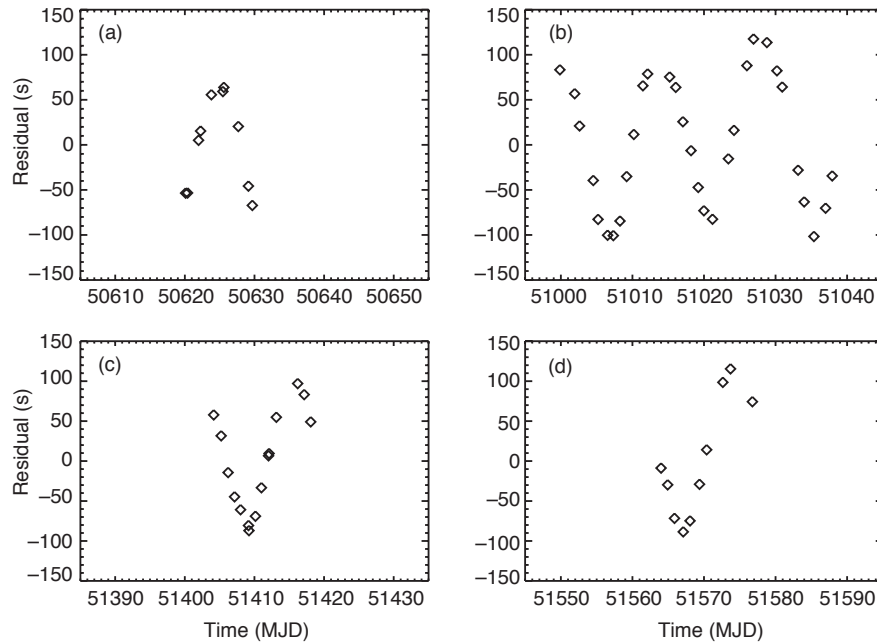


FIGURE 3

Pulse arrival time residuals from a constant-period model for each of the four observation epochs of 1E1145.1–6141.

Clearly, orbital effects are present. A roughly sinusoidal pattern is seen in each set of residuals, with a period of about 14 days. In such a plot, the pulses arrive late when the pulsar is behind its companion (farther from the Earth) and early when the pulsar is in front of its companion. The total observed delay immediately reveals that the projection of the orbit in the direction of Earth has a radius of about 100 light-seconds. This is about one fifth the size Earth’s orbit around the Sun.

A much more precise determination of the orbital parameters is possible by fitting a timing model that includes a Keplerian orbit in addition to the spin of the pulsar. We first determined the orbital period by

using the measured minima in the arrival time residuals in Fig. 3. Assuming a constant orbital period P_{orb} , these five minima must be separated by integer multiples of P_{orb} . The best-fit orbital period determined in this way is $P_{orb} = 14.37 \pm 0.02$ days.

To derive the remaining binary parameters and refine the orbital period determination, the effects of the binary motion must be decoupled from intrinsic changes in the pulsar’s spin due to accretion torques. We performed a combined fit of all the arrival time measurements shown in Fig. 3. Because of the effect of accretion torque during the time between observations, we could not produce a fully phase-connected orbital fit. Instead, we used a model in which the

frequency and phase of the pulsar were allowed to jump discontinuously between each epoch of observation and the orbital parameters applied globally. Other than the orbital effects, the pulse frequency was held constant within each epoch.

Table 1 lists our best-fit orbital parameters, and Fig. 4 shows the resulting model with all data folded at the orbital period. The five parameters in Table 1 are the standard Keplerian orbital parameters for an eccentric binary orbit: P_{orb} is the orbital period measured in days, T_0 is the epoch at which the neutron star crosses orbital phase 0 measured in MJD, $a_x \sin i$ is the projected semi-major axis of the orbit measured in light-seconds, e is the orbital eccentricity, and ω is the longitude of periastron, which describes where in the orbit the neutron star is closest to the companion star. The errors quoted in Table 1 are statistical only; any biases introduced by unmodeled accretion torques are not included. However, these systematic effects should be quite small since the data cover more than six cycles of the binary orbit and such effects are expected to average out.

Table 1. Orbital Parameters of 1E1145.1-6141

Parameter	Value
P_{orb}	14.365 ± 0.002 d
T_0 (MJD)	51008.1 ± 0.4
$a_x \sin i$	99.4 ± 1.8 light-s
e	0.20 ± 0.03
ω	$-52^\circ \pm 8^\circ$

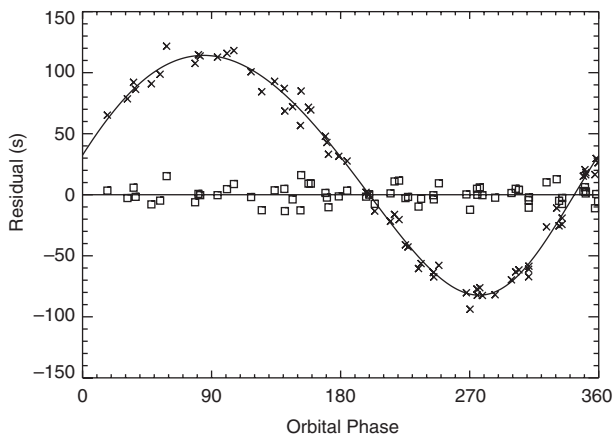


FIGURE 4 Observed pulse arrival time residuals to a constant-period model (crosses) with the best-fit eccentric orbit solution overplotted as a solid line. The squares are the same data after the orbit model is subtracted.

With the orbit determined, we can measure the precise intrinsic pulse period at each epoch with the contaminating effects of the orbit removed. Figure 5 shows these determinations along with all historical period measurements of this source. The pulsar has shown significant spin up since its discovery in 1978. Fitting the frequencies to a straight line yields an average frequency derivative of 1.2×10^{-14} Hz/s, which implies a spin-up timescale of 1000 years. This is similar to other supergiant X-ray pulsars.

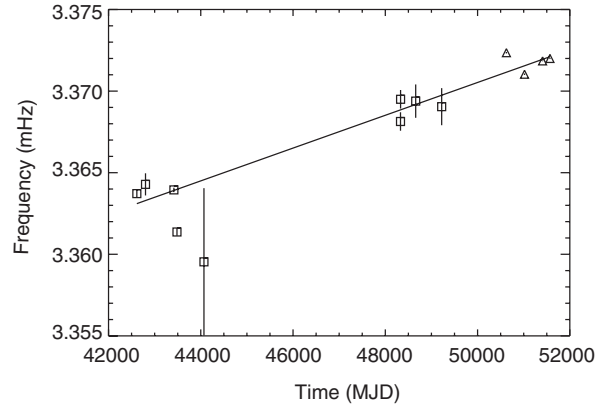


FIGURE 5 Barycentric pulse frequency as a function of time for 1E1145.1-6141. Squares are previously published data points, and the triangles are the data from our RXTE observations.

Discussion

This new discovery adds to the number of well-determined orbits in X-ray binary systems. In the search, we found no convincing evidence for X-ray eclipses, although the pulsar was not detected in one observation. Further X-ray observations of this source are underway. Also, optical studies of the Doppler shifts of spectral lines from the companion star could potentially provide further constraints on the orbit and the mass of the neutron star (as has been possible in a few other binary systems to date).

LONG-TERM TIMING OF AN LMXB ORBIT

We now turn to the second investigation, which involves precise timing of the eclipses of the LMXB EXO0748-676.² The physical process that drives the accretion in low-mass X-ray binary systems is not known with any certainty. The accretion may be driven by the loss of angular momentum through gravitational radiation or magnetic braking, or by the nuclear evolution of the secondary, which causes it to overflow its Roche lobe. The mass transfer from the

secondary can be either conservative (meaning that all mass lost by the secondary eventually ends up on the neutron star) or nonconservative. Models incorporating these physical processes make specific predictions for the rate at which the binary orbital period (P_{orb}) changes. For instance, the orbital period of an LMXB undergoing conservative mass transfer at a typical rate of 10^{-10} to 10^{-8} solar masses per year from a Roche-lobe-filling 1 solar mass companion is expected to decrease with a timescale of 10^8 to 10^{10} years. Unfortunately, none of the published orbital period derivative measurements in LMXBs are in agreement with theoretical expectations!

Six LMXBs are currently reported to have observed orbital period derivatives. Three of these systems (X1820–303, X1658–298, and Her X-1) have apparently negative period derivatives, indicating that the orbital separation is shrinking. The other three systems (X1822–371, X2127+119, and EXO0748–676) have positive orbital period derivatives, implying that the binary orbital separation is increasing. In each of these systems, the orbital period appears to be evolving at a considerably faster rate (by a factor of 10 or more) than theoretical predictions for a system undergoing conservative mass transfer. Clearly, the theoretical understanding of the processes driving orbital evolution of LMXBs is still very poor.

The best systems for addressing this problem are the eclipsing LMXBs, which are in an orientation so close to edge-on that the X-rays from the neutron star

are eclipsed by the companion once per orbit as the companion passes between the neutron star and the Earth. Only three LMXBs are known to show full eclipses. Full, sharp eclipses are important since the observed beginning of eclipse (ingress) and end of eclipse (egress) give precise timing markers that can be used to study the evolution of the orbit. The best candidate for such a study is the LMXB EXO0748–676, which is relatively bright in X-rays and has been persistently visible for the last 20 years, while the other known eclipsing LMXBs are transient systems and are faint or not visible much of the time. Thus motivated, we began a detailed long-term study of EXO0748–676 to greatly increase the observational data on LMXB orbital period evolution. This was made possible recently by the fact that the RXTE and USA instruments had very flexible automated scheduling. This allows many short observations of the source for the purpose of making repeated eclipse measurements over a long period of time without using a large amount of satellite observing time.

Eclipse Timing Observations

We observed EXO0748–676 with both RXTE and USA beginning in 1996 and continuing to the present time. EXO0748–676 exhibits complete eclipses that last about 500 seconds out of each 3.82-hour binary orbit. (Figure 6 shows an example of an eclipse observation along with a fit to the observed eclipse

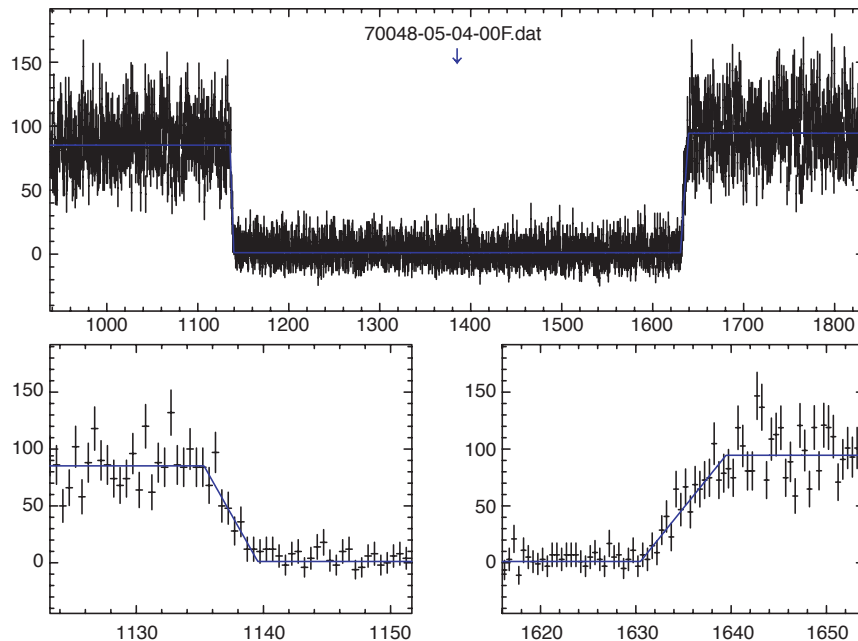


FIGURE 6 Sample eclipse observation of EXO0748–676. The lower plots are detailed views of the ingress and egress regions. The solid line represents the piecewise-linear model used to fit the eclipse, and the arrow marks the best-fit mid-eclipse time.

profile.) Typically, we observed 5 to 6 consecutive eclipses once every two months. The data are processed by selecting photons in the 2 to 8 keV energy range, converting the observed times to the arrival time at the solar system barycenter, binning the data into 0.5 s bins, and subtracting a background model. This results in a clean eclipse light curve for each observation. These light curves are then fitted to a model eclipse profile (a piecewise linear ramp-and-step model) to determine the precise time of mid-eclipse. Most observations result in a mid-eclipse time determination accurate to about 0.5 seconds. The mid-eclipse time is chosen as the most stable orbital phase marker because the eclipse ingress time, egress time, and total duration vary significantly from eclipse to eclipse, possibly due to changes in the structure of the companion star's atmosphere.

To analyze the eclipse timing data, we compare the observed times to those that would be calculated by a simple model in which the eclipses occur at a constant period. This is called an observed minus calculated or “O–C” plot, and Fig. 7 shows all of the RXTE and USA data on such a plot. Clearly, the data are not consistent with a simple constant period, and the observed variations are considerably larger than the measurement error. This is shown by the error bars on the plot. In addition, no simple model of orbital period evolution significantly improves the fit. The solid line is the best fit model with a constant period derivative, $\dot{P}_{orb} \equiv dP_{orb}/dt$, and also yields a very poor fit. Apparently, some other process is at work, causing the observed eclipse phases to do a random walk about a smooth solution. This problem is

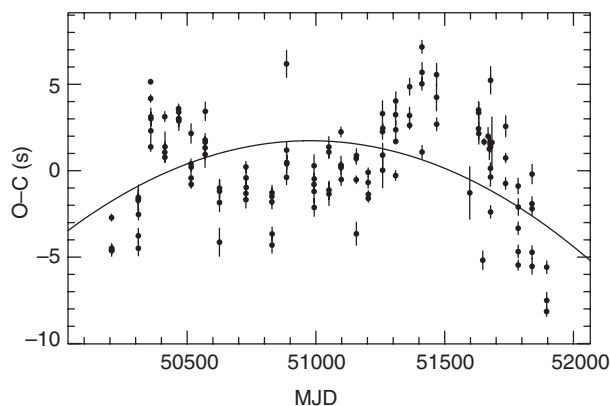


FIGURE 7
O–C plot of mid-eclipse times of EXO0748–676 measured with RXTE and USA. The residuals show a random walk about the constant-period model. The solid line is the best-fit model with constant period derivative (which is still a very poor fit).

even more apparent when all the historical eclipse measurements are added to the plot, as seen in Fig. 8. No matter what simple model is chosen, extremely significant residuals remain.

Intrinsic Period Jitter

To model this random walk, we added a term to account for small, random (zero-mean) fluctuations of the orbital period around the true underlying orbital period. This results in a cumulative random walk in orbital phase as seen in our measurements. If the underlying orbital period evolution is known, the O–C residuals can be represented as

$$(O-C)_j = \sum_{i=1}^{N_j} \varepsilon_i + e_j,$$

where ε_i is a random, zero-mean fluctuation in the length of orbit period i , and e_j is the measurement error in the j th mid-eclipse time. The cumulative nature of the ε_i causes the systematic wandering of the mid-eclipse residuals apparent in Fig. 7. We performed a maximum-likelihood analysis of the residuals to determine whether such a process could account for the observations and what the magnitude of the ε and e terms were (called σ_ε and σ_e , respectively). Looking at the RXTE and USA data only (Fig. 7), we found that such a model fit well with a period jitter σ_ε of 0.12 seconds and a measurement error σ_e of 1.62 seconds. When we extend this analysis to the full data set in Fig. 8, we find that a model that includes an intrinsic orbital period derivative plus intrinsic period jitter is preferred to one with period jitter alone.

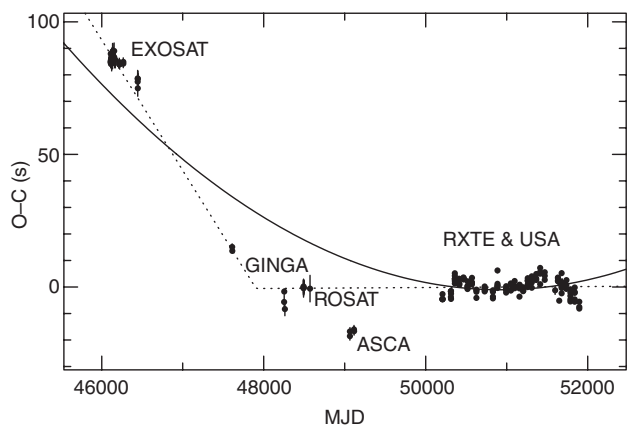


FIGURE 8
O–C plot of all published eclipse timings of EXO0748–676, including data from five different satellites from 1985 to the present day. The solid line is the best-fit model with constant period derivative, and the dotted line is a model with a sudden change in orbital period.

This random jitter has caused quite a bit of confusion over the last 20 years in interpreting eclipse timings of EXO0748–676. Previous authors, looking at small samples of data, have variously concluded that the orbital period is constant, increasing, decreasing, or sinusoidally varying. The maximum-likelihood analysis combined with the large and well-sampled data set we acquired allow us to begin to separate the random jitter from the longer-term orbital period evolution and rule out a number of these models.

We verified our result with a Monte Carlo technique in which we simulated a system with a period jitter of 0.12 seconds but no underlying orbital period evolution. We generated many simulated data sets and sampled them with the same sampling times as the real observations. These data sets demonstrated that spurious positive or negative period derivatives could easily be created by the random walk process. However, a random walk with a magnitude of 90 seconds, as seen in Fig. 8, was extremely unlikely. We therefore conclude that in the EXO0748–676 system there is both period jitter and orbital period evolution with a magnitude of

$$\dot{P}_{orb} = 1.2 \times 10^{-11}.$$

This corresponds to an orbital period evolution timescale of about 40 million years, whereas the timescale expected from the amount of mass moving around the system is more like a billion years.

Discussion

Based on our analysis, we conclude that the orbital period of EXO0748–676 has increased by ~8 ms over the past 16 years. This measured \dot{P}_{orb} implies that the two stellar components are moving away from each other instead of toward each other, as current theoretical models indicate they should and at a rate much faster than expected. Furthermore, the intrinsic period jitter that we see is certainly not expected from previous theoretical work. This jitter may correspond to very large changes in the orbital angular momen-

tum over very short timescales, much too short to be explained by changes in the rate at which the companion is losing mass. So, we are forced to look for other explanations for the jitter. One possible reservoir of angular momentum is the rotating companion star. The jitter could be due to exchange of angular momentum between the orbit and internal modes in the companion star. These internal mode changes might be associated with shape changes in the companion star and thus might be able to be probed by a careful analysis of the eclipse profiles. Probing internal dynamics of Sun-like stars is a challenge that astronomy is only now beginning to take on. X-ray eclipse methods in close binaries, where the Sun-like companion star is subject to extreme stresses, could complement information obtained in other ways such as helioseismology.

CONCLUSIONS

The X-ray astronomy group at NRL continues to make use of instruments constructed in-house as well as facilities provided by NASA and the international community to study the population, characteristics, and evolution of a wide variety of cosmic X-ray sources. Future plans include the use of next-generation X-ray telescopes that incorporate solid-state detectors, which are lighter and far more durable than gas-based detectors. These designs will be much closer to a package that can realistically be used for autonomous satellite navigation and timekeeping using celestial X-ray sources. Careful studies of the behavior of the celestial clocks like pulsars and eclipsing binaries will provide the raw data on which such a system will be based.

[Sponsored by ONR and NASA]

References

- ¹ P.S. Ray and D. Chakrabarty, "The Orbit of the High-Mass X-ray Binary Pulsar 1E1145.1–6141," *Astrophys. J.* **581**, 1293–1296 (2002).
- ² M.T. Wolff, P. Hertz, K.S. Wood, P.S. Ray, and R.M. Bandyopadhyay, "Eclipse Timings of the Low-Mass X-ray Binary EXO 0748–676. III. Orbital Period Jitter Observed with the Unconventional Stellar Aspect Experiment and the Rossi X-ray Timing Explorer," *Astrophys. J.* **575**, 384–396 (2002).



THE AUTHORS



PAUL S. RAY graduated from the University of California, Berkeley in 1989 with an A.B. degree in physics. He received a Ph.D. in physics from the California Institute of Technology in 1995 where his thesis research involved high-sensitivity searches for radio pulsars. He came to NRL in 1995 as an NRC-NRL postdoc jointly in the Space Science Division and the Remote Sensing Division and became a member of the NRL staff in 1997. His research centers on the astrophysics of compact objects, particularly accreting binaries and radio pulsars in our Galaxy. His studies have ranged over the electromagnetic spectrum from the longest radio wavelengths to high-energy gamma rays. He is a member of the NASA RXTE User's Group, has authored or co-authored 18 articles in refereed scientific publications, and has been awarded an Alan Berman Research Publication Award.



MICHAEL T. WOLFF received his B.S. degree from the University of Maryland in 1977 and his Ph.D. in astronomy from Indiana University in 1985. He has worked at the Naval Research Laboratory since 1986, first as a Universities Space Research Association Visiting Scientist until 1991 and then as a civil servant. His research activities have included the hydrodynamic modeling of high-temperature accreting plasmas in magnetic cataclysmic variable systems, participating in the design, construction, testing, and then commanding of the USA X-ray timing experiment that orbited the Earth as part of the U.S. Air Force ARGOS mission, and investigated the properties of a wide range of compact object binary systems including white dwarf, neutron star, and black hole systems. He currently works in the High-Energy Space Environment Branch in NRL's Space Science Division.



KENT S. WOOD received his B.S. degree from Stanford University in 1967 and his Ph.D. from the Massachusetts Institute of Technology in 1973. He came to NRL in 1973 and has remained here to the present time. He worked on the HEAO A-1 Experiment, a mission to map the brightest sources in the X-ray sky. Since then, his work has centered on the study of compact objects such as neutron stars and black holes, using mainly X-ray timing methods. He is the Principal Investigator for the USA Experiment on ARGOS, which has conducted timing studies and explored applied uses of X-ray astronomy and computing in space. He is co-investigator on the GLAST mission, a NASA gamma-ray facility being prepared for launch. He is Head of the X-ray/UV Astrophysics and Applications Section in the High-Energy Space Environment Branch at NRL.



PAUL HERTZ was an astrophysicist in the Space Science Division from 1985 to 2000. During that time his primary research interests were X-ray binaries, although his work ranged from globular clusters and supernova remnants to gamma ray bursts. He also coordinated NRL's participation in NASA guest investigator programs and pioneered the use of the NRL Connection Machine for the analysis of astrophysical data. Dr. Hertz received a B.S. in physics and mathematics from the Massachusetts Institute of Technology and a Ph.D. in astronomy from Harvard University. He has been awarded the Alan Berman Research Publication Award twice, and was awarded the 1985 Robert Trumpler Award of the Astronomical Society of the Pacific. Since 2000, Dr. Hertz has been a Senior Scientist in the Office of Space Science, NASA Headquarters, Washington, DC.

ACOUSTICS



BATTLESHIP *MAINE* MEMORIAL.

USS *Maine* was sunk in the harbor at Havana, Cuba, in February, 1898, and helped precipitate the start of the Spanish-American War.

- 91** Through-The-Sensors Concepts to Refresh the Environmental Picture
W.E. Avera, M.M. Harris, D.J. Walter, L.D. Bibee, and D.N. Lambert
- 93** Simultaneous Inversion of Bio- and Geo-Acoustic Parameters in the Yellow Sea
O.I. Diachok and S.C. Wales
- 95** Simulations of Low-Frequency Bubble Pulsations Generated by Impacting Cylindrical Water Jets
W.G. Szymczak and S.L. Means

[BACK TO CONTENTS](#)

THROUGH-THE-SENSORS CONCEPTS TO REFRESH THE ENVIRONMENTAL PICTURE

W.E. Avera, M.M. Harris, D.J. Walter, L.D. Bibee, and D.N. Lambert

Marine Geosciences Division

Introduction: The Naval Research Laboratory's (NRL) Marine Geosciences Division is advancing "Through-The-Sensor" (TTS) concepts that use ship and airborne sonar systems to obtain tactical environmental data and refresh the environmental picture in near real time. NRL's Acoustic Seafloor Classification System (ASCS) uses inversion and signal processing techniques developed under the NRL S&T program to determine acoustic impedance and seafloor properties. Classification of surficial seafloor sediments has been demonstrated using normal incidence beams from the AQS-20, UQN-4, BQN-17 acoustic systems, and backscatter from the EM-121 multibeam sonar. Signal and image processing algorithms were also developed to produce multibeam bathymetry and imagery from the AQS-20 mine-hunting sonar and the submarine Precision Underwater Mapping (PUMA) system. The UQN/Bottom Sediment Classifier (BSC) is currently installed on the USS *Dextrous* (MCM-13) in the Persian Gulf. The BQN-17/Submarine Sediment Classifier (SSC) was demonstrated aboard the USS

Key West (SSN-722) off the California coast. Efforts include transitioning these capabilities for use with tactical decision aids (TDAs), environmental assessments, and integration into historical databases at the Naval Oceanographic Office (NAVOCEANO).

Surficial Sediment and Bathymetry: Two key environmental data types needed in the littoral are bottom type and bathymetry. The ASCS system displays a profile of the seismic stratigraphy and inferred bottom type beneath the vessel. Figure 1 shows two displays from the system. Classification of surficial seafloor sediments has been demonstrated using normal incidence beams from the UQN-4 fathometer on mine countermeasures (MCM) ships, the BQN-17 submarine fathometer, and the AQS-20 mine-hunting system. These data can be used in onboard decision aids and ultimately stored in historical databases.

SEDIMAP™ is another system being developed at NRL for NAVOCEANO to determine bottom type using the angular dependence of backscatter from commercial multibeam sonars. SEDIMAP™ gives areal coverage by providing a swath of bottom type information below the vessel. Simulated annealing data inversion techniques are used to extract sediment grain size and roughness parameters.

Multibeam bathymetry and imagery are being extracted from the AQS-20 mine-hunting sonar (Fig. 2) and the submarine PUMA system. Data from the AQS-20 volume search sonar, designed to locate

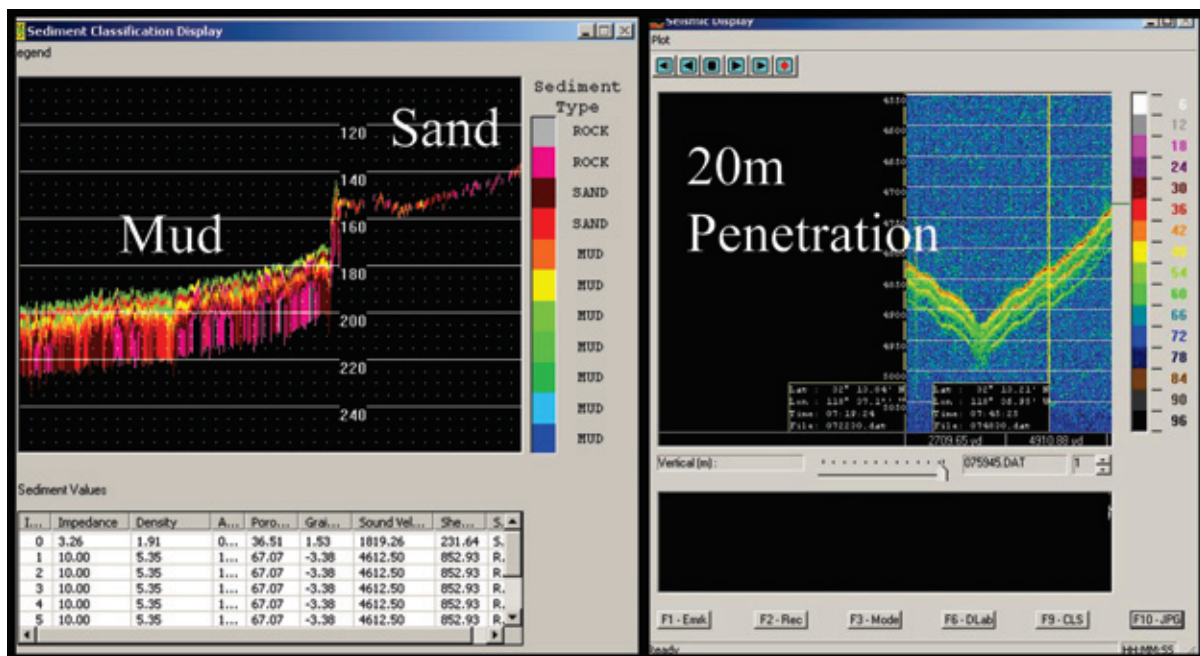


FIGURE 1

Acoustic Sediment Classification System (ASCS) displays showing (left) bottom type and (right) 20-m penetration into the seafloor.



FIGURE 2
AQS-20 with the four sonars. The Volume Search Sonar is used to obtain multibeam bathymetry and sediment type.

mines in the water column, is being used to generate multibeam bathymetry across swaths of the ocean bottom. The bathymetry can be imported into TDAs supporting mine warfare operations and used to augment the historical databases with bathymetry in areas where historical data are lacking, sparse, or perishable.

PUMA bathymetry is sent to the Tactical Environmental Data Services (TEDS) system for distribution to onboard TDAs. Acoustic images of the seafloor are also extracted from the PUMA data. These images are combined with bathymetry from the system to produce an automated bottom feature extraction capability. The bottom feature extraction will support Navy databases with detailed bottom characteristics that are not otherwise available.

Ship Installations and Demonstrations: UQN-4 fathometers on MCM ships are being adapted to characterize bottom sediments. Real-time processing and display of seismic stratigraphy and inferred sediment parameters are used for situational awareness in real time. In the future, sediment parameters will automatically be provided to MCM tactical decision aids onboard ship. The UQN/Bottom Sediment Classifier (BSC) was installed in October 2001 for 1-year demonstration on the USS

Dextrous (MCM-13), a forward deployed mine hunter in the Persian Gulf (Fig. 3). The demonstration was extended until Spring 2003 based on positive feedback.

The BQN-17 Submarine Sediment Classifier was demonstrated aboard the USS *Key West* off the California coast. Tests with the BQN-17 demonstrated mapping of subbottom sediment layers in water depths up to 3000 meters, with penetration up to 20 meters below the bottom. Dedicated tests with the AQS-20 sonar towed by an MH-53 helicopter (which can also be towed by the Remote Mine-hunting System) have been completed off the coast of Panama City, Florida, and modifications to record the data are being made to ensure this will be operational for the Fleet.

Summary: In summary, NRL's Marine Geosciences Division is advancing the TTS concept to produce ocean bottom type and bathymetry data from existing Fleet sonar systems. Recent research has focused on implementing and testing the technology. Concurrently, advances are being made toward combining data from multiple sonar systems and developing innovative ways to characterize the environmental battlespace.

[Sponsored by SPAWAR, ONR, NAVSEA] 

FIGURE 3
UQN-4/Bottom Sediment Classifier (BSC) installed on the USS *Dextrous* (MCM-13). UQN-4 fathometer display is located in the Chart Room, and the BSC display is located in the Combat Information Center (CIC) for real-time visualization of bottom type.



SIMULTANEOUS INVERSION OF BIO- AND GEO-ACOUSTIC PARAMETERS IN THE YELLOW SEA

O.I. Diachok and S.C. Wales
Acoustics Division

Introduction: Bio-acoustic absorptivity due to fish with swim bladders can have large (nominally as large as 40 dB at 5 km) frequency selective effects on transmission loss (TL) at frequencies between approximately 0.5 and 5 kHz in shallow waters.^{1,2} TL, which is defined as the difference between signal levels measured at one meter and at other ranges, is one of the parameters that controls the detection range of operational sonars. It is the most challenging to predict. TL is determined primarily by the oceanic sound speed profile, the geo-acoustic properties of the bottom, and the bio-acoustic properties of fish layers. Geo-acoustic parameters may be inferred from TL measurements. To date however, the effects of bio-absorptivity on TL have been disregarded in inversions of geo-acoustic parameters in both the scientific and operational literature. As a result of this omission, the scientific value and operational usefulness of inverted geo-acoustic parameters at/near the resonance frequencies of fish swim bladders at fish-dominated sites, such as the Yellow Sea, are highly questionable. We introduce here a new inversion method that permits simultaneous inversion of bio- and geo-acoustic parameters.

Traditional Approach to Observation of Bio-acoustic Effects: The most compelling demonstrations of bio-acoustic effects on TL have relied on long-term (at least 7-hour) broadband measurements between fixed sources and receivers.^{1,3} This experimental configuration permits monitoring of changes in resonance frequencies associated with the vertical migrations of fish, such as sardines and anchovies, at twilight. This method, however, is not “robust.”

Under some environmental circumstances, these species remain near the surface day and night. Furthermore, other species with swim bladders, such as cod, generally remain near the bottom day and night. In addition, this approach has proved to be logistically cumbersome.

Simultaneous Inversion: To overcome these difficulties, we have developed a new inversion method that permits simultaneous inversion of bio- and geo-acoustic parameters from short-term, broadband TL measurements between multiple source and receiver depths. To illustrate the power of this new technique, we summarize the results of simultaneous inversion of bio-acoustic parameters of fish (anchovies) and geo-acoustic parameters of the bottom from transmission loss measurements in the Yellow Sea that were reported by Chinese scientists at a shallow (40-m) water site near Qingdao.² This data set was selected because the bio-absorptivity at the site was extremely large, 40 dB, and their measurements were made between two source depths and two receiving depths. Figure 4 shows the results of the measurements at a range of 5.7 km. Highest losses occur at 1.35 kHz. This is the resonance frequency of 10-cm long anchovies, which are the dominant species in the Yellow Sea. Losses were highest when both source and receiver were placed at 7 m; they were lowest when both source and receiver were placed at 25 m.

Replica fields (theoretically generated acoustic fields for comparison with TL measurements) were calculated with a normal mode model that incorporates the effects of bio-acoustic absorption layers and the geo-acoustic properties of the bottom. The inversion was based on minimizing the root-mean-square (rms) difference Δ between measured and calculated values of TL at multiple ranges and multiple source and receiver depths. It involved a simultaneous search for bio-layer depth d , bio-layer thickness t , bio-alpha α_B , geo-sound speed c_p , and geo-alpha α_p . Figure 5 shows the two-dimensional

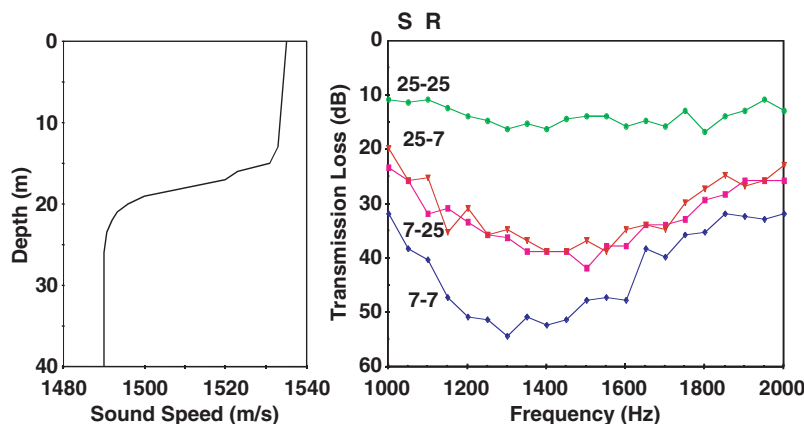


FIGURE 4
Measurements of sound speed profile and transmission loss at 5.7 km vs source and receiver depths (from Ref. 2).

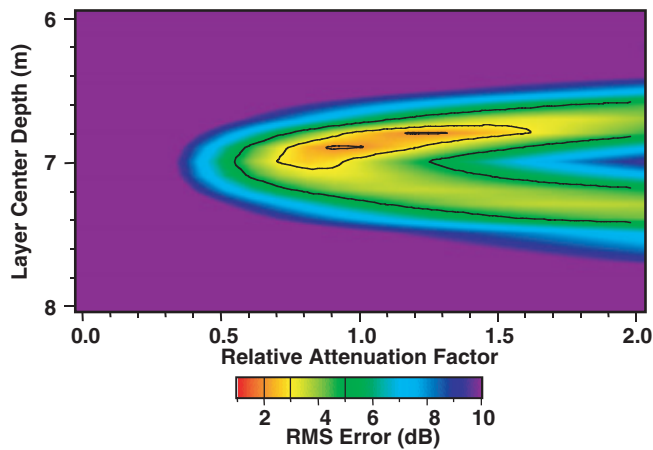
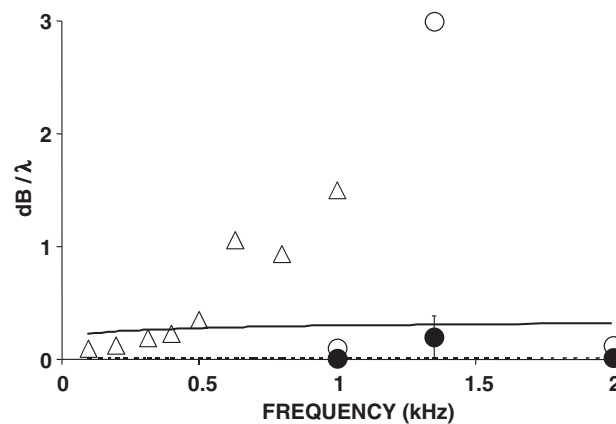


FIGURE 5
Ambiguity surface of the rms difference Δ between measured and calculated transmission loss at 1.35 kHz vs layer depth and absorption coefficient with the layer. Layer thickness equals 0.4 m. The inverted layer depth is approximately equal to 6.9 m. A relative attenuation of 1 corresponds to 0.3 dB/ λ in a 1-m thick layer. Contours: 2, 3, and 5 dB.

FIGURE 6
Inversions from data of Ref. 2 with (\bullet) and without (\circ) bio-alpha, Ref. 5 data without bio-alpha (Δ), and upper and lower bounds according to Ref. 4.



ambiguity surface of Δ at 1.35 kHz as a function of d and α_B with t , c_P and α_P held constant. The resultant extremely small value of Δ (1.9 dB) confirmed that the model, which was assumed in replica field calculations, was realistic, and that inverted parameters were meaningful. The inverted value of d , 6.9 ± 0.3 m, is consistent with theoretical calculations of d , 5.8 ± 1 m, of 10-cm long anchovies, the dominant species in the Yellow Sea, and with laboratory measurements of resonance frequencies of anchovies. The inverted value of t , about 0.4 m, is consistent with the nominal thickness of biological layers on continental shelves. The values of c_P (1700 m/s) and α_P (0.2 dB/ λ) are consistent with Bowles' review⁴ of previously reported measurements of these parameters.

By contrast, inversion calculations, which assumed that all excess attenuation (above geometrical spreading) at this site was due to the bottom, resulted in an unacceptably large value of Δ (9.5 dB) and an unrealistic value of α_P (3 dB/ λ). Figure 6 shows inverted values of α_P from Ref. 2 data with and without α_B , other inversions⁵ of α_P (which disregarded α_B) at a nearby site, and upper and lower bounds according to Ref. 4.

Conclusions: We have shown that it is possible to simultaneously invert geo-acoustic parameters of the bottom and bio-acoustic parameters of biological absorbing layers in the water column from TL measurements between multiple source and receiver depths. This method is expected to prove useful for inversion of bio- and geo-acoustic parameters at operationally mandated sites where the concentrations of fish are high.

[Sponsored by ONR]

References

- ¹O. Diachok, "Effects of Absorptivity Due to Fish on Transmission Loss in Shallow Water," *J. Acoust. Soc. Am.* **105**, 2107-2128 (1999).
- ²X. Qiu et al., "Frequency Selective Attenuation of Sound Propagation and Reverberation in Shallow Water," *J. Sound Vib.* **220**, 331-342 (1999).
- ³P. Ching and D. Weston, "Wide Band Studies of Shallow Water Acoustic Attenuation Due to Fish," *J. Sound Vib.* **18**, 499-510 (1971).
- ⁴F.A. Bowles, "Observations on Attenuation and Shear Wave Velocity in Fine Grained Marine Sediments," *J. Acoust. Soc. Am.* **101**, 3385-3397 (1997).
- ⁵J.X. Zhou, "Normal Mode Measurements and Remote Sensing of Sea Bottom Sound Velocity and Attenuation in Shallow Water," *J. Acoust. Soc. Am.* **78**, 1003-1009 (1985).

SIMULATIONS OF LOW-FREQUENCY BUBBLE PULSATIONS GENERATED BY IMPACTING CYLINDRICAL WATER JETS

W.G. Szymczak and S.L. Means
Acoustics Division

Introduction: The impact of a water jet onto a water surface can entrain air bubbles whose pulsations provide acoustic sources. Such impacts can occur during the breaking of a wave or, on a smaller scale, when a raindrop strikes a puddle of water. A better understanding of this phenomenon can lead to improved characterizations of ambient noise and acoustic detection algorithms for Navy sonar systems. NRL has developed a method for simulating the impact of water jets by using a generalized hydrodynamics model. These simulations provide details of not only the initial formation of the air-entrained bubble during the cavity collapse, but also the bubble's subsequent pulsations as it rises to the surface. Validations are provided by comparisons to experiments of impacting cylindrical water jets.

Generalized Hydrodynamics Model: The simulations rely on a computational method based on a constrained system of conservation laws. The primary constraint is on the density, namely $\rho \leq \rho_0$, where ρ_0 is the intrinsic density of the incompressible liquid. The density is used as a fluid of volume variable that delineates the liquid region (where $\rho = \rho_0$) from the nonliquid regions (where $0 \leq \rho < \rho_0$). The distinguishing feature of the model is the imposition of this constraint using a density and momentum redistribution algorithm. This algorithm was derived from an approximation to the solution of a Stefan-Boltzmann equation.¹ This algorithm not only enforces the density constraint but also conserves mass and momentum, is spatially invariant, and ensures that the energy is nonincreasing.

This feature allows for a physically rational treatment of liquid collisions while providing stability.

Another important feature of the model is that it allows for regions of “spray” where $0 < \rho < \rho_0$. Such regions will form when free surfaces become unstable, in particular when Rayleigh-Taylor instabilities occur. These instabilities are, in general, unavoidable in most violent free surface flows, such as the breaking of a wave on the beach or the oscillations of an underwater bubble. Therefore, these spray regions are not a priori suppressed through the use of surface tracking or level set approaches.

The model treats bubbles, defined as connected subsets of the region where $0 \leq \rho < \rho_0$, as uniform pressure regions. For air-entrained bubbles, the pressure is initialized as the ambient air pressure. During the flow field dynamics, the pressure is assumed to behave adiabatically, $PV^\gamma = C$, where V is the volume of the bubble that changes due to the fluid motion, is a constant determined at the time the bubble formed, $\gamma = 1.3$ is the adiabatic exponent, and P represents the time-dependent bubble pressure.

Computational Results: The generalized hydrodynamics model has been implemented into computer codes denoted BUB2D, for the solution of two-dimensional and axially symmetric problems, and BUB3D for three-dimensional problems. To study details of jet impacts and air entrainment of bubbles, consider an idealized experiment of a falling cylinder of water onto a still water surface. Figure 7 shows the setup of experiments conducted by Kolaini et al.² The case when the water cylinder has radius $R = 0.054$ m, length $L = 0.45$ m, and height above the surface $H = 0.15$ m is considered here. Figure 8 shows images of the experiment from a video of this experiment. The formation of a cavity after the cylinder impacts the air-water surface and the pinching off of a bubble are clearly displayed in these images. For comparison, Fig. 9 shows the

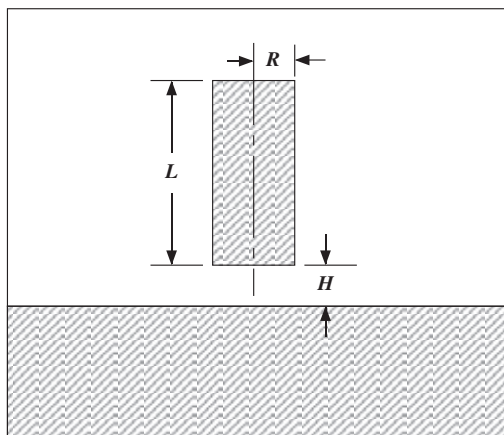


FIGURE 7
Experimental setup of a liquid cylinder above still water.

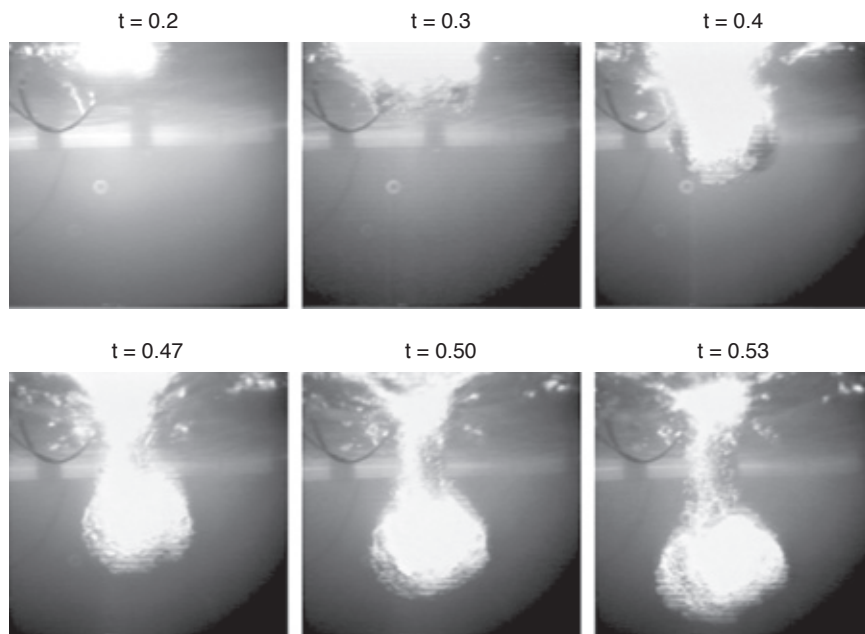


FIGURE 8
Images from video of the experiment.

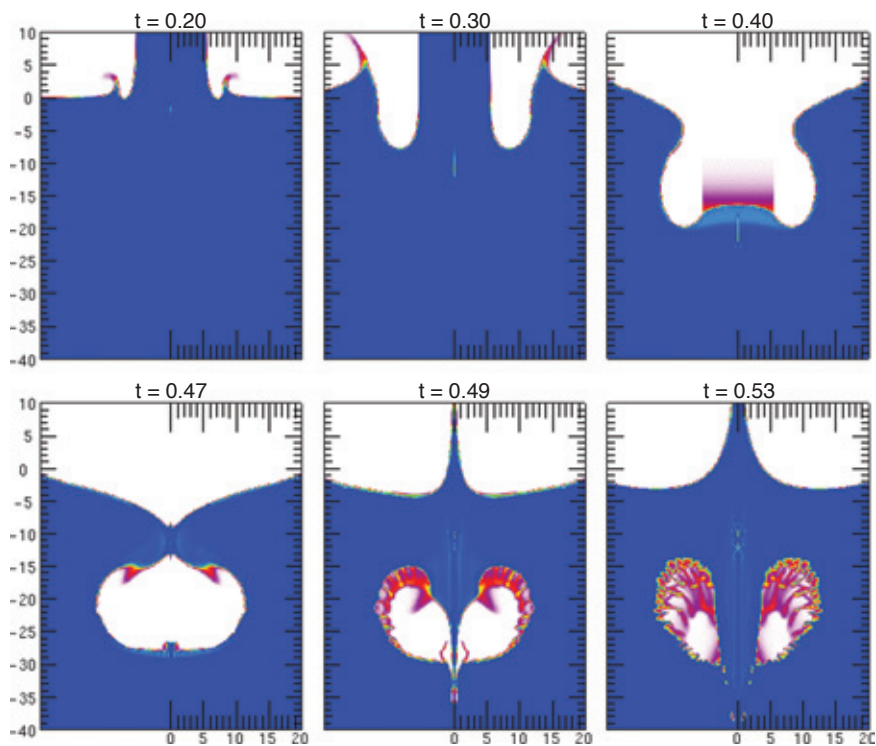


FIGURE 9
Computed density contours.

results of an axially symmetric computation using BUB2D. In this figure, an annular water jet ejected upward can be seen surrounding the cylinder at time $t = 0.2$ s, shortly after the impact. The cavity enlarges as the cylinder falls into the water surface at times $t = 0.3$ s and $t = 0.4$ s. The cavity has just closed at time $t = 0.47$ s. Shortly after the cavity closes, two water jets form: one moving downward, piercing the bottom of the bubble and the second, moving upward above the surface as seen at time $t = 0.50$ s. These water jets have also been observed in high speed photographs of the experiment.² After the formation of the bubble, it begins to pulsate according to the adiabatic pressure assumption. At time $t = 0.53$ s, the bubble has pulsated twice, each time exhibiting Rayleigh-Taylor instability during the time it is near its minimum volume (maximum pressure). These instabilities are exhibited in the profile of the bubble and the amount of spray seen inside.

Figure 10 shows a comparison of the computed and measured pressure time series at a location 0.4 m from the radial axis and 0.2 m below the original air-water interface. The label "(1)" in the graph of the measured values indicates the time of the initial impact of the cylinder on the quiescent surface and corresponds to the first "spike" in the computed series at time $t = 0.175$ s. The measured fundamental frequency of 43 Hz is accurately reproduced by the computed frequency of 43.88 Hz. The decay of the amplitude of the pressure pulsations was 10.12% per period for the first 10 oscillations. This value is

slightly greater than shown in the experimental data, where the decay is approximately 8% per oscillation. Computationally, this decay is expected from both energy losses due to liquid collisions, and numerical dissipation.

Conclusions: A computational code based on a generalized hydrodynamics model has been shown to be capable of not only predicting bubble formation as the result of liquid impacts, but also the acoustic sources that the bubbles produce as they undergo low-frequency pulsations. This represents an important first step for predicting and characterizing air-entrained bubbles caused by plunging breaking waves, which in turn can be used to enhance acoustic detection and classification algorithms.

Acknowledgments: The authors thank Ali Kolaini for introducing us to this interesting and important benchmark problem and for providing the video tape from which the images of Fig. 8 were extracted.

[Sponsored by ONR]

References

- ¹J.C.W. Rogers and W.G. Szymczak, "Computations of Violent Surface Motions: Comparisons with Theory and Experiment," *Phil. Trans R. Soc. Lond.* **A 355**, 649-663 (1997).
- ²A.R. Kolaini, R.A. Roy, L.A. Crum, and Y. Mao, "Low-Frequency Underwater Sound Generation by Impacting Transient Cylindrical Water Jets," *J. Acoust. Soc. Am.* **94**(5), 2809-2820, (1993).

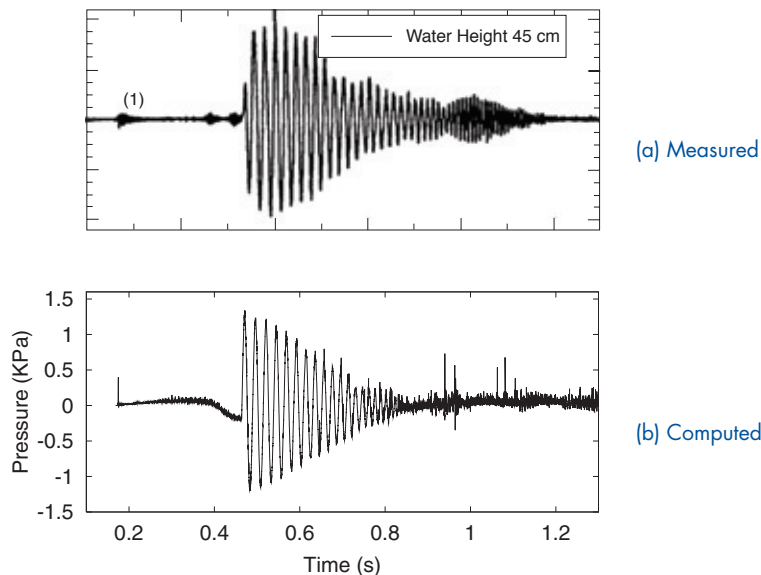


FIGURE 10
Pressure time series (measured values from Ref. 2, Fig. 4).

ATMOSPHERIC SCIENCE AND TECHNOLOGY



TOMB OF THE UNKNOWN DEAD FROM THE CIVIL WAR.

The tomb contains the remains of 2,111 unknown soldiers who were found in trenches or scattered over battlefields within a 25-mile radius of Washington, DC.

- 101** High-Resolution Modeling of Tropical Cyclones Using Moving Grids
C.-S. Liou and T.R. Holt
- 103** A “Satellite Focus” for the War on Terror
S.D. Miller
- 105** NRLMSISE-00: A New Empirical Model of the Atmosphere
J.M. Picone, D.P. Drob, R.R. Meier, and A.E. Hedin
- 108** Free-Space High-Speed Laser Communication Link Across the Chesapeake Bay
C.I. Moore, H.R. Burriss, M.R. Suite, M.F. Stell, M.J. Vilcheck, M.A. Davis, R.T. Smith, R. Mahon, W.S. Rabinovich, J.P. Koplrow, S.W. Moore, W.J. Scharpf, and A.E. Reed

[BACK TO CONTENTS](#)

HIGH-RESOLUTION MODELING OF TROPICAL CYCLONES USING MOVING GRIDS

C.-S. Liou and T.R. Holt
Marine Meteorology Division

Introduction: Tropical cyclones or hurricanes are serious threats to both Navy operations and the general public because of the potential for severe and hazardous weather conditions. Although the accuracy in tropical cyclone track forecasting has been significantly improved in recent years, uncomfortably large uncertainty still exists in predicting tropical cyclone structure and intensity. Besides the lack of a sufficient number of observations for properly describing the initial tropical cyclone circulation, complexity in cyclone structure represents another difficulty in predicting tropical cyclones with numerical models. As shown in the AVHRR satellite image for super hurricane Floyd (Fig. 1), vigorous deep convection appears adjacent to the calm hurricane center, the eye. Wind speed increases rapidly from near zero in the eye to higher than 50 m/s within 50 km. Beyond the deep convective eye wall, small-scale convective cells and asymmetric, spiral convective bands dominate the hurricane circulation. This sharp gradient wind distribution and the small-scale nature of deep convection require very high model grid resolution to properly simulate the tropical cyclone structure and intensity. However, a hurricane typically moves with a speed of 25 to 30 km/h. Therefore, to maintain a high-resolution grid centered on the tropical cyclone and to make the most efficient use of computer resources, numerical techniques must be developed for moving high-resolution grids to follow a selected tropical cyclone. We have developed and implemented such numerical techniques in the Navy's operational mesoscale model, the Massive Parallel Processing (MPI) version of the Coupled Ocean/Atmosphere Mesoscale Prediction System (COAMPS™).*

Moving Grids for Tropical Cyclone Prediction: We need to dynamically and automatically locate the position of a tropical cyclone in a high-resolution grid domain in order to move the grids following the selected cyclone. To ensure a smooth cyclone track that follows and represents an area center of cyclone circulation, we use a "mass center" to define a tropical cyclone position. The mass center is defined as the gravity center of pressure deficits

with respect to a reference pressure. When a COAMPS™ high-resolution inner grid is assigned to follow a tropical cyclone, the inner grid is initially centered at the tropical cyclone position. The cyclone position is then dynamically tracked at every time step of the forecast. When the tropical cyclone moves away from the inner grid center more than one grid distance of its parent grid, the inner grid is moved to its new location where the grid is once again centered over the tropical cyclone. The inner grid remains fixed when the tropical cyclone movement would shift the grid into the lateral boundary zone of its parent grid.

As a high-resolution inner grid follows a selected tropical cyclone, the grid will move into an area where only coarser-resolution information is available from its parent grid. We use bi-linear interpolation to project the coarse-resolution information onto the high-resolution grids in that area. A dynamic consistence adjustment is applied afterward to reduce any imbalance generated by the interpolation. For terrain height and land-sea-ice index fields, which are time independent, we prepare the two fields initially with high resolution covering the whole domain of the outer-most coarse grid and ensure the terrain height and index to be the same at collocated grid points of all grids. In this way, the high-resolution fields are easily extracted for any high-resolution moving grid, regardless of where it moves.

Results: We choose tropical cyclone Bilis to demonstrate the ability of moving high-resolution grids in modeling the detailed structure of a tropical cyclone. Figure 2 shows the 850 hPa winds (about 1.5 km above ground) of a 27-km resolution parent grid at the initial time, with white boxes indicating locations of the moving high-resolution inner grids at different forecast times. Figure 3 shows the 850 hPa winds of the 9-km resolution moving grid for the 42-h forecast. The high resolution simulates well the complicated wind distribution when the tropical cyclone interacts with the complex terrain of Taiwan. By ensuring the same terrain height at all collocated grid points, the high-resolution grid smoothly moves over the complex terrain areas without generating any obvious numerical noise. Comparisons of COAMPS™ forecasts from moving grids and larger-area fixed grids also indicate that the grid movement introduces very minimal errors in numerical calculation (not shown). More than 100 tests have been conducted to ensure the accuracy of the numerical techniques implemented in the MPI computational environment.

*COAMPS™ is a trademark of the Naval Research Laboratory.

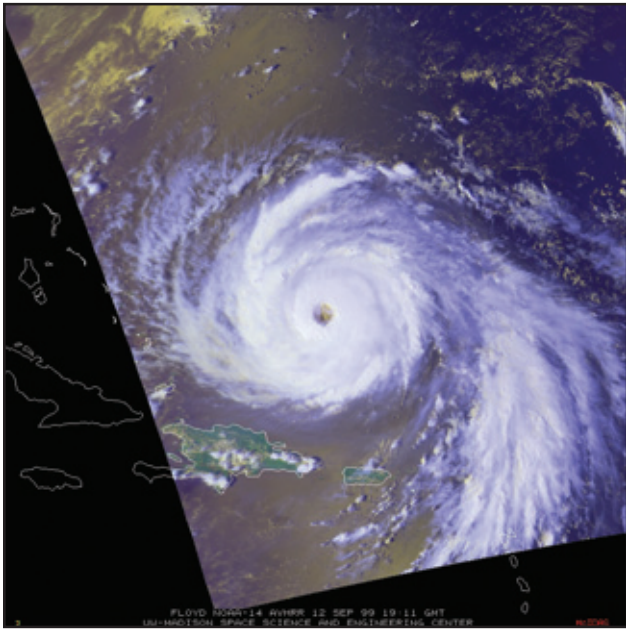


FIGURE 1
 AVHRR satellite image of super hurricane Floyd at 19:00 GMT 12 September 1999 (courtesy of CIMSS, University of Wisconsin).

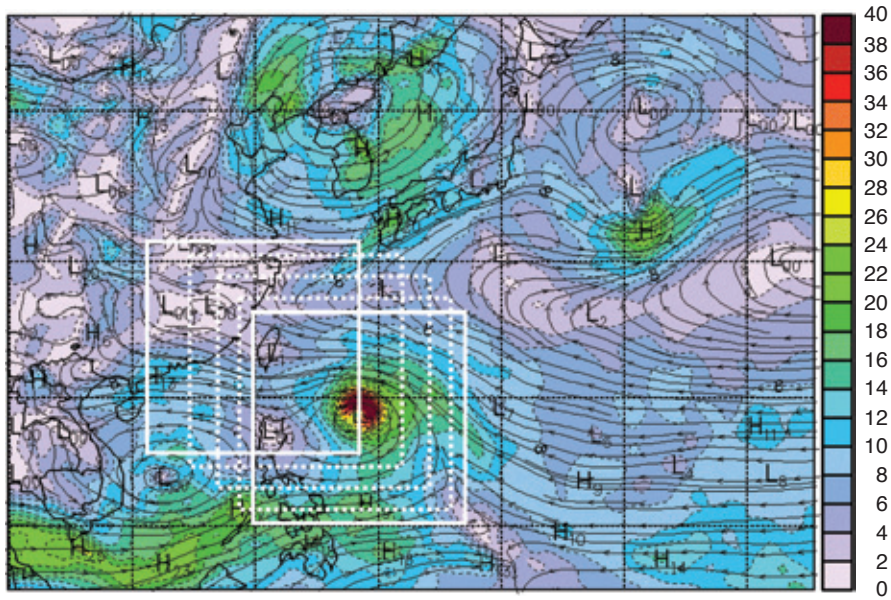


FIGURE 2
 850 hPa wind speed (color, m/s) and streamlines of 27-km grid at the forecast initial time. White boxes are locations of the 9-km moving grid at different forecast times.

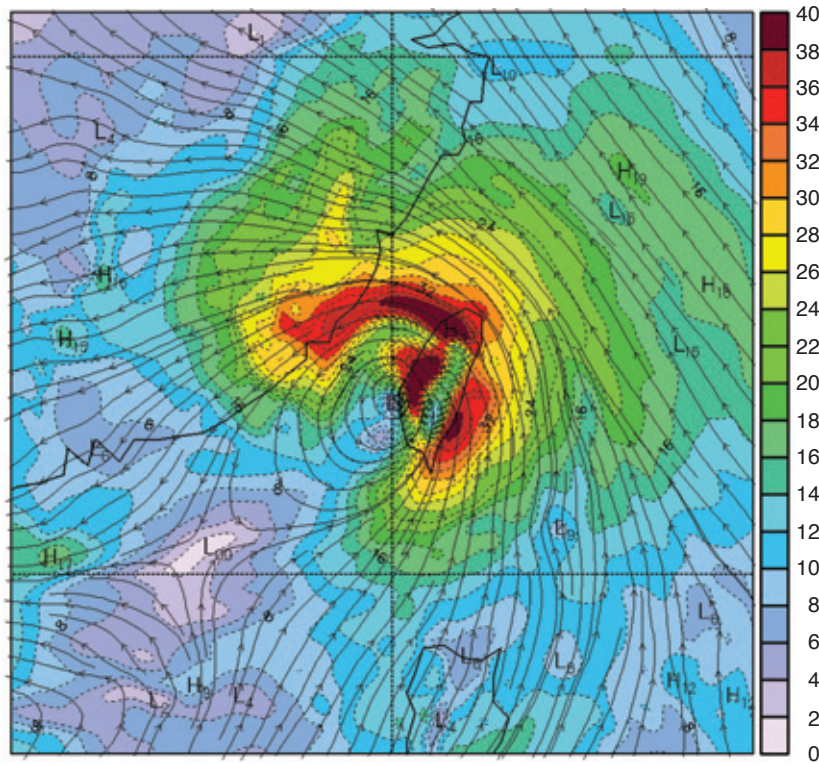


FIGURE 3
850 hPa wind speed (color, m/s) and streamlines of 9-km moving grid for a 42-h forecast.

Summary: To improve tropical cyclone structure and intensity forecasts by better resolving its complicated circulation, we have developed and implemented algorithms to move high-resolution COAMPS™ grids following a selected tropical cyclone. The success of this development provides us with a capability to run very high-resolution inner grids with affordable computer resources to further develop other modeling components, such as model physics, for improving tropical cyclone structure and intensity forecasts.

[Sponsored by ONR and SPAWAR]



A “SATELLITE FOCUS” FOR THE WAR ON TERROR

S.D. Miller
Marine Meteorology Division

Introduction: Following the September 11, 2001 attacks, the Office of Naval Research called on all Navy performers to address a pressing question: What resources could be provided in the short-term (~60 days), medium-term (~60 weeks), and long-term

(~60 months) time frames to assist the Department of Defense (DOD) in the War on Terror? The Naval Research Laboratory responded in part by developing a fully dynamic, web-based satellite product demonstration tool—Satellite Focus. A resource of proven value during Operation Enduring Freedom (OEF), Satellite Focus promises to empower Meteorology/Oceanography (METOC) operations well into the future.

Understanding METOC Needs: The ability to provide effective tactical METOC guidance in the extreme, harsh weather environments characteristic of the Southwest Asia OEF domain hinges on the availability of thorough, timely, and accurate environmental information. At the onset of the OEF campaign, the fundamental problem in meeting rapidly escalating demands for satellite data support was not as much a matter of technical readiness as it was one of resource coordination and distribution. Recognizing that a number of potentially useful satellite value-added products existed at various stages of development but were not yet forward-deployed to the operational centers via the normal research and development transition channels, we began a demonstration project to show the here-and-now utility of these products in the current

conflict. The concept of a Satellite Focus web page was born.

“Sector-Centric” Design: From the perspective of the METOC officer, the operating area is the known parameter. The Satellite Focus design is therefore sector-centric, with a “sector” defining the local operating domain—the finest resolution of a dynamically scalable hierarchy of spatial domains. Figure 4 illustrates the simple concept of sectors residing within a larger focus region. Overlaid on this Meteosat-5 enhanced infrared image are colored boxes delineating various sectors within a region of interest. For example, the Arabian Gulf (green box) sector resides in the OEF Middle East region. The OEF Middle East region, in turn, is defined as a box within the greater Southwest Asia region (not shown), and the entire globe is partitioned into many such regions. All satellite imagery products created for a sector share common dimensions and therefore are easily compared against each other—an invaluable utility for analysis.

The Product Suite: The Satellite Focus web page features many new products tailored to the difficult realities of this region. Among these products are tools for observing desert dust storms; nocturnal low clouds and fog; snow/cloud distinction; deep convection and rainfall; aircraft contrails; and general mesoscale meteorology. Several existing products required careful refinement to function properly in the OEF environment. Others, such as the desert dust enhancement

(see “A New Desert Disenhancement Technique Applicable to Near Real-time MODIS Data over both Ocean and Land,” by S.D. Miller, feature article in this *Review*), represent new technologies developed specifically for OEF applications. Near real-time telemetries from a growing constellation of civilian and DOD geostationary and polar orbiter satellites fuel the Satellite Focus “engine.” Thanks to considerable efforts by NOAA/NASA agency counterparts to support DOD efforts during OEF, a streamlined flow of global data from the MODerate-resolution Imaging Spectroradiometer (MODIS) now provides a boon of new information over previously data-void locales throughout the Southwest Asia domain.

The Web Interface: The internet-based graphical user interface of Satellite Focus evolves dynamically as users introduce or remove basins, regions, sectors, and imagery products. Pop-up buttons display all available products, with additional options for viewing archived imagery, customized animation, and multi-image mosaics. Online tutorials support steep learning curves for new satellite products. Low-bandwidth accommodations include intermediate thumbnail imagery at reduced quality, with secondary options for full-quality download. Figure 5 depicts an example page layout, with orientation buttons in the upper panel, available products in the left panel, and the current display in the main field. The Satellite Focus codes are forward-deployable and customizable to specific user domain/product needs.

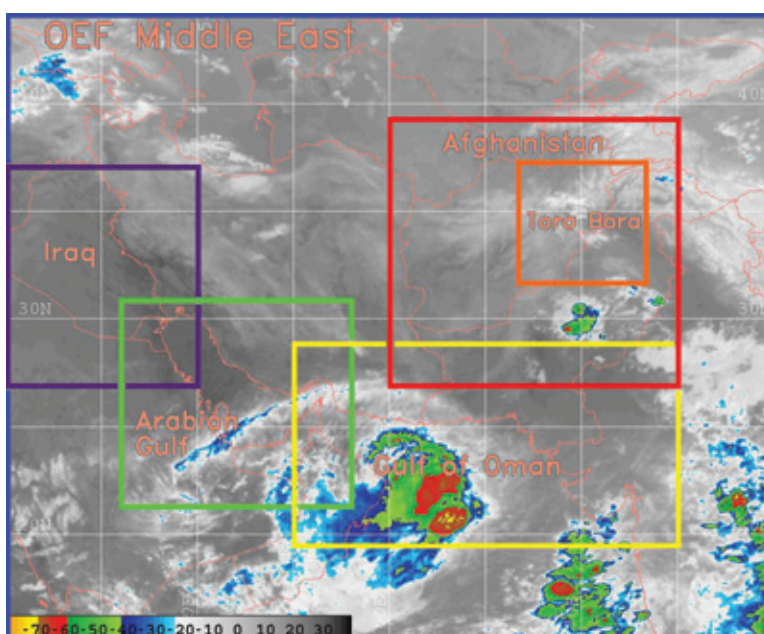


FIGURE 4
The OEF Middle East region is partitioned into several sectors (colored boxes), from which users can zoom-in to view higher resolution products.

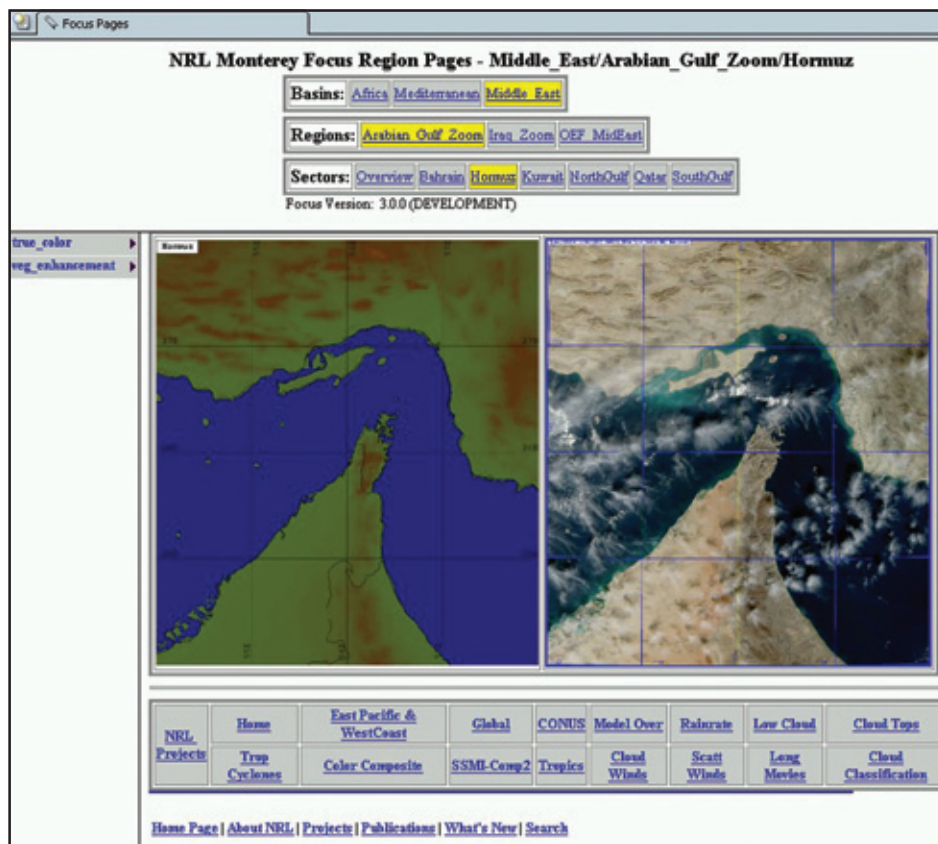


FIGURE 5
Example of the Satellite Focus web interface layout, honing in on the Strait of Hormúz with 250-m resolution MODIS true-color imagery.

Payoff—Linking to the WarFighter: Network bandwidth constraints aboard Navy ships required hosting Satellite Focus on Secure Internet (Siprnet). Coordination with Fleet Numerical Meteorology and Oceanography Center (FNMOC) made this access possible. Regular correspondence between NRL scientists and METOC officers has accelerated the spin-up for products now being used in daily briefings both ashore and afloat (distributed from carrier and amphibious assault ships among battle group members and coalition forces). NRL currently maintains seven focus regions within the Southwest Asia OEF domain, with the majority of these initiated upon direct requests from users in the arena. With the current package, we are poised to react literally in a matter of minutes to any need, worldwide, with a fully dynamic interface for NRL value-added satellite products—an agility that is critical to supporting DOD METOC in the War on Terror.

Acknowledgments: We thank FNMOC for Siprnet coordination, NOAA/NASA for MODIS data support, and METOC officers aboard the USS *Abraham Lincoln* (CVN 72) and USS *Belleau Wood* (LHA 3) for their valuable feedback.

[Sponsored by SPAWAR]



NRLMSISE-00: A NEW EMPIRICAL MODEL OF THE ATMOSPHERE

J.M. Picone, D.P. Drob, and R.R. Meier

Space Science Division

A.E. Hedin

Universities Space Research Association

Introduction: NRL has completed the new NRLMSISE-00 empirical model of the atmosphere for worldwide distribution to operational users and scientists.¹ MSIS stands for Mass Spectrometer and Incoherent Scatter Radar, the two primary data sources underlying early versions of the model, and E indicates that the model extends from the ground to space, as opposed to early versions that covered only the upper atmosphere or “thermosphere” (altitude > 90 km). NRLMSISE-00 represents the culmination of an effort to preserve and radically extend NASA’s MSIS technology so that future military and scientific users could exploit the model’s advantages. The model calculates composition, temperature, and total mass density, and is the standard for international space research. Improvements have focused on the thermosphere, which offers the potential for a number of vital operational and scientific applications.

NRLMSISE-00 accounts for the main drivers of the upper atmosphere: the solar extreme ultraviolet (EUV) flux and geomagnetic heating. The 10.7-cm solar radio flux ($F_{10.7}$) is the standard proxy for the solar EUV, while the A_p daily geomagnetic index measures the geomagnetic component of space weather. The next section outlines improvements that make NRLMSISE-00 a strong candidate to replace the 30-year-old Jacchia-70 model as the standard for space object orbit determination and prediction by the Navy and the Air Force. The next-generation Air Force orbit model has already adopted the MSIS representation of the lower atmosphere to eliminate a glaring deficiency of Jacchia-70, which works only for altitudes above 90 km.

Revolutionary Improvements: For the first time, this MSIS-class model assimilates total mass density values determined from drag on satellites and other space objects while retaining the traditional mass spectrometer and radar databases. The addition of drag data to the NRLMSIS database on composition and temperature gives the model a foundation superior to that of the Jacchia models, which are based primarily on orbital drag data produced in the 1960s. In contrast, the NRLMSIS database now covers the last four decades, with notable NRL

upgrades of the temperature and molecular oxygen (O_2) data sets. As a result, the NRLMSISE-00 model has potential applications in precision orbit determination, space object re-entry, ionospheric forecasting, ionospheric D-region absorption of high-frequency signals, and infrasound site location.

Our development work has opened several important areas of scientific study, including the resolution of contradictory measurements of molecular oxygen in the lower thermosphere, enhancement of molecular ions in the ionospheric F-region by geomagnetic storms, and spacecraft drag due to ionospheric oxygen ions and hot atomic oxygen. Molecular oxygen is of critical importance in prediction of the ionospheric F-region and in the inversion of new remote sensing data from the NRL/Space Test Program ARGOS satellite mission. Earlier MSIS-class models lacked data for O_2 at higher solar activity and depended primarily on data from mass spectrometers flown by NASA during the 1970s when the EUV flux was low. The early models then used temperature data to extrapolate the estimated O_2 concentration to elevated solar conditions.

NRL has now acquired O_2 data from solar ultraviolet absorption measurements aboard the NASA Solar Maximum Mission (SMM) to generate

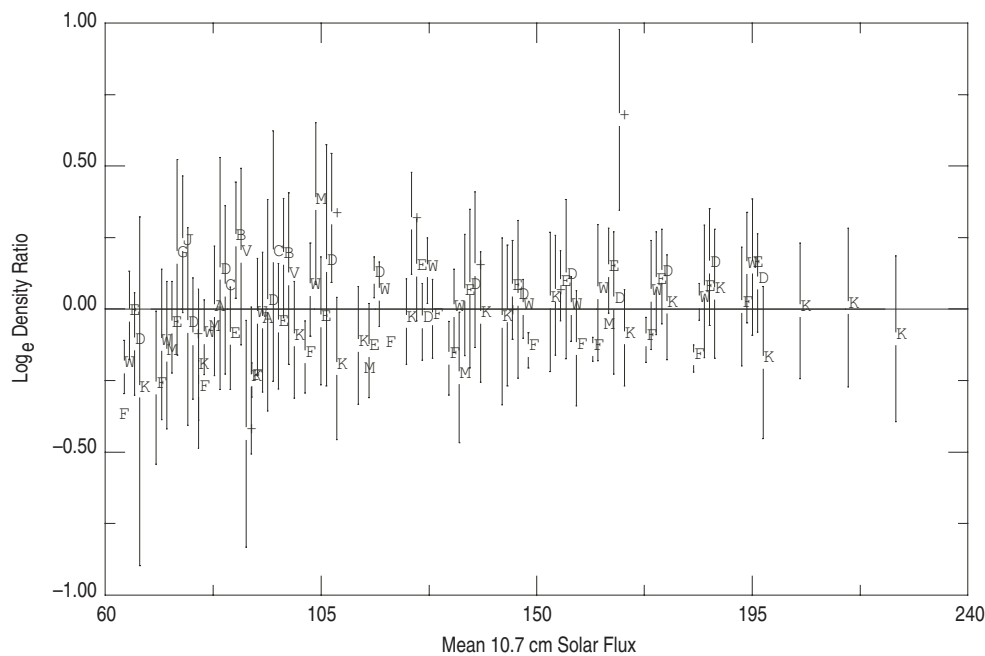


FIGURE 6(a) Natural logarithm of lower thermospheric $[O_2]$ vs 81-day mean $F_{10.7}$, averaged within bins of 10 flux units. The plot shows the bin-averaged data values normalized by NRLMSISE-00. Vertical bars correspond to the $\pm 1\sigma$ range of normalized $[O_2]$ values within each bin. NRLMSISE-00 corresponds to the horizontal line at 0.0. Symbols: C, G, J, +, mass spectrometer data; A, B, D, E, F, M, V, W, solar ultraviolet absorption data (100-150 km); K, SMM data (140-200 km).

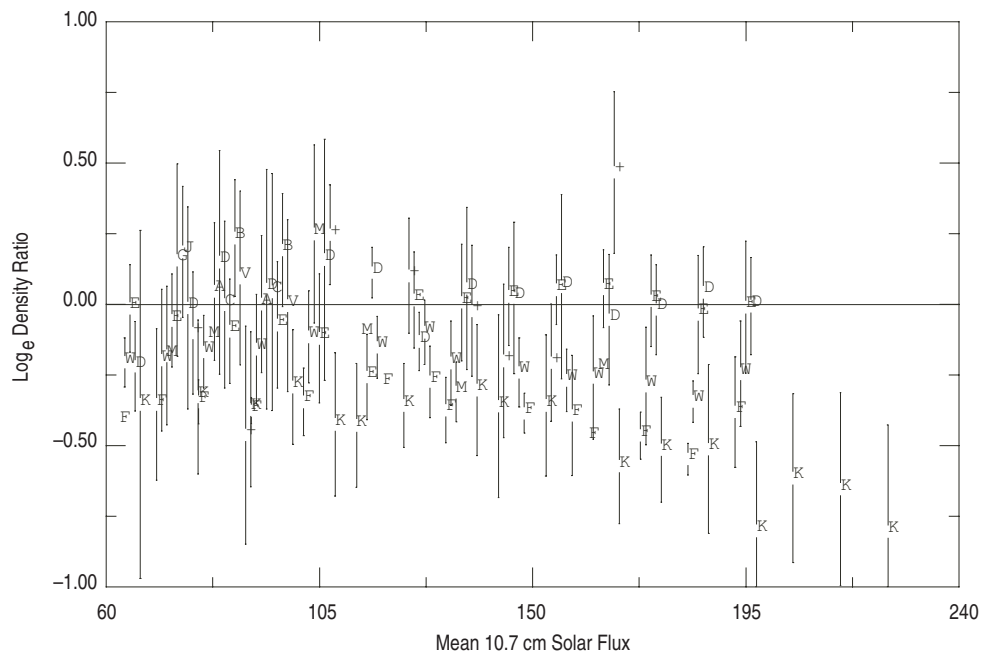


FIGURE 6(b)

Same as (a), but with data normalized to the older MSISE-90 model, which corresponds to the horizontal line at 0.0.

NRLMSISE-00 across a wide range of solar EUV and altitude. This has drastically changed the model predictions (Fig. 6). Figure 6(a) shows the logarithm of the ratio of the O_2 data to the NRLMSISE-00 model density as a function of solar activity ($F_{10.7}$). The horizontal line at a value of 0.0 corresponds to the new model (ratio = 1). The vertical bars signify the range of values of the data relative to the model, and the clustering of the data around the NRLMSISE-00 line signifies a good fit across several decades of data, including the SMM data (symbol “K” on the plots). Figure 6(b) shows a similar comparison to the previous model, NASA’s MSISE-90, which does not match the weak solar EUV dependence of SMM. Early applications of the new model by ionospheric scientists have shown great promise in resolving past paradoxes and improving the model predictions.

Recent investigations of low Earth orbit (LEO) drag have shown that the operational atmospheric model, Jacchia-70, erroneously attributes nonthermospheric drag sources to atomic helium (He). We now have evidence that these sources consist of “hot” atomic oxygen and ionospheric atomic oxygen ions (O^+), which can be of primary importance during the summer at high latitudes and altitudes above 600 km. Since neither of these species is in thermal equilibrium with the thermosphere, the new NRLMSISE-00 model treats them as a new component to drag called

“anomalous oxygen.” In addition to capturing the effects associated with anomalous oxygen, NRLMSISE-00 provides a superior fit to the corresponding *winter* Jacchia drag data at altitudes above 600 km, as compared to the Jacchia-70 model. The new model also eliminates deficiencies found in the Jacchia model for the summer hemisphere at very low solar activity.

New Directions: NRL has now become an international center for assimilative upper atmosphere models and is developing new applications of the NRLMSISE-00 model, including analysis of ultraviolet remote sensing data for precise orbit determination and prediction, accurate upper atmospheric composition for ionospheric forecasting, and ground-to-space atmospheric data assimilation for infrasound site location. NRL scientists are also using NRLMSISE-00 along with long-term orbital drag data to evaluate human-induced change in the upper atmosphere over several decades and to test new solar EUV proxies for more accurate prediction of the thermospheric state.

[Sponsored by ONR]

Reference

¹J.M. Picone, A.E. Hedin, D.P. Drob, and A.C. Aikin, “NRL-MSISE-00 Empirical Model of the Atmosphere: Statistical Comparisons and Scientific Issues,” *J. Geophys. Res.*, doi:10.1029/2002JA009430, in press (2003).



FREE-SPACE HIGH-SPEED LASER COMMUNICATION LINK ACROSS THE CHESAPEAKE BAY

C.I. Moore,¹ H.R. Burris,² M.R. Suite,¹ M.F. Stell,² M.J. Vilcheck,¹ M.A. Davis,³ R.T. Smith,¹ R. Mahon,⁴ W.S. Rabinovich,⁵ J.P. Koplrow,⁵ S.W. Moore,⁵ W.J. Scharpf,¹ and A.E. Reed¹

¹Space Systems Development Department

²Research Support Instruments, Inc.

³Honeywell T.S.I.

⁴Jaycor, Inc.

⁵Optical Sciences Division

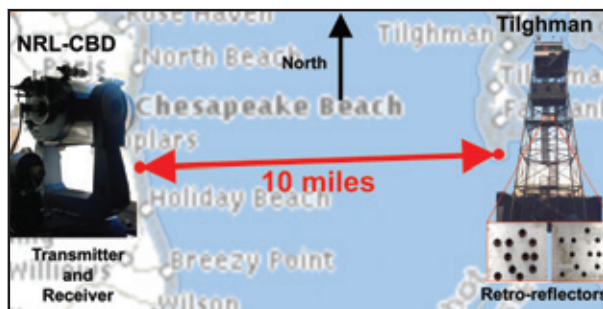
Introduction: The development of free-space optical laser communications (FSO lasercomm) is key to DOD's effort to transform the country's National Security Space Infrastructure. FSO lasercomm offers great advantages over conventional RF communications technology. Advantages include higher data rates, low probability of intercept, lower power requirements, smaller packaging, and lower frequency allocation requirements. However, there are also difficulties in implementation of a practical FSO lasercomm system for Naval and space-based platforms: attenuation in the atmosphere, scattering of signal due to atmospheric turbulence, high-precision tracking requirements between moving platforms, etc. The Space Systems Development Department (SSDD) and the Optical Sciences Division have joined forces to investigate and solve many of these difficulties. This joint effort involves the Optical Sciences Division's development of compact and high-efficiency laser amplifiers and high-speed modulators suitable for space-based or Naval platforms¹ and the SSDD's development of an FSO lasercomm test bed at NRL Chesapeake Bay Detachment (CBD) to test these components in a realistic environment.² A maritime environment provides an excellent location to test the worst-case limits of a Naval FSO lasercomm system in a wide range of atmospheric conditions.

FSO Lasercomm Test Bed at CBD: The test bed uses an eye-safe 1550-nm laser operating at 2.5 W, and it consists of a round-trip FSO lasercomm link across the Chesapeake Bay between CBD and NRL-Tilghman Island (Fig. 7). The transmitter and receiver of the lasercomm system are both located at CBD, and an array of corner cube retro-reflectors is located on Tilghman Island. Because only approximately 0.4% of the beam is intercepted by the retro-reflectors, this link is equivalent to a one-way link distance of approximately 72 km.

The received beam is collected with a 16-in. telescope and focused on either a high-speed detector for communication link-quality assessments or a position sensitive detector (PSD) for studies of atmosphere-induced turbulence effects.

High-speed Communication Link: Initial experiments at the CBD-Tilghman Island test bed have successfully demonstrated a communication link operating at up to 500 Mbps. Communication link-quality is measured using a high-speed transmitter and receiver, with modulation rates from 100 to 500 Mbps. The transmitter is modulated with a pseudorandom-bit-sequence (PRBS) from the pattern generator of a bit-error-rate (BER) tester. The received signal is processed in the receiver portion of the tester where a BER is output. The BER of the received signal is measured at 5-s intervals over 2 min for 100, 200, 300, 400, and 500 Mbps. No significant change in average BER is observed between these data rates. Figure 8 is a histogram of the BERs observed at these five data rates. The data show that the BER is below 10^{-5} 89.7% of the time and below 10^{-4} 97.4% of the time.

Atmospheric Turbulence: Turbulent cells in the atmosphere induce significant variation in both the pointing (angle-of-arrival) and intensity (scintillation) of laser beams used in terrestrial FSO lasercomm links. These angle-of-arrival variations and scintillations are the same effects that cause "image dancing" of objects observed over hot surfaces and the flickering of stars. Figure 9 is an example of data



Background courtesy of MAPQUEST

FIGURE 7 NRL-CBD to Tilghman Island FSO lasercomm test bed. Bistatic transmitter and receiver at CBD (left) and corner-cube retro-reflector arrays mounted on the tower on Tilghman Island (right).

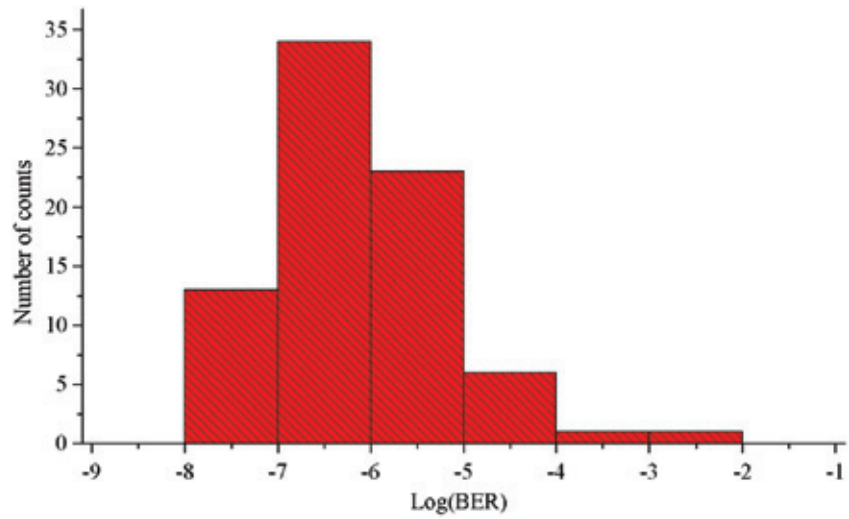


FIGURE 8
Histogram of all bit-error-rates measured at 100, 200, 300, 400, and 500 Mbps.

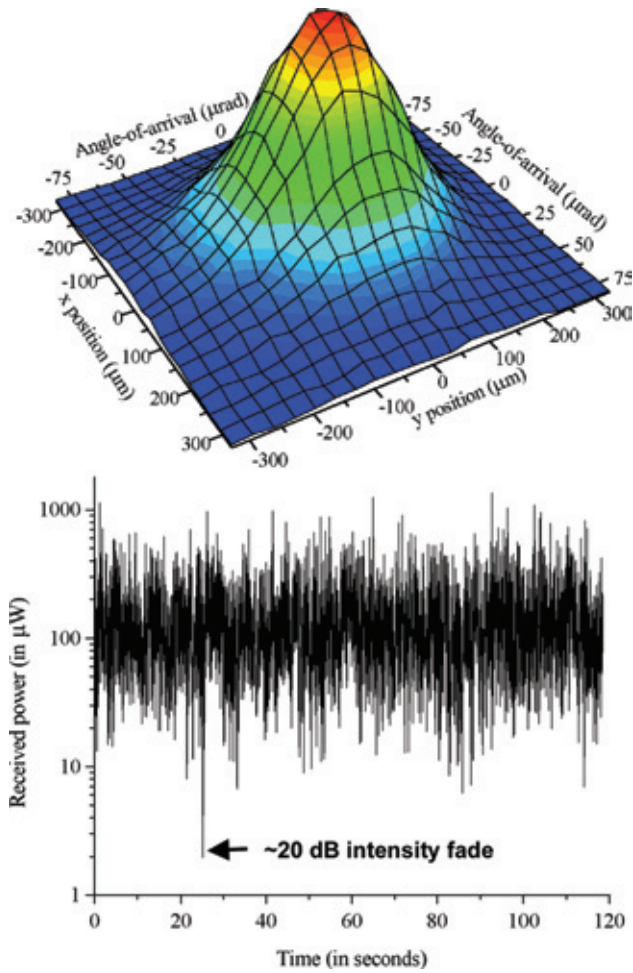


FIGURE 9
Histogram of the angle-of-arrival of received beam centroid (top) and intensity of received signal over a 2-min interval (bottom). The angle-of-arrival histogram has centroid displacement labeled in both millimeters of displacement on the PSD and angle-of-arrival into the telescope.

acquired with the PSD. This figure shows the angle-of-arrival (top) and scintillation (bottom) of the received beam over a 2-min interval. The angle-of-arrival plot is a histogram of the received spot centroid position on the PSD and the corresponding angle-of-arrival into the receiver telescope. Since high-speed data links typically require small detectors (~10s of microns), these angle-of-arrival variations can cause the received beam to miss the detector and introduce errors in the link. The scintillation plot shows the large variations in received intensity and a particularly deep "fade" (~20 dB) at 25 s. Intensity scintillations can introduce errors in a link as the results of received intensity levels falling below the detection threshold of the receiver. These turbulence effects are the greatest difficulty associated with a terrestrial FSO lasercomm system, and the mitigation of these effects is the main subject of FSO lasercomm research at NRL and elsewhere.


Future Work: Future work will concentrate on improving the quality, reliability, and speed of the link. The experiments described above do not use active tracking or atmospheric mitigation techniques. A fast steering mirror is being added to the system to reduce angle-of-arrival fluctuations and improve the overall BER and reliability of the link. Higher speed transmitters, receivers, and drive electronics will be used to allow increased data rate transmission, with the ultimate goal of 40 Gbps. Error control coding, adaptive thresholding,³ and

other processing techniques will also be implemented to further reduce the BER of the link.

Summary: The establishment of this test bed allows multiple experiments to be performed. These experiments include testing of FSO lasercomm components, studies of atmospheric turbulence and transmission effects on an FSO lasercomm system, atmospheric turbulence mitigation techniques, and maximum achievable data rates as a function of atmospheric conditions. The successful demonstration of this link shows that high-speed FSO lasercomm links in a maritime environment are possible between locations separated by large distances. The link demonstrated here is the longest, highest speed FSO lasercomm link near ground level ever demonstrated.

[Sponsored by ONR]

References

- ¹J.P. Koplow, S.W. Moore, and D.A.V. Kliner, "A New Method for Side-Pumping of Double-Clad Fiber Sources," in *J. Quantum Electron.*, to be published.
- ²C.I. Moore, H.R. Burris, M.R. Suite, M.F. Stell, M.J. Vilcheck, M.A. Davis, R. Smith, R. Mahon, W.S. Rabinovich, J. Koplow, S.W. Moore, W.J. Scharpf, and A.E. Reed, "Free-space High-speed Laser Communication Link across the Chesapeake Bay," in *Free Space Laser Communication and Laser Imaging II, SPIE Proc.*, to be published.
- ³H.R. Burris, N.M. Namazi, A.E. Reed, W.J. Scharpf, C.I. Moore, M.J. Vilcheck, M.A. Davis, M.F. Stell, M.R. Suite, W.S. Rabinovich, and R. Mahon, "A Comparison of Adaptive Methods for Optimal Thresholding for Free-space Optical Communication Receivers with Multiplicative Noise," in *Free Space Laser Communication and Laser Imaging II, SPIE Proc.*, to be published. 



KOREAN WAR MEMORIAL.

From 1950 to 1953, the United States joined with United Nations forces in Korea to take a stand against what was deemed a threat to democratic nations worldwide. The Korean War Veteran's Memorial honors those Americans who answered the call, those who worked and fought under the most trying of circumstances, and those who gave their lives for the cause of freedom.

- 113** Protein Crystal Surfaces at Molecular Resolution
J.H. Konnert and S. Gorti
- 114** Orientation, Manipulation, and Assembly of Carbon Nanotubes
P.E. Pehrsson and J.W. Baldwin
- 117** Creating Chemical and Biological Diamond Interfaces
J.N. Russell, Jr., J.E. Butler, R.J. Hamers, L.M. Smith, and S.F. Bent
- 120** An Improved Method for TNT Analysis in Ground Water, Seawater, and Soil
E.R. Goldman, G.P. Anderson, and J.M. Mauro
- 122** An Automated, Portable Array Biosensor
F.S. Ligler, J.P. Golden, Y.S. Shubin, L.C. Shriver-Lake, J.B. Delehanty, K.E. Sapsford, and C.R. Taitt

[BACK TO CONTENTS](#)

PROTEIN CRYSTAL SURFACES AT MOLECULAR RESOLUTION

J.H. Konnert
Laboratory for Structure of Matter
S. Gorti
Marshall Space Flight Center

Introduction: The atomic force microscope (AFM) is becoming an important tool for studying biologically active macromolecules. In particular, this concerns protein molecules that are appearing in great quantities in biological and medical research laboratories because of the success in determining the human genome. The profound importance of protein research lies in understanding biological processes and the implications for human health. X-ray crystallography is the most powerful analytical tool available for determining the three-dimensional arrangements of the atoms in these molecules. Because great advances have been made in techniques to extract the atomic structure of these molecules from X-ray diffraction data collected from single crystals,¹ the rate-determining step in these analyses is now often the growing of the required single crystals. The mechanisms by which crystals of these macromolecules grow are quite varied and complicated. The AFM, by probing the crystal surface in situ with a sharp tip, allows direct observation of these mechanisms.

Image Collection and Interpretation: The resolution of the AFM has improved to the point that images may contain features of 0.8 to 1.0 nm. When such features are observed, they result from small protrusions extending from the tip contacting the sample surface. Even though it is difficult or impossible to directly measure subnanometer features on a tip, these features must be characterized when analyzing a molecular resolution image. Additionally, surface atoms may be displaced from their equilibrium positions by interactions with the tip

To address these difficulties, analytical techniques have been developed at NRL. A theoretical image is constructed as a function of a molecular model of the crystal surface and a tip geometry. The molecular model and tip shape are adjusted to yield the best possible fit between the model and experimental AFM images. The experimental data illustrated here (and collected by S. Gorti while at NRL) are more accurate than earlier data² because much smaller forces were applied with the AFM. Although the model of the crystal surface is improved, the basic conclusions remain the same.

Example: We illustrate this technique with the analysis of the (110) face of tetragonal lysozyme, a protein molecule that is used in many laboratories to study the mechanisms of protein growth. Earlier low-resolution AFM data revealed that the growth steps on this face are two molecules in height, or 0.56 nm. Analysis of the known crystal structure revealed two distinct ways that molecules might add to the crystal to produce the 0.56-nm steps. Each may be associated with a different growth mechanism. Analysis of the AFM image displayed in the upper half of Fig. 1 indicated the surface structure to be quite similar to only one of the two possible "ideal" structures present in the interior of the crystal. The vertical columns of what appear to be dumbbells in the upper half of Fig. 1 are really columns of pairs of molecules. The molecules in each column are related by what will become vertically oriented 4_3 screw axes when they are covered by another growth step of molecules. The nearly correct model was refined by adjusting the positions of the molecules and the parameters defining the tip to maximize the agreement between the theoretical and the experimental images. The bottom half of Fig. 1 displays the molecules in the configuration determined by the refinement. Each molecule displayed in the bottom half of Fig. 1 has been moved approximately 0.4 nm from the positions they occupy within the bulk of the crystal. The result is that the surface molecules contact their nearest neighbors related by 4_3 screw axes more closely on the surface than within

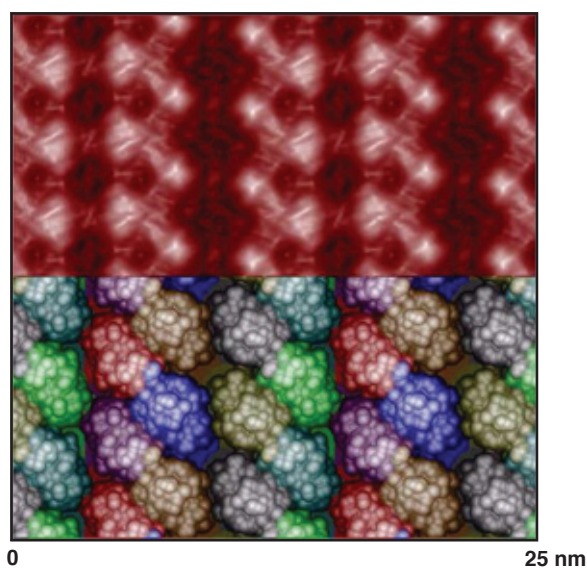


FIGURE 1
The top half displays an experimental image of the (110) face of a lysozyme crystal; the bottom half shows a proposed molecular model.

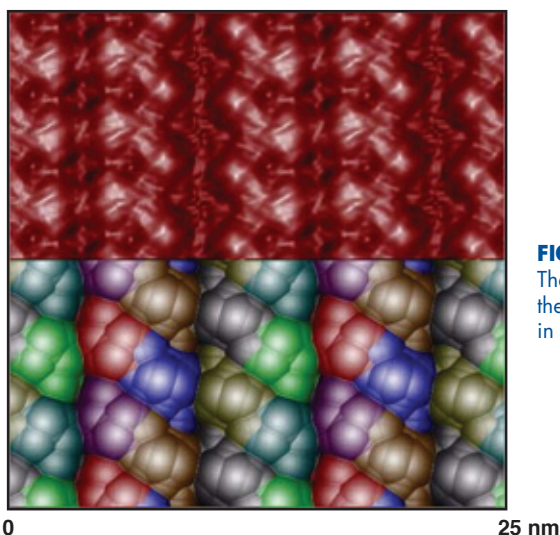
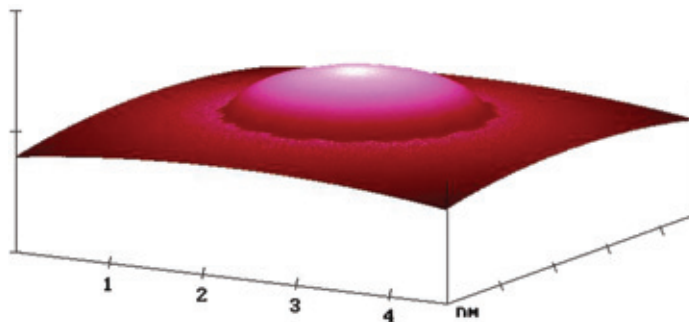


FIGURE 2

The top half is the experimental image; the bottom is the theoretical image formed by convoluting the model in Fig. 1 with the AFM tip in Fig. 3.

FIGURE 3

The AFM tip used to calculate the theoretical image in Fig. 2.




the crystal. Figure 2 compares the experimental image with the theoretical one computed by convoluting the “best” tip with the molecular surface displayed at the bottom of Fig. 1. The correlation coefficient relating the two images is a desirable 0.92. Figure 3 illustrates the “best” tip that is defined with four parameters.

Summary: Interpretation of the AFM data for the (110) face of has demonstrated which of the two mechanisms proposed for the addition of molecules to the growing crystal face is correct. Additionally the analysis reveals a surface reconstruction with intermolecular contacts at the surface different from those within the crystal.

[Sponsored by ONR and NASA]

References

¹J. Karle, “Some Developments in Anomalous Dispersion for the Structural Investigation of Macromolecular Systems in Biology,” *J. Quantum Chem.* **7**, 357-367 (1980).

²H. Li, M.A. Perozzo, J.H. Konnert, A. Nadarajah, and M.L. Pusey, “Determining the Molecular-packing Arrangements on Protein Crystal Faces by Atomic Force Microscopy,” *Acta Cryst.* **D55**, 1023-1035 (1999). 

ORIENTATION, MANIPULATION, AND ASSEMBLY OF CARBON NANOTUBES

P.E. Pehrsson and J.W. Baldwin
Chemistry Division

Introduction: Single-wall carbon nanotubes (SWNTs) are important because of their small size, quasi one-dimensionality, and potentially near-perfect lattice structure.¹ Variations in the SWNT diameter, chirality, and functionalization can render them metallic or semiconducting, with either n-type or p-type.² These properties will be exploited in applications using tubes for molecular wires, switches, nanoelectromechanical systems (NEMS), sensors, and other devices. But their small size and flexibility also pose major problems, because large numbers of tubes must be sorted and deposited onto specific locations and orientations on surfaces based on those properties. Unfortunately, present techniques for manipulating individual tubes (e.g., with a probe microscope) are slow and cumbersome, so other methods are needed.

We are exploring the use of nonuniform electric fields to selectively move electrically neutral nanotubes by dielectrophoresis (DEP) and charged tubes by electrophoresis (EP). Dielectrophoresis moves particles to the region of highest or lowest electric field, depending on the relative frequency-dependent conductivity and permittivity of the solvent and particle, the particle size, shape, and surface chemistry. The dielectrophoretic and electrophoretic forces are strongly affected by surface dipoles on the nanotube and at the electrode/liquid interface. A full description of the process includes Coulomb and dielectric forces, the frequency-dependent formation of an ionic double layer, and electroosmosis and electrohydrodynamics.

Using these techniques, we seek to purify, select, and direct the deposition of different tube types, and use detection and feedback to deposit specific numbers of tubes on a surface. This approach should also work for other nanostructures, e.g., nanoparticles and ensembles of tubes chemically or physically attached to other nanostructures, and facilitate efficient assembly of nanoscale circuits and other architectures from preassembled components.

Experimental: Nanotubes are deposited on a thermally oxidized Si wafer across opposing Au microelectrodes separated by a 1- μm gap. Figure 4 shows single-wall nanotubes suspended in dimethylformamide (DMF) deposit onto the electrodes when an ac sine wave (1 kHz to 2 MHz, 0-2 V peak to peak) with a DC offset is applied to one electrode while the other remains grounded. The resistance across the microelectrodes and a current-limiting resistor is monitored. Post-deposition current-voltage (I-V) data elucidate the electrical properties of the deposited tubes, and the solvent effects

on the inter- and intra-tube conductivity and tube/contact resistance. Some nanotubes are used as-grown, while others are chemically modified, e.g., with oxygen or fluorine, to introduce surface dipoles and change the tube polarizability; the latter can be used to adjust the forces exerted on the tube by the applied fields.

Results and Discussion: Appropriate ac and dc voltages separate the nanotubes and the contaminant particles present even in highly purified nanotube suspensions. The tubes typically deposit between the electrodes as 10-20 nm diameter bundles that can be isolated and straight (Fig. 5(a)) or tangled. Nanotube agglomeration is energetically favorable and probably partially responsible for the observed bundling, but it is also possible that the voltages used selectively deposit bundles rather than single tubes. Fluorinated tubes, shown in Fig. 5(b), also deposit between the electrodes with application of an ac voltage. Contaminant particles and tubes with charged functional groups such as the carboxylic acids and hydroxyls terminating acid-purified or damaged SWNTs respond differently than untreated tubes. In a static dc field, the tube ends align toward the positively charged anode and surround the electrode (seen as the dark corona around the left electrode in Fig. 5(c)). Such perimeter deposition does not occur for unfluorinated tubes. Only contaminant particles deposit between the electrodes Fig. 5(d), potentially presenting a method for their removal from the nanotubes solution.

Figure 6 shows that the I-V curve of tubes deposited between the electrodes is less linear (Ohmic) than that of the starting material, indicating that the deposited tubes may have a smaller ratio of metallic to semiconducting tubes. However, the properties of

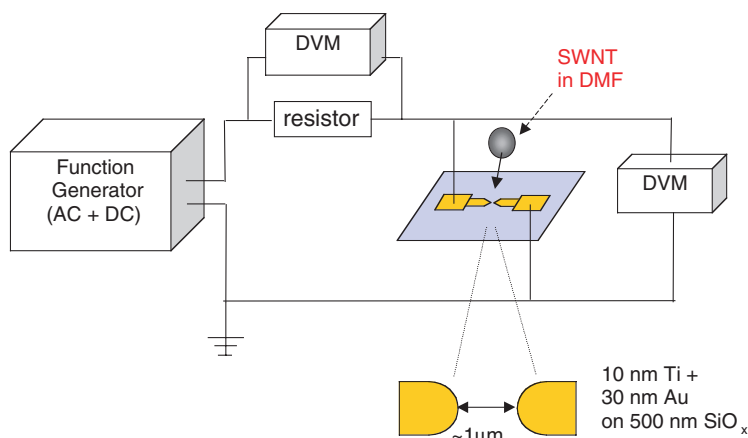


FIGURE 4
Schematic of the apparatus for deposition and alignment of carbon nanotubes.

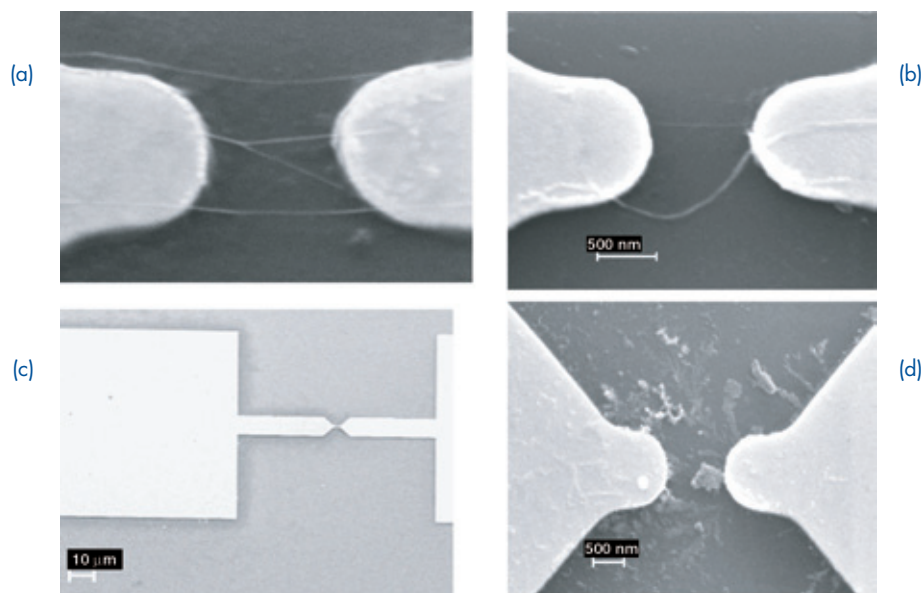


FIGURE 5
 (a) Untreated SWNT bundles deposited across electrode gap with 1 MHz ac and dc offset; (b) fluorinated nanotube (FSWNT) bundles deposited across gap with 100 kHz ac bias; (c) FSWNTs deposited around perimeter of (left) electrode biased with ac and dc offset; no tubes deposit on the grounded (right) electrode; (d) contaminant particles deposited between electrodes shown in c.

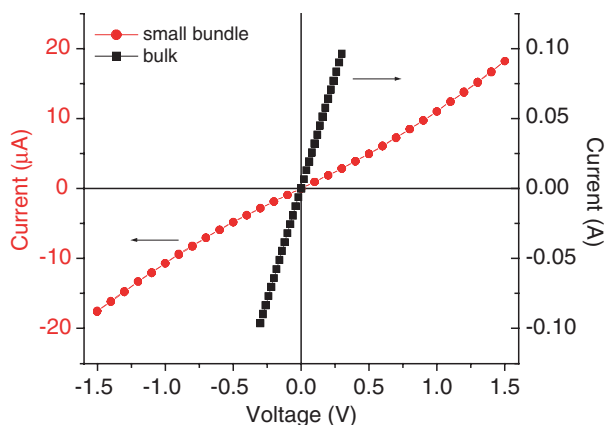


FIGURE 6
 I-V curve of nanotubes shown in Fig. 5(a) after solvent removal (circles) and a mat of the tubes deposited directly from solution (squares).

the tubes themselves are not the only consideration in characterizing the observed electrical behavior of the deposited nanotubes. The solvated tubes may have a higher contact resistance and intertube transmission barrier, which complicates the development of detection and feedback schemes to limit deposition to a desired number.

Conclusions: We use electric fields to separate metallic and semiconducting nanotubes, remove non-nanotube contaminants, and controllably assemble tubes at desired locations. These steps are essential prerequisites to practical, large-scale assem-

bly of nanoelectronic devices based on the potential of these materials.

Acknowledgments: The authors thank D.S.Y. Hsu for providing the electrodes.
 [Sponsored by ONR]

References

¹R. Saito, G. Dresselhaus, and M.S. Dresselhaus, *Physical Properties of Carbon Nanotubes* (Imperial College Press, London, 1998).
²Y. Cui and C.M. Lieber, "Functional Nanoscale Electronic Devices Assembled Using Silicon Nanowire Building Blocks," *Science*, **291**, 851-853 (2001).

CREATING CHEMICAL AND BIOLOGICAL DIAMOND INTERFACES

J.N. Russell, Jr.,¹ J.E. Butler,¹ R.J. Hamers,²
L.M. Smith,² and S.F. Bent³

¹*Chemistry Division*

²*University of Wisconsin*

³*Stanford University*

Overview: Developing organic synthetic routes for attaching organic and biological materials/structures to semiconductor substrates is important for the development of molecularly based electronic and sensing devices. We demonstrate several methods that promise to lead to molecular structures and functionality on diamond via thermal and photochemical means. We focus on diamond because of its chemical stability and biocompatibility.

Surface Cycloaddition Reactions:^{1,2} We draw our inspiration for chemical functionalization of the diamond surface from organic chemistry. To determine whether the hydrogen-free diamond (001) surface could be functionalized using cycloaddition chemistry, we used cyclopentene and 1,3-butadiene as chemical tests of the π -bonding nature of the hydrogen-free surface dimer bond. A type IIa natural diamond trapezoidal prism, oriented with the major faces exposing the (001) crystal planes, was mounted in an ultrahigh vacuum (UHV) chamber on a manipulator with a temperature range of 90 to 1473 K. Multiple internal reflection infrared spectroscopy (MIRIRS) was used to monitor the CH stretching region of the infrared spectrum. When the hydrogen-terminated diamond (100) surface was heated above 1323 K, the surface hydrogen recombined and H₂ desorbed. The resulting hydrogen-free surface was composed of partially π -bonded (partially di-radical) surface dimers.

Neither cyclopentene nor 1,3-butadiene reacted with the hydrogen-terminated surface. The molecules physisorbed intact at 90 K and desorbed without reaction. In contrast, the hydrogen-free C(001) surface reacted with both molecules at room temperature. Figure 7(a) shows unpolarized MIRIRS for cyclopentene chemisorbed on the C(001) surface at room temperature compared to the spectrum of a physisorbed multilayer of cyclopentene at 90 K. Note the alkene C-H stretch at $\sim 3050\text{ cm}^{-1}$ disappeared upon chemisorption, indicating the removal of the C=C bond in the chemisorbed molecule. The spectrum is consistent with cyclopentene chemisorbing via the reaction mechanism shown in Fig. 7(b).

We also examined whether butadiene would react with the H-free surface dimer to yield a [2+2] (cis or trans conformation) and/or a [4+2] (Diels-Alder) reaction product (Fig. 7(c)). The room temperature MIRIR spectra for the perhydro-butadiene and 1,1,4,4-d₄-butadiene dosed H free C(001) are compared in Fig. 7(d). The asymmetric and symmetric alkane (-CH₂-) stretches are observed. Using deuterium labeling, the alkene C-H stretch in the reaction product is associated with H on the 2 and 3 positions of the butadiene molecule. Meanwhile, the vinylic =CH₂ stretch in perhydro-butadiene disappeared upon reaction with the surface. The data are consistent with predominately a concerted [4+2] cycloaddition reaction mechanism.

The observation of a [2+2] reaction product for cyclopentene indicates a low symmetry reaction route, which accesses the di- σ -radical character of the dimer. In the case of butadiene, where the molecule could react to yield a product via the [2+2] or [4+2] reaction pathways, the [4+2] reaction product is favored. This illustrates the π -bonding character of the C(001) dimer bond and the higher probability of the high symmetry reaction when it is available. Thus, the surface is composed of partially π -bonded dimers. This work demonstrates the viability of organic synthetic routes for functionalizing diamond surfaces.

Photochemical Surface Attachment:^{3,4} As noted above, the hydrogen-terminated diamond surface is unreactive at room temperature. By leveraging the UHV studies, we developed a UV photochemical process for reacting alkenes with the “chemically inert” hydrogen-terminated diamond surface under ambient conditions. Five to 10 μL of trifluoroacetamide-protected 10-aminodec-1-ene (“TFAAD”) were placed directly on a freestanding (1-mm thick) hydrogen-terminated diamond film in a nitrogen-purged Teflon reaction chamber with a quartz window. The sample was exposed for about 12 hours to ultraviolet light from a low-pressure mercury vapor quartz grid lamp ($\lambda_{\text{max}} = 254\text{ nm}$, $0.35\text{ milliwatt/cm}^2$). The samples were rinsed in chloroform, then methanol, before X-ray photoelectron spectroscopy (XPS) analysis.

Figure 8 shows the C(1s), F(1s), and N(1s) XPS before and after photochemical surface modification with TFAAD. Before modification, the carbon spectrum has one major peak centered at 285.5 eV, corresponding to bulk carbon (off-scale on the right-hand side of the spectrum). After modification, the carbon spectrum developed two new peaks at 293.9 eV and 289.8 eV from the -CF₃ and carbonyl (C=O) groups, respectively. Fluorine (F(1s): 689.6 eV) and nitrogen

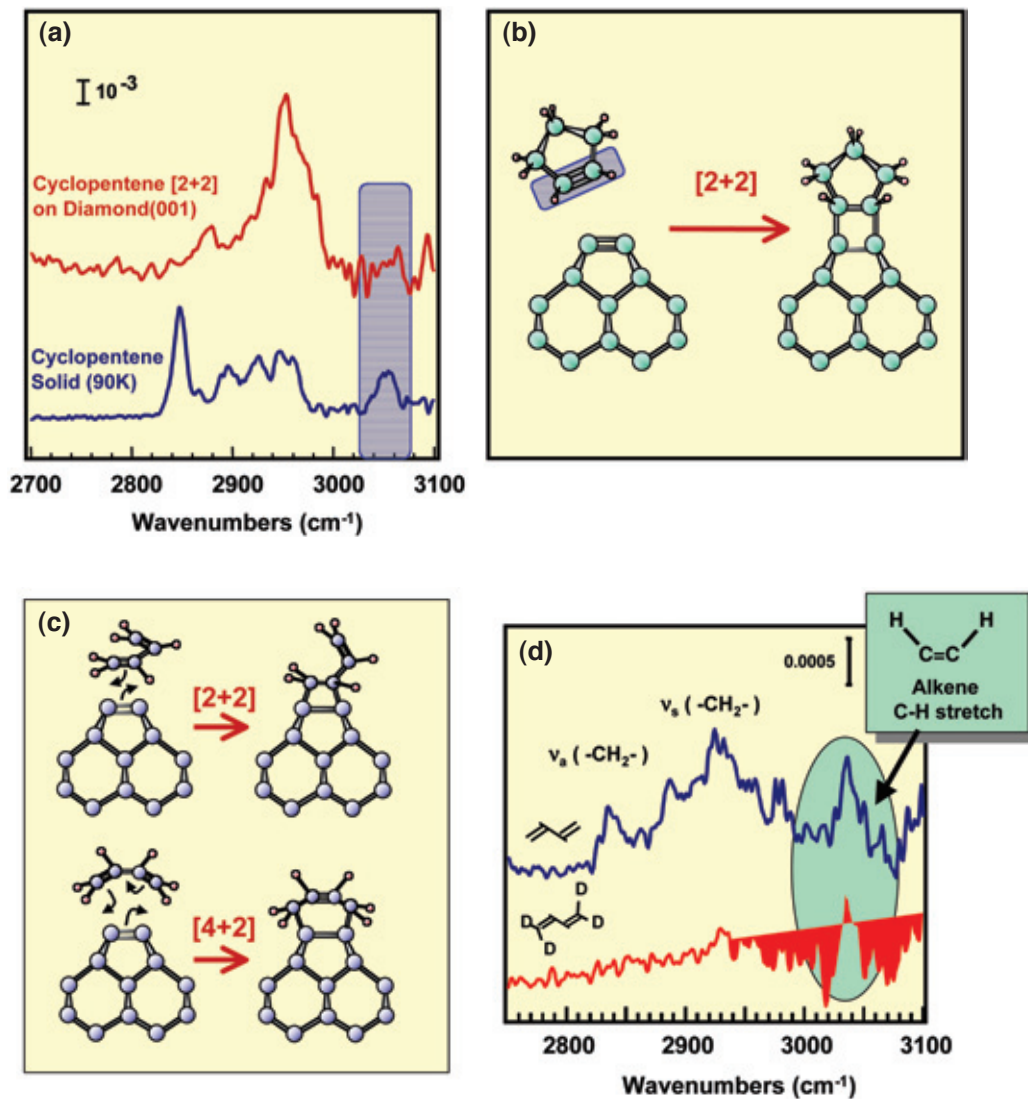


FIGURE 7

(a) MIRIRS of cyclopentene on a diamond (001) surface (note the loss of the alkene C-H stretch at $\sim 3050 \text{ cm}^{-1}$); (b) Illustration of the [2+2] cycloaddition reaction; (c) Possible surface reaction mechanisms for 1,3-butadiene; (d) MIRIRS of butadiene on a diamond (001) surface.

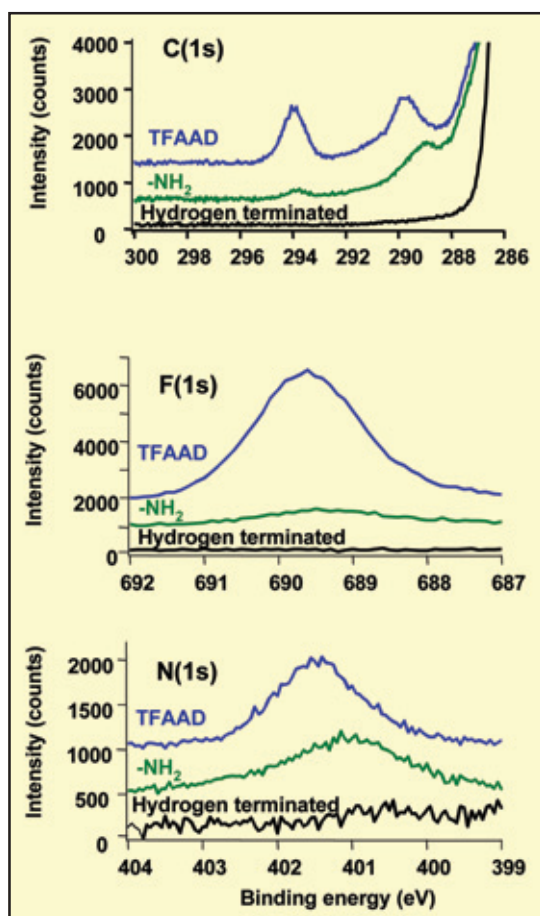


FIGURE 8
XPS data of TFAAD on diamond before and after deprotection. The hydrogen-terminated diamond spectra are shown for reference.

(N1(s): 401.4 eV) peaks from the trifluoroacetamide (TFA) protecting group also verified TFAAD attachment. TFAAD did not adhere to the surface without UV irradiation.

By refluxing the TFAAD-modified surface in 2:5 MeOH:H₂O with 7% (w/w) K₂CO₃, the trifluoroacetamide protecting group was removed, leaving the surface terminated with chemically reactive amine groups. Figure 8 also shows XPS spectra of the same sample after deprotection. Based on the changes in the C(1s) and F(1s) data, ~85% of the -CF₃ groups are removed by the deprotection process. The shift in the N1(s) binding energy is also consistent with a free amine.

DNA functionalization and stability:⁴ The amine-terminated diamond surface can be reacted with linker molecules that connect single-stranded DNA oligonucleotides to the surface. The stability of the oligonucleotide functionalized surface was investigated for repetitive cycles of hybridization and denaturation. In each cycle, the surface-bound DNA was hybridized with its fluorescently labeled complement and the fluorescence intensity was

measured. Then the sample was denatured at room temperature in an aqueous solution of 8.3M urea and rinsed with distilled water. No significant fluorescence loss was measured for the hybridized DNA-modified diamond after repeating the hybridization/denaturation process 15 times (Fig. 9). However, similarly prepared DNA-modified silicon surfaces lost 1.8 ± 0.4 % fluorescence per hybridization cycle or an ~27% loss after 15 cycles. We conclude that diamond substrates are well-suited for reproducible DNA sensing applications.

Impact: Schemes for chemically functionalizing the hydrogen-free and hydrogen-terminated diamond surfaces that use thermal and photochemical processes were demonstrated. The modified diamond surfaces are chemically robust. In particular, the DNA-functionalized diamond surface is well-suited to repeated and reproducible sensing applications.

Acknowledgments: The cycloaddition work was performed in collaboration with the University of Wisconsin and Stanford University groups. The pho-

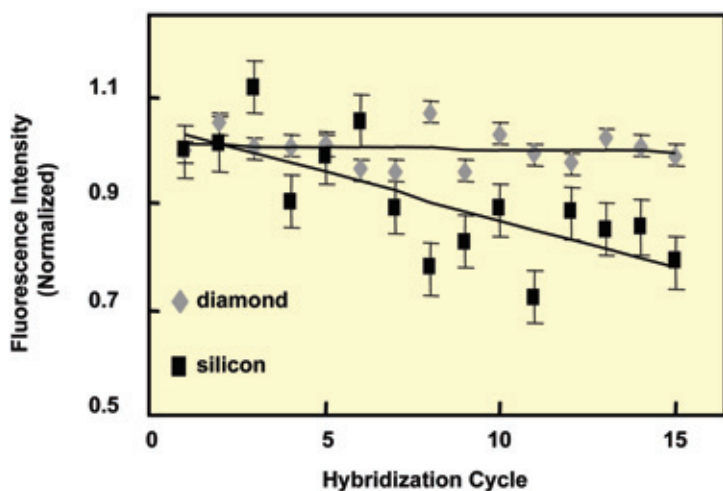


FIGURE 9
Direct comparison of the hybridization stability of DNA on diamond and silicon surfaces.

tochemical attachment and DNA work was in collaboration with the University of Wisconsin group. We thank Tanya Knickerbocker, Todd Strother, Michael Schwartz, Jennifer Hovis, and Sarah Coulter from the University of Wisconsin and George Wang from Stanford University for their valuable contributions.

[Sponsored by ONR, NSF, and NIH]

References

- ¹J.S. Hovis, S.K. Coulter, R.J. Hamers, M.P. D'Evelyn, J.N. Russell, Jr., and J.E. Butler, "Cycloaddition Chemistry at Surfaces: Reaction of Alkenes with the Diamond (001)-2x1 Surface," *J. Am. Chem. Soc.* **112**(4), 732-733 (2000).
- ²G.T. Wang, S.F. Bent, J.N. Russell, Jr., J.E. Butler, and M.P. D'Evelyn, "Functionalization of Diamond(100) by Diels-Alder Chemistry," *J. Am. Chem. Soc.* **112**(4), 744-745 (2000).
- ³T. Strother, T. Knickerbocker, J.N. Russell, Jr., J.E. Butler, L.M. Smith, and R.J. Hamers, "Photochemical Functionalization of Diamond Films," *Langmuir* **18**(4), 968-971 (2002).
- ⁴T. Knickerbocker, T. Strother, M.P. Schwartz, J.N. Russell, Jr., J.E. Butler, R.J. Hamers, and L.M. Smith, "DNA-Modified Diamond Films," *Langmuir* (2003), in press.

AN IMPROVED METHOD FOR TNT ANALYSIS IN GROUND WATER, SEAWATER, AND SOIL

E.R. Goldman, G.P. Anderson, and J.M. Mauro
Center for Bio/Molecular Science and Engineering

Introduction: The Navy is interested in TNT (2,4,6-trinitrotoluene) detection for monitoring the clean up of soil and ground water at former munitions manufacturing and storage facilities. On-site test methods are useful for assessing the nature and extent of contamination as well as for monitoring clean up processes. Current on-site tests involve

multiple steps and can require up to 2 hours to complete. We have invented a rapid, simple, and sensitive test method that is amenable to high throughput screening for the presence of TNT in water and soil samples.

The new assay was made possible by our discovery that binding a fluorescent TNT analog to an anti-TNT antibody increases the fluorescence emission of the analog. Free TNT added to a solution containing the antibody-bound fluorescent TNT analog competes with the analog for binding to the antibody. When fluorescent TNT analog releases from the antibody as TNT binds in its place, fluorescent emission from the sample decreases (Fig. 10), providing the basis for the analytical method we have developed. As more TNT is added, the signal decreases until TNT has replaced all the fluorescent TNT analog.

The Assay: We have developed two configurations of the new TNT assay: a solution-based assay format in which all reagents are in solution, and a solid-phase assay format in which the anti-TNT antibody is immobilized on a surface.¹ We routinely perform these assays in 96-well microtiter plates, allowing us to simultaneously process many samples.

The solution-based assay format has the advantage of having no washing or incubation steps. We add the antibody and fluorescent TNT analog to wells, then add the TNT-containing liquid sample to each test well, and read the fluorescence output in a standard fluorescent microtiter plate reader. A 96-well microtiter plate filled with samples can be processed in approximately 5 minutes. We have been able to detect TNT at a level of 0.5 ng/ml (0.5 ppb) in laboratory buffer (Fig. 11). TNT quantitation can be achieved by constructing standard curves in the appropriate concentration range using TNT standards of known concentration.

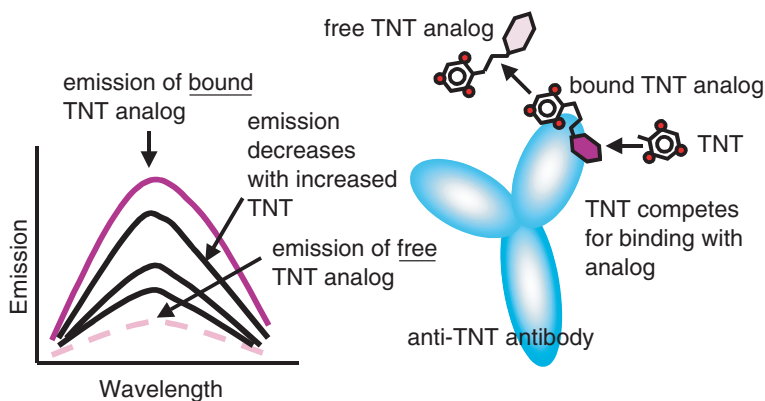


FIGURE 10
Fluorescent emission decreases as the antibody binds TNT in place of the fluorescent TNT analog.

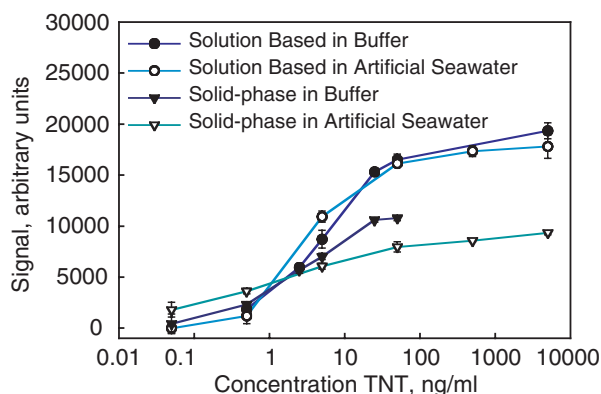


FIGURE 11
Analysis of TNT in laboratory buffer and artificial seawater.

In the solid-phase assay format, anti-TNT antibody is pre-bound by adsorption within the wells of polystyrene microtiter plates and then loaded with the fluorescent TNT analog. Excess unbound fluorescent analog is washed away, TNT-containing samples are added to the wells, and fluorescence output is measured for each sample. This format allows us to detect TNT down to a level of 0.5 ng/ml (0.5 ppb) in buffer (Fig. 11). This analysis format requires more setup than the solution-based assay. Antibody-coated plates are prepared a day before use, and about 15 minutes are needed to saturate the immobilized antibody with fluorescent TNT analog. We believe it should be possible to prepare and store plates loaded with antibody and fluorescent TNT analog to allow an assay time of less than 5 minutes per 96-well plate.

The limits of detection we have obtained using these assay formats are competitive with other on-site test methods for monitoring TNT in water. Comparing six on-site analysis methods for detecting explosives in water, only the RaPID Assay Kit had a lower reported level of detection (0.07 ppb TNT in water samples); however, it takes approxi-

mately 70 minutes to run 51 samples using the RaPID method.² In comparison, the solution-based format of the new assay can perform triplicate analysis of 51 samples in less than 10 minutes.

Our new test method also performs well for analyzing TNT present in artificial seawater. In this case, we can detect TNT at levels of 0.5 ng/ml (0.5 ppb) using the solution-based method and 0.05 ng/ml (0.05 ppb) with the solid-phase format (Fig. 11). This is an important finding, as some methods for detection of TNT do not work well in high saltwater concentrations like seawater, and often require additional dilution or extraction steps. Finally, we have tested methods for extracting TNT from contaminated soil samples followed by rapid screening or quantitative analysis using the new assay.

Conclusions: Based on our observation that binding of a fluorescent TNT analog to an anti-TNT antibody increases the fluorescence emission of the TNT analog, we have developed a test method that has great potential for use in efficient on-site detection and quantitation of TNT levels in ground water and soil. The formats we have tested are simple, rapid, and should be readily adaptable for high-throughput, parallel sample processing and automation. Our next goal is to use the new methodology to test for TNT in the field and to evaluate its sensitivity and reliability directly compared to other available detection and standard high-performance liquid chromatography-based methods.

[Sponsored by ONR]

References

- ¹E.R. Goldman, G.P. Anderson, N. Lebedev, B.M. Lingerfelt, P.T. Winter, C.H. Patterson, and J.M. Mauro, "Analysis of Aqueous 2,4,6-Trinitrotoluene (TNT) Using a Fluorescent Displacement Immunoassay," *Anal. Bioanal. Chem.*, in press.
- ²A.B. Crockett, H.D. Craig, and T.F. Jenkins, "Field Sampling and Selecting On-Site Analytical Methods for Explosives in Water," EPA/600/S-99/002; <http://www.epa.gov/swertio1/tsp/download/water.pdf>

AN AUTOMATED, PORTABLE ARRAY BIOSENSOR

F.S. Ligler,¹ J.P. Golden,¹ Y.S. Shubin,² L.C. Shriver-Lake,¹ J.B. Delehanty,¹ K.E. Sapsford,³ and C.R. Taitt¹

¹Center for Bio/Molecular Science & Engineering

²Geo-Centers, Inc.

³George Mason University

Introduction: To respond to a bioterrorist incident or enemy attack, rapid, easy-to-use sensors are urgently needed. Currently, several commercially available sensors are available that are capable of detecting biological weapons (BW) and other pathogens, but most of these sensors are not designed for rapid testing of multiple biological threats at the same time. We are developing an Array Biosensor to fill this unique requirement: rapid, field-deployable detection of multiple biological threats in different kinds of samples. The Array Biosensor uses antibodies as recognition elements to detect targets with high sensitivity and selectivity. A series of different “capture” antibodies are attached to the surface of a microscope slide at specific locations (arrays) and are used to grab threat agents out of the sample. A second, fluorescent “tracer” antibody binds to the captured target, and the resulting fluorescent “sandwich” is detected using a CCD camera. If multiple “capture” or “tracer” antibodies are used, each binding to a different BW agent or pathogen, we can simultaneously detect and identify multiple different targets on the same slide. The optical components of the system include a red diode laser, like that used in a laser pointer, and a digital camera. The assays are fast (10-15 min), sensitive, and specific.

To make the array biosensor portable for field use, we have developed and optimized a novel fluidics component milled in a plastic cube (Fig. 12). The fluidics cube allows the operator to preload all the necessary solutions and perform the test while simultaneously imaging the microscope slide. The en-

tire fluidics control system fits within a small tacklebox and can be operated in a fully automated fashion.

Variety of Tests: Because food and water sources are potential targets for bioterrorists, we have recently developed tests for pathogens for use in a wide variety of foods. Tests for a food poisoning agent, staphylococcal enterotoxin B (SEB), conducted on milk, homogenized ham, ground beef, cantaloupe, and eggs, were as sensitive as tests conducted in laboratory buffer. Tests for *Salmonella* showed equivalent results in ground cantaloupe, washes of chicken carcasses, bean sprouts, and eggs as in buffer. The presence of irrelevant bacteria, even in 1000-fold excess, did not interfere with *Salmonella* detection.

To increase the number of tests performed on a single slide, we used state-of-the-art technology developed during the Genome Project, an automated dispensing system, to deposit “capture” antibodies onto our slides. We have demonstrated that 32 tests can be performed in each lane, with up to six samples analyzed simultaneously. While 192 separate tests are shown (Fig. 13), this number can potentially be much greater. The limitation on the number of targets that can be screened for in each sample is primarily a function of image resolution and antibody availability.

Conclusions: The portable array biosensor (Fig. 14) addresses the need for rapid, sensitive, and specific analysis for multiple biohazards at the site of sample collection. We have demonstrated that the sensor is effective for rapid detection of pathogens, toxins, and clinical markers in a wide variety of sample types. Real-world testing is now underway for bioterrorism defense, infectious disease detection, food and water safety, and environmental monitoring applications.

[Sponsored by ONR, NSWC, NASA, EPA, and USDA]

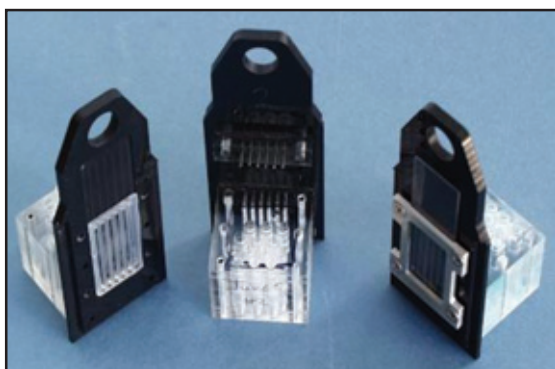


FIGURE 12

Ergonomically designed fluidics cube. The cube includes six reservoirs for sample and six reservoirs for fluorescent “tracer” antibodies. The solutions can be dried and stored inside the cube for extended periods. The cube unit also includes a flow channel device for passing the fluids over the microscope slide and a specially molded gasket for a fluid-tight seal. The protruding end of the unit is designed for easy handling and insertion into the optics box. The entire unit minimizes potential sources of leakage, size, and weight.

FIGURE 13

An automated printer, designed for depositing high-density arrays of DNA, was used to create patterns of capture antibodies on microscope slides. Eight spots of each capture antibody (indicated at the top) were immobilized in each lane. Six samples (indicated to the right of the image) were analyzed simultaneously for all four targets. Thus, 32 assays were performed per sample, yielding a total of 192 assays in 12 minutes. CT: Cholera toxin; B. glob: *Bacillus globigii*; SEB: Staphylococcal enterotoxin B.

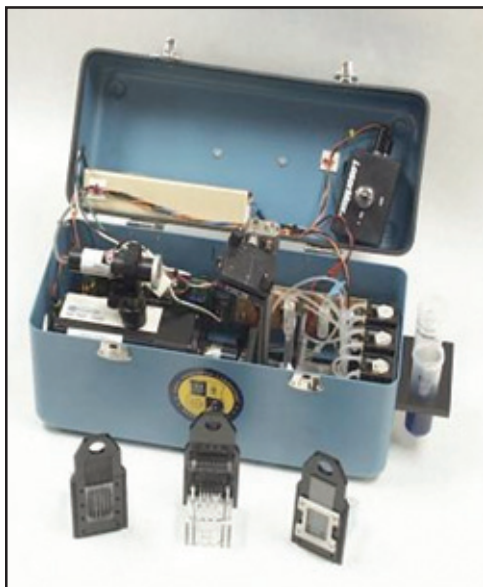
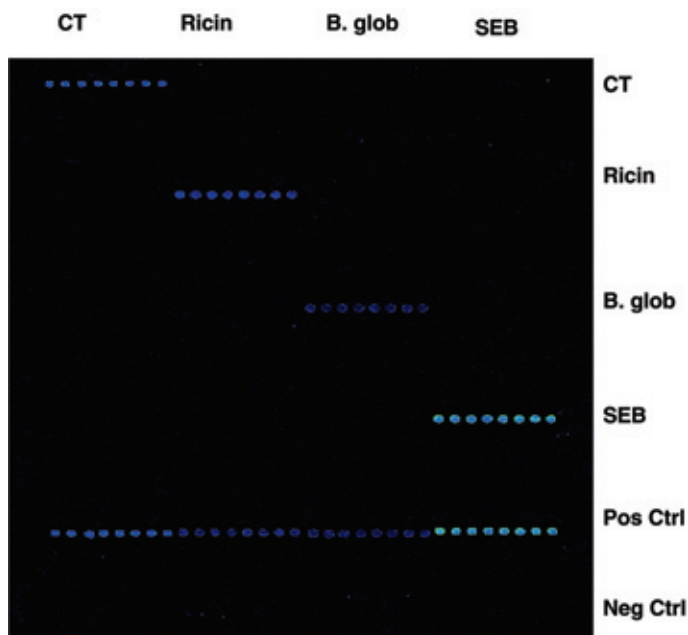


FIGURE 14

The portable array biosensor with fluidic cubes. To conduct a test, the cube is filled with six samples and fluorescent “tracer” antibodies. It is inserted into a spring-loaded Teflon slot. Three finger-sized peristaltic pumps draw the samples and fluorescent reagents across the microscope slide. Light emitted from a laser shines across the end of the waveguide, exciting any fluorescent “sandwiches” that form on the surface. A digital camera records the location of the fluorescent spots, and image analysis software quantifies the bound target.



MARINE CORPS WAR MEMORIAL.

Based on a Pulitzer Prize-winning photograph by Joseph Rosenthal, Felix de Weldon's powerful bronze work is popularly known as the "Iwo Jima Statue." By special presidential proclamation, its flag flies twenty-four hours a day.

- 127** EMI and EM Energy Transport in the Near Field
D.J. Taylor, M.G. Parent, and S. Samaddar
- 128** Detection and Imaging of Buried Objects
K.M. Scheff and J.P. Hansen
- 130** Imaging Stacking Fault Growth in SiC Diodes
R.E. Stahlbush, M.E. Twigg, and M. Fatemi
- 133** Long Spin Coherence Lengths for Quantum Devices
M.J. Yang, C.H. Yang, and Y.B. Lyanda-Geller

[BACK TO CONTENTS](#)

EMI AND EM ENERGY TRANSPORT IN THE NEAR FIELD

D.J. Taylor and M.G. Parent
Radar Division
S. Samaddar
Sachs Freeman Associates

Introduction: The propagation of electromagnetic (EM) energy through stratified dielectric media is a topic relevant to numerous Navy applications. Devices such as multilayer radomes, frequency-selective surfaces, and radar absorbers are designed based on models of how EM waves move through stratified dielectric media. However, the use of such devices in the near field of radiating or receiving antennas requires that knowledge of how electromagnetic waves interact with dielectric media be expanded beyond the simple models used to date. An understanding of the basic physics in this area will allow engineers to successfully design and integrate multiple antenna apertures into composite structures that will be part of next-generation naval vessels such as the DD(X) destroyer.

Research Approach: NRL is developing analytical and experimental methods at microwave frequencies for electromagnetics in the near fields of stratified dielectric media. These methods are aimed at detecting and characterizing wave motions with a noninvasive technique that will allow energy transport in laminated materials to be studied by using only EM wave fields measured in a region external to the structure. The research involves a combination of analytical studies of classic wave motion in laminated media of infinite extent, numerical simulations of electromagnetic wave interactions with dielectric media of finite size, and the development of sub-wavelength sensors to measure the EM fields associated with finite media. The fundamental issue is to extract information from the propagating and evanescent fields that exist near the surface of stratified dielectric media and are intimately coupled to energy transport within the structure. This extracted information can then be used to identify the spatio-temporal “fingerprint” of the transport mechanism involved.

EM Waves in Layered Media: EM wave transport in planar layered media of infinite extent is a classic boundary-value problem. When the source of the EM fields is at infinity and the incident fields are plane waves, the transport is expressed solely in terms of reflected and transmitted plane waves. If the source of the EM fields is a finite distance from

the dielectric interfaces, then the solution becomes multimodal in the sense that it contains physical mechanisms other than the reflected and transmitted plane-wave components. The wave-transport physics in the near field include not only the geometric-optics transmitted and reflected modes but also the guided-wave energy trapped in the layers and the interface modes (or “lateral waves”) that are excited due to the proximity of the source. It is these EM wave-transport mechanisms that will contribute to the EM interference (EMI) between future embedded phased-array antennas. The distribution of the EM fields associated with these modes is such that they extend into the region outside of the dielectric media. Depending on the nature of the mode, the corresponding component of the field can be propagating or evanescent. Sampling the fields just outside the dielectric, in the free-space region but very close to the interface, allows the detection of field energy from the propagating and evanescent modes. Classification and identification of these modes requires a transform to the temporal-frequency/spatial-frequency domain where dispersion, characteristics of the group and phase velocities, and determination of propagating versus evanescent can be made and associated with EM wave-transport mechanisms in the structure.

Simulating and Measuring Near EM Fields: The physical models for EM wave transport are based on solutions for unbounded, infinite-dimension, layered media; the physical problems encountered by the Navy are naturally finite in size. The analysis of EM fields near finite structures must be accomplished using numerical solutions of Maxwell’s equations or direct measurements. NRL is conducting research in both areas to provide EM field data for analysis. Figure 1 shows a snapshot of a time-domain simulation of fields generated by an array of 2-dimensional, electric line sources excited with a Gaussian pulse waveform that interacts with a planar dielectric slab. The array generates an EM wave with a localized planar wavefront that is reflected from and transmitted through the dielectric slab. At the time step shown in the figure, the radiated field from the array has passed through the slab; however some energy remains near the slab. This energy implies the existence of higher-order modes and has two origins: energy trapped in the slab, and diffracted energy from the termination of the structure.

Measurements of the fields very near to such a structure require a different type of sensor—one with high spatial resolution that faithfully captures the evanescent field modes, which exhibit a high spatial frequency component. Figure 2 shows a simple current-loop sensor designed to measure

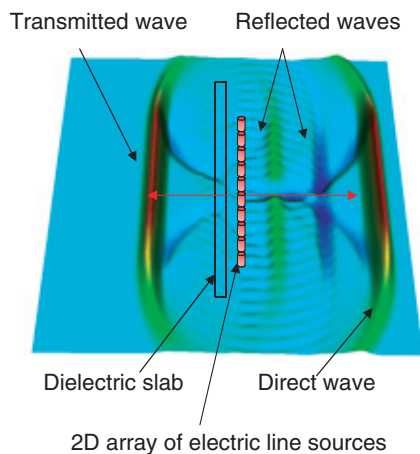
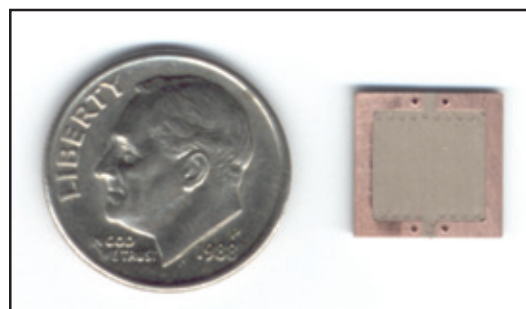


FIGURE 1 Simulated near-field amplitudes generated with a 2-dimensional FDTD (finite-difference time-domain) technique, for an array of 17 electric line sources that are excited by a Gaussian waveform in the presence of a dielectric slab (30-cm wide by 1.5-cm thick) with $\epsilon = 2.56$. At this particular time step, the pulse has passed completely through the slab; however, the presence of trapped energy in the slab and diffracted energy near the slab indicates the existence of higher-order modes in the structure.

FIGURE 2 Square current-loop probe for measuring the microwave magnetic field component normal to the loop at 3 GHz. The loop has an outer length of $\lambda/10$ (1 cm) at 3 GHz.



magnetic field strength at 3 GHz. This probe, others like it,¹ and the Radar Division's large planar scanner form the basis for experimental investigations into near-field EM wave phenomena exhibited by planar dielectric structures.

[Sponsored by ONR]

Reference

¹P.H. Harms, J.G. Maloney, M.P. Kesler, E.J. Kuster, and G.S. Smith, "A System for Unobtrusive Measurement of Surface Currents," *IEEE Trans. Antennas Propag.* **49**(2), 174-184 (2001).



DETECTION AND IMAGING OF BURIED OBJECTS

K.M. Scheff and J.P. Hansen
Radar Division

Introduction: A state-of-the-art ultrawideband (UWB) radar, designed and implemented by the Radar Division, is being used to develop techniques for the detection, imaging, and ultimate identification of objects buried near the Earth's surface.¹ This dual-frequency, dual-polarization, UWB radar system has performed ultra-high resolution measurements (2-

cm range resolution) of land mines and other objects in a laboratory setting. Initial free-space measurements are currently being used to develop and test imaging algorithms, as well as to explore the feasibility and limitations of various synthetic aperture radar (SAR) configurations.

Hardware and Measurement Geometry: This laboratory version of the UWB system has video impulse-excited X-band and S-band traveling wave tubes (TWTs) that produce transmit pulses with 2 W of peak power and durations of 0.15 and 0.25 ns (3 dB power envelope). Separated, dual-polarized, UWB (2-18 GHz) horn antennas are used for transmit and receive to maintain receiver isolation without the use of a duplexer. The receive system detects signals in coherent baseband quadrature form with a unique direct-sampling detector based on a multiple-sampling-head, 8-bit, digital sampling oscilloscope. The heads simultaneously sample the in-phase and 90° phase-shifted components of a received signal.

For this experiment, synthetic aperture is achieved by positioning and directing the transmit and receive antennas at fixed locations of a 1-m² data-collection grid via a rail system above the ground. With respect to the center of the grid, each target is centered in the y-dimension and is offset in

the x-direction (Fig. 3). The measurement system is configured so that the distance between the transmit-antenna and receive-antenna rails in the x-direction is constant. Both antennas are pointed at the target such that polarization direction is preserved (that is, vertical polarization is in the x-direction and horizontal polarization is in the y-direction). Data were collected every 2.5 cm along the receive-antenna rail at fixed antenna positions at X-band (0.15 ns) for three targets (a metallic land mine, a plastic land mine, and a calibration sphere) in free space.

Analysis: The amplitude images are formed in the time domain using

$$\text{Amplitude}_{x,y,z} = \sqrt{I_{x,y,z}^2 + Q_{x,y,z}^2},$$

where

$$I_{x,y,z} = \sum_{t,r} V_I \left(\sqrt{(x-x_t)^2 + (y-y_t)^2 + (z-z_t)^2} + \sqrt{(x-x_r)^2 + (y-y_r)^2 + (z-z_r)^2} \right)$$

and

$$Q_{x,y,z} = \sum_{t,r} V_Q \left(\sqrt{(x-x_t)^2 + (y-y_t)^2 + (z-z_t)^2} + \sqrt{(x-x_r)^2 + (y-y_r)^2 + (z-z_r)^2} \right)$$

for all points in the image volume. After the time delays for the transmit (x_t, y_t, z_t) and receive (x_r, y_r, z_r) positions are calculated, voltages (V_I, V_Q) with the proper time delay are algebraically summed for a

given position in the image volume to form the in-phase (I) and quadrature (Q) components of the image. Signals from objects outside the volume of interest are range gated out to avoid degradation of the image. The beauty and the power of using an UWB short-pulse system over conventional radars is in the ability to form images with this simple algorithm.

Experimental Observations: Figure 4 is a side view of a 15-cm diameter calibration sphere above its radar image. The extent of the measurement geometry can be inferred from the extent of the crescent shape, which indicates that the measurement covers a small fraction of the sphere. Because the positioning in the x-direction was off-center, the sphere was not illuminated on the right side, and the image of its top is somewhat asymmetric. This asymmetrical artifact is present in the following images of metallic (Fig. 5) and plastic (Fig. 6) mines and will be removed in subsequent measurements. For example, Fig. 5 provides a cross-sectional image in the xz-plane of an inert, cylindrical (33-cm diameter, 11.5-cm high), metallic, anti-tank mine. Observe that the image realistically includes corners, where the top portion of the mine joins the main body, and the rim around the base of the mine. However, because the positioning in the x-direction was off-center, the rim about the base was not illuminated on the right side, and the image of the top of the mine is somewhat asymmetric.

Figure 6 shows a side-view image of an inert, plastic, square mine with comparable dimensions (32-cm length, 11.5-cm height). Despite being plastic, the image has significant returns that appear to be internal to the mine. In addition, the image has the correct width and shape, but its vertical extent is greater than the actual physical height, which could be caused by scattering or resonance within the

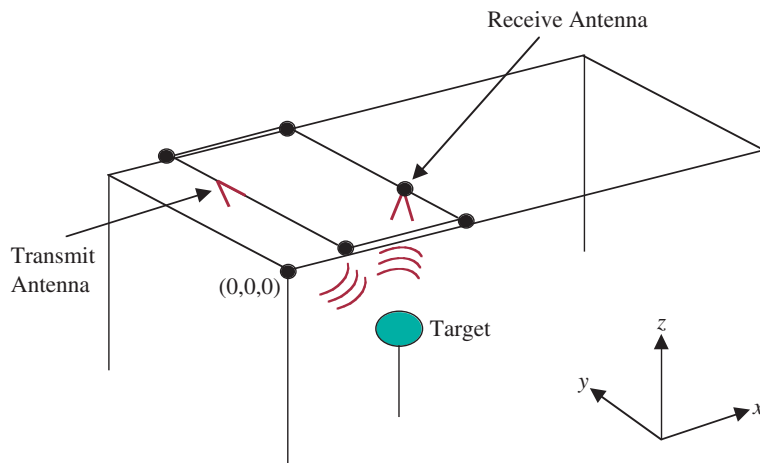


FIGURE 3 Collection geometry. The receive antenna moves in the y-direction on a mounting rail, the transmit antenna is placed at fixed position along a parallel rail, and both antennas move in unison in the x-direction.

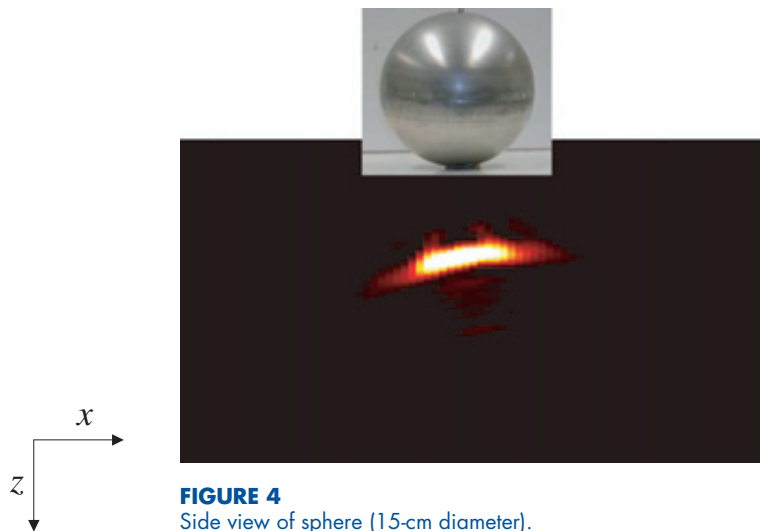


FIGURE 4
Side view of sphere (15-cm diameter).



FIGURE 5
Side view of metallic mine.

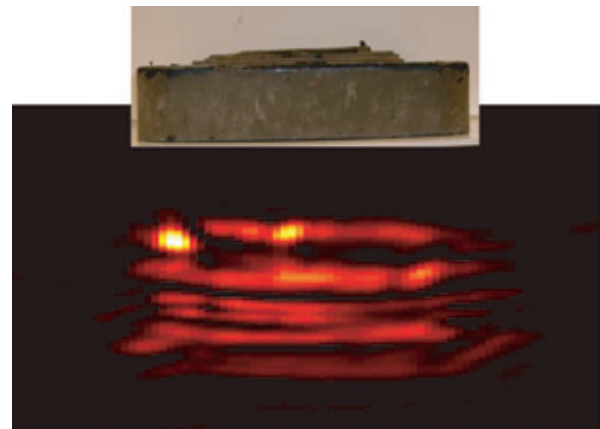



FIGURE 6
Side view of plastic mine.

mine. Unfortunately, the contents of the mine were not known at the time of the measurements. The origins of the height discrepancy and the apparent return from internal scatter are currently being investigated.

These initial results show promise for detecting and imaging shallow-depth, anti-personnel mines (nonmetallic and conventional) with a short-pulse UWB radar at S-band and X-band. Research continues on characterizing and imaging the radio-frequency scatter from these objects.

[Sponsored by ONR]

Reference

¹ P. Hansen, K. Scheff, E. Mokole, and E. Tomas, "Dual Frequency Measurements of Ocean Forward Scatter with an Ultrawide-band Radar," *Proceedings of the IEEE 2001 National Radar Conference*, Atlanta, Georgia, pp. 366-371, May 2001. 

IMAGING STACKING FAULT GROWTH IN SIC DIODES

R.E. Stahlbush, M.E. Twigg, and M. Fatemi
Electronics Science and Technology Division

Introduction: As the Navy converts more of its propulsion and weapon systems to electric power, the performance demands placed on power devices are exceeding the capability of silicon-based devices. Silicon carbide (SiC)-based devices offer the best prospect for meeting the high voltage and current, and elevated temperature that will be required for the Navy's future power conversion systems. However, there are material defect problems that afflict SiC devices. A recent problem that has stymied attempts to commercialize SiC bipolar devices such as

PiN diodes is the tendency to grow stacking faults within the active region during its high current operation.^{1,2}

Figure 7 shows an example of the resulting electrical degradation in PiN diodes. This diode lacks the stable and reliable operating characteristics necessary for the active components in a power conversion system. The desired current densities for SiC power devices are in the range from 100 to 500 A/cm². Even at the low end of this range, the diode has an increase in its forward voltage drop of several volts after moderate electrical stressing.

A number of perplexing aspects to the degradation are introduced by stacking faults. Diodes fabricated on the same wafer can have voltage increases that vary by more than an order of magnitude. Furthermore, the onset of degradation is erratic. Some diodes start degrading when first operated, while others operate without degradation for a while followed by a spurt of degradation. Still others operate for extended times with minimal degradation.

We present imaging techniques developed to examine the stacking fault growth and discuss how the imaging shows how many characteristics of stacking fault growth can be explained by the complicated stress field in SiC wafers.

Degradation Due to Stacking Faults: We have developed imaging techniques based on electroluminescence to investigate stacking fault growth of during diode operation. By using diodes with the solid metal anode contact replaced by a metal grid, light from the diode drift region can be collected. Figure 8 shows the close correlation between the growth of stacking fault area and the increased voltage drop. The total area of the stacking faults is determined from light emission images collected concurrently with the electrical stressing. Two of the images, before and partially through the stressing sequence, are included in the figure. For the imaging conditions used, the dislocations bounding the stacking faults show up as bright lines. The image of the stressed diode exhibits multiple stacking faults, and the leading edges of three of them are circled.

The electrical effect of the stacking faults explains the close correlation between stacking fault growth and electrical degradation. When stacking faults develop in the drift region of a SiC PiN diode (schematically shown in the Fig. 7 inset), they introduce quantum wells that serve as recombination centers. This, in turn, reduces the minority carrier lifetime, increases the resistance of the drift region, and increases the voltage drop to conduct the same current.

Stacking Fault Growth Dynamics: Tracking the growth of individual stacking faults provides insights into their nucleation and growth processes. Stacking faults are nucleated throughout the diode drift region and often grow from dislocations present before stressing. The stacking faults expand within the SiC basal plane, which is tilted 8° with respect to the diode (see Fig. 7 inset). They expand within the drift region. Transmission electron microscopy (TEM) images show that they stop about 100 nm from the SiC surface. Their growth stops before the surface because within the heavily doped anode, there is no electron-hole recombination to drive the expansion. The growth near the n⁺ substrate is more difficult to track and may provide additional insights into the nucleation process as we investigate this region more closely. The stacking faults also grow laterally through the diode drift region. The stacking faults either continue growing until they span the diode or are pinned by internal stress barriers. The barrier can often be overcome temporarily increasing the current density. The increased electron-hole recombination rate overcomes the local stress and the stacking fault continues growing. The growth velocity of all of the stacking faults have strong fluctuations, indicating that the internal stress varies with a range of length scales with a lower limit less than 10 μm.

TEM images provide more details about the internal stress within the diodes. We have developed a large area (1 mm × 50 μm) sample preparation technique for site-specific plan view TEM imaging. This makes it possible to investigate stacking faults over an area that spans the diode. TEM on the same diodes imaged by light emission shows a one-to-one correspondence between stacking faults imaged by the two techniques. All stacking faults are Shockley type. This type of stacking fault is due to stress and involves a shearing of the SiC crystal. The alternate types are formed by the coalescence of vacancies or interstitials. Figure 9 shows how the three types of stacking faults are distinguished. Comparing the TEM images to simulations of the three types shows that only Shockley stacking faults are present. The sign of the stress—compressive or tensile—at the dislocations bounding the stacking faults has also been determined from the dislocation's Burgers vector. This mapping shows the complex nature of internal stress because regions within 1 mm reverse between compressive and tensile stress.

Summary: Before SiC power devices with superior characteristics can replace silicon power devices, the reliability problems due to stacking fault

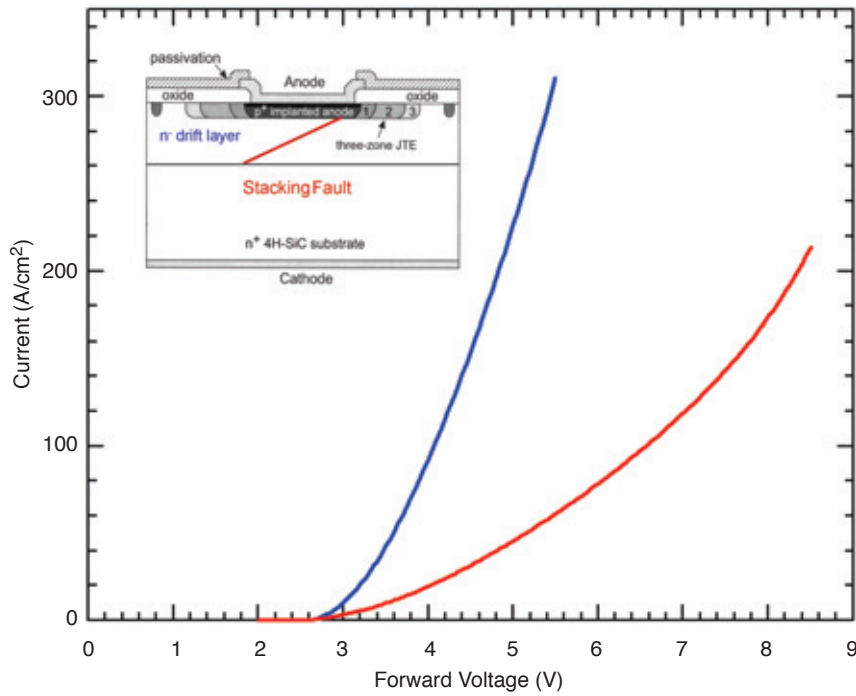


FIGURE 7 Forward-biased current-voltage curve of a SiC PiN diode before (blue) and after (red) current stressing. Stressing consisted of 4 h at 160 A/cm² and 30 s at 800 A/cm². The inset shows a schematic cross-section of a SiC PiN diode with a stacking fault across the drift region.

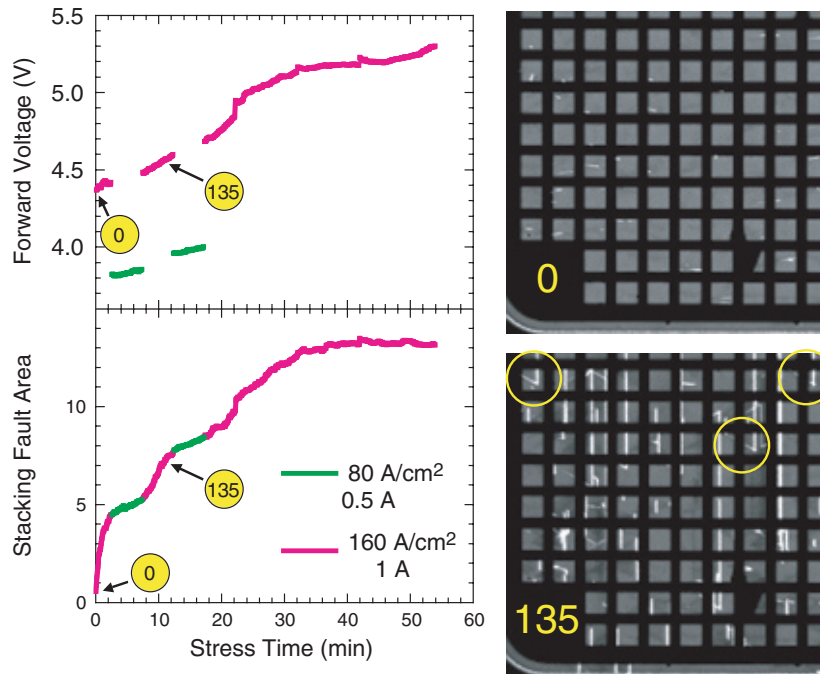


FIGURE 8 Diode forward voltage and stacking fault area vs time stressed at 80 and 160 A/cm². The images show dislocations before stressing, frame 0, and partially through the stressing, frame 135. Three of the leading edges of stacking faults are circled in yellow. The opaque metal grid that contacts the anode partially blocks the light emission.

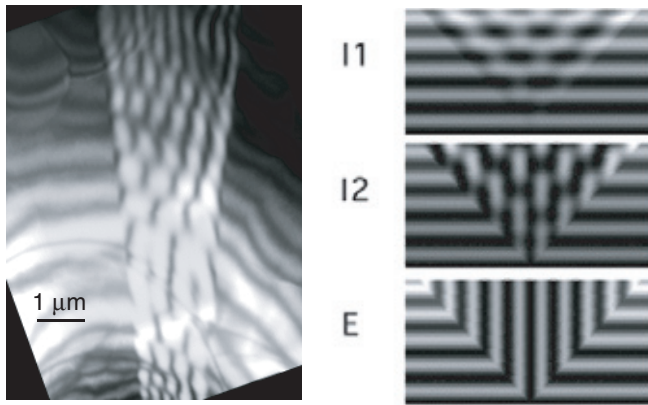


FIGURE 9

Determining the stacking fault type by comparing the TEM image on the left to simulated images for the three possible stacking fault types: I1 from vacancy condensation, I2 from shear (Shockley), and E from interstitial condensation. All of the stacking faults have the "chain link" pattern of the Shockley fault.

growth must be solved. Light emission and TEM imaging techniques that we have developed provide an understanding for the complicated degradation behavior and the material properties responsible for degradation. The imaging reveals nucleation at dislocations and a complex internal stress pattern within the SiC wafers that both promotes and impedes stacking fault growth. We are working with wafer and epitaxial growers of SiC material to produce the next generation of power devices.

[Sponsored by ONR and DARPA]

References

¹ H. Lendenmann, F. Dahlquest, J.P. Bergman, H. Bleichner, and C. Hallin, "High-Power SiC Diodes: Characteristics, Reliability, and Relation to Material Defects," *Mat. Sci. Forum* **389-393**, 1259-1264 (2002).

² R.E. Stahlbush, M. Fatemi, J.B. Fedison, S.D. Arthur, L.B. Rowland, and S. Wang, "Stacking Fault Formation and Propagation in 4H SiC PiN Diodes," *J. Elec. Mat.* **31**, 370-375 (2002).

RE

LONG SPIN COHERENCE LENGTHS FOR QUANTUM DEVICES

M.J. Yang,¹ C.H. Yang,² and Y.B. Lyanda-Geller^{1,3}

¹*Electronics Science and Technology Division*

²*University of Maryland*

³*University of Illinois*

Introduction: Electron spin in semiconductor quantum devices is currently attracting great attention—in part because of potential applications for quantum information and spintronics. The critical issue for quantum computation is to maintain electron spin coherence over quantum structures. The observation of spin interference phenomena, such as quantum beating in the conductivity of ring-shaped structures is a crucial challenge in making spin-coherent quantum devices possible. Long-range

spin coherence can be tested by observation of the phenomena related to the phase in the electron wave function, and lately it has become a "holy grail" in many areas of modern physics.

Spin Berry's Phase: When the parameters of a quantum system are changed and then return to their original values, the wave function acquires dynamical and geometric phases. In contrast to the dynamical phase that records how long these changes take place, the geometric phase depends only on the path taken by the parameters of the system during these changes. Since the discovery by M. Berry,¹ the geometric phases have captured the imagination of physicists and have been demonstrated experimentally in optics and atomic physics. For electronic transport in solids, it has been proposed that conducting rings provide a physical setting in which the spin Berry phase can be observed due to intrinsic spin-orbit (SO) coupling.² In particular, for rings with Rashba SO coupling, the electron momentum defines a radial in-plane Zeeman-like magnetic field (B_{in} in Fig. 10). This results in energy splitting for fixed wave vector $k \neq 0$. When electrons circumnavigate the ring in a perpendicular external magnetic field B_{ext} , the values of the total magnetic field ($\vec{B}_{eff} = \vec{B}_{ext} + \vec{B}_{in}$) form a cone-shaped path, so that the Berry phase is half the solid angle of the cone.

Nanofabricated Ballistic Rings: We have recently achieved a breakthrough in nanofabrication³ at NRL. Among other opportunities, it has enabled us to create spin-coherent devices for observing the spin Berry phase. The novel device proposed and realized here has a one-collimating-contact (OCC) configuration, in which the current lead is tangent to a ring, as depicted in Fig. 10. The collimating contact between the lead and the ring allows most of electrons to move essentially without diffraction. We

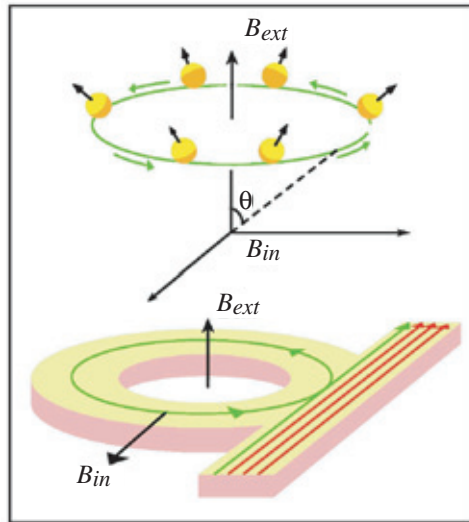


FIGURE 10
Trajectories of electrons in the real space and of their spins in the parameter space for the one-collimating-contact ring.

used AlSb/InAs/AlSb single quantum wells grown by molecular beam epitaxy to create these structures. Figure 11 is a schematic diagram of the structure and the electrostatic lateral confinement of the conducting channel. The newly developed nanofabrication technique utilizes the large difference of the surface properties of InAs from that of AlSb. We first define device patterns using electron-beam lithography, and remove the 3-nm InAs cap by wet-etching. This shallow etch process results in a drastic change of the band bending and creates a conducting electron channel in the InAs quantum well. We used this technique to process OCC rings with radii (r) of 150, 250, 350, and 500 nm. The right-hand inset in Fig. 12(a) shows an atomic force micrograph (AFM) of a 350-nm ring. The lithographic width of the wire is 95 nm, and the estimated conducting channel width is 70 nm. The magnetoresistance of a 500-nm ring is shown in the left-hand inset of Fig. 12(a). The data indicate that there are four transverse modes in the wire when $B_{ext} < 2.3$ T. The estimated longitudinal wavelengths for the first three transverse modes are 44, 50, and 66 nm, smaller than the contact size determined from atomic force microscopy (AFM) images. Because of the collimation effect, these modes do not enter the ring unless B_{ext} reaches 0.9 T, at which magnetic focusing becomes important.

Quantum Beating of the Aharonov-Bohm Oscillations: Figure 12(a) displays the Aharonov-Bohm (AB) interference effect in the resistance of 250 nm ring at 1.9 K. There are two distinct features in ΔR : (1) the unambiguous $h/2e$ oscillations around zero B_{ext} and (2) the quantum beating pattern with five visible transitions to the fundamental frequency

h/e . The noticeable nodes, indicated by arrows in Fig. 12(a), are aperiodic on B_{ext} . The observed features in ΔR are the result of the superposition of two interference signals associated with two spin eigenstates. The double frequency in the vicinity of zero magnetic field is a result of two conditions; (1) the existence of two spin states at $B_{ext} = 0$, and simultaneously; (2) the π phase difference between dynamical phases of these two spin states after a single passage in this particular ring. In other rings that we have studied, the double-frequency signal manifests itself at different magnetic fields, determined by the ratios of the spin-orbit energy and the frequency of electron rotation in those rings. For example, the AB oscillations for a 350-nm ring, shown in Fig. 12(b), indicate that the phases of two spin states differ by 1.5π after one passage of the ring.

Implications: The interplay of the Berry's and dynamical phases leads to transitions in AB conductance between double and single frequency oscillations. The spin Berry's phase has a profound impact on the AB oscillations. In our experiments, Berry's phase determines ΔR at low B_{ext} , shifts the occurrence of the first in-phase beating to the higher field for $r = 250$ nm, and results in a dramatic turnabout feature in $r = 350$ nm oscillations. The observations of quantum beating and double-frequency oscillations indicate a long spin coherent length, more than $3\ \mu\text{m}$ at 1.9 K.

A ring with two spin-orbit states is an interesting example of quantum two-level systems, which are currently the focus of attention as the building blocks of quantum computers. This system can also generate other prospects for future quantum tech-

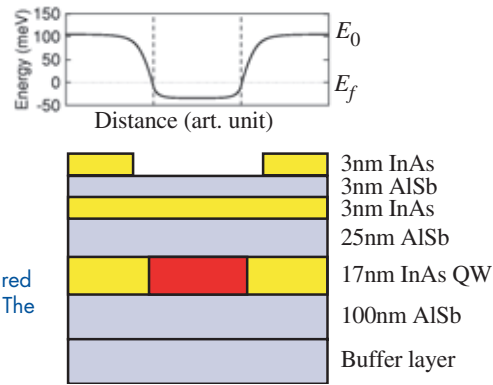


FIGURE 11
Schematic diagram of the sample structure. The red area indicates the induced conducting channel. The inset above depicts the lateral confinement.

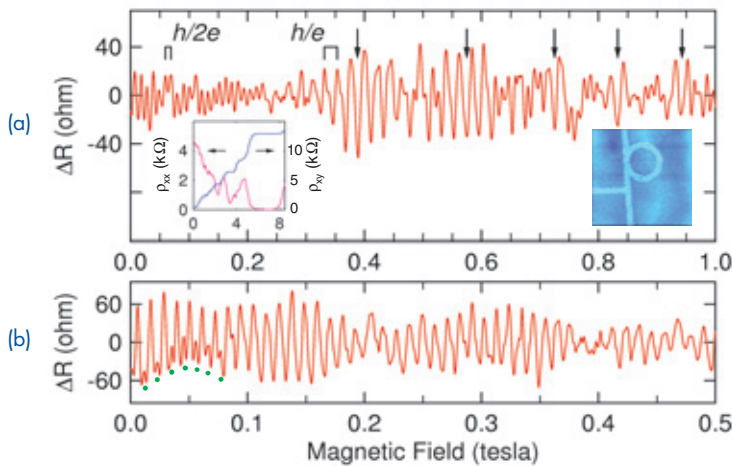


FIGURE 12
(a) The experiment quantum beating pattern for an OCC InAs ring with a radius of 250 nm. The arrows indicate the in-phase nodes for two spin chiral states. The right inset is a $2 \times 2 \mu\text{m}$ atomic force micrograph of an InAs ring. The left inset shows the magnetoconductance of an InAs ring. (b) The measured beating pattern for a 350-nm ring where the additional turnabout feature due to the existence of Berry's phase is marked with dots.

nologies. Our work shows that interference signals in nanostructures can be modified by creating electrical gates to these devices, we anticipate further achievements in controlling and manipulating spin-orbit states.

[Sponsored by ONR, NSA/ARDA, and DARPA]

References

- ¹ M.V. Berry, "Quantal Phase Factors Accompanying Adiabatic Changes," *Proc. R. Soc. London A* **392**, 45-57 (1984).
- ² A.G. Aronov and Y.B. Lyanda-Geller, "Spin-Orbit Berry Phase in Conducting Rings," *Phys. Rev. Lett.* **70**, 343-346 (1993).
- ³ M.J. Yang, K.A. Cheng, C.H. Yang, and J.C. Culbertson, "A Nanofabrication Scheme for InAs/AlSb Heterostructures," *Appl. Phys. Lett.* **80**, 1201-1203 (2002).

ENERGETIC PARTICLES, PLASMAS, AND BEAMS



MILITARY NURSES STATUE.

"To commemorate devoted service to country and humanity by Army, Navy, and Air Force nurses." Frances Rich's sculpture captures the compassion, the gentleness, and the strength, which are exemplified by the nurses of the United States Armed Forces.

- 139** Tactical Aircraft Directed Infrared Countermeasures System Overview
K.A. Sarkady, H.A. Romero, D.M. Cordray, J.G. Lynn, R.M. Mabe, K. Strothers, J.A. Schlupf, and R.C. Cellucci
- 141** Nested Multi-Wire Array Implosions for KeV X-ray Generation
J. Davis, A.L. Velikovich, and V.I. Oreshkin
- 143** Dusty Plasma Dynamics in the NRL Space Physics Simulation Chamber Laboratory
W.E. Amatucci, D.N. Walker, and G.I. Ganguli

[BACK TO CONTENTS](#)

TACTICAL AIRCRAFT DIRECTED INFRARED COUNTERMEASURES SYSTEM OVERVIEW

K.A. Sarkady, H.A. Romero, D.M. Cordray, J.G. Lynn, and R.M. Mabe

Optical Sciences Division

K. Strothers, J.A. Schlupf, and R.C. Cellucci
Raven, Inc.

An Emerging Weapon of Choice: Shoulder-fired surface-to-air missiles (SAM) are widely proliferated, relatively inexpensive, and easy to conceal. An emerging market now exists making these weapons available to numerous insurgency and terrorist organizations. In November 2002, al-Qaida claimed responsibility for firing two SAMs at an Israeli civilian aircraft during take-off in Kenya, raising concern throughout the Western world about the safety of civilian air travel. By contrast, military aircraft have long been susceptible to infrared (IR) guided SAMs and air-to-air missiles (AAMs). Results of a worldwide survey, shown in Fig. 1, indicate that these missiles are responsible for well over 50% of all military aircraft losses. These three factors (availability, price, and record of performance) make IR SAMs and AAMs an emerging weapon of choice.

TADIRCM: The Tactical Aircraft Directed Infrared Countermeasures (TADIRCM) system has been designed to provide Navy and Marine Corps fixed and rotary wing platforms with covert, highly effective protection against even the most advanced IR-guided SAMs and AAMs. The system uses a suite of two-color IR sensors to passively detect the afterburning signature of a threat missile plume. Judicious choice of the operating wavelengths and system optics allows for the detection of these missiles' boost ignition signature well beyond their maximum

kinematic launch range, even if operating in severe (measured) urban clutter conditions. An onboard digital processor provides the system with the capability to autonomously cue a directed jamming system that can establish a precision track on the approaching missile using a high-resolution IR camera. A modulated laser beam is then used to create false targets in the missile seeker, causing optical break-lock (OBL) of the targeted platform. The use of an onboard laser provides for essentially unlimited platform protection. This constitutes an extremely desirable capability since the protection currently available to Navy platforms is severely limited by the number of countermeasure assets that can be carried onboard.

Live-Fire Testing of the TADIRCM System: Figure 2 shows the TADIRCM system components. These components were installed on an aircraft pod mounted on a QF-4 drone aircraft (Fig. 3). System performance was tested on the QF-4 from the spring of 2001 to November 2001. Testing resulted in OBL in each one of an advanced SAM and AAM fired against the QF-4. The ability of the TADIRCM system to rapidly declare the onset of boost ignition resulted in very large miss distances in each of these live-fire exercises.

Confidence in the capabilities of the TADIRCM system was established in a number of intermediate tests conducted at the Navy's weapons test range in China Lake, California. The ability of the system to reliably declare a threat missile was conducted (frequently) with the help of the Optical Beam Evaluation and Wander (OBEWAN) instrument. This instrument generates an IR signature whose intensity, spectral content, and temporal properties closely resemble NRL's large database of exploited threat missile signatures. For this portion of the test, the OBEWAN signature needed to correspond only to that seen in the missiles' boost motor ignition phase.

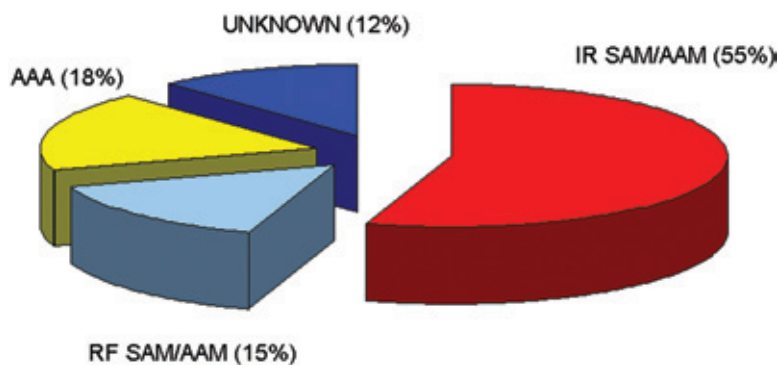


FIGURE 1
Survey of worldwide military aircraft losses (1991-1998).

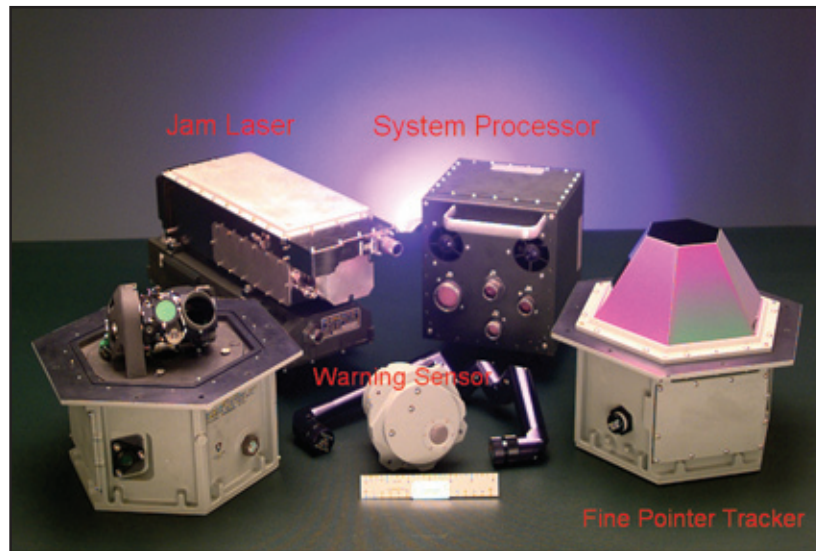


FIGURE 2
The TADIRCM system components.



FIGURE 3
TADIRCM installed on a pod on the drone QF-4.

Testing of the TADIRCM system then focused on evaluating its ability to deliver laser beam energy at the desired target. To this end, a number of seekers of the two selected live-fire missiles were placed in the vicinity of the OBEWAN instrument. While flying in a racetrack pattern, TADIRCM was repeatedly stimulated and the OBEWAN instrument was used to measure the spatial and temporal properties of the laser beam. Simultaneously, the missile seeker electronics were monitored to determine OBL of the QF-4 target. This portion of system testing was very successful and resulted in OBL of all tested seekers in every pass of the QF-4. In all cases, OBL was measured to occur on very fast time scales. This portion of the test also confirmed the favorable power levels

and spatial properties of the laser beam at all launch ranges of tactical interest.

At this point, all checks of system performance were successfully achieved and testing proceeded by firing one advanced SAM and AAM at the drone QF-4. In each case, the missiles were equipped with special telemetry packages that monitored the internal state of the missiles' seeker electronics. Timelines for all of the system events (missile launch, missile threat declaration, time to slew and establish track by the fine pointer-tracker, time to deliver laser energy, and time to OBL) were carefully monitored and cross-correlated. In each case, system performance was excellent and corresponded closely to that established in all preliminary tests of



FIGURE 4
Chase plane view of TADIRCM at work. Note the missiles' dive trajectory effected shortly after jamming.

the TADIRCM system. The ability to rapidly declare the onset of boost motor ignition resulted in timelines for laser energy on target prior to the missile achieving a guided proportional navigation flight pattern. Hence, the miss distances in each of these tests well exceeded those needed for aircraft self-protection. In the case of the AAM, this test constitutes the first time that such a threat has been successfully countered in a live-fire scenario. For completeness, Fig. 4 is a graphic illustration of a TADIRCM live-fire engagement.

Conclusions: The Navy has successfully tested TADIRCM, resulting in a great deal of interest in establishing a production program for this system. Current planning calls for the production of several pod units to be delivered to the Fleet to establish configurational and operational procedures for this electronic warfare system.

[Sponsored by ONR]



NESTED MULTI-WIRE ARRAY IMPLOSIONS FOR KEV X-RAY GENERATION

J. Davis,¹ A.L. Velikovich,¹ and V.I. Oreshkin²

¹Plasma Physics Division

²High Current Electronics Institute, Tomsk, Russia

Introduction: The brightest sources of keV X-ray radiation used for nuclear weapons effects testing, weapons physics, and a variety of other applications are pulsed-power driven Z-pinch plasma radiation sources (PRS). Hundreds of kJ of 2-4 keV radiation have been produced on the 20 MA Z facility at Sandia National Laboratories. The production of harder X rays is increasingly difficult (Fig. 5), largely because heating of high-atomic-number plasmas is a serious problem due to the energy losses through

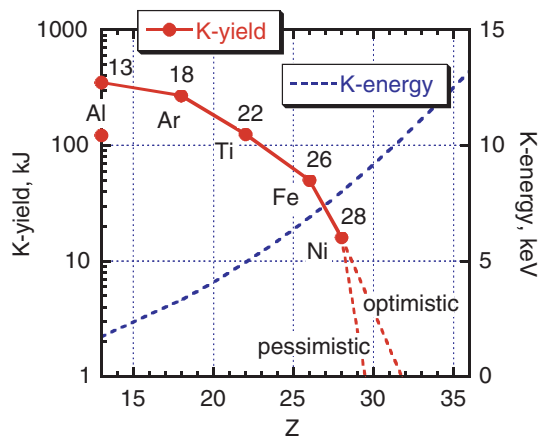


FIGURE 5 K-shell yields produced in recent experiments on Z and the corresponding K-shell energies vs atomic number. Dashed lines show interpolation of these results to higher photon energies.

subkilovolt line radiation that rapidly increase with the atomic number.¹ Even the “optimistic” scaling of the experimental results to the photon energy range of >10 keV predicts the yields not exceeding ~1 kJ (Fig. 5). To do better than this, we need improved PRS load design and maybe other than K-shell line radiation emission mechanisms. Combining the innovative approaches recently suggested at NRL—nested wire array load design and the use of continuum recombination radiation of low-Z elements^{2,3}—seems to be the most promising way to increase the PRS X-ray yields in the high-energy range.

Nested Wire Arrays: Magnetic field lines in a conventional cylindrical wire array are shown in Fig.

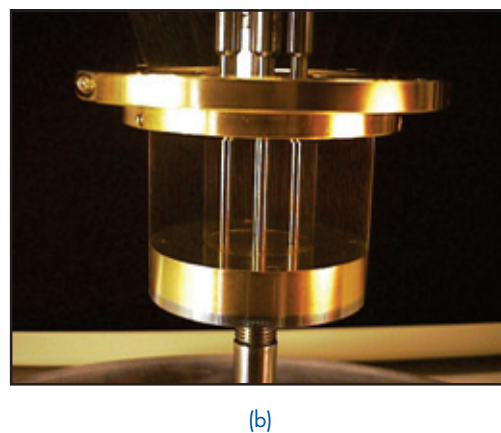
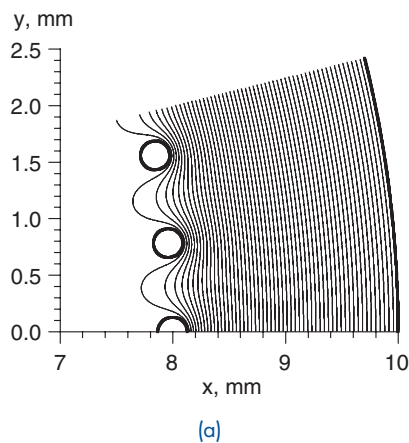
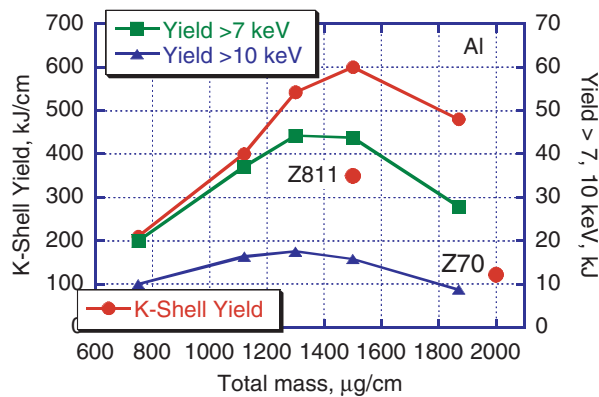


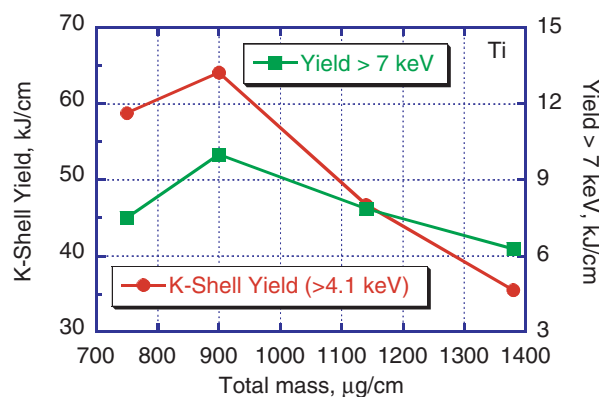
FIGURE 6 (a) Geometry of magnetic field in a single 64-wire wire array. The pressure of the azimuthal field concentrated between the wires and the return current pushes the wires to the axis. (b) Sandia nested wire array load: 240 tungsten wires in the outer array, 120 in the inner.

6(a). The pressure of global azimuthal magnetic field accelerates the wires to the axis, where their kinetic energy is eventually converted into radiation. In a nested load, an inner concentric cylindrical wire array is placed inside the outer one, as shown in Fig. 6(b). When the imploded outer array hits the inner, the two arrays can interact either as continuous gas shells (colliding shell mode), or the outer array plasma can penetrate through the gaps between the inner wires, all or some of its current being switched to the inner array. In either case, this interaction tends to stabilize the implosion, which results in a higher radiation power. The nested wire array loads are now used at Sandia for generating both soft X rays (nesting increased the record radiation power on Z by 40%) and hard X rays. The efficiency of the nested load design for the latter purpose is illustrated by Figs. 5 and 7. The Al single-wire array shot Z70 in 1997 is compared to the Al nested wire array shot Z811 (October 2001). The improved load design contributed to increasing the K-shell yield and power by factors of 3 and 4, respectively.

Recombination Continuum: When higher atomic-number elements are difficult to heat to multi-keV temperatures, we suggest using the continuum radiation of lower atomic-number elements at energies well in excess of their K-shell excitation potentials. An advantage of lower atomic-number plasmas is that one need not pay the large energetic price of stripping many electrons to reach a K-shell radiating hard X-ray lines. Our theoretical and simulation results indicate that the recombination continuum may have an advantage for generating 7-10 keV quanta on pulse power facilities operating in the range of 15-20 MA. The largest recombination



(a) Al in a "colliding shells" mode (experimental K-shell yields from shots Z70 and Z811 are also shown).



(b) Ti-Ni in a 50-50 current-splitting mode.

FIGURE 7
Simulated mass scans of K-shell and recombination yield for 2:1 nested wire array loads imploded on Z.


yield is expected from a highest atomic-number element that could efficiently produce K-shell yield on a given pulse power machine, at conditions corresponding to higher plasma temperatures, tighter pinches, and lower load masses than in most conventional single arrays loads. It could be achieved using either aluminum or titanium low-mass nested wire array loads. Figure 7(a) shows the K-shell and high-energy yields predicted for Al nested wire arrays with outer/inner mass and radius ratio 2:1, as in shot Z811, imploded on Z in a 1D radiative-MHD simulation for the best-case "colliding shells" mode of the interaction between the inner and the outer arrays. The optimum conditions for the K-shell emission are close to those of shot Z811, total mass 1.5 mg/cm, and the predicted K-yield is even higher than the observed one because of energy coupling, which seems to be unrealistically high in the colliding shell mode. Optimum masses for generating higher-energy quanta are predicted to be slightly lower. Figure 7(b) shows similar predictions for

nested Ni-clad Ti wire arrays, with inner/outer arrays interacting at collision in a more realistic 50-50 current splitting mode. Although the reduction in the energy coupling efficiency and 30% of the higher atomic-number Ni ions decrease the temperature of the pinch, and hence, the keV X-ray yields, the predicted radiative performance, if confirmed in experiment, will be of high practical significance.

Summary: We describe an approach to load design that can significantly improve the radiative performance of PRS in the keV energy range. It has already proved to be very successful in increasing both the yield and power of Al K-shell emission produced on the Z. Experiments underway at Sandia National Laboratories are testing our predictions of considerable yields in higher-energy photons that could be produced with low-mass nested wire array loads.

[Sponsored by DTRA]

References

- ¹J. Davis, J.L. Giuliani, and M. Mulbrandon, "Influence of L-shell Dynamics on K-shell Yields for Imploding Krypton Z-pinch Plasmas," *Phys. Plasmas* **2**, 1776-1774 (1995).
- ²J. Davis, N.A. Gondarenko, and A.L. Velikovich, "Fast Commutation of High Current in Double Wire Array Z-pinch Loads," *Appl. Phys. Lett.* **70**, 170-172 (1997).
- ³A.L. Velikovich, J. Davis, V.I. Oreshkin, J.P. Apruzese, R.W. Clark, J.W. Thornhill, and L.I. Rudakov, "High Energy Photon Radiation from a Z-pinch Plasma," *Phys. Plasmas* **8**, 4509-4517 (2001). 

DUSTY PLASMA DYNAMICS IN THE NRL SPACE PHYSICS SIMULATION CHAMBER LABORATORY

W.E. Amatucci, D.N. Walker, and G.I. Ganguli
Plasma Physics Division

Introduction: Dusty plasmas have become a topic of great interest because they provide an excellent tool for exploring many of the fundamental assumptions used in plasma physics. A dusty plasma consists of electrons, ions, neutral gas, and charged microparticles ("dust") with diameters ranging from a few nanometers to a few micrometers. They exist naturally in space, being found in the low Earth orbit region, planetary rings, comet tails, and in planetary nebulae. From its early beginnings with observations of astrophysical phenomena, this area of plasma physics research has grown to encompass industrial plasma, space plasma, and basic plasma issues ranging from

strongly coupled systems, to transport, to waves and instabilities. In the laboratory, experiments have evolved from observations of the behavior of the microparticles in the plasma to direct manipulation of the microparticles and use of the microparticles themselves for plasma diagnosis. However, most dusty plasma experiments have been performed in relatively small setups, most often with dust cloud scale sizes of the order of 2-3 cm.

DUPLEX: The Naval Research Laboratory (NRL) DUPLEX—the DUSty PLAsma EXperiment—device was developed to investigate fundamental issues in the physics of large-scale dusty plasmas in an environment far from the chamber boundaries. The chamber, shown in Fig. 8 with plasma, is unique among laboratory dusty plasma devices. It is 80 cm in diameter and 80 cm in height and is constructed from 0.5-in. thick optically transparent polycarbonate plastic, providing a 360° view of the experimental region. The top and bottom endcaps of the device are also transparent. Alumina microparticles with an average particle diameter of $\langle d \rangle \sim 1.2 \pm 0.5 \mu\text{m}$ are typically used in these experiments.

The large-scale nature of the experiment makes it ideal for investigation of the interaction of dusty plasmas with materials of various shapes, sizes, and electrical characteristics, and allows for the study of phenomena that have not been previously observed in dusty plasma experiments. Individual charged dust clouds with diameter as large as 70 cm and heights as large as 50 cm have been observed in DUPLEX. The clouds often have complex spatial structures with apparent void regions and considerable internal transport.

Argon dc glow discharge plasmas are created in DUPLEX. A 10-cm diameter disk anode biased in the range 300 to 1000 V is suspended vertically above a grounded 75-cm diameter cathode. The separation between the anode and cathode can be adjusted to a maximum of 75 cm, but typically the separation is maintained between 15 and 20 cm. Experiments are performed at pressures ranging from 50 to 300 millitorr.

One of the primary diagnostic techniques used to observe the dust particles is Particle Image Velocimetry (PIV). This technique was pioneered for dusty plasmas by Dr. Edward Thomas, Jr. and the dusty plasma group at Auburn University. It involves illuminating suspended microparticles with a pair of 30-ns laser pulses that are expanded using cylindrical lenses into vertically or horizontally oriented light sheets, separated in time. The laser pulses are synchronized to the frame grabbing rate of a CCD camera, ensuring that each pulse appears on a single

video frame. The displacement of the particles can then be calculated by viewing their relative positions in subsequent video frames. From the displacement and the known time interval, two-dimensional velocity vectors can be computed in the plane of illumination.

Dust Cloud Structuring: Dusty plasmas in DUPLEX are observed to have complex structure. Figure 9 is an example. This image shows a structured cloud suspended above the cathode. The neutral pressure is 250 millitorr and the anode bias voltage is 1000 V. The cloud in this image has a horizontal extent of ~5 cm and a vertical extent of ~3 cm. The “banding” observed in the cloud is not due to reflections or shadows in the experiment, but are real regions that have a significantly lowered—possibly zero—dust density as compared to adjacent regions. The motion of particles within the clouds, as measured using the PIV diagnostic and shown in Fig. 10, suggests that the particles are generally constrained within each band. This observation, combined with the upward flow of the particles suggests that the exchange of particles between the different bands probably occurs at the boundaries of the clouds.

Dusty plasmas of the size and nature observed in the DUPLEX device can be generated because there are none of the usual sheath effects near the walls that are present in most smaller experiments. This allows the dust clouds to expand to the size where an equilibrium is achieved between the mutual repulsion of the negatively charged microparticles and an inward pressure force from the

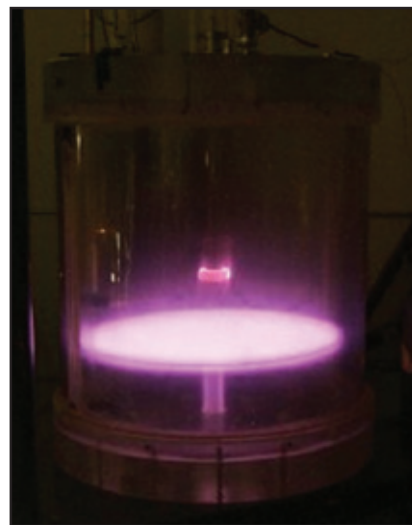


FIGURE 8
The NRL DUPLEX device with argon dc glow discharge plasma.

FIGURE 9
 Example of complex structuring
 observed in DUPLEX dusty plasma
 clouds with 1- μm alumina
 microparticles.

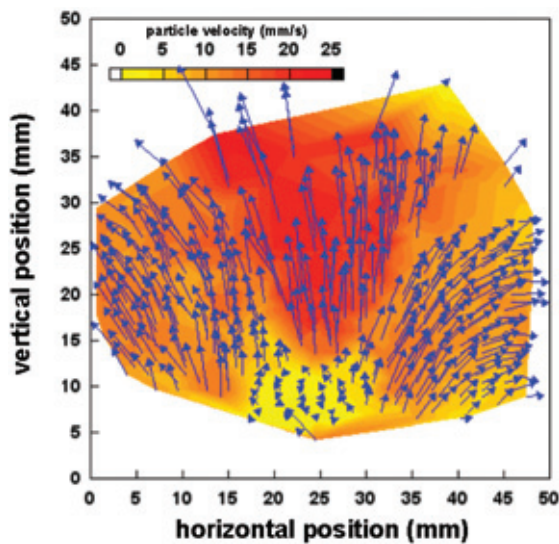
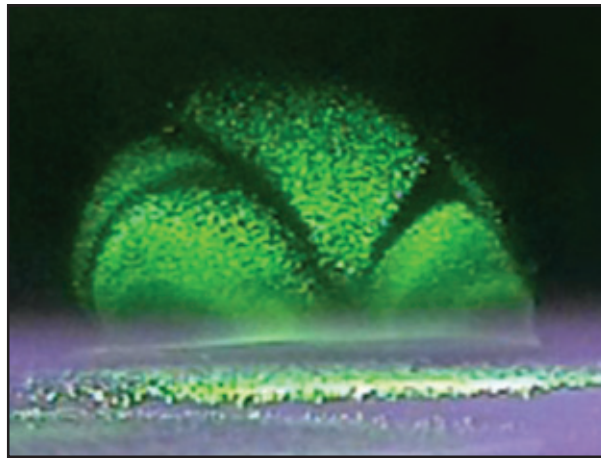


FIGURE 10
 Particle Imaging Velocimetry measurement
 of the charged microparticle velocities in the
 dust cloud shown in Fig. 9.

plasma. The dust cloud internal structure suggests a possible underlying electrostatic potential structure in the region where the particles are suspended. Because these highly structured clouds form above the dust sources, it is possible that the insulation provided by the unlevitated dust on the cathode alters the local potential profile directly above the source. Future work on this experiment will focus on the

nature of the formation of such void structures by using electrodes to control the potential structures in the plasma.

Acknowledgments: The experimental assistance of Dr. E. Thomas, Jr., C. Compton, and B. Christy of Auburn University is gratefully acknowledged.

[Sponsored by ONR]



INFORMATION TECHNOLOGY AND COMMUNICATION



THE SPACE SHUTTLE *CHALLENGER* MEMORIAL.
This memorial is dedicated to the crew of the *Challenger*, which was destroyed in a fireball shortly after launch in January 1986. The crew included Christa McAuliffe, a teacher who was to be America's first "ordinary citizen in space."

- 149** Multimodal Interactions with Dynamically Autonomous Robots
D.J. Perzanowski, A.C. Schultz, W.L. Adams, M. Bugajska, M.S. Skubic, G. Trafton, D.P. Brock, E. Marsh, and M. Abramson
- 151** Demonstration of a High-Rate Tactical Reconnaissance System with Real-Time Airborne Image Exploitation
J.N. Lee, D.C. Linne von Berg, M.R. Krueger, and M.D. Duncan
- 153** Real-Time Tactics Planning Aid for Weapons of Mass Destruction Defense
G.E. Layman
- 156** Better Codes—Better Communication
R.A. Echard and S.C. Chang
- 159** Programmable Embeddable INFOSEC Product
S.J. Chincheck

MULTIMODAL INTERACTIONS WITH DYNAMICALLY AUTONOMOUS ROBOTS

D.J. Perzanowski,¹ A.C. Schultz,¹ W.L. Adams,¹
 M. Bugajska,¹ M.S. Skubic,² G. Trafton,¹ D.P. Brock,¹
 E. Marsh,¹ and M. Abramson³

¹Information Technology Division

²University of Missouri-Columbia

³ITT Industries

Introduction: Intelligent interaction between humans and robots requires that they interact naturally, intelligently, and cooperatively to accomplish goals. This interaction is dependent on their roles. In other words, a sense of teamwork needs to be built in to the interface. This kind of interaction and the ability to act as cooperative or independent agents is known as *dynamic autonomy*.

Natural interactions, such as natural language and gestures, facilitate dynamic autonomy. They affect easy communication, allowing the participants to concentrate on the task and not on the ways to communicate. Awareness of the environment is also important. Thus, our interface incorporates both spoken utterances, natural gestures, and a cognitive model of spatial relations to indicate such elements as the location of objects and other spatial information about the environment. Given this model of the environment, humans and robots have a common ground for interacting with each other and the environment.

As robots and autonomous vehicles become more prevalent, human-robot interaction is becoming

increasingly important. Current state of the art requires many humans to control a single, seemingly autonomous vehicle. For example, Global Hawk, a high-altitude, long-endurance unmanned air vehicle, currently requires a team of 10 operators to control it, while Predator, a medium-altitude, long-endurance unmanned aerial vehicle, requires three. Future autonomous systems must work closely and cooperatively with humans, sometimes exhibiting full autonomy while at other times collaborating with varying numbers of humans in close proximity. To facilitate collaboration and cooperation in such systems, we have designed a multimodal interface² that incorporates both natural language and gestures, touch screen modalities, and a cognitive model of spatial relations (Fig. 1).

Robot Platforms: We are using several robots—Nomad 200s, a B21r, and several ATRV-Jrs (Fig. 1). They are equipped with range sensors (sonars, structured light or LIDAR rangefinders, etc.) to enable environment mapping, crude object detection, and gesture detection. The robots are also equipped with a wireless microphone for speech input and an optional camera to provide the user with a real-time video of the environment.

Multimodal Interface: When using the interface, human users need not conform to predetermined methods of interaction to complete a task. Speaking a command and gesturing may seem appropriate and natural at times (Fig. 2). Or, the human user can use graphical modes, such as a hand-held personal digital assistant (PDA) (shown in Fig. 1) or an end user terminal (EUT) (Fig. 3). Menu buttons on the

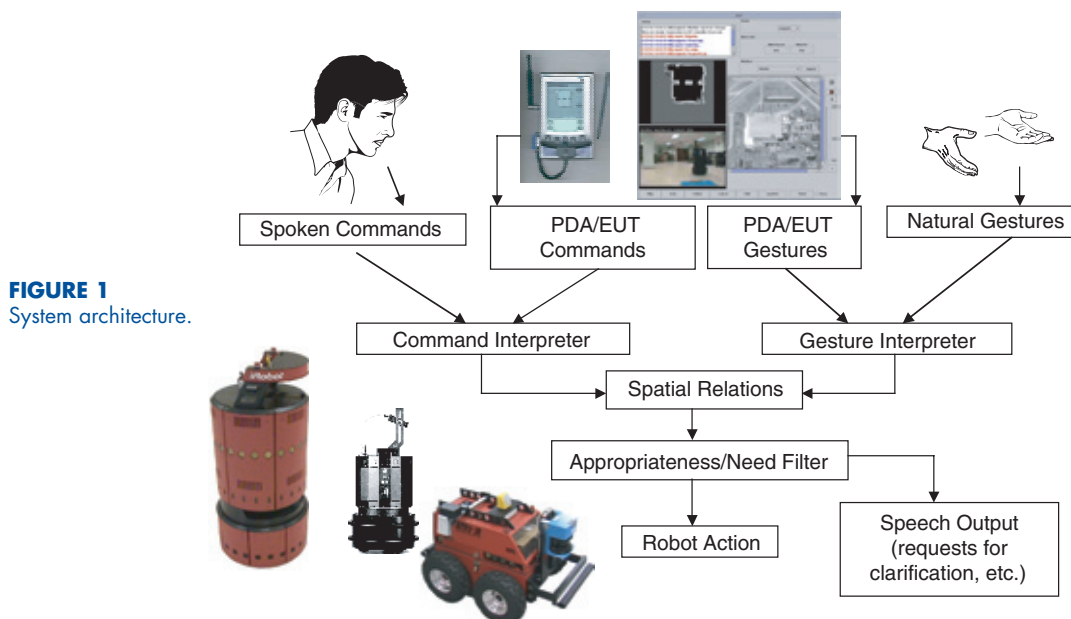


FIGURE 1
System architecture.

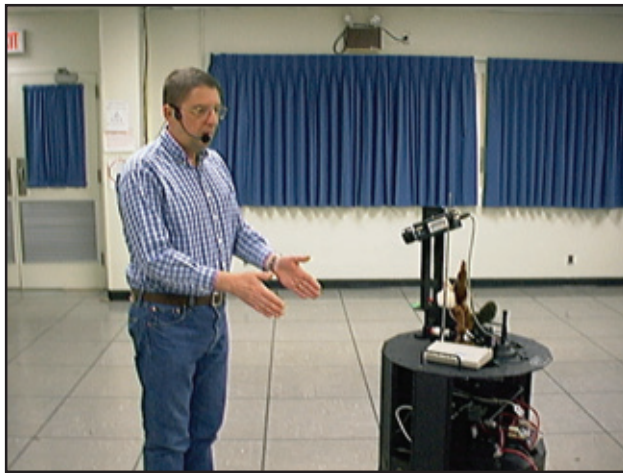


FIGURE 2

A researcher interacts with a mobile robot using natural language and gestures.

PDA and EUT (top right-hand screen in Fig. 3) replace spoken commands and queries. An EUT satellite image (bottom right-hand screen in Fig. 3) provides an aerial view of the robot's environment. The lower left-hand screen (Fig. 3) shows a live robot-eye-view of the immediate environment, and a mapped representation of the latter is on both the PDA and EUT (middle left-hand screen in Fig. 3). A text window (upper left-hand screen in Fig. 3) displays the human-robot dialog. Users can combine any of the

various modalities to interact with the robot, e.g., speaking and clicking on a location on the robot's map.

Commands or queries are linguistically parsed,⁴ and the resulting representation is correlated with gesture data, knowledge of other participating agents, and with spatial information from the robot sensors. The result is then mapped to a robot command, which produces either the requested action or invokes a further interchange of information.

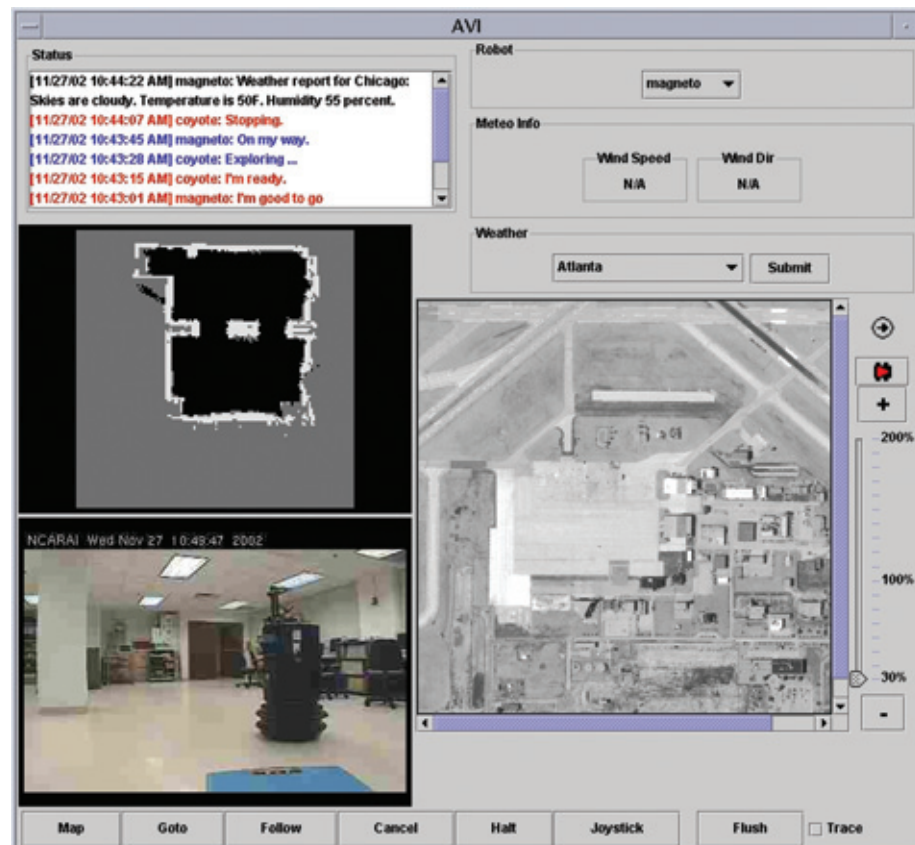


FIGURE 3
Multi-screen display of the end user terminal (EUT).

Thus, humans and robots become cooperative and collaborative agents in completing a task.

The spatial reasoning component³ clusters the sonar data to define discreet objects. Objects can be named for easy reference, and spatial information, such as *left of* and *behind*, is derived, which can then be used for further interactions.


Finally, human-robot interaction is facilitated by shared cognitive models of behavior. Humans communicate, cooperate, and collaborate because they share these models. Using ACT-R, a cognitive architecture for simulating and understanding human cognition and behavior,¹ the robots can reason about spatial relations and objects, and behave in ways analogous to humans. With a similar model of behavior, humans and robots can interact and communicate more effectively and efficiently.

Thus, the robot can understand complex navigational commands, such as “Go between the two buildings on your left and hide on the northwest corner behind the storage container.” Not only must the robot understand what the various objects in these utterances are, but it must also be able to identify significant locations on or near those objects. With this information, it can then perform an action, such as hiding, which involves a complex set of heuristics.

Conclusions: We are concentrating on two research areas to facilitate cooperation and collaboration in human-robot interaction. The first area is the design and implementation of a multimodal interface. By providing a natural or intuitive multimodal interface, users can concentrate on the task, not on the modes of interaction. The second research area is the use of computational models of human cognition to facilitate spatial reasoning in robots that share information about the environment, objects, and locations with humans and with each other. By incorporating human cognitive models, we enable collaborative and cooperative interactions that enhance dynamic autonomy in robots.

[Sponsored by ONR and DARPA]

References

- ¹J.R. Anderson and C. Lebiere, *The Atomic Components of Thought* (Lawrence Erlbaum, Mahwah, NJ, 1998).
- ²D. Perzanowski et al., “Communicating with Teams of Cooperative Robots,” in *Multi-Robot Systems: From Swarms to Intelligent Automata*, A.C. Schultz and L.E. Parker, eds. (Kluwer: The Netherlands, 185-193, 2002).
- ³M. Skubic, D. Perzanowski, A. Schultz, and W. Adams, “Using Spatial Language in a Human-Robot Dialog,” in *Proceedings of the IEEE 2002 International Conference on Robotics and Automation*, Washington, DC, 2002, pp. 4143-4148.
- ⁴K. Wauchope, “*Eucalyptus: Integrating Natural Language Input with a Graphical User Interface*,” NRL/FR/5510-94-9711, Naval Research Laboratory, Washington, DC. 

DEMONSTRATION OF A HIGH-RATE TACTICAL RECONNAISSANCE SYSTEM WITH REAL-TIME AIRBORNE IMAGE EXPLOITATION

J.N. Lee, D.C. Linne von Berg, M.R. Kruer, and M.D. Duncan
Optical Sciences Division

Introduction: The NRL Optical Sciences Division has been at the forefront of reconnaissance system development. The division has not only developed basic technology, such as large focal plane arrays, but has also designed, implemented, and demonstrated complete prototype systems. NRL demonstrated the first all-digital tactical reconnaissance system for the Navy, TARPS-CD (Tactical Air Reconnaissance Pod System—Completely Digital). In 2001, NRL demonstrated a prototype of the SHARED Reconnaissance Pod (SHARP) system for the F/A-18 Super Hornet; virtually all the features of this prototype have carried over into the Engineering and Manufacturing Development (E&MD) phase of the SHARP program. In the meantime, activity on the TARPS-CD effort for the F-14 has continued as risk reduction for advanced capabilities being considered for inclusion into the SHARP system. As part of the TARPS-CD effort, we have produced an upgraded digital reconnaissance pod payload to address fleet user responses to the original TARPS-CD system. The resultant pod system, denoted as Full-Capability (F-CAP), is based on the SHARP prototype architecture and is a test bed for advanced technology for SHARP. Figure 4 is a view of the F-CAP pod and its payload. Among the improvements we have implemented are:

- The NRL-developed Airborne Real-time Image Exploitation System (ARIES), with a new cockpit control box that allows the aircrew to examine and select imagery in real time;
- A high-performance Inertial Navigation System (INS), tightly coupled to GPS, mounted internal to the pod to provide accurate sensor attitude and position data for target geolocation;
- A solid state digital recorder that allows rapid access of imagery for routing and processing;
- Automated mission execution, system debug, and mission review via mission and maintenance PCMCIA memory cards; and
- A directional antenna for increased Common Data Link (CDL) transmission range.

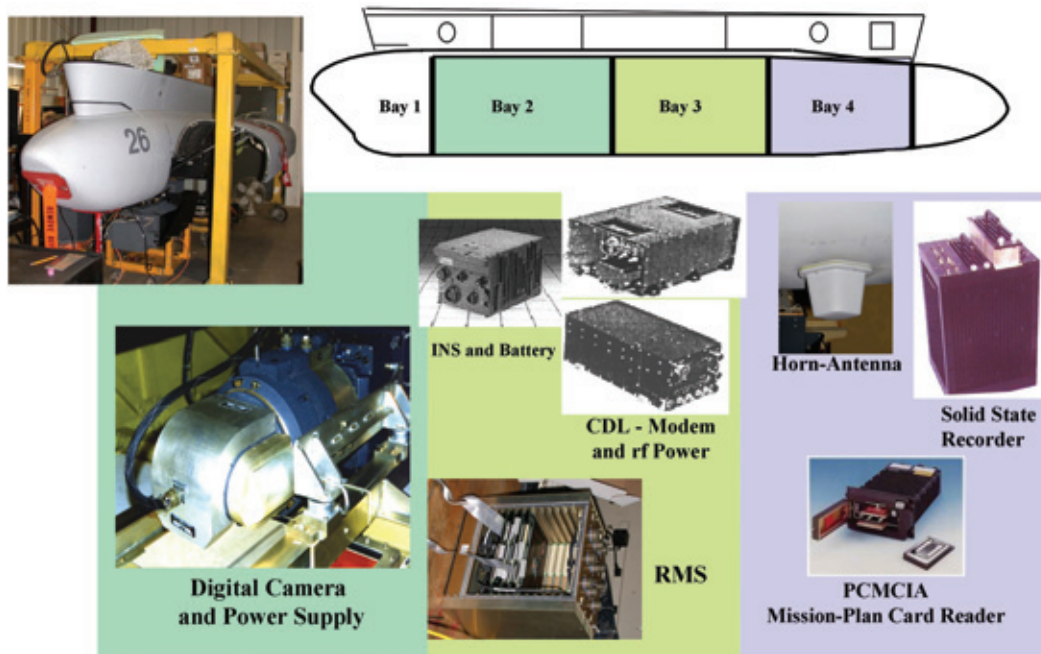


FIGURE 4
F-CAP payload components and their location within the TARPS pod.

Special Cockpit Control Panel: One key improvement we have made with F-CAP is the incorporation of the ARIES circuit card into the Reconnaissance Management System (RMS) for in-cockpit display, processing, and geolocation of images obtained from the TARPS-CD digital framing camera. We designed and built a special cockpit control panel to allow the aircrew to quickly manipulate the image data on the cockpit display (e.g., pan, zoom, and roam) and create an image segment. This image segment can be a full-sized camera image reduced in resolution or it can be a smaller area of the full image, but with higher, or even full, resolution. Images are automatically annotated with useful information such as latitude and longitude. The annotated image segment can then be transmitted via the Fast Tactical Imagery (FTI) low-bandwidth (10 kbps) radio link to either an aircraft carrier, a strike aircraft, or ground special forces for target prosecution. FTI can also relay images from aircraft to aircraft, allowing transmission over the horizon. This capability enables an entirely new way to identify and prosecute time-critical targets. Figure 5 is an example of an image that was captured by air crew and transmitted by FTI.

The current TARPS-CD system uses knowledge of sensor attitude and location to perform aero-triangulation to determine the latitude and longitude of targets within an image. The original TARPS-CD design relied on the aircraft's INS data to determine

sensor attitude; such an approach is inadequate for the precision targeting needed by new, GPS-guided weapons. The improved F-CAP design uses a separate, high-performance INS in the pod. This improved design uses GPS to augment the INS and has been shown to operate successfully in early flights of the F-CAP pod, although measurements of the increased precision using this approach have not yet been completed. This new design will allow the insertion of new technology in passive aero-triangulation techniques as they are developed. In addition to INS improvements, digital terrain elevation data are being incorporated into the ARIES system to allow more accurate geo-location in mountainous terrain.

Improved F-CAP: We have also improved the F-CAP system over the original TARPS-CD system by replacing the older, mechanically based digital tape recorder with a solid-state recorder. The solid-state recorder in F-CAP has over 30 GB of nonvolatile flash memory and records data at up to 40 MB/s. Because such a recorder has random access memory, any data stored in the system can be retrieved very quickly. When operated by the F-CAP RMS, the solid-state recorder allows near-instantaneous retrieval of previously recorded full-resolution imagery. This imagery can be sent to the cockpit by the ARIES card and can be transmitted to the ground or to ships via the 274-Mbps CDL link.

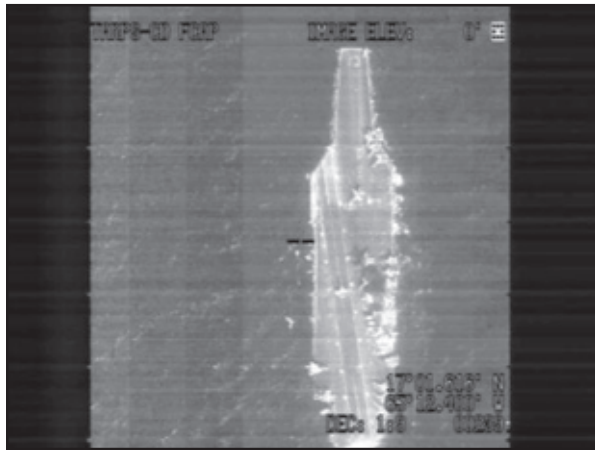


FIGURE 5
F-CAP image of the USS *Harry S. Truman* captured from the F-14 cockpit video display and transmitted via the FTI system.

The transmission of real-time and recorded imagery to the ground is an important function of the TARPS-CD system. The original TARPS-CD system used an omnidirectional antenna in a small rf enclosure for CDL transmission in the X-band. We placed a small horn antenna within the same rf enclosure for the F-CAP pod. Using input navigational data, the CDL hardware automatically steers the horn in the azimuthal direction at a fixed depression angle to point toward a designated latitude and longitude position. This design allows 274-Mbps CDL to be received at up to 180 nautical miles, $\sim 2.5\times$ the range of the original antenna. We have demonstrated the successful downlink of imagery with this new design.

“Automode”: The original TARPS-CD system was able to record image data only when commanded to do so by a pilot operating the pod control panel in the F-14 cockpit. This meant that a busy pilot might leave the system on continually, resulting in a huge amount of extraneous data, or that targets might be missed. To help solve this problem, we implemented an automatic mission mode for the F-CAP system. This “automode” can be programmed onto a PCMCIA memory card using a laptop computer and graphically based mission-planning software we developed. The automode information can include the location of point targets, area targets, and strip targets, as well as the location of the CDL receiver. The automode information is read into the RMS prior to an actual mission. If the pod is switched to automode, then the entire mission can be executed automatically, with the camera, recorder, and CDL data link turned on and operated automatically as the aircraft approaches the appropriate locations. In addition to storing the automode

program, the PCMCIA card is used to store the sequence of events that actually occurs during the execution of a mission, even when the mission is run completely manually. Finally, in the F-CAP pod another PCMCIA card records every operator action and anomaly report during a mission, allowing mission review and identification of any hardware, software, or operator errors.

Evaluation: The F-CAP pod was evaluated in operational exercises by F-14 squadron VF-32 at NAS Fallon in July 2002 and aboard the carrier USS *Harry S. Truman* (CVN-75) in September and November 2002. The F-CAP pod and spare electronic components accompanied VF-32 and the *Truman* on its deployment in December 2002.

[Sponsored by NAVAIR]



REAL-TIME TACTICS PLANNING AID FOR WEAPONS OF MASS DESTRUCTION DEFENSE

G.E. Layman
Tactical Electronic Warfare Division

Introduction: The Weapons of Mass Destruction Defense (WMDD) Mission Application is a prototype tactical decision and planning aid designed for integration into several Command, Control, Communication, Computer and Intelligence (C4I) Systems.

The WMDD is used to assess hostile nuclear, biological, and chemical (NBC) weapon attacks and perform course-of-action (COA) analysis and operations planning for WMD defense. It contains embedded simulations that predict propagation and lethality effects of fallout and contamination clouds.

Development Challenge: A serious problem in modern C4I systems is the difficulty of developing simulations within mission applications such as the WMDD. C4I systems are designed primarily to present the military forces a Common Operational Picture (COP) that represents the best assessment of the current situation as close to real time as possible.

Few provisions have been made in C4I to manage simulated (nonreal-time, nonreal-world) data required for time projection and COA analysis. The Navy Modeling and Simulation Management Office (NAVMSMO) recognized the challenge and tasked the Naval Research Laboratory to conduct research into embedded simulation technologies.

C4I Embedded Simulation Infrastructure (ESI)

Program: An embedded simulation infrastructure concept was conceived that includes simulation-to-C4I links and modeling and simulation (M&S) extensions to the Common Operational Environment (COE: the software baseline for most modern C4I systems).

M&S Services were developed that are common to a broad range of mission applications. Applications using these services, including Embedded Operator Level Training, the C4I Team Training System (CTTS), and the WMDD described here.

WMDD Operational Requirements: Operational requirements are organized into four categories. Upon completion the WMDD will provide these general functions:

- *Nuclear, Biological, and Chemical (NBC) Common Operational Picture (COP)*—Perform NBC sensor fusion, and source location and analyze downwind contamination effects. Report NBC event alerts, tracks, and plume analysis results to the C4I COP.
- *Force Protection*—Perform real-time, wide-area situation assessment and course-of-action analysis to determine proper NBC event responses (avoidance, protection decontamination).
- *Zone/Urban Defense*—Perform high-resolution, zero latency contaminant transport and lethality analysis for urban areas and fixed defensive positions (e.g., bases). Analyze sensor deployments, determine escape routes, and plan decontamination and recovery operations.
- *Operations Planning*—Provide capabilities for scenario-based planning, WMD defense posture analysis, and strike planning analysis for unintended NBC secondary effects.

Figure 6 shows a contamination plume, calculated from NBC event data, weather information, and terrain data. Analysis is conducted with the embedded Hazard Prediction Assessment Capability (HPAC) simulation, developed by the Defense Threat Reduction Agency (DTRA).

This figure illustrates a simple COA analysis conducted by time-projecting the contamination cloud and ship's path of intended movement (PIM). Mission Editing services allow users to generate and evaluate alternate courses of action to avoid the contamination or determine when to take protective measures.

Mission Editor: The Mission Editor, shown in Fig. 7, permits a ship commander or battle group

planner to rapidly synthesize, display, and store dynamic route planning scenarios. The scenarios are entered into the C4I system for evaluation using other analytical tools. Ship and aircraft tracks are defined by their PIM as waypoints. Waypoints define state changes such as bearing or speed changes.

The planned positions can be projected in time for analysis and modified to satisfy mission requirements. The Mission Editor is the first dynamic scenario planning capability fully integrated within COE-based C4I systems; it is also used in training applications.

Host Application Concept: Simulation-based applications within a domain such as planning or training will duplicate many functions, regardless of the specifics of those applications. A large part (e.g., >85%) of software development may be eliminated through the use of common software functions.

Host Applications organize M&S services into shell programs. This approach isolates unique functions to a small percentage of the code, primarily within the embedded simulations. Using well documented M&S services, applications and embedded simulations can be easily developed.

Figure 8 illustrates the architecture for the WMDD Host Application. The COE, shown at the bottom, provides a wide range of common applications and services such as mapping, visualization, data base management, and network services.

The WMDD Application consists of several segments and embedded simulations servers, as shown. The application segments, containing the M&S Services, are clients to the embedded simulations. Currently, two simulations are contained in the WMDDA.

M&S Services: The following M&S services support scenario-based applications such as training, planning, and COA analysis.

- Scenario Generation/Planning.
- Plan Preview.
- Virtual Track Management.
- COP Capture.
- Time Base Management.
- Visualization.
- Tactical Data Base Access.
- Simulation COP Displays.
- Archive/Replay/Debrief.
- Communications.

These M&S Services have been used in the WMDD and the C4I Team Training System, another Host Application. The M&S Services are being proposed as new COE components for FY03.

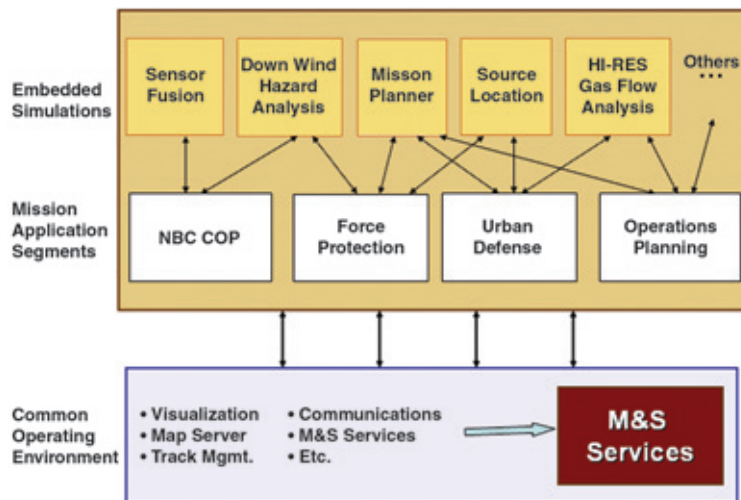


FIGURE 8
WMDD host application architecture.

Summary: The Weapons of Mass Destruction Defense Application provides needed functionality to C4I. The benefit of the WMDD Host Application design is that it manages system complexity, thereby reducing development effort and maintenance costs. The embedded simulations are generally smaller, containing well defined functions that can be more easily developed and modified.

Acknowledgments: WMDD software developers are Dan Robinson, Brenda Weber and Nam Le. Participants in the ESI Program include Dennis McGroder, Trinh Nguyenphan, Jennie Womble, John Daly and Peter Kunkel.

[Sponsored by NAVSMO]



BETTER CODES—BETTER COMMUNICATION

R.A. Echard
Space Systems Development Department
S.C. Chang
George Mason University

Introduction: “Can you hear me now?” This popular phrase, familiar to everyone in today’s fast pace world, is more than just an indicator of convenience. To a Naval communicator, maintaining communications (Comms) during military operations is vital to the survival of U.S. and allied forces. How do we ensure that our forces have the best communication systems available? This question boils down to a special mathematical theory discovered by Claude

Shannon more than 50 years ago¹ but only recently exploited to its full potential. Researchers at NRL and George Mason University have refined a system of error control coding that enables new possibilities for a variety of communication products. Our codes, known as π -rotation codes, offer error correction capability approaching the fundamental mathematical limit while maintaining a small and simple circuit configuration.

Background: All messages can be represented by a string of ones and zeros. Coding for error control is simply a matter of mapping these binary message patterns to longer sequences with deterministic relationships. The amount of information, as measured by the number of information bits, is still maintained in the coded transmission. However, the longer sequence with predetermined arrangement allows the decoder in the receiver to recover the information, even when the transmission has been corrupted.

An important parameter of coding is the ratio between the number of information bits to the number of bits in the encoded string or codeword. We call this the “rate” of the code, and it determines the additional bandwidth required to implement the error control scheme. For example, a rate 1/2 code would nominally require twice the bandwidth, a rate 1/3 code, three times the bandwidth, and so forth. The cost of additional bandwidth is well offset by the improved power efficiency if the codes are properly designed.

More than 40 years ago, a coding scheme was invented called low-density parity-check (LDPC) codes.² These codes were recently rediscovered as having the capability to reach the efficiencies prom-

ised by Shannon's original theory.³ In general, to describe LDPC codes that perform at these high efficiencies requires a massive amount of memory for each code design. With the introduction of π -rotation codes, the amount of memory required is reduced to just a few bytes. In addition to the memory savings, π -rotation codes are easily encoded by using a unique encoding architecture based on a single permutation mapping. The performance of π -rotation codes places them among the best performing error control codes known today.

LDPC Codes: LDPC codes are described by the parity check matrix \mathbf{H} . The code C is defined as the set of all codeword vectors \mathbf{y} , such that $0 = \mathbf{H}\mathbf{y}$. Thus, C is the set of all vectors orthogonal to the row vectors in the matrix \mathbf{H} . Good performance requires a large \mathbf{H} matrix formed from randomly placed one/zero patterns. Figure 9 shows a simple example. The dots in this figure represent the locations of the ones, and the blank regions represent zeros. A good performing matrix may have row and column dimension of many tens of thousands. In general, to create codewords from information messages, this matrix must be inverted to obtain the generator matrix. Although conceptually this is a simple procedure, the large

size makes conversion to the generator matrix a significant computational process. In general, the LDPC coding system requires the storage of both the parity-check matrix and the generator matrix for encoding and decoding the messages. Thus a substantial amount of memory and processing power is required to implement LDPC codes.

The π -Rotation Codes: The π -rotation codes are a form of LDPC codes that do not require a generator matrix and are described by a set of three integers for the *classic* version and an additional four integers for the *extended* version.⁴ The three integers $[m, a, b]$ are used to define a permutation matrix through a unique chaotic generator. This permutation matrix has a single "one" in each column and row of the matrix. Its size is determined by the value of m . Calling this matrix π_A , we create four matrices by rotating the π_A permutation matrix, as shown in Fig. 10. Using these four matrices as a basis, we create the mosaic pattern as shown to produce the larger matrix \mathbf{H}^d . This matrix is combined with a pair of diagonal matrices to create the complete \mathbf{H} matrix. The circuit to create codewords is easily implemented, as shown in Fig. 11. The results in Figs. 12 and 13 provide an example of the bit error correcting performance of π -rotation codes.

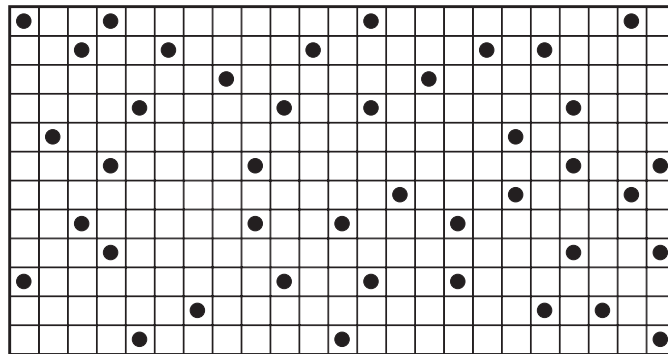


FIGURE 9
Example of an arbitrary parity-check matrix.

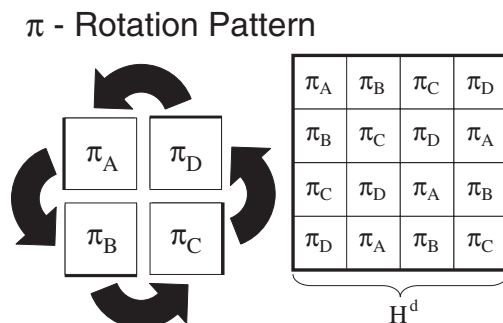


FIGURE 10
The four π -rotation permutation matrices are arranged to create the larger \mathbf{H}^d composite matrix.

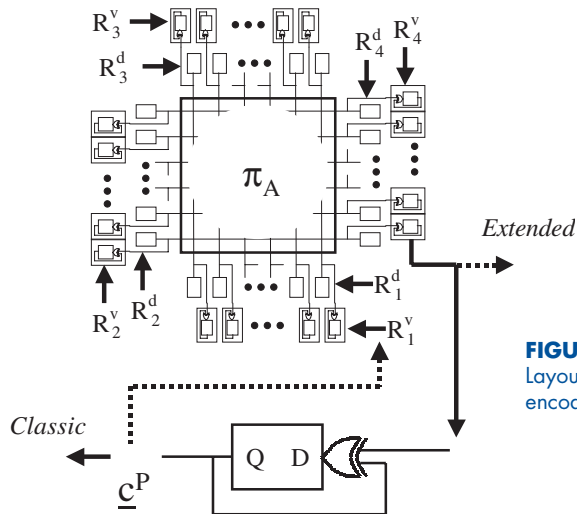


FIGURE 11
Layout of the classic and extended π -rotation encoding circuit.

FIGURE 12
Bit error rate (BER) performance curves for irregular (extended)- π -rotation LDPC codes in the additive white Gaussian noise channel. All information lengths are 15,000 bits.

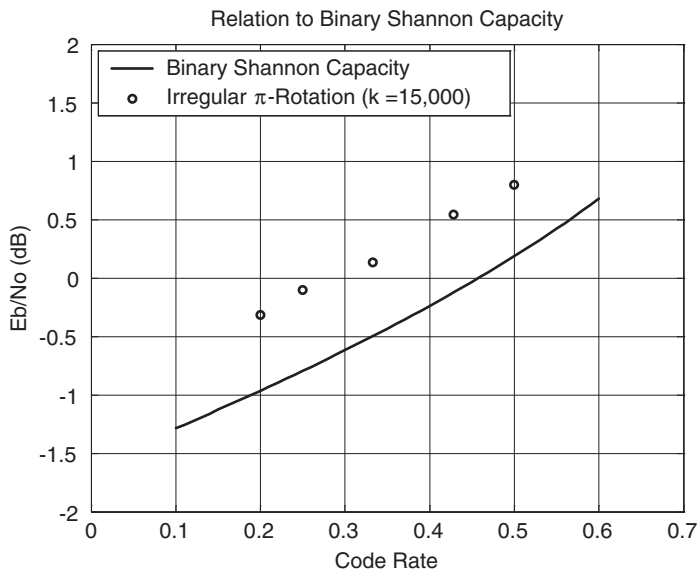
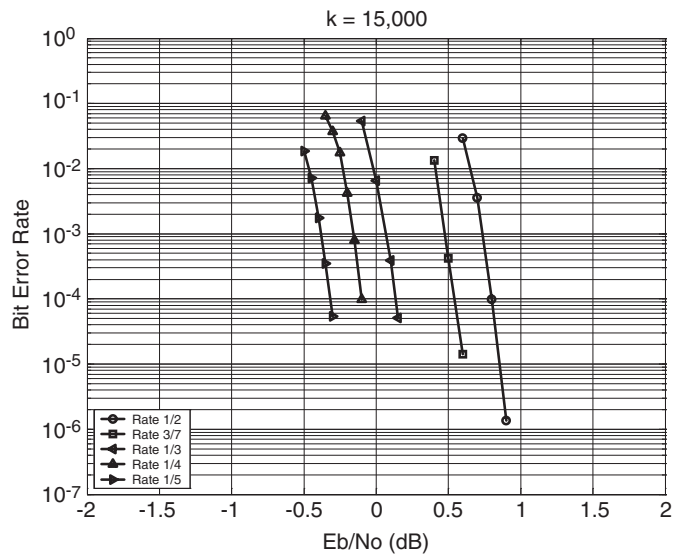


FIGURE 13
Signal-to-noise ratio required to obtain 10^{-4} BER performance with irregular π -rotation LDPC codes compared to the binary Shannon limit. Each code is completely defined by a 7-integer vector.

Summary: We can see that these codes easily perform within 1 dB of the theoretical limit. Also, since these codes are defined with a short description, the exact code is easily stored or transmitted for exchange between radios. The circuit implementation is an added plus to the usefulness of the π -rotation codes since code rate and code length are easily adapted to dynamic channel conditions. This research is an example of NRL's contribution to the continued improvement of communication resources available to our Service personnel.

Acknowledgments: Richard Echard acknowledges support from the Naval Research Laboratory to pursue studies at the George Mason University through the Edison Memorial Graduate Training Program.


[Sponsored by ONR]

References

¹C.E. Shannon, "A Mathematical Theory of Communication," *Bell Sys. Tech. J.* **27**, 379-423 (1948).

²R.G. Gallager, "Low Density Parity Check Codes," Ph.D. thesis, Massachusetts Institute of Technology, Cambridge, MA, 1960.

³D.J.C. MacKay and R.M. Neal, "Near Shannon Limit Performance of Low Density Parity Check Codes," *Electron. Letts.* **33**(6), 457-458 (1997).

⁴R. Echard and S.C. Chang, "Irregular π -Rotation LDPC Codes," *Proceedings of IEEE GLOBECOM 2002*, Taipei, Taiwan, 17-21 November 2002. 

PROGRAMMABLE EMBEDDABLE INFOSEC PRODUCT

S.J. Chincheck
Information Technology Division

The Problem: Information critical to the defense of our country must be protected from exploitation and exposure. Information specific to military applications may include nuclear command and control launch codes, troop movements, deployments and locations, classified mission data, and other information that falls under the broad heading of "classified information." Examples of other, nonmilitary information that must be maintained and transmitted in a secure environment would include strategic information provided by agents of the U.S. Government, plans for handling situations of civil or military unrest among nations of strategic interest to the U.S. Government, and communications between and among U.S. Government top officials including the President of the U.S.

The Requirements: Protecting this information to ensure that the defense mission of this country is successful requires a flexible security system that will support backward compatibility with legacy hardware and software and accommodate new, emerging algorithms for future secure applications. Requirements include:

- A universal system that is not tied to one particular hardware implementation, i.e., will not become obsolete with the development of more advanced hardware.
- A flexible system that enables secure upgrades as more robust algorithms are developed to thwart an increasingly sophisticated hacker community and nation state attacks.
- A standardized system that can serve as the foundation on which additional application-specific functions may be built, incorporating all the security aspects of the core system.

Communications Security (COMSEC) Modernization Strategy: The COMSEC Systems Section of the Naval Research Laboratory (NRL) analyzed the existing state of the art and determined that a software-based approach would best meet the information security requirements with respect to flexibility for the future while supporting backward compatibility. A strategy was developed that involved providing all COMSEC users with a software-programmable system compatible with legacy operations. Upon development and validation of new cryptographic algorithms by the National Security Agency (NSA), these algorithms can be introduced in a unified COMSEC modernization scheme. Moreover, future upgrades can be accommodated using the same process.

The PEIP Solution: Primary goals in the development of the Programmable Embeddable INFOSEC Product (PEIP) are to design a single module that encapsulates most of the Information Systems Security (INFOSEC) requirements levied on a system in a well defined area, thus minimizing or completely removing INFOSEC requirements levied on the host system, and to provide the functionality essential in meeting the critical requirements defined above. The plan for achieving these goals was to complete the development of PEIP technology in two phases, with the second phase adding additional capabilities while remaining backward compatible with the first phase. This phased approach allows components of the architecture to be added in future revisions, thus increasing the flexibility built into the device, minimizing costs associated

with initial developments, and increasing the robustness of the design.

The PEIP is a reprogrammable software cryptographic device that provides a single INFOSEC solution in a standard module format. In addition, PEIP implements existing cryptographic algorithms in software. Moreover, PEIP has been designed to accommodate new cryptographic algorithms as they are developed. The PEIP is adaptable to a variety of input/output (I/O) modules to allow implementation in applications as varied as aircraft, submarines, minuteman silos, and man-portable systems, to name a few. The PEIP can be configured to emulate multiple devices by associating algorithms and keys in cryptographic channels. PEIP currently supports up to 10 simultaneous channels.

The First Application—The KOV-17: The first application of the NRL PEIP technology occurred as a consequence of the need to find a successor to the KG-38, the cryptographic device used in the Navy submarine program. The KG-3X family of cryptographic devices is the workhorse cryptographic platform for the nuclear command and control (NC²) community. The KG-38 successor, the first pillar of the PEIP family, was developed in support of the Submarine Low-frequency/Very Low-frequency VMEbus Receiver (SLVR). This device, denoted the KOV-17, is a receive-only cryptographic unit, capable of being reprogrammed with new operational software, algorithms, and keys material in the field. These capabilities allow this device to maintain connectivity when installed in systems using current KG-38 capabilities while providing the capability to easily field a successor algorithm that can be used when the KG-38 algorithm reaches obsolescence. The programmable nature of the device also sup-

ports simultaneous support of both algorithms during a transition phase.

Maximizing the multichannel aspects of the PEIP has allowed the KOV-17 to provide the Fleet the ability to monitor 10 communications circuits concurrently, thus enhancing Fleet communications with submarines. The KOV-17 is currently used in the attack submarines (nuclear propulsion) (SSNs) and the ballistic missile submarines (nuclear propulsion) (SSBNs), and is scheduled for deployment aboard submarine tenders. A variant of the KOV-17, the KOV-17-1 is used by the Air Force in the Minuteman ballistic missile silos.

The KOV-17 implementation within SLVR provides the functionality of 10 KG-38s for each submarine platform. Each KG-38 weighs 37 lb, is 1230 in.³ in size, and consumes 57 W of power. A single KOV-17, which plugs into an SLVR chassis, is a 6u VME card weighing less than 2 lb and uses only 7 W of power. Figure 14 illustrates the benefits of the PEIP within SLVR.

Summary: The PEIP has wide ranging cryptographic applications benefiting the Navy, the Air Force, NSA, and the Department of Defense (DOD). Because the PEIP provides functionality essential to emerging INFOSEC products, the PEIP technological solution has become critical to the future of Navy programs. Continued research in PEIP technology, defined as PEIP Phase II, will address additional features and functions such as support for transmit and Multiple Independent Levels of Security. The PEIP Phase II is a cornerstone component of the DOD Crypto Modernization Program and has been chosen as the cryptographic solution for the DOD Nuclear Command and Control Program.

[Sponsored by SPAWAR and NSA]



FIGURE 14 Graphic illustration of the savings in size and complexity of the PEIP solution replacing KG-38s.



PEACE MONUMENT.

(Originally known as the Navy Monument). The two allegorical female figures at the top represent America weeping on the shoulders of History over the loss of her naval defenders during the Civil War.

- 163** Image-based Modeling of Naval Steels
A.B. Geltmacher, G. Spanos, and J.F. Bingert
- 165** Molecular Beam Epitaxial Growth of AlGaN/GaN High Electron Mobility Transistors
S.C. Binari, D.S. Katzer, D.F. Storm, B.V. Shanabrook, E.R. Glaser, and J.A. Roussos
- 167** A New Ferromagnetic Semiconductor: $\text{Mn}_x\text{Ge}_{1-x}$
A.T. Hanbicki, Y.D. Park, B.T. Jonker, S.C. Erwin, J.M. Sullivan, C.S. Hellberg, A. Wilson, and G. Spanos

[BACK TO CONTENTS](#)

IMAGE-BASED MODELING OF NAVAL STEELS

A.B. Geltmacher,¹ G. Spanos,¹ and J.F. Bingert²

¹Materials Science and Technology Division

²Detailed to NRL from LANL

Introduction: Alloy steels will continue to be the main structural material in Navy surface ships and submarines for the foreseeable future because of their relatively low cost, their good combination of mechanical properties, and the existing infrastructure for processing and fabrication. The desire to optimize or improve materials has traditionally required lengthy and expensive experimental programs. The development of a different approach, guided by material modeling and simulation¹ and validated by selected experiments, would enable significant improvements in the design of Naval materials. This approach is an important part of the Navy's Material by Design Grand Challenge. The ultimate goal of this challenge is to provide design engineers with enhanced/optimized alloy compositions and processing procedures to meet performance criteria for Naval structures, within reasonable time frames. Currently, alloy development time lines consist of many years using standard material development techniques because of their reliance on trial-and-error approaches. To significantly reduce this development time, state-of-the-art computational techniques over a wide range of length scales (from first principles to macroscopic) will be applied in conjunction with critical validation experiments. The objective of the research presented here is to use image-based finite-element models to investigate the effect of material microstructure on continuum-level response as part of the larger framework in the Navy Grand Challenge. Image-based modeling consists of using realistic, experimentally measured microstructural features as a basis for mesoscale stress/strain simulations.

Material Selection: Performance criteria for new alloy steels for Naval applications include eliminating magnetic signature to produce better stealth capabilities and improving corrosion resistance to reduce total ownership costs of future Naval structures. It is well known that the addition to steels of certain alloying elements (e.g., nickel and chromium) reduces magnetic signature by transforming the steel to the nonmagnetic austenite phase. Similarly, corrosion resistance is normally increased by the addition of chromium to the steel. AL-6XN, a "superaustenitic" stainless steel, was selected as a model material for this research. This

nonmagnetic alloy has good corrosion and strength properties due to its high nickel (~24 wt.%), chromium (~20 wt.%), and molybdenum (~6 wt.%) content. AL-6XN is currently being considered for certain Naval applications and represents a baseline composition for future alloy design exercises. The desire to reduce alloy content for cost and environmental concerns means that materials engineers will need to consider the possibility that stress-induced phase transformations can produce magnetic crystal structures in these "leaner" steels, due to loading events. Thus, image-based mesoscale modeling is needed to determine local stress and strain states generated within material microstructures under various loading conditions. Initiation of failure events such as stress-corrosion cracking, fatigue, and fracture, is also critically dependent on these local stress and strain states.

Experimental Characterization: We have characterized AL-6XN to develop statistically meaningful data sets in support of mesoscale finite-element modeling and to examine structure-property relationships in this stainless steel. The principal interrogation method involves automated electron backscatter diffraction (EBSD) analysis, which provides crystal orientation information, in combination with standard imaging of the microstructure. Figure 1 shows a typical crystal direction map for AL-6XN along with a subset of grains identified for further analysis. In this figure, different colors represent different crystallographic orientations of the atomic lattices within each grain. Analysis of the EBSD data reveals grain misorientation relationships and grain boundary distributions for the microstructure. Special grain boundary types can also be identified, including low-energy coincident site lattice boundaries, and these are delineated by color in the grain subset. The EBSD results also provide direct input for realistic polycrystal image-based models. Relative plastic response of AL-6XN to various loading conditions may also be predicted locally through mapping of the Taylor factor for a given applied deformation gradient and set of slip systems. Figure 2 shows the Taylor factor map for the subset of experimentally determined grains highlighted in Fig. 1. This map is useful for validating simulation results.

Finite-Element Modeling: Image-based finite-element models have been used to determine the location and level of stress incompatibilities at the mesoscale. Drs. Papaconstantopoulos and Mehl of the Center for Computational Materials Science at NRL calculate the elastic constants for use in the

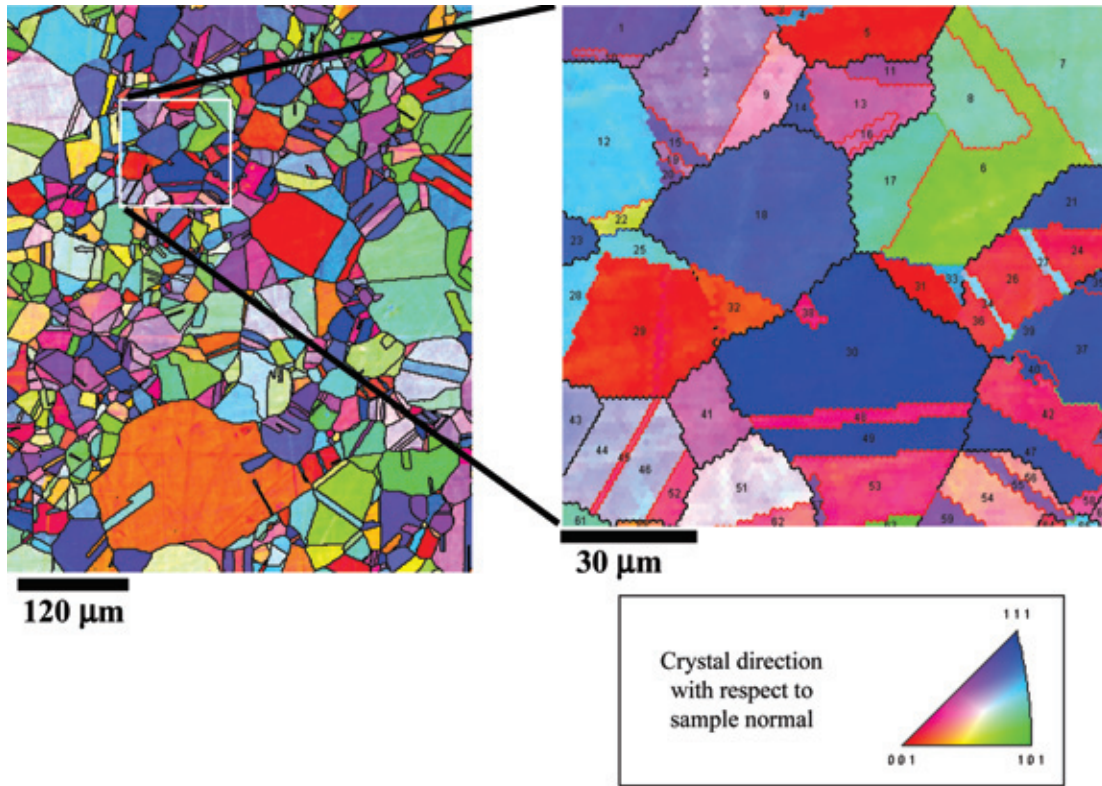


FIGURE 1 An experimental crystal orientation map measured using electron backscatter diffraction (EBSD) for AL-6XN. A subset of grains from the large map is highlighted on the right-hand side. The grains are color-coded by the crystal direction normal to the measured surface plane. Grain boundary types are differentiated by color.

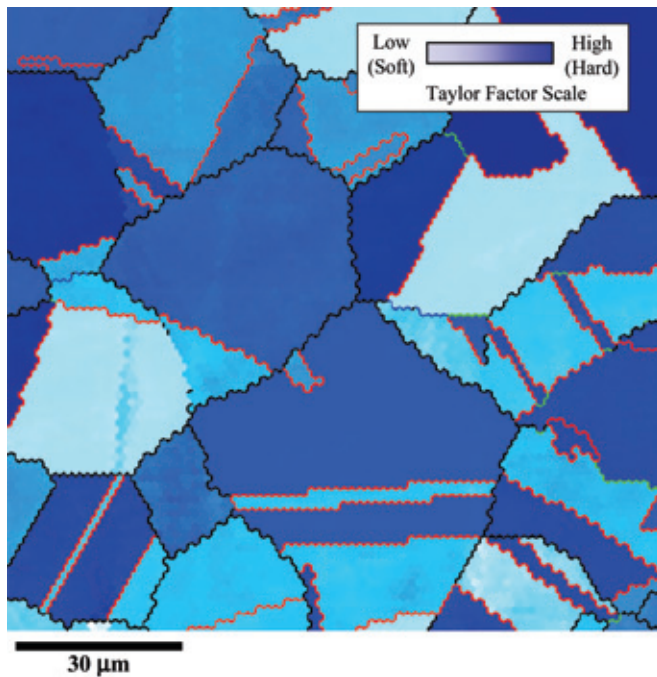


FIGURE 2 A Taylor factor map calculated for the highlighted subset from Fig. 1. The relative yield strength of the grains is scaled to the color key.

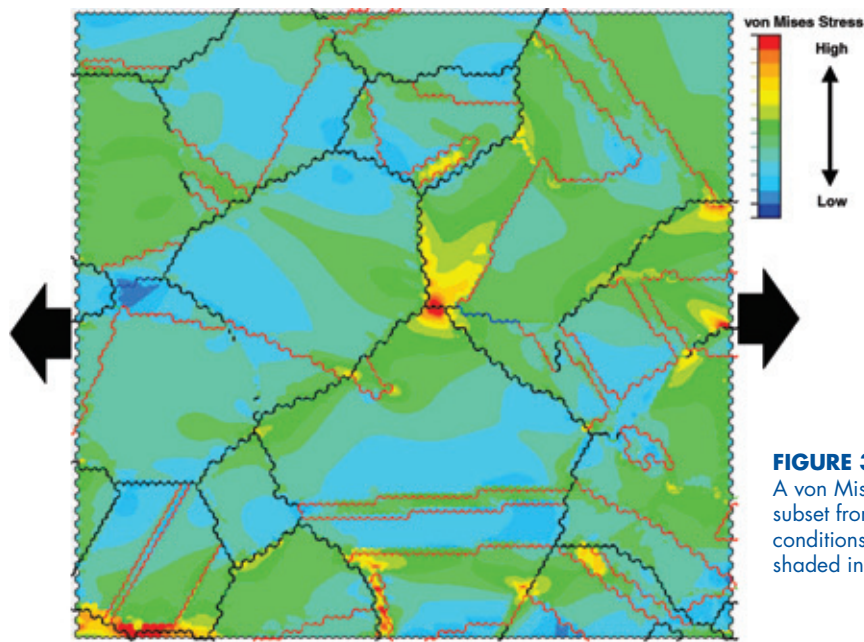


FIGURE 3
A von Mises stress contour plot for the highlighted subset from Fig. 1 under highly constrained loading conditions. Regions of high stress concentration are shaded in red.

models from first-principles and atomistic models. The image-based model results show that regions of large stress and strain gradients can be developed due to neighboring grain misorientations. For example, Fig. 3 shows the generation of high local von Mises stress regions under highly constrained loading conditions for the grain subset highlighted in Fig. 1. Comparison of these regions to the experimental EBSD maps shows the local grain configurations where phase transformations, plasticity, and damage may be nucleated.

Conclusions: A goal of the Navy's Materials by Design Grand Challenge is to develop the framework for computation-based design and selection of materials well into the future (~50 years). An important component of the Grand Challenge is the use of multiple computational techniques to design a material to meet specific property requirements. The computational models must cover a wide range of length scales—from atomistic, through microstructural, to macroscopic scales. The research briefly presented here shows the development of an experimental/computational technique that is useful in linking the microstructural scale to the macroscopic response in two dimensions. Full three-dimensional (3-D) models based on 3-D experimental data will be a future focus at NRL.

[Sponsored by ONR]

Reference

¹G. Olsen, "Computational Design of Hierarchically Structured Materials," *Science* **277**, 1237-1242 (1997). 

MOLECULAR BEAM EPITAXIAL GROWTH OF ALGaN/GaN HIGH ELECTRON MOBILITY TRANSISTORS

S.C. Binari, D.S. Katzer, D.F. Storm, B.V. Shanabrook, E.R. Glaser, and J.A. Roussos
Electronics Science and Technology Division

Introduction: The results achieved through the research and development undertaken in the GaN high electron mobility transistor (HEMT) technology are expected to have a significant impact on future DOD systems. The key performance factor that makes the GaN technology of interest is the high microwave-output-power density that has been achieved. As a result of this power performance advantage, this technology has been proposed for use in several DOD applications, including active arrays for ships, towed decoys, airborne arrays, and unmanned combat air vehicles.

GaN HEMTs have demonstrated a power density greater than 10 W/mm, which is an order of magnitude higher output-power density than commercially available technologies. This level of power performance is due to the high voltage and current density capability of the AlGaN/GaN materials system. GaN has a breakdown field of 3×10^6 V/cm, which is about 10 times higher than that of GaAs. The high breakdown permits high voltage operation, and this enables high power output. High voltage operation is also useful for reducing the requirements for dc voltage conversion in both

commercial and military systems. High drain currents are a direct result of the high electron density that can be formed at the AlGa_{0.25}N/GaN interface and the high velocity with which these electrons move. The high electron velocity also is a critical factor that determines the high-frequency operation of these transistors.

Although impressive performance has been demonstrated, significant developmental work remains before GaN HEMTs can become a viable technology. Improvements in substrate and epitaxial layer quality are key aspects that require further development. Research at NRL on the epitaxial growth of GaN and related compounds by molecular beam epitaxy (MBE) is structured to further this development. In the MBE growth process at NRL, elemental sources of Ga, Al, and In and a gaseous source of N are directed at a heated substrate. The active nitrogen is obtained from a nitrogen RF-plasma source. Mg and Be are available for use as acceptors and Si is used as a donor. Through precise control of the incident fluxes onto the substrate, high-quality epitaxial layers, with near-atomic thickness control, can be attained.

Results: Figure 4 shows the cross section of a typical GaN HEMT. The structure consists of a 0.1- μm -thick AlN buffer layer, a 1- μm -thick undoped GaN buffer/channel layer, and an undoped 250- \AA -thick Al_{0.25}Ga_{0.75}N barrier layer. These layers were grown on SiC substrates at temperature of about 750 °C. Reference 1 provides additional growth details. These layers generally have a sheet resistance of about 550 Ω/\square , a Hall mobility greater than 1200 $\text{cm}^2/\text{V}\cdot\text{s}$, and sheet carrier concentration of $1 \times 10^{13} \text{ cm}^{-2}$. Devices grown, fabricated, and characterized at NRL have demonstrated a continuous wave output power density of 6.3 W/mm, with a gain of 11.5 dB and a power-added efficiency of 36% at 2 GHz. Figure 5 shows these results. This is one of the highest power densities achieved for GaN HEMT structures grown by MBE, and it establishes a benchmark performance level for advanced device designs and material structures that are being pursued under internal programs.

One materials growth issue that can limit the performance of GaN HEMTs is parasitic conduction in parallel with the active channel. Parasitic conduction paths can be responsible for poor pinch-off behavior of transistors and poor interdevice isolation. Poor pinch-off can result in reduced power performance because the drain current and voltage swings that are available under ac drive will be reduced. Work was conducted at NRL to identify and eliminate sources of parasitic conduction.²

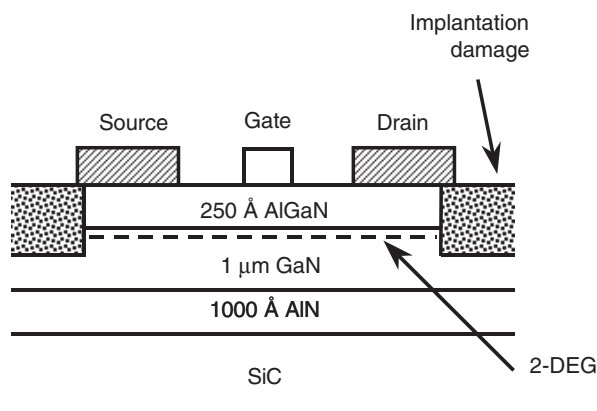


FIGURE 4
AlGa_{0.25}N/GaN HEMT cross section.

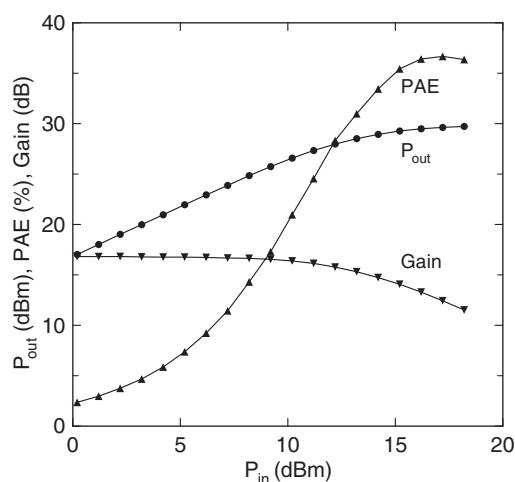


FIGURE 5
Measured continuous wave power performance at 2 GHz for a passivated, undoped AlGa_{0.25}N/GaN HEMT grown on semi-insulating SiC. Gate length = 1.5 μm , source-drain spacing = 4 μm , width = 150 μm .

Through the use of capacitance-voltage profiling of Schottky barrier test structures, we observed an increase in the GaN buffer layer carrier concentration near the interface with the underlying AlN layer under most growth conditions. We have compensated for this by introducing Be-doping immediately adjacent to the AlN interface. Device isolation was improved by a factor of 10^3 and, as shown in Fig. 6, the transistor pinch-off characteristic was dramatically improved. The use of Be-doping is a technique that should control parasitic buffer conduction under a wide range of growth conditions and, as a result, should provide additional flexibility in the design and growth of GaN device structures.

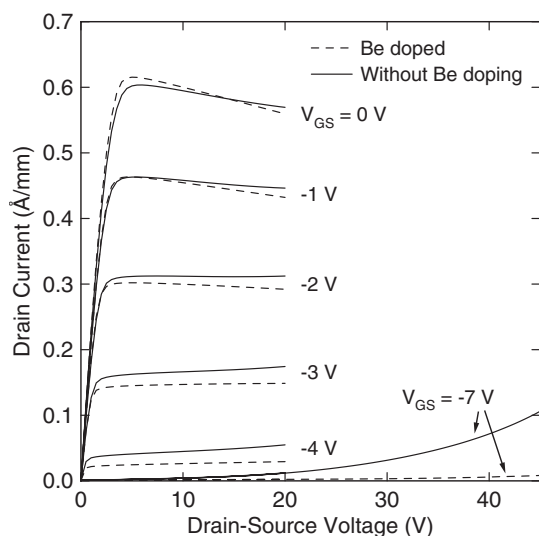


FIGURE 6 HEMT drain characteristics for devices without (solid lines) and with (dashed lines) Be doping. Note the improved pinch-off characteristics at a -7 V gate-source bias for the doped sample compared to the undoped sample.

Acknowledgments: The authors thank H.B. Dietrich for valuable discussions and N. Green for device fabrication.

[Sponsored by ONR]

References

- 1 D.S. Katzer, S.C. Binari, D.F. Storm, J.A. Roussos, B.V. Shanabrook, and E.R. Glaser, "MBE Growth of AlGaIn/GaN HEMTs with High Power Density," *Electron. Lett.*, in press.
- 2 D.F. Storm, D.S. Katzer, S.C. Binari, E.R. Glaser, B.V. Shanabrook, and J.A. Roussos, "Reduction of Buffer Layer Conduction Near Plasma-assisted Molecular-beam Epitaxy Grown GaN/AlN Interfaces by Beryllium Doping," *Appl. Phys. Lett.* **81**(20), 3819-3821 (2002).

A NEW FERROMAGNETIC SEMICONDUCTOR: Mn_xGe_{1-x}

A.T. Hanbicki,¹ Y.D. Park,² B.T. Jonker,¹ S.C. Erwin,¹ J.M. Sullivan,² C.S. Hellberg,¹ A. Wilson,³ and G. Spanos¹

¹Materials Science and Technology Division

²Present address: Seoul National University

³NRL/ASEE Postdoc

What is a Ferromagnetic Semiconductor:

Ferromagnetic semiconductors (FMSs) are materials that simultaneously exhibit semiconducting properties and spontaneous long-range ferromagnetic (FM) order. Classic examples, studied decades ago,

include the europium chalcogenides and the chalcogenide spinels. The coexistence of these properties in a single material provides fertile ground for fundamental studies as well as a host of new applications. Development of novel devices languished for some time due to the inability to incorporate these materials with mainstream semiconductor device materials.

Interest in FMSs was rekindled with the discovery of spontaneous FM order in $In_{1-x}Mn_xAs$ in 1989 and $Ga_{1-x}Mn_xAs$ in 1996,¹ when FM properties were realized in semiconductor hosts already widely recognized for semiconductor device applications. Although these new FMS materials have magnetic ordering, or Curie, temperatures (T_c) below room temperature, they have been closely studied for their potential in future spin-dependent semiconductor device technologies, with the expectation that further research will increase T_c . $Ga_{1-x}Mn_xAs$, for example, has been used as a source of spin-polarized carriers in both light-emitting diodes and resonant tunneling diode heterostructures.

A New Material: We have prepared the first Group-IV ferromagnetic semiconductor, Mn_xGe_{1-x} .² While most recent experimental work on FMSs has focused on III-V and II-VI compounds, there is broad interest in the Group IV semiconductors, namely C, Si, Ge, and $Si_{1-x}Ge_x$. Ge is of particular interest because it is closely lattice matched to the technologically important $Al_yGa_{1-y}As$ family and has higher intrinsic hole mobilities than either GaAs or Si. A high hole concentration is essential to mediate the necessary FM exchange.¹

We used nonequilibrium growth techniques such as molecular beam epitaxy and low substrate growth temperatures to minimize phase separation and the formation of unwanted compounds because of the low solubility of Mn in Ge. Mn_xGe_{1-x} single-crystal films can be grown on both Ge and GaAs substrates, and we have discovered that the electronic and magnetic properties are very promising for FMS device applications. In particular, electric field control of the FM order should be achievable at gate voltages compatible with present CMOS technology (± 0.5 V). Implementation of such a device is described below.

Magnetic and Electric Properties: Figure 7 shows magnetization as a function of temperature for a typical sample; Curie temperatures are derived from this type of data. Our films have T_c 's in the range of 25 to 116 K, with a linear dependence on Mn concentration for $0.006 \leq x \leq 0.035$. Magnetization loops (Fig. 7 inset) exhibit hysteretic behavior and have significant remanence—both clear signs of

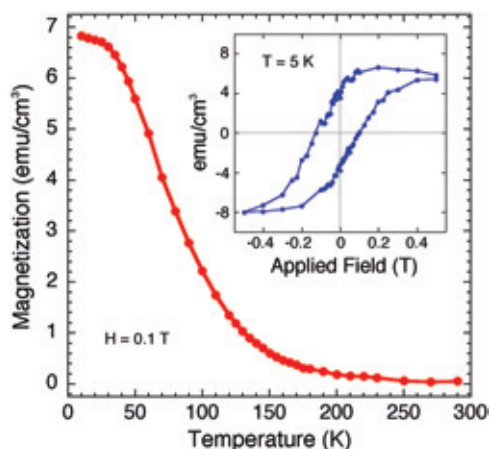


FIGURE 7

Temperature dependence of the magnetization for a 61.5 Å thick $\text{Mn}_{0.02}\text{Ge}_{0.98}$ film [inset shows the B-H loop at 5 K for the same sample].

FM order. Saturation magnetizations up to 30 emu/cm^3 indicate that only 45-60% of all the Mn atoms are magnetically active, and theory provides some insight into this behavior.

Hole densities at room temperature can be obtained from Hall measurements. The hole density increases with Mn concentration and ranges from 10^{19} to 10^{20} cm^{-3} . Below the magnetic ordering temperature, transport measurements clearly show a large extraordinary Hall effect (EHE), another clear signature of FM order. Finally, the resistivity of our $\text{Mn}_x\text{Ge}_{1-x}$ films decreases with temperature, indicating that samples are semiconducting rather than metallic in nature.

Insights from Theory: To investigate the microscopic origins of ferromagnetism in $\text{Mn}_x\text{Ge}_{1-x}$, we used electronic-structure calculations based on density-functional theory (DFT) with the aim of providing a first-principles foundation for future model descriptions. Mn preferentially occupies

substitutional sites and creates only negligible distortion of the host lattice—Ge atoms are perturbed by less than 0.05 Å. Figure 8 illustrates how a Mn atom affects the Ge lattice; electron density (Fig. 8(a)) is shown as green, and spin density (Fig. 8(b)) is shown as blue. Note that the bonding density between a Mn and Ge atom near the Ge atom is nearly the same as between neighboring Ge.

The calculated magnetic moment of Mn in Ge is $3\mu_B$, in agreement with other DFT studies but contrary to Hund's rules (as applied to defects). By mapping DFT results for the spin interactions onto a Heisenberg model, we extract spin couplings whose sign and magnitude depend on both distance and crystallographic direction, with ferromagnetic interactions ultimately dominating. The interactions are hole mediated, and are reduced when the material is strongly compensated. Nearest-neighbor Mn pairs are strongly antiferromagnetically coupled and hence do not participate in the FM ordering. This is consistent with our experimental data.

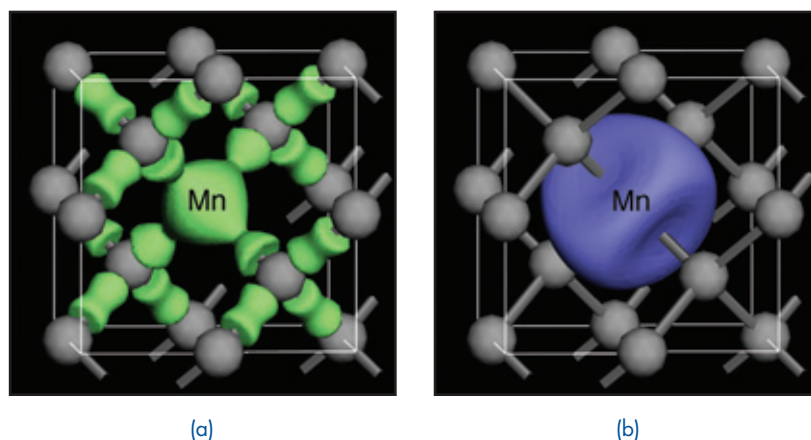
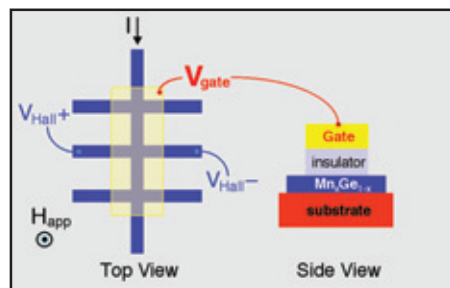
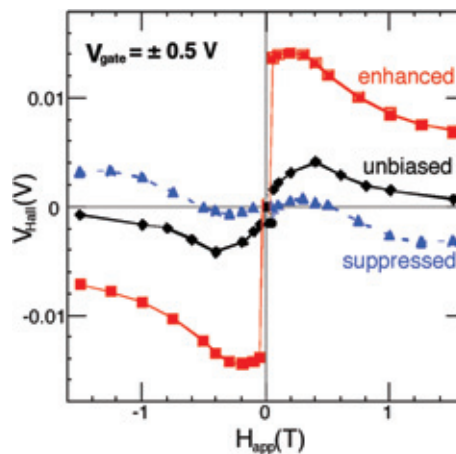


FIGURE 8

An isolated Mn atom in a Ge lattice showing the (a) calculated electron density and (b) calculated spin density.



(a)



(b)

FIGURE 9

(a) Schematic diagram of a gated Hall bar. (b) Hall voltage vs applied magnetic field at 50 K. The EHE voltage reflects the magnetization of the film. A ± 0.5 V gate voltage is used to vary the hole density in the $\text{Mn}_{0.015}\text{Ge}_{0.985}$ active layer. At zero gate voltage (diamonds), a small EHE signal is observed. As the hole density in the MnGe layer is enhanced (squares) or suppressed (triangles) by the gate voltage, the EHE signal and corresponding FM order is enhanced or suppressed.

A Unique Application: The nonmetallic character of our samples permits control of the carrier density in simple gated structures (Fig. 9(a)) via application of a small gate voltage. Since the FM exchange is mediated by the holes, we should be able to control the FM order, an effect demonstrated with $\text{In}_{1-x}\text{Mn}_x\text{As}$, but with very high gate voltages (± 125 V).³ The effect of gate voltage on FM order is shown in Fig. 9(b). The extraordinary component of the Hall voltage is clearly enhanced (suppressed) as the hole density is enhanced (suppressed) by a ± 0.5 V gate voltage, confirming that FM exchange is hole mediated in $\text{Mn}_x\text{Ge}_{1-x}$.

Summary and Implications: Epitaxially grown $\text{Mn}_x\text{Ge}_{1-x}$ is FM with semiconducting character.

Electric field control of the FM order, a unique property of FMS compounds, has been demonstrated with conventional low voltage circuitry. This suggests a variety of applications including low power control of magnetic fields, voltage-tunable dichroic devices, and gated optical isolators.

[Sponsored by ONR and DARPA]

References

- ¹ H. Ohno, "Making Nonmagnetic Semiconductors Ferromagnetic," *Science* **281**, 951 (1998).
- ² Y.D. Park, A.T. Hanbicki, S.C. Erwin, C.S. Hellberg, J.M. Sullivan, J.E. Mattson, T.F. Ambrose, A. Wilson, G. Spanos, and B.T. Jonker, "A Group-IV Ferromagnetic Semiconductor: $\text{Mn}_x\text{Ge}_{1-x}$," *Science* **295**, 651 (2002).
- ³ H. Ohno, D. Chiba, F. Matsukura, T. Omiya, E. Abe, T. Dietl, Y. Ohno, and K. Ohtani, "Electric Field Control of Ferromagnetism," *Nature* **408**, 944 (2000).





SEABEES MEMORIAL.

"Seabees" is the nickname for the U.S. Navy Construction Battalions (CBs). Formed during World War II, they were trained in both construction and combat and built naval facilities and living quarters in the Pacific.

- 173** Roughness-Induced Ocean Bottom Scattering
R.J. Soukup and R.F. Gragg
- 175** Global Ocean Nowcasts and Forecasts with the Navy Coastal Ocean Model (NCOM)
C.N. Barron, R.C. Rhodes, L.F. Smedstad, C.D. Rowley, P.J. Martin, and A.B. Kara
- 178** The Influence of Microbial Fe(III) Reduction on Clayey Sediment Flocculation
J.-W. Kim, Y. Furukawa, T. Daulton, S.E. O'Reilly, and S. Newell
- 181** Dissociation of Sub-Seafloor Gas Hydrates and Seafloor Stability: What Thermobaric Models Show
P.R. Vogt and W.-Y. Jung

[BACK TO CONTENTS](#)

ROUGHNESS-INDUCED OCEAN BOTTOM SCATTERING

R.J. Soukup and R.F. Gragg
Acoustics Division

Introduction: Given the increasing need to project Naval power into littoral regions, we expect that our Navy's active sonars will operate over ocean bottoms that will represent a kind of "hostile terrain." This hostile terrain contains high levels of acoustic backscattering that will degrade sonar performance. Generally, this backscatter is caused by the roughness of the water/bottom interface and by inhomogeneities in the sediments. Straits and other areas closely delimited by landmasses are prime examples of such environments. NRL has been at the forefront of important developments in predicting acoustic scattering from such water/bottom interfaces. In many of these areas, increased current flows have, over time, removed sediments and exposed rocky bottoms. In 2002, NRL researchers concluded an important study that identified bottom roughness as the driving mechanism that produces both high scattering levels and complex angular and frequency dependence.

Scattering and Active Sonar Performance:

In the Cold War era, when sonars usually operated in the open ocean, simple empirical descriptions of backscattering were often used, e.g. $BSS = \mu + 10 \log(\sin^2 \theta)$, where BSS is the bottom backscattering strength in decibels (dB) and θ is the bottom-grazing angle. μ is a constant, taken to be -27 dB on the relatively soft, sedimented bottoms typical of ocean basins. However, the littoral picture is more complex. For example, for an exposed limestone bottom, the best μ would be closer to -14 dB. Figure 1 illustrates the difference in predicted sonar performance for these two μ values and shows that the limestone bottom can severely limit a sonar's ability to find a target. Given the importance of bottom scattering in active sonar operations, it is crucial that the Navy use physics-based scattering models that can be incorporated into performance predictions.

Roughness-Induced Scattering: NRL has recently developed a scattering model based on the in situ physical parameters that specify both the geoacoustics and roughness of the seafloor.¹ Figure 2 shows predictions for limestone at 2000 Hz, with one of the two roughness parameters varied to simulate both smooth and rough bottoms. Note that these predictions differ substantially from the empirical model for limestone, and that their scattering

strengths are considerably enhanced at lower grazing angles, which are the most important angles in typical sonar operation. This illustrates the importance of characterizing the bottom roughness to make predictions about this type of seafloor. Although techniques such as stereo-photography do exist to extract this information, they are practical only for measuring very small areas. Consequently, in addition to quantifying the dependence of the acoustics on bottom roughness, we also must be able to estimate the roughness parameters themselves.

Tests on Limestone: One way to estimate these parameters is to use our physics-based model to invert for them from acoustic measurements. We illustrate this with data from a limestone bottom off the Carolina Coast for which the geoacoustic and roughness parameters were not known. The data exhibit the predicted complexity in grazing angle dependence, with intervals of rapid variation and others that were relatively flat. Figure 3 presents data at 2000 Hz together with a model prediction, where we evaluate all the unknown bottom parameters by using a multidimensional search technique to optimize the data-model fit. The results are consistent with typical limestone values in the geophysical literature. Multiple runs of the algorithm with random starting points produce a clear hierarchy of importance for the parameters—establishing the roughness parameters (and one of the geoacoustic parameters) as the main drivers of scattering for this ocean bottom.² The key role of the roughness motivates our designation of this type of scattering as "roughness-induced." Our ability to mathematically describe the statistical properties of this roughness, and our ability to model the observed scattering behavior allows us to confidently predict performance of sonar systems in these types of environments.

The Future: The results of this study underscored the role of roughness in seafloor scattering, but the difficulty of obtaining ground-truth measurements for the in situ roughness remains a significant problem. Controlled experiments are not practical for systematic study of the roughness properties of ocean bottoms. However, experiments in tank facilities with scale models made of appropriate materials afford an efficacious alternative. A slab of plastic or aluminum can be given a prescribed roughness with computer-controlled milling equipment. In 2002, we scattered ultrasound beams from a roughened polyvinyl chloride sample, and are currently analyzing the results as an analog to ocean-bottom limestone. With scale models, it is possible

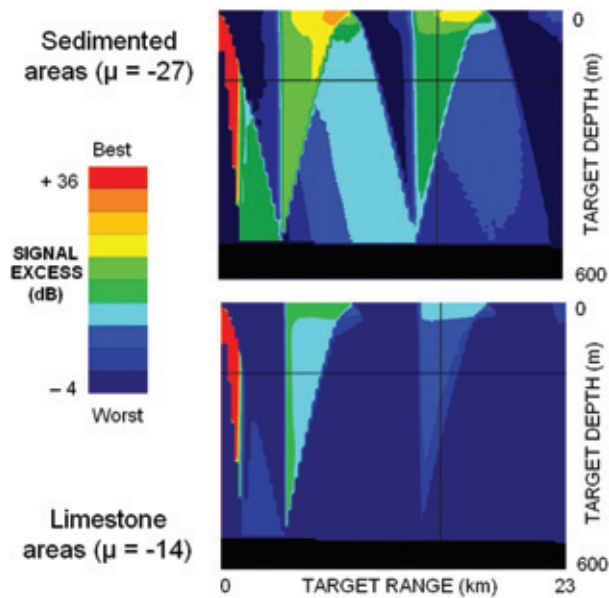


FIGURE 1 Predictions of sonar performance off the Carolina Coast for two different values of m , a constant described in the text. Signal excess (color) is a measure of confidence in a sonar's ability to find a target, with higher positive values indicating greater probability of successful detection. The signal excess is plotted for potential targets at different values of depth and range—one possible target location is shown by the intersection of the two black lines. (Model runs courtesy of J. Clements, Applied Research Laboratory, University of Texas.)

FIGURE 2 NRL model predictions of bottom backscattering strength at 2000 Hz for different values of an input parameter relating to the roughness of the limestone bottom (red curves), and the predicted curve for the empirical model for limestone mentioned in the text (blue curve).

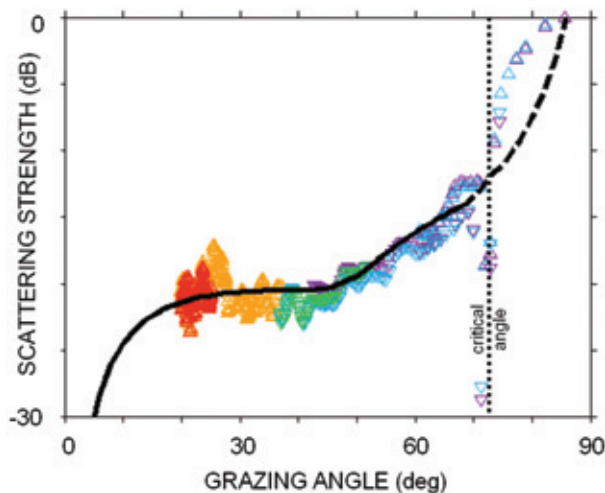
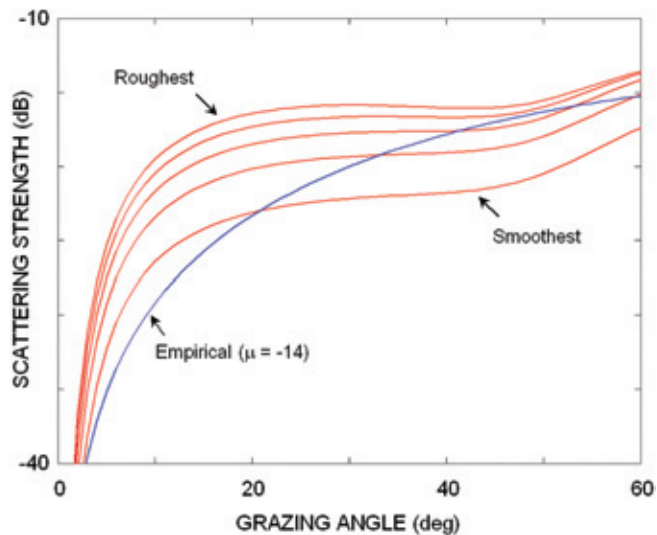



FIGURE 3 Bottom backscattering strength for Carolina Coast limestone plotted vs grazing angle. The NRL model prediction (solid line) gives an excellent fit to measured data up to the critical angle of 72 degrees (vertical line). Near the critical angle, data processing produces outlying values; above the critical angle, the model underpredicts because scattering mechanisms other than interface scattering make strong contributions. The different colors represent data subsets collected in different received directions and different deployments of the measurement system.

to directly verify predictions such as those of Fig. 2. Such efforts will require an interdisciplinary approach, involving NRL researchers with expertise in a variety of areas: design of acoustic experiments, scattering theory, materials science, laser profilometry, ground-truth geoacoustic measurements, and the operation of NRL tank facilities with computer-controlled sources and receivers.

[Sponsored by ONR]

References

¹ R.F. Gragg, D. Wurmser, and R.C. Gauss, "Small-slope Scattering from Rough Elastic Ocean Floors: General Theory and Computational Algorithm," *J. Acoust. Soc. Am.* **110**, 2878-2901 (2001).

² R.J. Soukup and R.F. Gragg, "Scattering from a Rocky Bottom at 2-3.5 kHz: Measurements and Modeling," *J. Acoust. Soc. Am.* (to appear). 

GLOBAL OCEAN NOWCASTS AND FORECASTS WITH THE NAVY COASTAL OCEAN MODEL (NCOM)

C.N. Barron, R.C. Rhodes, L.F. Smedstad,
C.D. Rowley, and P. J. Martin
Oceanography Division
A.B. Kara
Florida State University

Introduction: The global ocean is a seamless body where open-ocean systems shape and are shaped by nearshore conditions, surface processes drive and respond to interior circulation, and localized events often can be predicted and understood only within a larger context. To support Navy operations and other research and operational activities within such an environment, we have developed and are transitioning to the Naval Oceanographic Office (NAVO) a fully global implementation of the Navy Coastal Ocean Model (NCOM). We have endeavored to produce a friendly environment for nesting higher resolution models wherever the need should arise. Some global NCOM data products of particular interest include surface currents and temperature, mixed-layer depth, current and thermohaline profiles, and shelf circulation.

Global NCOM extends present global Navy operational model capabilities¹ into the Arctic and to nearshore regions, with a minimum depth of 5 m. Operational roles of global NCOM include providing standalone data where global resolution is sufficient and timely overviews of local circulation as detailed localized products are prepared. Perhaps its most important purpose is to provide boundary conditions used by regional or relocatable models, giving re-

quired information regarding the surrounding environment to localized models more specialized for a particular task or domain. In general, nested models will have more detailed forcing, topography, additional data for assimilation, or higher resolution necessary for improved local detail. The global model includes inflow from almost 1000 rivers to improve the fidelity of coastal salinity. Global NCOM is designed to be suitable for inclusion in a coupled ocean-atmosphere modeling system, and it is also designated as the host for an embedded ice model, PIPS3, which is in development for transition.

Implementation: NCOM is a free-surface, primitive-equation model based primarily on two other models, the Princeton Ocean Model and the Sigma/Z-level Model.² In its global configuration, we have implemented NCOM on a curvilinear horizontal grid designed to maintain a grid-cell horizontal aspect ratio near 1. Horizontal resolution varies from 19.5 km near the equator to 8 km or finer in the Arctic, with midlatitude resolution of about 1/8° latitude (~14 km). Figure 4 shows a sea surface temperature (SST) snapshot from the full domain in a projection that shows the actual distribution in the logical domain. Horizontal resolution has been sacrificed to allow increased vertical resolution. To improve the detail of upper-ocean dynamics, we maintain a maximum 1-m upper level thickness in a hybrid sigma/z vertical configuration with 19 terrain-following sigma-levels in the upper 137 m over 21 fixed-thickness z-levels extending to a maximum depth of 5500 m. Model depth and coastline are based on a global 2-minute bathymetry produced at the Naval Research Laboratory (NRL).

The present daily model run consists of a 72-hour hindcast to assimilate fields that include recent observations, and a 72-hour forecast. Longer forecasts are being evaluated. Global NCOM uses atmospheric forcing from the Navy Operational Global Atmospheric Prediction System, with latent and sensible heat fluxes calculated internally using NCOM SST. Tidal heights and currents can be added using a separate user-specified model, with validation and boundary condition experiments focusing on using the NAVO operational model PC Tides.

Assimilation: Data assimilation is based on global profiles of temperature and salinity derived using operational sea-surface fields and in situ data within the Modular Ocean Data Assimilation System (MODAS)³. The operational global 1/16° Navy Layered Ocean Model (NLOM), while limited to subpolar waters deeper than 200 m, has higher horizontal resolution than Global NCOM and is better suited to directly assimilate altimeter data and fore-

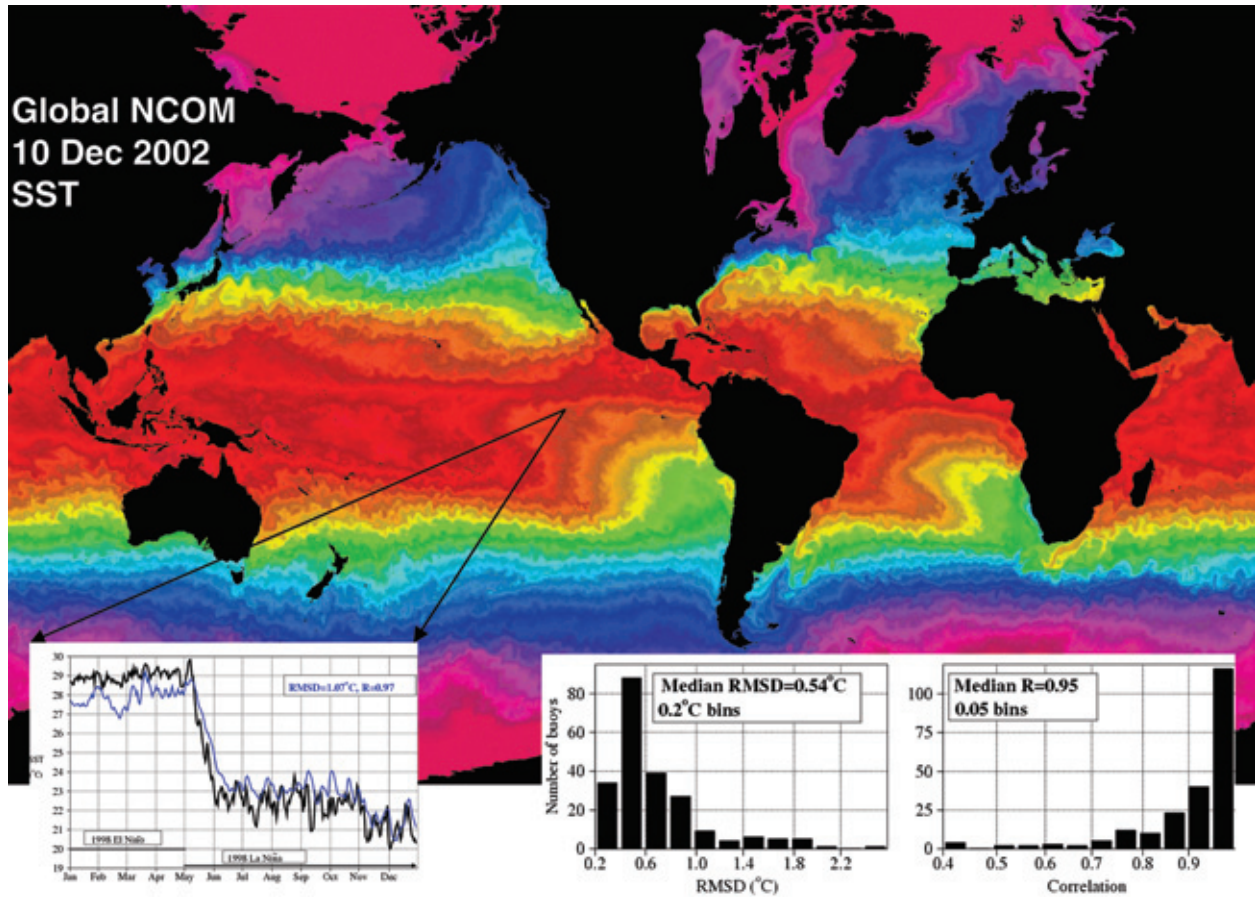


FIGURE 4

The global Navy Coastal Ocean Model (NCOM) extends from the Arctic Ocean to the coast of Antarctica and from the open ocean over the shelf break to nearshore regions. Plots of model products such as this sea surface temperature field are available from www.ocean.nrlssc.navy.mil/global_ncom. A variety of global NCOM validation tests continue. For example, the histograms summarize comparisons with 219 unassimilated, year-long buoy SST time series in the Equatorial Pacific, North Pacific, and shelf regions of the United States. One of these cases (line plot) shows NCOM agreement (blue) with one TAO buoy (black) during the extreme 1998 El Niño to La Niña transition.

cast the location of fronts and eddies. To take advantage of this capability, NLOM sea surface height (SSH) fields are paired with MODAS2D SST to derive temperature and salinity profiles using the MODAS dynamic climatology. NCOM relaxes toward these profiles according to a spatially variable weighting function. Figure 5 shows four year-long time series that demonstrate the progression from background climatology, to assimilation field, to model result, with the unassimilated observations for comparison.

Validation: Validation of global NCOM against observation-based standards uses a variety of experiments and criteria. Some are climatological comparisons against historical means, including evaluation of mean eddy kinetic energy at various depths and transport and velocity distributions through straits or other sections. NCOM nowcasts and forecasts are compared with satellite observations, prior to assimilation, or with independent in situ data, as shown in Fig. 4. In situ data are also used to evaluate subsurface temperatures and mixed layer depth (Fig. 5). Validations of ocean currents are based on com-

parisons with drifter trajectories and ADCP sections. Finally, event comparisons in regions of interest may be made using a variety of observational sources, such as the comparison shown in Fig. 6 of ocean color products compared with NCOM surface height and currents in the Arabian Sea.

Plans: We are transitioning global NCOM to NAVO, with delivery for operational testing scheduled for February 2003. Testing continues on modified assimilation schemes, boundary condition extraction, and mixed-layer tuning. Global NCOM data provide boundary information for a number of ongoing research efforts.

Acknowledgments: The authors thank Dr. H. Hurlburt (NRL) and Dr. W. Schmitz (WHOI emeritus) for their advice and guidance during development and transition of the Global NCOM system; Dr. A. Wallcraft (NRL) for his work in making NCOM code portable and scaleable; Dr. D. Ko for his work on the global bathymetry and model grid; and Dr. R. Arnone (NRL) and Dr. J. Kindle (NRL) for help in the comparison with ocean color. We also

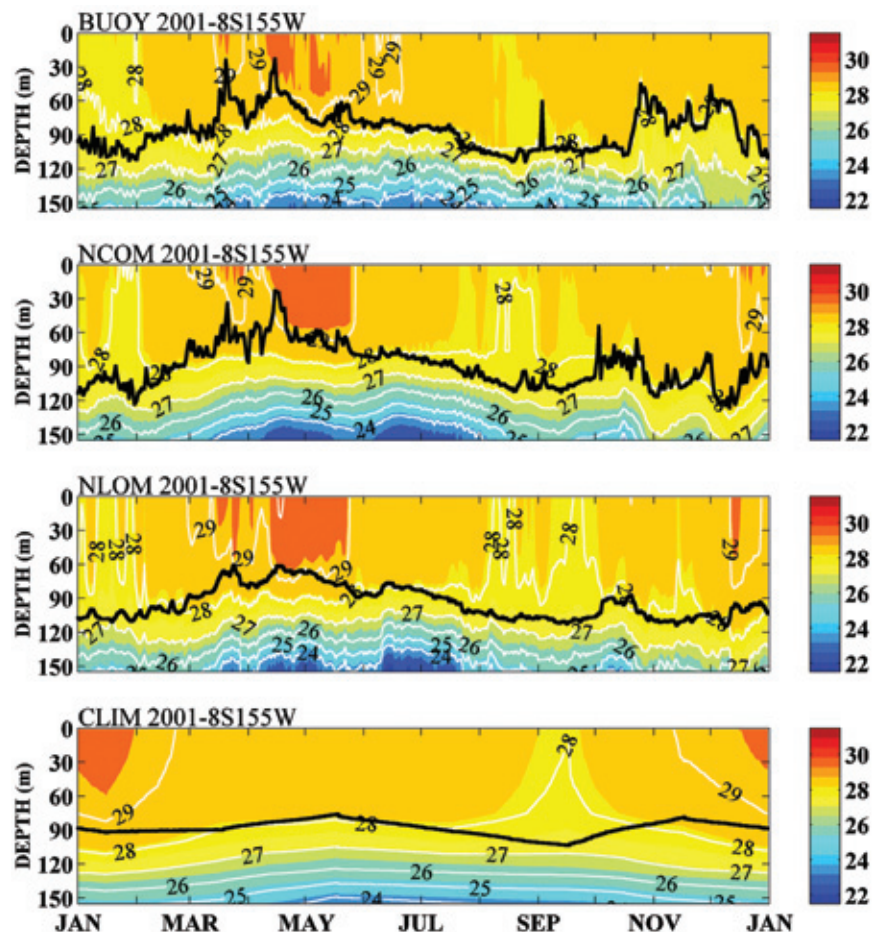


FIGURE 5 Time-series from 2001 at a TAO buoy location in the equatorial Pacific (8°S, 155°W). The bottom series indicates the MODAS climatological background. Using real-time MODAS SST and NLOM SSH, the MODAS dynamic climatology produces a field that is assimilated into global NCOM. The ability of global NCOM to resolve the mixed-layer dynamics allows it to produce a mixed-layer depth (black line on each series) in closer agreement with the variability measured in the observations.

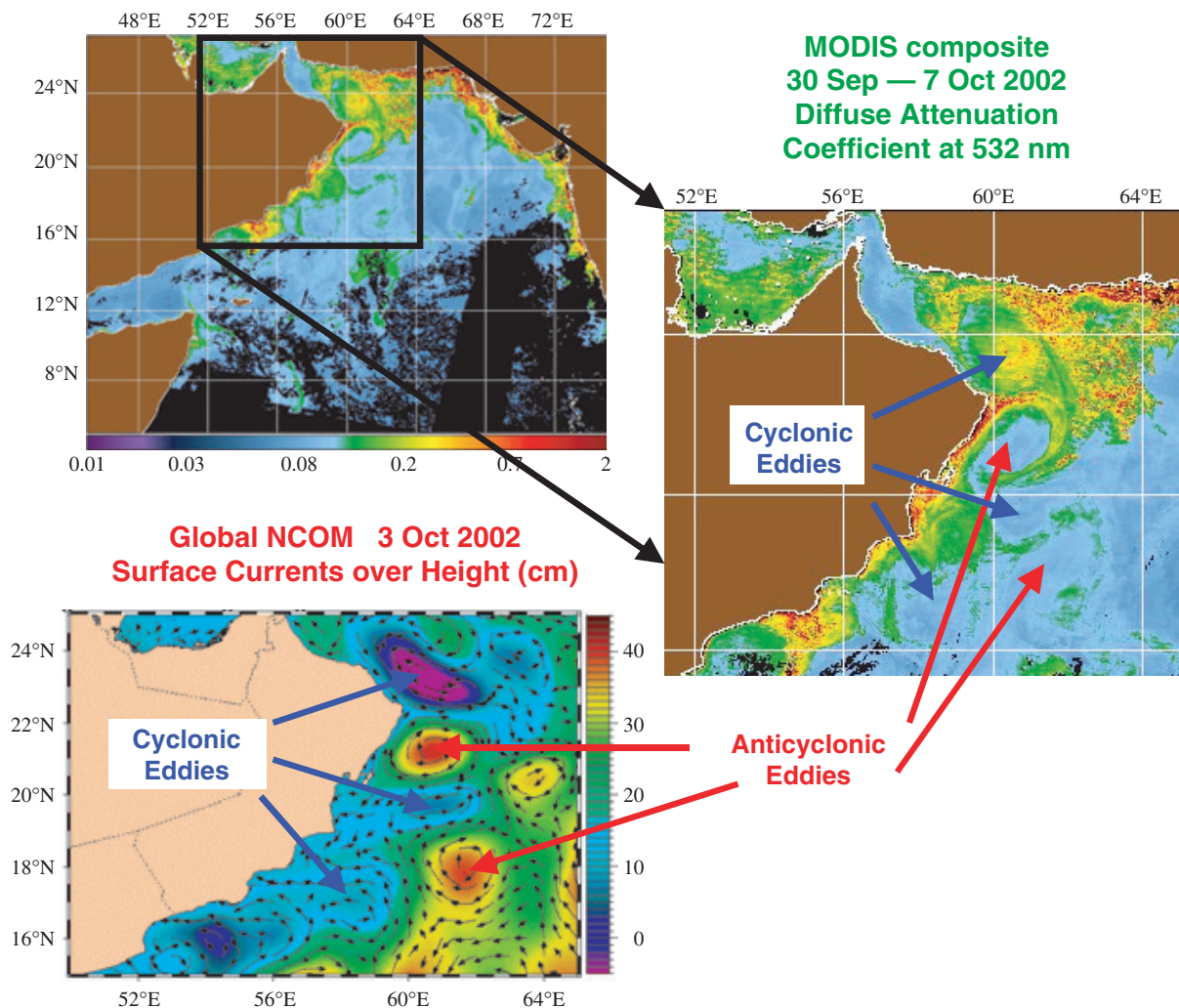


FIGURE 6
Global NCOM SSH and surface currents in the Arabian Sea are compared with a MODIS composite produced by the Ocean Optics section at NRL (Ocean Color at <http://www7300.nrlssc.navy.mil/products.html>). Eddies located in the global NCOM analysis agree with observed features delineated by gradients in diffuse attenuation coefficient.

thank Ms. J. Dastugue for her assistance in developing the Global NCOM web site at www.ocean.nrlssc.navy.mil/global_ncom. This work is made possible through the support of Space and Naval Warfare Systems Command PMW155 and computational resources provided by the Department of Defense High Performance Computing Modernization Program.

[Sponsored by SPAWAR]

References

- ¹R.C. Rhodes et al., "Navy Real-time Global Modeling Systems," *Oceanog.* **15**, 29-43 (2002).
- ²P.J. Martin, "Description of the Navy Coastal Ocean Model Version 1.0," NRL Report FR/7322-00-9962, 45 pp. (2000).
- ³D.N. Fox, W.J. Teague, C.N. Barron, M.R. Carnes, and C.M. Lee, "The Modular Ocean Data Analysis System (MODAS)," *J. Atmos. Ocean. Technol.* **19**, 240-252 (2002).

THE INFLUENCE OF MICROBIAL Fe(III) REDUCTION ON CLAYEY SEDIMENT FLOCCULATION

J.-W. Kim, Y. Furukawa, T. Daulton, S.E. O'Reilly, and S. Newell
Marine Geosciences Division

Introduction: Understanding the role of flocculation of suspended sediments carried by rivers is important to industries and naval undersea operations. This "fluid mud" can be responsible for the variability of littoral sediment properties such as turbidity, shear strength, and compressibility. Many theoretical and laboratory studies have dealt with the physical chemistry and fluid dynamics of interactions among sedi-

mentary particles.¹ Nevertheless, previous studies have given little consideration to the environmental variables that are important in the actual sedimentary environment such as the variability of particle compositions (i.e., bacteria, particulate organic matter, and clay mineralogy) and the temporal and spatial dynamics of redox chemistry controlled by the microbial diagenesis. Furthermore, few direct observations of suspended particles in fluid mud were reported, which may be due to the difficulties of sampling or handling the materials. In this study, we aim to quantify the role of microbial diagenesis in controlling particle flocculation.

Material and Methods: Nontronite from the Uley graphite mine, South Australia (Clay Mineral Society standard, NAu-1) was used in this study. Nontronite is an iron-rich smectite widely distributed in marine and terrestrial environments. Powdered nontronite (< 0.2 mm) and iron-reducing bacterium, *S. oneidensis*, were mixed in a tube, and then incubated anaerobically for 48 hours. Similarly, a control lacking cells was prepared and incubated. Reduced and nonreduced (control) nontronite were then suspended in separate settling columns placed in an anaerobic chamber. The size distribution of suspended aggregate particles and their settling velocity was measured using a Micromeritics Sedigraph and calculated based on Stokes' Law. A JEOL JEM-3010 transmission electron microscope (TEM) operating at 300 keV was used to characterize changes in the floc architecture, in particular the changes in structure of nontronite particles that were induced by microbial reduction of Fe(III) in nontronite. Reference 2 provides details of sample preparation and experimental methods.

Results: Figure 7 shows the reduced nontronite (with cells) in settling tube A and the nonreduced nontronite (without cells) in settling tube B. The substantial color change of clay that resulted from reduction of Fe(III) is apparent in tube A compared to tube B, which displays the original color of the clay. The reduced nontronite suspension began to flocculate in 30 minutes, as indicated by the arrow, and was almost completely settled in 80 minutes (tube A). In contrast, the controlled nontronite suspension remained dispersed in the water column, even after 80 minutes (tube B). Nontronite aggregate size distributions were measured using a Micromeritics Sedigraph in various durations of incubation time (0 – 48 hr) compared to controlled nontronite, as shown in Fig. 8. Depending on a given condition, the reduced nontronite suspen-

sions show variations of aggregate sizes ranging from 2.5 to 4 μm in equivalent spherical diameter at 50 cumulative mass percent, which is about 5 to 8 times larger than controlled suspensions (0.5 μm). The calculated mean settling velocity of reduced nontronite suspensions is 6.9×10^{-4} cm/s based on 25 degrees in temperature, average grain density = 2.5 g/cc, and average grain size = 3.2 μm , while 2.1×10^{-5} cm/s averaged settling velocity is calculated for nonreduced nontronite suspensions with 0.5- μm average grain size. The aggregate size distributions of 0- and 3-hour incubation experiments are similar, and 12-, 24-, and 48-hour incubation experiments are similar. Previous studies have shown that there is no structural Fe(III) reduction at 0 hour, and less than 10% of total structural Fe(III) is reduced to Fe(II) within the first 3 hours of incubation.³ Consequently, the formation of flocs in these samples is considered to be controlled by microbial biopolymers rather than by the change in particle redox chemistry. However, small aggregates (less than 2.5 μm) are found only in 0 to 3 hour samples, not in 12 to 48 hour samples, suggesting the role of further microbial reduction of clay layers and further production of biopolymers in coagulation of small aggregates into larger macro-flocs.

The TEM-imaged floc architectures of the control and reduced nontronite suspensions are illustrated in Fig. 9(a) and 9(b), respectively. Typically, hexagonal-shaped single nontronite particles are well-dispersed, and large pore areas are dominant features of nonreduced nontronite (Fig. 9(a)). In comparison, reduced nontronite occurs in clusters containing *S. oneidensis* (S) and biopolymers with few if any pore areas observed (Fig. 9(b)). The structural changes in nontronite upon Fe(III) reduction are shown in Fig. 9(c) and 9(d). The mean basal layer spacing decreases from 1.5 to 1.2 nm, and the diffuse ring patterns in the selected area diffraction (SAED) patterns gain discrete Bragg reflections upon Fe(III) reduction. The structural changes are mainly caused by the increase in net negative charge on reduced nontronite; therefore, coagulation of the clay particles is accelerated by cations such as Na^+ and Ca^{2+} .

Conclusions: Microbial Fe(III) reduction promotes the flocculation properties of clay particles: (1) biopolymers play an important role of forming micro-flocs of dispersed nonreduced clay particles (<2.5 μm); (2) upon microbial Fe(III) reduction, both surface charges increase and further production of biopolymers promotes the coagulation of clay aggregates forming macro-flocs (>2.5 μm).

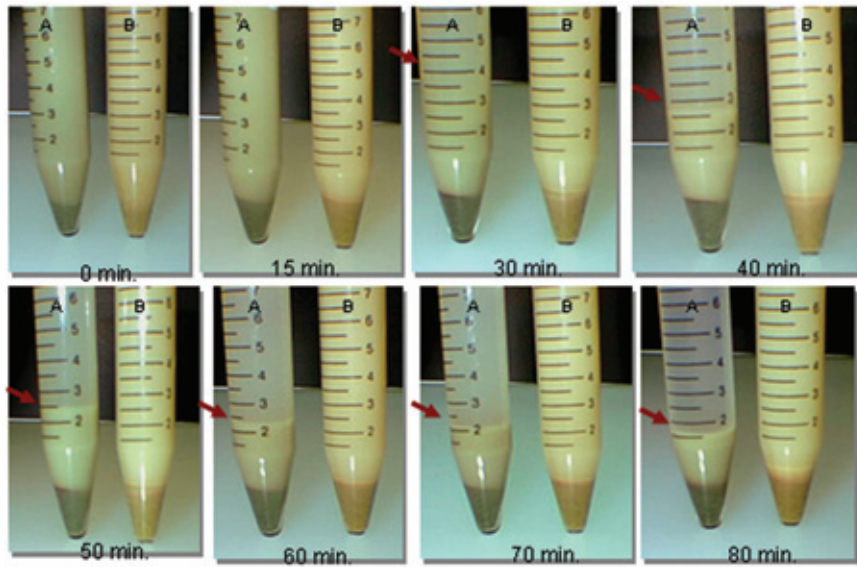


FIGURE 7
Settling behavior of microbially Fe(III) reduced nontronite suspensions (tube A) and non-reduced (control) nontronite suspensions (tube B).

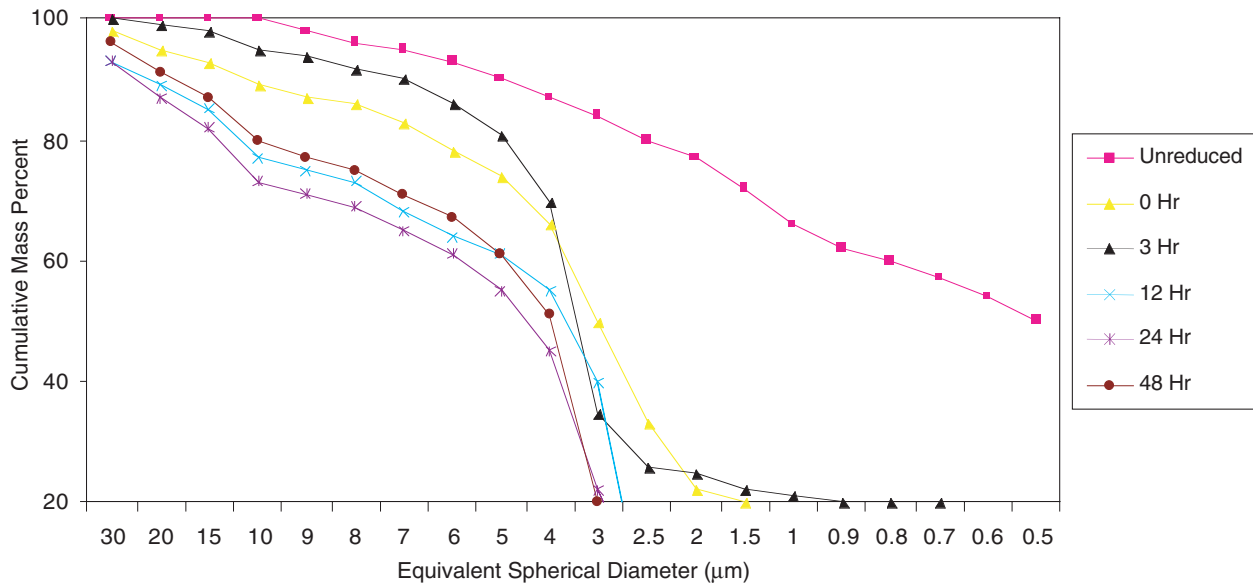


FIGURE 8
Aggregate size distribution of nonreduced (control) nontronite and microbially Fe(III) reduced nontronite suspensions (over 48 hours).

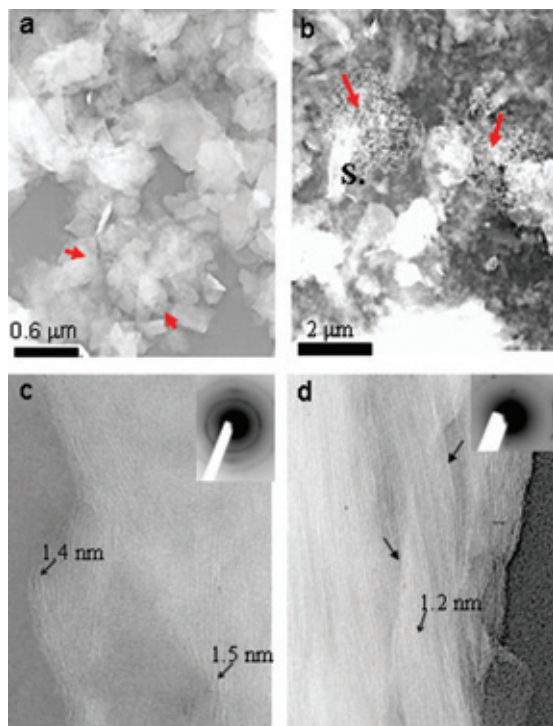



FIGURE 9
Conventional transmission electron microscopy (TEM) micrographs of flocc architectures of (a) nonreduced (control) nontronite suspensions and (b) microbially Fe(III) reduced nontronite suspensions inoculated with *S. oneidensis* (S). Environmental cell (EC)-TEM micrographs with selected area electron diffraction (SAED) patterns showing; (c) nonreduced (control) nontronite (lattice fringe spacing \approx 1.4 – 1.5 nm) and (d) reduced nontronite (lattice fringe spacing \approx 1.2 nm).

Acknowledgments: We thank J. Watkins of NRL for helping the experiments.
[Sponsored by ONR]

References

- ¹A.J. Manning and K.R. Dyer, "A Laboratory Examination of Flocc Characteristics with Regard to Turbulent Shearing," *Marine Geol.* **160**, 147-170 (1999).
- ²J.W. Kim, Y. Furukawa, T. Daulton, D. Lavoie, and S. Newell, "Characterization of Microbially Fe(III)-reduced Nontronite: Environmental Cell-Transmission Electron Microscopy Study," *Clays & Clay Minerals* (in press).
- ³J.E. Kostka, J.W. Stucki, K.H. Neelson, and J. Wu, "Reduction of Structural Fe(III) in Smectite by a Pure Culture of *Shewanella Putrefaciens* Strain MR-1," *Clays & Clay Minerals* **44**, 522-529 (1996). 

DISSOCIATION OF SUB-SEAFLOOR GAS HYDRATES AND SEAFLOOR STABILITY: WHAT THERMOBARIC MODELS SHOW

P.R. Vogt and W.-Y. Jung
Marine Geosciences Division

Introduction: Gas hydrates, which are stable at the high pressures of seafloor more than a few hundred meters deep, are crystalline solids with a cage-like (clathrate) structure of water molecules enclosing larger host molecules, most commonly methane. The material is present between sediment grains or in larger veins and nodules under most continental

margins, with enormous aggregate volumes. Ongoing research, some at NRL, is motivated by the potential use of hydrates as a fuel source, the possible release of greenhouse gas by hydrate dissociation, and the influence of such dissociation on seafloor sediment stability, which forms the basis for our study.

The association of undersea landslides with geophysical evidence for hydrates below the U.S. East Coast continental slope led G. Carpenter to hypothesize in 1981 that low sea levels of the last Ice Age (ca. 18,000 years ago, abbreviated 18ka (millenia ago)) may have caused hydrate to dissociate at depth, reducing sediment shear strength and facilitating failure. Other researchers elaborated on this idea—suggesting that the methane liberated by slides could have warmed the atmosphere, forming a "shut-off valve" for ice ages. While these ideas have gained wide acceptance, Norwegian scientists found the three major slides they studied along their margin (Fig. 10) to have happened when they should not—during the rapidly rising sealevels of post-glacial times. The largest (Storegga, 5,500 cubic kilometers!) and best known slide—and one that NRL and Norwegian collaborators have studied, including 1999 dives by USN nuclear submarine NR-1—occurred 8,150 years ago (8.15ka), generating a major tsunami. Intrigued by this contradiction but still suspicious that hydrate dissociation helped cause the failures, we began modeling the evolution of the gas hydrate stability zone at Storegga and other margins.

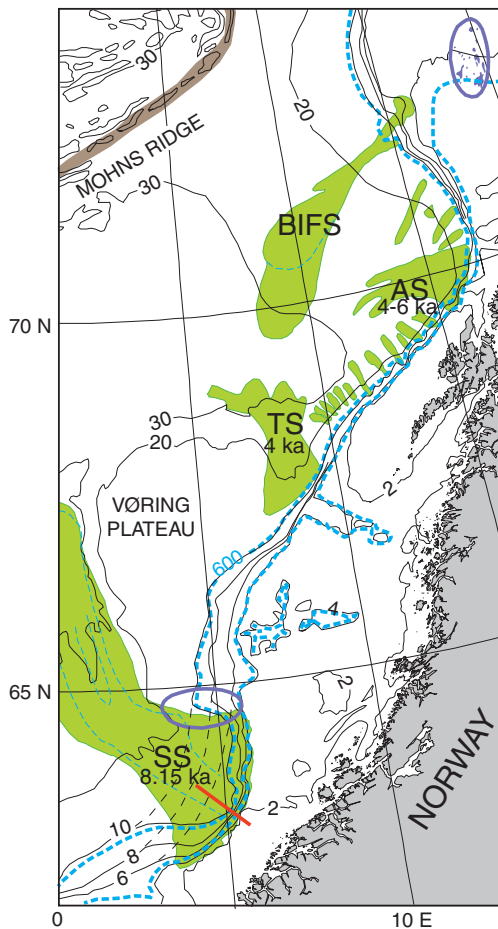


FIGURE 10 Norwegian continental margin, showing relatively recent giant underwater landslides in green: SS, Storegga slide; TS, Traenadjupet slide; AS, Andøya slide; and BIFS, Bear Island Fan slide. Gas hydrate stability models shown in Figs. 11 and 12 were computed along line #1. Black contours show water depths in 100s of meters; thickness of modern methane hydrate stability zone, in meters, is shown by dashed blue contours (600 and 0 m). Blue ovals and patches show areas where seismic surveying has detected hydrates to date.

If major slides can happen in post-glacial times, could they occur today or tomorrow?

Research Approach: Starting with a “slice” through the sea and seafloor in the middle of the Storegga slide scar (red line in Fig. 10), we calculated the thickness of the Methane Hydrate Stability Zone as a function of rising sea level and bottom water temperatures, which have opposing effects on hydrate stability: A rising sea level, due mostly to melting glaciers, increases pressure at all depths and makes hydrate stable to greater depths. However, seawater warming at the ocean floor has the opposite effect—once this warmer boundary condition diffuses to the base of the hydrate stability zone, any hydrate in that basal region would become unstable, liberating free gas and water, and thus reducing the shear strength of the mud.

As in other physical modeling studies, we need reasonably accurate estimates for various physical quantities—either from laboratory or field measurements. For example, sediment density determines the pressure exerted on the hydrate by the overlying mud. Previous NRL cores gave us near-bottom den-

sity, but at greater depths (10s to 100s of meters) we rely on published seismic and borehole results. The subbottom temperature gradient controls the pressure (depth) at which hydrate becomes unstable—the steeper the gradient, the thinner the stability zone. To get this gradient, we combined shallow (a few meters penetration) thermal probe data from past NRL cruises with other published values. The thermal diffusivity is needed to calculate the rate at which seafloor warming propagated (“diffused”) down into the subbottom. Because we are interested in what happened in the Storegga slide area over time, we have to figure out what the topography looked like *before* the slide altered it. Such topographic reconstruction can be done by extrapolating depth contours from one side of the horseshoe-shaped slide scar to the other (Fig. 10 shows concept). One can think of the pre-slide margin as a cookie, from which a bite has been taken. Even if the bitten-off piece is missing, the cookie’s original shape can be estimated. For Storegga, the volume of the “bite” has been checked by seismic reflection techniques against the amount of slide debris in the Norway Basin.

The phase boundary separating hydrate from methane+water depends on pore water chemistry. Laboratory studies show that if the water between the sediment grains is salty, the boundary is shifted to decreasing stability (“A” side of gray band in Fig. 11). On the other hand, if some higher hydrocarbons, for example ethane, are mixed with the methane, the stability field is expanded (“B” in Fig. 11). Uncertain pore water chemistry led us to show the boundary as a band, vs a sharp line. Fresh pore water with pure methane lies in the middle of the band. The “truth,” likely varying with depth and locale, probably lies somewhere within. Future deep drilling and pore water chemistry will some day provide a more precise answer.

Since seawater sulfate ions oxidize methane in the upper sediments (light blue regions in Fig. 12),

methane hydrate, although stable, is largely absent there.

A most critical dataset is the history (more precisely the *PRE*-history) of how sea levels and water temperatures rose starting 18,000 years ago, when the last Ice Age “maxed out.” One of the two sea level rise curves we used was derived from a joint NRL-US Geological Survey sediment coring expedition to our own Chesapeake Bay, and similar curves have been derived by others. When a branch of the Gulf Stream entered the Norwegian Sea ca. 11,000 years ago, it left a different assemblage of planktonic fossils in the sediments below from which past ocean temperatures can be reconstructed.

Although we cannot go back in a time machine to directly measure past gas hydrate distribution, present (0ka) model validation can and has been per-

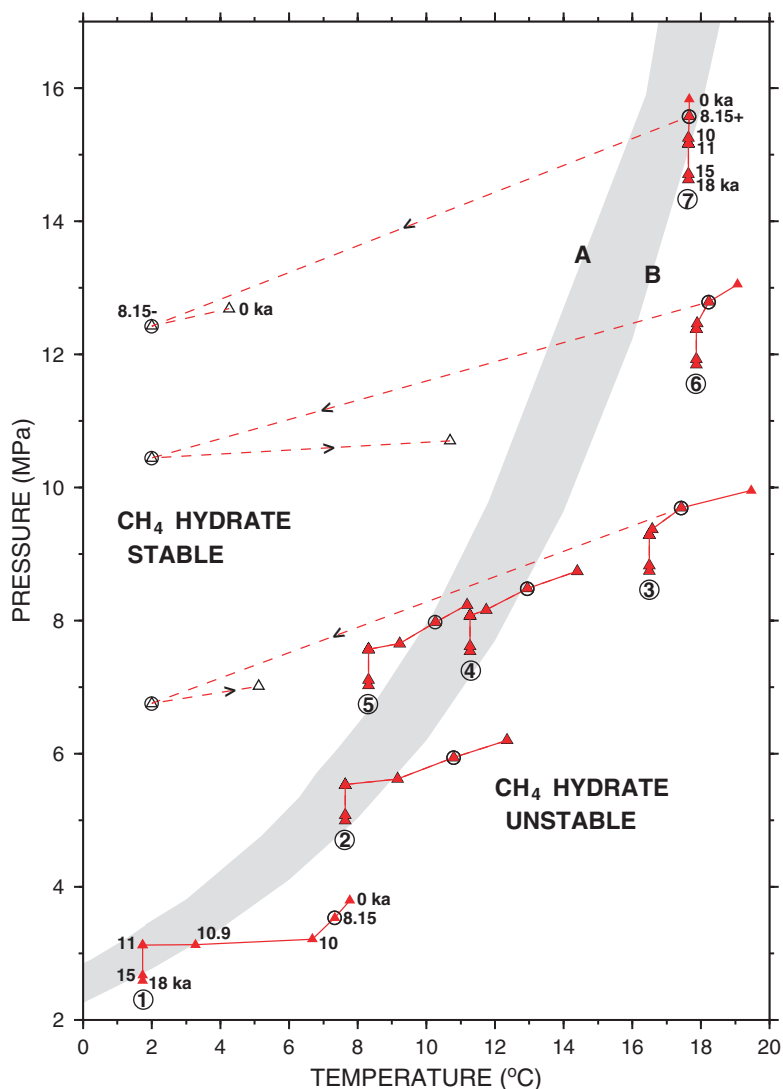


FIGURE 11
Trajectories (from last Ice Age at 18ka, to the present) of seven sub-seafloor points (see Fig. 12 for locations) in temperature and pressure space, in relation to boundary of methane hydrate stability. Circled points correspond to 8.15ka, time of Storegga slide. Trajectory branches for points within the slide area and covered by slide debris are shown dashed. Because the phase boundary depends on pore water salinity and admixed higher hydrocarbons, it is shown here as a band. The left-hand edge (A) reflects pore water with the salinity of seawater, while the right-hand edge (B) reflects fresh water with 2% ethane.

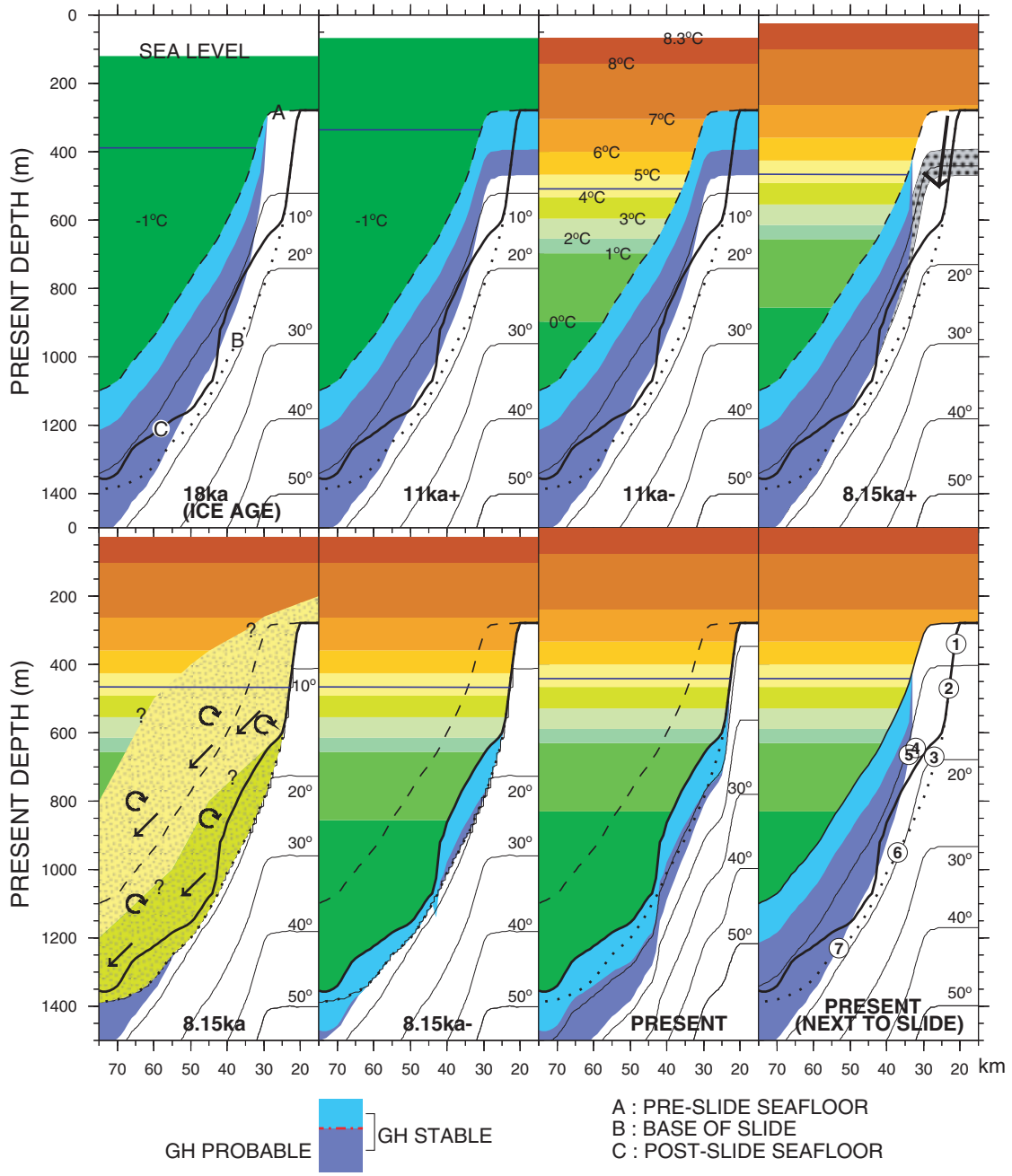


FIGURE 12
 Computed changes in methane hydrate stability zone (MHSZ) over time from last glacial maximum (18,000 years ago, or 18ka) to ocean warming at 11ka, Storegga landslide at 8.15ka, and to present conditions in slide area and on adjacent, not (yet) failed seafloor. 11ka+ means just prior to 11,000 years ago, etc. Stippled zone in 8.15ka+ profile shows area of hydrates dissociated from previous profile (11ka-). Top of each profile is modern sealevel. The sub-seafloor MHSZ is shown in blue, with the upper 115 m (light blue) probably lacking hydrate. Horizontal blue line is upper limit of MHSZ in ocean. Dashed line (A) shows the restored, pre-slide seafloor, heavy line (B) is the present seafloor, and dotted line (B) is the failure surface (base of slide). Conditions during the actual slide (8.15ka) are schematic only. Small numbers show points whose trajectories in (P, T) space are shown in Fig. 11.

formed by seismic determination of hydrate distribution.

Results and Implications: Our models predict how the Methane Hydrate Stability Zone must have changed during the last 18,000 years in the area of the great Storegga Slide. We show this change in two ways: Figure 11 shows how selected parcels of sediment (numbered in Fig. 12) moved in temperature-pressure ('thermobaric') space. Figure 12 shows conditions at various times along line #1 (Fig. 10) across the upper slide scar.

During the greatest extent of glaciation (18ka), sea level, and hence subbottom pressure, was too low for hydrate to be stable on the Storegga shelf. By 11ka, rising sea level had expanded the stability zone onto the shelf. Sometime after upper waters warmed, the stability zone was forced to retreat from the shelf once more. The time between 18ka until somewhat after 11ka years ago would not have been favorable for dissociation, and therefore slides. However, comparison of profile 11ka- and 8.15ka+ shows how hydrate dissociation could have promoted the Storegga slide when it happened—hydrate present in the dark blue zone at 11ka- would have dissociated, creating gassy, low-shear strength sediment (stippled at 8.15ka+), which then failed when the right earthquake came along. Failure most likely began where the dissociation zone (stippled in Fig. 12, 8.15ka+) intersects the known slide base.

Although we did not try to model the transient slide event, we know it stripped off most of the hydrate stability zone (8.15ka-), which then rethickened as the warm subbottom exposed by the slide was cooled by the overlying water. Some authors have suggested that reduced post-slide pressure would have caused additional hydrate dissociation and secondary slides but at Storegga, most hydrate-infested sediment, except in deep water, was removed. Even if some had been left, the large (negative) latent heat of dissociation would have


cooled the remaining hydrate, delaying further dissociation.

The solid red tracks in Fig. 11 illustrate how shallower sediment parcels (#1,2,4,5) first moved upward toward hydrate stability as sea levels rose, and then veered back out towards instability due to post-11ka warming. Deep parcels (e.g., #7) were unaffected by warming, while other parcels (e.g., #3,6) never approached the stability field, except in the slide scar, where they were abruptly jerked toward lower pressure and temperature by the slide event (dashed lines), only to warm again as thermal equilibrium was restored after 8.15ka.

Summary and Conclusion: Modeling the thermobaric evolution of the Storegga slide area may explain why this and other slides occurred during post-glacial times, when pressures were rising and hydrate stability should have been on the increase. The reason has to do with bottom water warming, which postdates most of the sea level rise, and which then took additional time to “diffuse” down far enough below the seafloor to cause hydrate to become unstable. Post-glacial slides could not have caused deglaciation, but were consequences of climate warming. Our results apply to other continental margins, except in polar and in deep waters, which have remained cold. Our study also shows that the risk of major slides (and resulting tsunamis) did not disappear after the last glaciation, but remains high today on the upper continental slope. Additionally, future ocean warming would exacerbate this risk.

[Sponsored by ONR]

References

- ¹ P.R. Vogt and W-Y. Jung, “Holocene Mass Wasting on Upper Non-Polar Continental Slopes—Due to Post-Glacial Ocean Warming and Hydrate Dissociation?,” *Geophys. Res. Lett.* **29**(9), 55-1-55-4 (2002).
- ² C.K. Paull and W.P. Dillon (eds.), “Natural Gas Hydrates: Occurrence, Distribution, and Detection,” *Geophys. Monograph 124* (American Geophysical Union, Washington, DC, 2001). 

OPTICAL SCIENCES



JOHN PAUL JONES.

"Surrender? I have not yet begun to fight." Relief on this statue shows Jones hoisting the flag on a United States man-of-war, following the tradition that he was the first to raise the new American flag on a war vessel.

189 Fiber-Optic Bottom Mounted Array
C.K. Kirkendall and G.A. Cranch

191 Athermal Solid-State Lasers
S.R. Bowman

[BACK TO CONTENTS](#)

FIBER-OPTIC BOTTOM-MOUNTED ARRAY

C.K. Kirkendall and G.A. Cranch
Optical Sciences Division

The Fiber-Optic Bottom-Mounted Array Program: The Fiber-Optic Bottom-Mounted Array (FOBMA) program has advanced the underlying technology for large-area, electrically passive, lightweight, seabed fiber-optic hydrophone arrays. We have developed a high dynamic range digital demodulator system and have incorporated three new optical technologies into the existing fiber-optic sensing technology base. These are: dense wavelength division multiplexing (DWDM), remote optical amplification, and high-performance fiber laser sources. The use of DWDM allows large numbers of hydrophones to be multiplexed onto a single optical fiber, while the use of remote amplification increases the passive array span by several tens of kilometers. Our prototype system, comprising 96 hydrophones interrogated through a 40-km fiber link, has been successfully tested in a sea trial off the coast of Nova Scotia, and demonstrated excellent acoustic performance and target tracking capability. This program is a collaboration between the Naval Research Laboratory and the Defence Science and Technology Laboratory (DSTL) sponsored by the U.S. Navy International Program Office and the U.K. Ministry of Defence.

Project Summary: Fiber-optic hydrophone arrays have been under development at NRL since the late 1970s. This technology has reached a level of maturity such that prototype systems comprising around 100 sensors have been successfully demonstrated in realistic sea trials.¹ The continued interest of the U.S. Navy in developing remote, electrically passive underwater acoustic surveillance arrays for littoral water applications has further driven the development of these systems. Figure 1 shows the deploy-

ment configuration of our system. Systems of this type can be deployed in either a vertical or horizontal configuration; our system is designed for horizontal deployment (i.e., a seabed array). The array is linked to the optoelectronic interrogation unit located either on a surface ship or at a shore station.

The underlying sensing mechanism uses fiber-optic interferometry to measure the acoustically induced strain in a fiber-wrapped mandrel hydrophone. Multiple sensors are interrogated sequentially using time division multiplexing (TDM), resulting in up to 64 sensors multiplexed per wavelength. Wavelength division multiplexing can then be added to increase the number of TDM signals carried by a single fiber. One aim of this project was to incorporate three new optical technologies into the existing fiber-optic sensor TDM technology base. These are DWDM, remotely pumped erbium-doped fiber amplifier (RPEFDF), and high-performance erbium fiber laser sources. Incorporating DWDM technology increases the number of sensors that can be interrogated over a single fiber by a factor equal to the number of wavelengths used. RPEDF technology is incorporated to increase the distance between the optoelectronic interrogation system and the array. Finally, fiber laser technology demonstrates a potentially low-cost, high-performance laser source, compatible with DWDM technology.

Figure 2 shows the system architecture. The launch optics comprises six erbium-doped distributed feedback fiber lasers multiplexed onto a single fiber in the multiplexer (MUX). The output of the lasers is modulated using acousto-optic modulators in a compensating interferometer and amplified with a power EDFA. Attenuators (ATTEN) are included to allow pre-emphasis of the signal powers and control the launch power. The receive optoelectronics contains the wavelength demultiplexers, optical preamplifier, RPEDF pump diode, and the digital demodulators. The digital demodulator incorporates a bi-cell polarization diversity receiver (PDR) to alleviate polarization-induced signal fading. While the demodulator supports > 60 kHz of

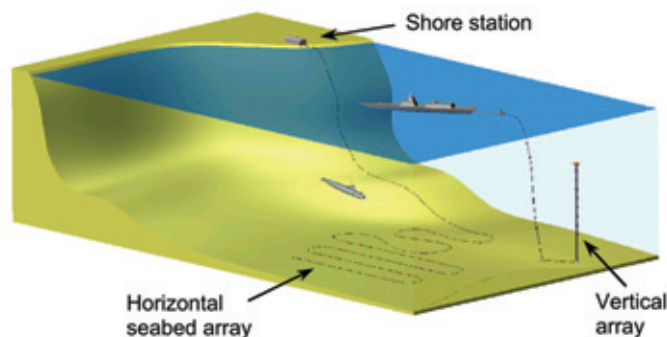


FIGURE 1
FOBMA deployment concept.

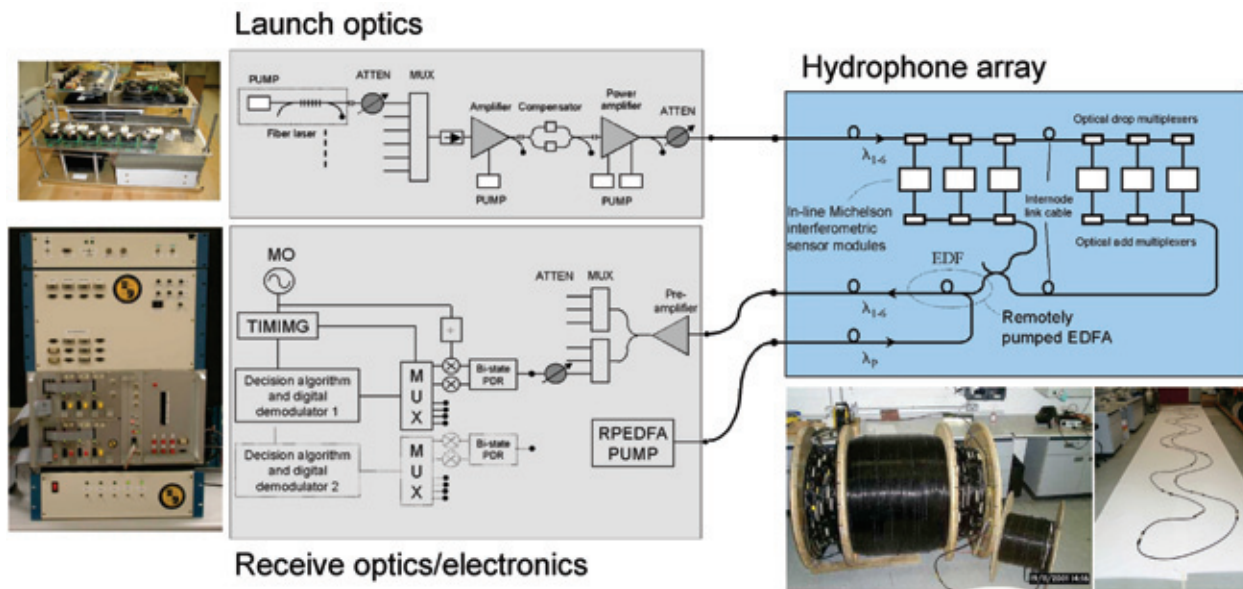


FIGURE 2
FOBMA system architecture.

acoustic bandwidth, the majority of the recorded acoustic data was band-limited to ~700 Hz to conserve storage space. A personal computer stores the acoustic data from the array. The RPEDFA pump power is delivered through a separate fiber. Thus, three fibers are required to interrogate the array.

The FOBMA system is designed to be directly scalable to a full-size system and comprises two nodes of 48 hydrophones (total 96) separated by a 3-km fiber-optic cable. Each wavelength interrogates 16 TDM sensors (expandable to 64) arranged in the architecture described in Ref. 2. The RPEDFA is incorporated into the first node and provides ~20 dB of small-signal gain per wavelength. A 5-km fiber-optic cable connects the first node to the opto-electronics at a shore station.

A 40-km link was simulated by adding bare fiber coils located with the optoelectronics.

Results and Conclusion: The array was deployed for 9 days at a depth of ~50 m off the coast of Halifax, Nova Scotia. Around 40 Gbytes of data were recorded over this period from various targets, both real and simulated. Figure 3 is an example of the target tracking capability of one of the arrays in this system. The target was a 450 Hz tone generated by a towed acoustic source. The image shows true bearing relative to the center of a 48-hydrophone array vs time. Color indicates sound pressure level. Curvature in the array, induced during the deploy-

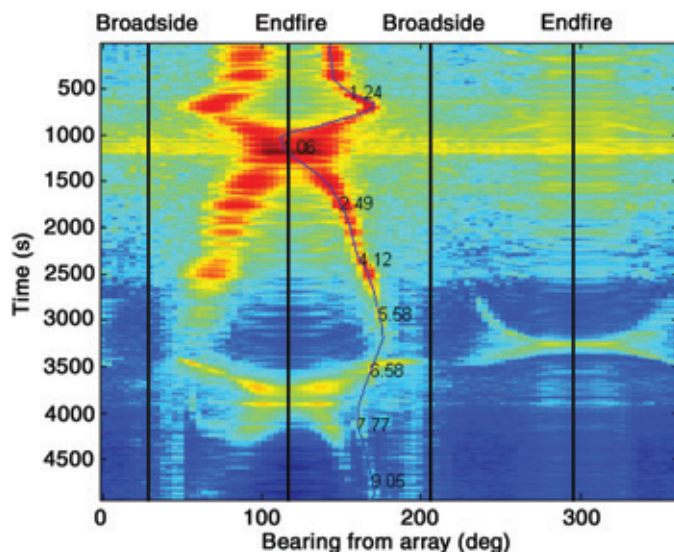


FIGURE 3
A 450 Hz tone tracked to a range of 9 km.

ment process, allows the left-right ambiguity in the response of the line array to be resolved (the sensor locations were determined using a chirp-based element location measurement conducted shortly after deployment). The actual track of the towed source can be identified to be along the narrower track following a bearing of $\sim 150^\circ$. The tone is visible to a range of ~ 9 km. Figure 3 was generated using a shape-corrected conventional beamformer. These data were recorded with a total standoff distance of 40 km. However, standoff distances in excess of 50 km are possible, depending on the array size and required acoustic performance.³ This technology enhances the U.S. Navy's capabilities in littoral water antisubmarine warfare and large-area surveillance.

Acknowledgments: NRL was responsible for developing the optoelectronics system and data recorder, and a number of people made significant contributions to this program. These are G. Cogdell and A. Dandridge of NRL and A. Bautista, K. Daley, S. Motley, and J. Salzano of SFA, MD. QinetiQ, UK, was responsible for developing the RPEDFA and underwater array portion and carried out the target tracking processing. Cogent Defense Systems, UK, designed and constructed the underwater array. The sea trial was part of the international Rapidly Deployable Sensors 4 trial.

[Sponsored by ONR and Navy IPO]

References

- ¹ C.K. Kirkendall, A.R. Davis, A. Dandridge, and A.D. Kersey, "64-channel All-optical Deployable Acoustic Array," *NRL Review*, 1997, 63-65.
- ² G.A. Cranch and P.J. Nash, "Large-scale Multiplexing of Interferometric Fiber-optic Sensors using TDM and DWDM," *J. Light. Tech.* **19**(5), 687-699 (2001).
- ³ G.A. Cranch, P.J. Nash, and C.K. Kirkendall, "Large-scale Remotely Interrogated Arrays of Fiber-optic Interferometric Sensors for Underwater Acoustic Applications," to be published in *IEEE Sensors Journal special edition on Fiber Optic Sensors*, February 2003.

ATHERMAL SOLID-STATE LASERS

S.R. Bowman
Optical Sciences Division

Introduction: Conventional solid-state lasers are exothermic. The processes of optical excitation and stimulated emission can never yield unit quantum efficiency. The residual energy from this quantum defect results in waste heat generation within the lasing medium. In high-power solid-state lasers, heat loads are often in excess of 500 W/cm^3 . This magni-

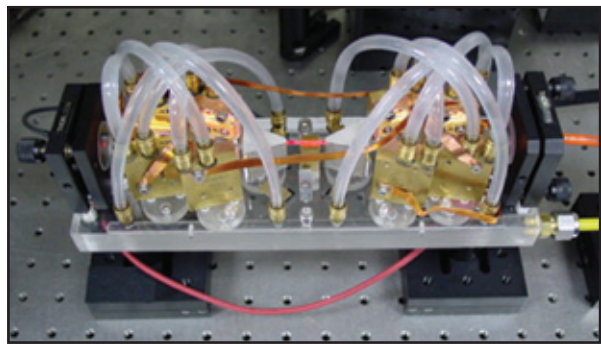


FIGURE 4
The prototype Radiation Balanced Laser included eight high-brightness diodes that end-pumped a small Yb:KGW crystal (red slab at the center).

tude heat load severely distorts laser beam quality and restricts the average power of laser systems.

In pursuit of higher power, NRL is investigating a new mode of laser operation called Radiation Balanced Lasers (RBLs). The basic concept of the RBL is to use anti-Stokes fluorescence to offset the quantum defect of the stimulated emission.^{1,2} Under ideal conditions, the absorbed power balances the radiated power at each point within the laser material and waste heat is eliminated. The radiative balance is maintained by controlling wavelengths and intensities within the cavity. Operation in the RBL mode removes thermal restrictions on the laser medium, allowing increased laser volume and average power.

The Prototype: A prototype device has been demonstrated at NRL. Material studies suggested that the prototype take the form of a Yb^{3+} doped $\text{KGd}(\text{WO}_4)_2$ resonator.³ This device used eight, 25-W laser diodes to end-pump a $1 \times 2 \times 10$ -mm slab of Yb:KGW (Fig. 4). The diode pumps were centered at 1001 nm, and the Yb laser operated at 1040 nm. The room temperature fluorescence of the Yb:KGW is centered at 992 nm. This laser operated at 3.3% wall plug efficiency with only 0.42% heat generation in the KGW crystal. Current efforts to optimize materials and lasing conditions should reduce this heat load even further. Scaling of this RBL concept to the kilowatt level is currently underway.

[Sponsored by ONR and NAVSEA]

References

- ¹ S.R. Bowman, "Lasers Without Internal Heat Generation," *IEEE J. Quantum Electron.* **35**, 115-122 (1999).
- ² S.R. Bowman, "Non-Exothermic Quasi-Two Level Laser," U.S. Patent #6,370,172, issued April 2002.
- ³ S.R. Bowman, N.W. Jenkins, B. Feldman, and S. O'Connor, "Demonstration of a Radiatively Cooled Laser," *Conference on Lasers and Electro-Optics*, Long Beach, CA, June 2002.

REMOTE SENSING



ADMIRAL RICHARD E. BYRD, JR.

"Upon this bright globe he carved his signature of courage." Polar explorer; flew over both North and South Poles; established base at Little America; head of "Operation Deep Freeze" – United States' contribution to the International Geophysical Year.

- 195** Synthetic Aperture Ladar
R.L. Lucke, L.J. Rickard, M. Bashkansky, J.F. Reintjes, and E.E. Funk
- 197** Dynamic Ocean Fronts
A.L. Cooper, R.P. Mied, G.L. Lindemann, and M.A. Sletten
- 199** Coastal Transport of Organic and Inorganic Matter
R.W. Gould, Jr. and R.A. Arnone

[BACK TO CONTENTS](#)

SYNTHETIC APERTURE LADAR

R.L. Lucke and L.J. Rickard
Remote Sensing Division

M. Bashkansky, J.F. Reintjes, and E.E. Funk
Optical Sciences Division

Introduction: Synthetic aperture radar (SAR) is a long-established imaging technique for air- or spaceborne radars: the motion of the platform sweeps out a “synthetic aperture” that can be many times larger than the radar’s antenna. By maintaining phase coherence of the radar’s RF radiation over this imaging time and using heterodyne detection to measure the phase of radiation reflected from the scene, the imaging resolution can be driven by the size of the synthetic, rather than of the physical, antenna. This provides high resolution in the dimension of the scene that is parallel to the direction of flight (azimuth resolution). High resolution in the other dimension (range resolution) is provided by an FM-chirped (i.e., frequency varying) waveform that supports accurate time-of-flight measurements: light that returns from one range is distinguished by its time delay (which changes its heterodyne beat frequency at the detector) from light that returns from another. If the same techniques can be extended to visible or infrared light, the potential exists for extremely high resolution with a very modest aperture size.¹ Using 1.55- μm light, we have produced the first laboratory demonstration of a synthetic aperture ladar (SAL) image,² using precisely the SAR technique outlined above. Developing SAL into an operational system will be difficult, in large part because the laser wavelength for SAL is 10^3 to 10^4 times shorter than the RF wavelength for SAR. This means that phase coherence is harder to maintain. But SAL has the advantage of building on three decades of SAR legacy, and many of the techniques developed for SAR, especially for signal processing, can be used by SAL.

High Resolution at Long Range: The laws of physics dictate that the highest angular resolution that any remote sensing system can achieve is about λ/D , where λ is the wavelength of the radiation and D is the diameter of the system’s RF antenna or optical aperture. The resolution with which the system can image the scene is therefore $R \times \lambda/D$, where R is the range to the scene. For a satellite-based system in orbit around a planet, the range to the scene is at least a few hundred kilometers. If resolution of a few centimeters is desired, the diameter of the aperture must then be several meters (for

visible or near infrared light). Only for the very biggest and most expensive satellites is it possible to contemplate flying such a large mirror. But a satellite, by its very nature, can sweep out a synthetic aperture many meters across in a few milliseconds.

SAL techniques have great potential for solar-system remote sensing. A candidate landing zone could be examined at the scale of all significant hazards before a vehicle is committed to it. Detailed scientific information could be obtained on small-scale geological features, such as strata on the walls of river valleys or lava channels. Furthermore, SAL is an active sensing method; it can supply images of places where sunlight is absent, such as wintertime polar regions, and increase coverage in single-pass encounters with targets like asteroids. In principle, SAL could offer similar benefits for Earth-surface measurements. But such a system would require further developments in atmospheric compensation techniques because the atmosphere can degrade beam quality substantially at visible wavelengths.

Laboratory Demonstration: NRL has taken the first step in developing a true imaging SAL. Figure 1 shows the experimental apparatus. Ninety percent of the output of a 1.5- μm laser is sent into a fiberoptic circulator that sends light through a lens to the target. The target was an aluminum mounting plate on which the letters “NRL” had been made with retroreflective tape. The 4% of the light that is reflected back from the polished end of the fiber constitutes the local oscillator (LO) for the heterodyne detection. (In heterodyne detection, the signal

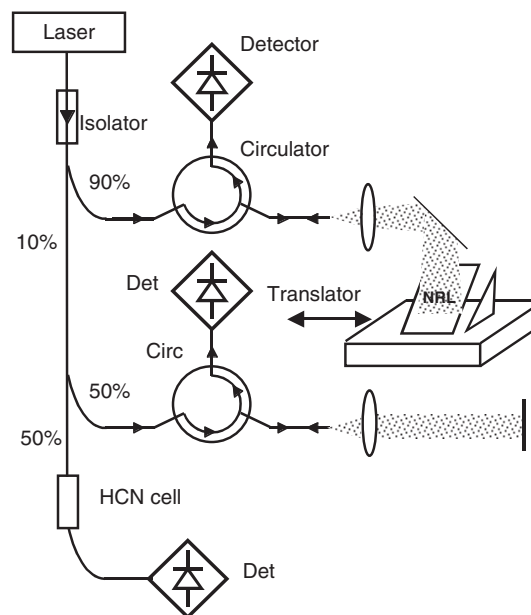


FIGURE 1
Experimental setup (from Ref. 2).

of interest is mixed with a similar LO signal to enable detection of a more tractable lower frequency signal.) A small fraction of the light returning from the target re-enters the fiber, thereby mixing with the LO light to provide a heterodyne signal, which is sent to the detector. The target is translated across the beam to provide the synthetic aperture. (As Galileo might have said, it doesn't matter whether the aperture or the target moves.) Half of the other 10% of the laser light is sent to a second interferometer, which is used as a reference to monitor nonlinearities in the laser's frequency chirp.

The object is a flat mirror perpendicular to the beam, so there is only one range element. Therefore, variations in the heterodyne beat frequency can be due only to scan nonlinearities. These variations are measured and used to correct data from the primary interferometer. (The second interferometer would not be needed in an operational system using a highly stabilized laser.) The last 5% of the laser light is sent to an HCN cell, which sets an exactly reproducible starting frequency for the laser's chirp.


Figure 2 shows the image provided by this apparatus—the first-ever true SAL image. On the left is the raw image. It is dominated by speckle, as is the case for any coherent-light imaging system. (SAR images also have speckle.) The circle overlaid on this image shows the approximate size of the resolution element that would result from the system's physical aperture alone (i.e., the resolution that could be obtained if there were no system-scene motion, and hence no synthetic aperture generation). The reso-

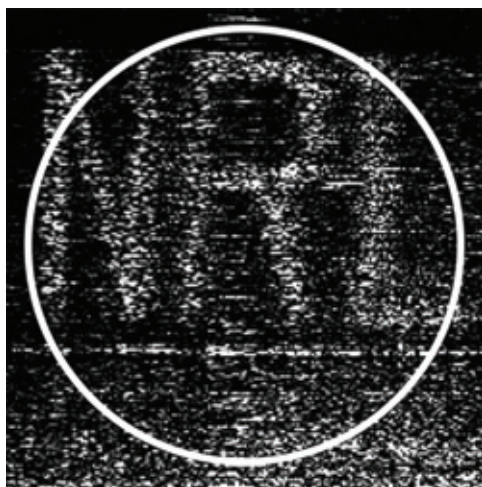
lution actually obtained is better by a factor of about 50. The image on the right shows the result of filtering the image to reduce the effect of speckle.

Engineering Problems: Now that the feasibility of SAL has been demonstrated, “only” engineering hurdles stand in the way of developing an operational system. But they are formidable. First of all, one needs high-power lasers (up to kilowatts or even more) that have very long coherence times (up to many milliseconds) and fast pulse-repetition rates (up to 100 kHz) that are tunable over about a 1 GHz bandwidth and can be space-qualified. Maintaining the phase coherence needed for synthetic aperture image processing requires compensating for platform vibrations to an accuracy better than the wavelength of the light used. This problem requires sensitive accelerometers but will be easier to deal with for the smooth motion of a spacecraft than for an airborne system. To some extent, problems with laser coherence times and platform stability can be alleviated in postprocessing by the focusing methods developed for SAR.

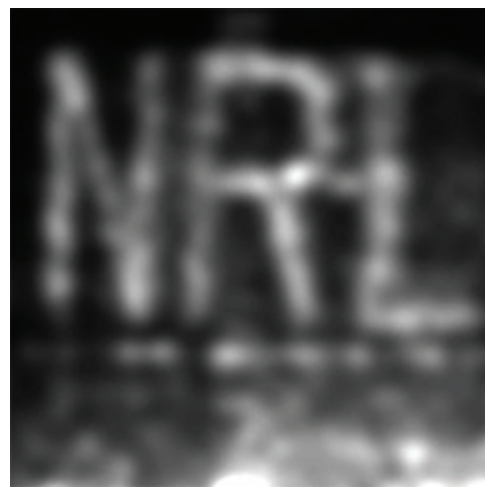
[Sponsored by USAF]

References

- ¹R.L. Lucke and L.J. Rickard, “Photon-Limited Synthetic Aperture Imaging for Planet Surface Studies,” *App. Opt.* **41**, 5,084–5,095 (2002).
- ²M. Bashkansky, R.L. Lucke, E. Funk, L.J. Rickard, and J. Reintjes, “Two-Dimensional Synthetic Aperture Imaging in the Optical Domain,” *Opt. Lett.* **27**, 1,983–1,985 (2002). 



(a) Raw image



(b) Filtered image

FIGURE 2

The image generated (from Ref. 2).

DYNAMIC OCEAN FRONTS

A.L. Cooper, R.P. Mied, G.J. Lindemann,
and M.A. Sletten
Remote Sensing Division

Introduction: Density fronts are ubiquitous in remote ocean imagery. They are driven by buoyancy effects associated with such phenomena as thermal plumes from power plant effluents, spreading oil and pollution slicks, and estuary and river discharges into a higher salinity environment. Understanding these features is important in enhancing the Navy's ability to interpret remotely sensed imagery for extracting useful environmental and tactical information.

Observations: Figure 3 is a radar image (9.375 GHz center frequency, horizontal polarization) of a front at the edge of the Chesapeake Bay tidal outflow plume. It displays distortions commonly observed in the frontal outcrop line. Waves, sharp corners, bulges, and other small-scale structure on scales of hundreds of meters to a few kilometers can be present. The bulges are oriented toward the heavier fluid, and the sharp corners are directed toward the lighter fluid. Fronts appear as regions of large radar cross section, which is generally attributed to an enhanced gravity-capillary wave spectrum and attendant wave breaking caused by surface convergence across the front.¹

Figure 4 shows the complete 4-hour frontal evolution sequence.² Each segment indicates the position and shape of the front as determined by a particular radar image in the sequence. Early in the sequence, a single bump can be observed in the front near (36°57'N, 75°57'W), and this structure is emphasized by delineating it with a thicker line than the one used to represent the remainder of the front. The bump appears to originate over a region with steep bottom topography. Over the next 4 hours, its amplitude and width grow substantially as the bulge translates to the southeast.²

Evolution Model: To understand the evolution of fronts such as those in Figs. 3 and 4, we have developed a new two-dimensional buoyant plume model based on gas dynamic shock-tube theory,³ but germane to the unique flows in gravity current fronts.⁴ In the model, we assume

- Geometric optics (the ray assumption), which presumes that each element of the front

propagates along a ray that is locally normal to the front.

- One-dimensional nonlinear fluid motion, which treats the frontal propagation as the collective motion of a bundle of gently bending ray tubes in which the dynamics in each one is governed locally by the one-dimensional equations of fluid mechanics.
- Reduced-gravity physics, which allows us to view the buoyant fluid as floating on top of a lower water layer of effectively infinite depth. This assumption is approximately satisfied in coastal waters, rendering the details of the underlying bathymetry unimportant.
- Frontal jump conditions, which constrain the velocity and layer thickness at the plume nose.

The resulting model is hyperbolic, and, therefore, the frontal evolution is an initial value problem with the self-generated subsequent behavior completely defined once initial conditions are prescribed.

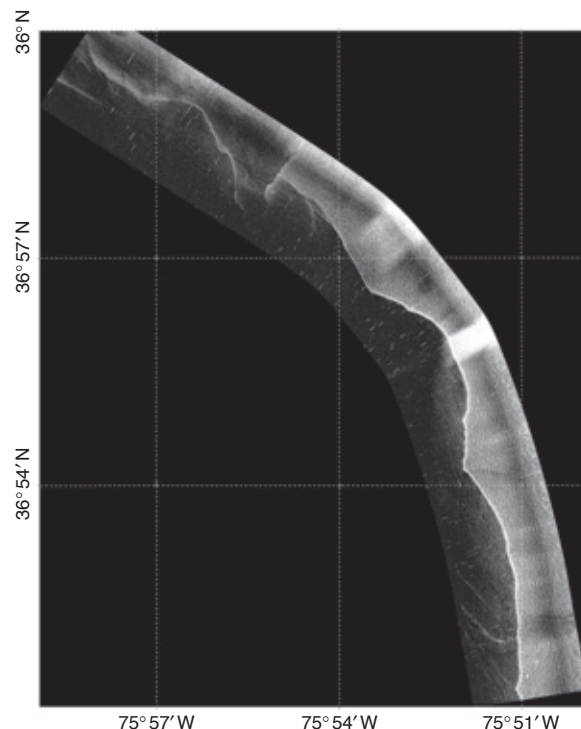


FIGURE 3 X-band real aperture radar (RAR) image of the Chesapeake Bay plume front. The bright line reflects the strong convergence and attendant wave breaking at the front boundary separating the fresh (less dense) plume water on the left from the higher salinity (heavier) shelf water on the right. The sharp cusp features point from the heavier fluid toward the lighter fluid. Corrugation scales ranging from 0.5 to 2.5 km are present.

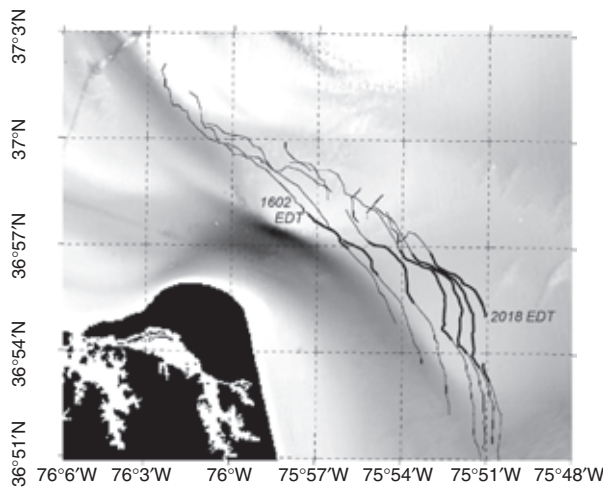


FIGURE 4

A line drawing (derived from airborne X-band radar imagery) indicating the successive positions of the Chesapeake Bay outflow plume boundary during the flood phase of the tidal cycle. Approximately 4 hours of evolved time are displayed. The main growing bulge is emphasized with a thicker line (from Ref. 5).

Model Results: The length scales of frontal perturbations can be as large as a few tens of meters to several kilometers. In Fig. 5, we assume an initial periodic perturbation

$$X_0 = a \cos(\delta y), \quad (1)$$

where $a = 0.04$ km, $\delta = 10.5 \text{ km}^{-1}$ (600-m wavelength), and a uniform initial local front-normal propagation speed of 0.18 m/s. Natural fluctuations with this magnitude might be induced by a number of mechanisms, such as an instability of an along-front current or a spatially varying wind stress.

Substantial frontal changes occur while the front oscillates. That is, a trough in the initial configuration evolves into a crest (and vice versa) in an astonishingly short time (≈ 0.75 h). This oscillatory process is explained by the nonlinear focusing of the front by its own curvature.^{4,5} By the end of the simulation (1.5 h), the front consists only of a series of crests joined at sharp angular junctions called “breaking frontal waves,” which point toward the lighter fluid as seen in the observations.

Along-front wavelengths vary temporally. At $t \approx 1$ h for instance, corrugations with wavelengths of ~ 0.4 and ~ 0.2 km are visible. This is similar to the observations in Fig. 4 and may suggest that these mixed-wavelength shapes are simply products of natural frontal evolution.

Conclusions: Under the idealized conditions assumed, the frontal evolution is a self-generated initial value problem. Clearly, the actual frontal conditions and evolution displayed in Figs. 3 and 4 are

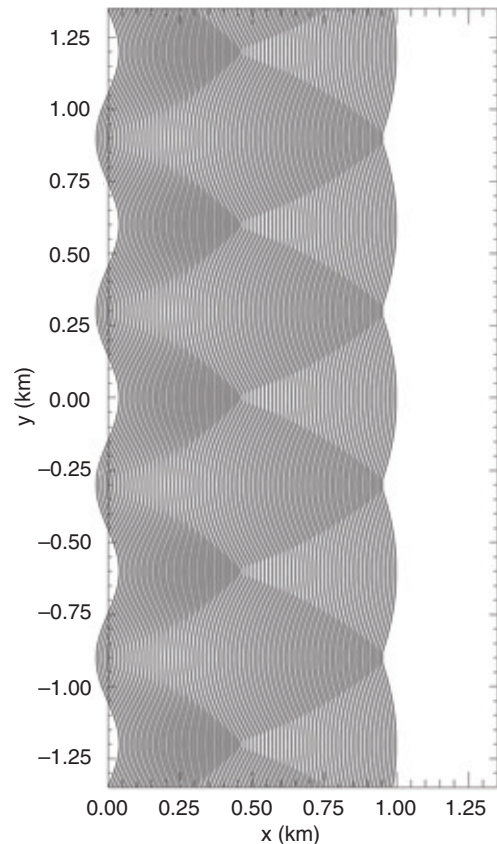


FIGURE 5

Simulated frontal evolution for the periodic initially perturbed frontal surface (Eq. (1)) described by $X_0 = a \cos(\delta y)$ and moving at a constant frontal speed of 0.18 m/s toward the heavier fluid on the right. The 90-min evolution corresponds to a complete oscillation, with 1-min intervals starting at the initial front at the left. The relatively sharp features, which always point toward the lighter fluid, are breaking frontal waves.

significantly more complicated than may be captured in the simulations. Nevertheless, a number of inferences have been drawn from the simulations shown, and much of the modeled behavior mimics the observations.

[Sponsored by ONR]

References

- ¹ R.W. Jansen, C.Y. Shen, S.R. Chubb, A.L. Cooper, and T.E. Evans, “Subsurface, Surface, and Radar Modeling of a Gulf Stream Current Convergence,” *J. Geophys. Res.* **103**, 18,723-18,743 (1998).
- ² M.A. Sletten, G.O. Marmorino, T.F. Donato, D.J. McLaughlin, and E. Twarog, “An Airborne, Real Aperture Study of the Chesapeake Bay Outflow Plume,” *J. Geophys. Res.* **104**, 1211-1222 (1999).
- ³ G.B. Whitham, *Linear and Nonlinear Waves* (John Wiley and Sons, Somerset, NJ, 1974).
- ⁴ A.L. Cooper, R.P. Mied, and G.J. Lindemann, “Evolution of Freely Propagating, Two-dimensional Surface Gravity Current Fronts,” *J. Geophys. Res.* **106**, 16,887-16,901 (2001).
- ⁵ R.P. Mied, A.L. Cooper, G.J. Lindemann, and M.A. Sletten, “Wave Propagation Along Freely Propagating Gravity Current Fronts,” *Dyn. Atmos. Oceans* **36**, 59-81 (2002).

COASTAL TRANSPORT OF ORGANIC AND INORGANIC MATTER

R.W. Gould, Jr. and R.A. Arnone
Oceanography Division

Introduction: Ocean optical properties provide the link between the spectral signature of ocean color and the composition of the water. By unraveling this signature, we can decouple the individual components that contribute to the signal and obtain a wealth of information about the concentration of the dissolved and particulate matter in the water. Furthermore, we can measure ocean color from space using satellites, so we can synoptically map spatial distributions of the bio-optically active components at ecologically relevant time scales. For the first time, using new satellite bio-optical algorithms that we have developed to partition the dissolved and particulate matter into organic and inorganic components, we are unraveling the complicated spectral signature and gaining valuable insight into a variety of physical and biogeochemical processes occurring in coastal and shelf regions.

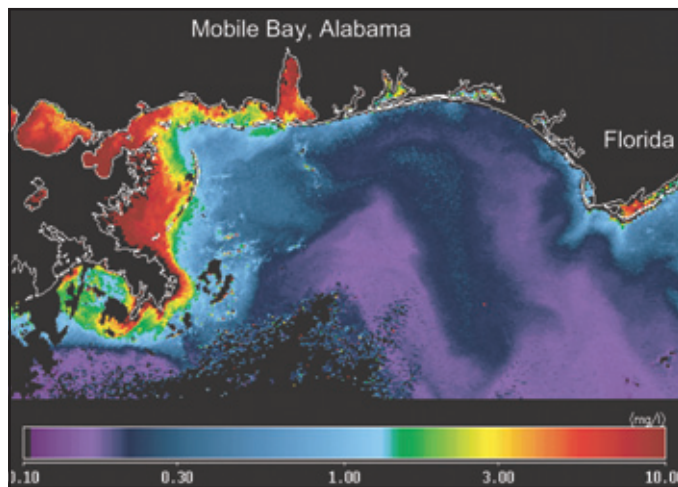
Ocean Color Remote Sensing: Starting with the Coastal Zone Color Scanner (CZCS), and more recently with the sea-viewing Wide Field-of-View Sensor (SeaWiFS), Moderate Resolution Imaging Spectroradiometer (MODIS), and MEdium Resolution Imaging Spectrometer (MERIS), ocean color satellites have provided synoptic estimates of bio-optical parameters such as chlorophyll for nearly 25 years.^{1,2} It is possible to estimate water composition from space because the water-leaving radiances at visible wavelengths measured by the satellite sensors are related to the particulate and dissolved substances in the water through the radiative transfer equations. These relationships enable us to estimate the inherent optical properties (IOPs) of the water, such as the absorption and backscattering coefficients, which affect phytoplankton primary production, biomass, heat flux, convective mixing, and naval applications (laser mine detection systems, diver visibility). Furthermore, the optical properties vary over short spatial and temporal scales in the coastal environments, so we can use these remote sensing estimates of the IOPs to optically track and classify water masses.

Before we can unravel the components and optical characteristics of the water, however, the satellite data must be atmospherically corrected. The atmosphere can contribute up to 90% of the total signal measured by the sensor at the top of the atmosphere, so accurate removal of this signal is

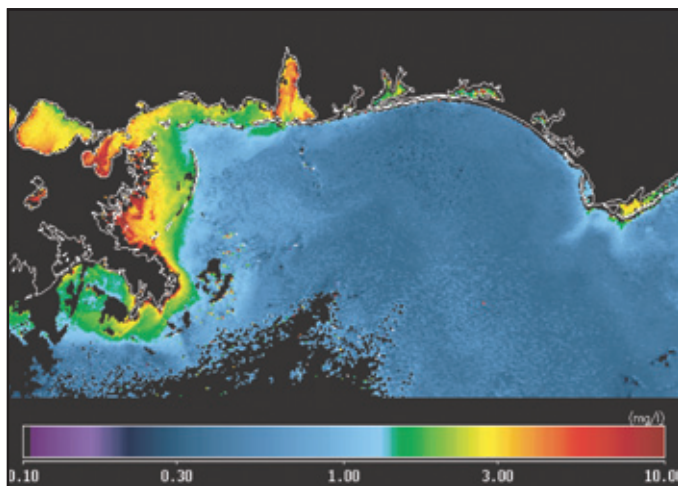
essential over the ocean where reflected radiances are lower than over land. The atmospheric correction and bio-optical algorithms were originally developed for open-ocean waters, where optical properties are primarily controlled by phytoplankton and correlated properties. Frequently, the algorithms failed near shore, precluding satellite retrievals along the coast, because the assumptions used for open-ocean areas are not valid in turbid coastal waters. Recently, however, algorithm modifications have extended estimates shoreward, enabling pixel retrievals all the way into turbid coastal waters, bays, and even estuaries where optical properties are controlled by a complex mix of phytoplankton, suspended sediments, and colored dissolved organic matter (CDOM).³ With a new suite of aircraft and satellite ocean color sensors currently on-line or planned for the near future, with increased spectral and spatial resolution, new algorithms are required to take advantage of these improved capabilities and provide new products in coastal areas.

Partitioning Organic and Inorganic Matter in Coastal Areas: Although optical instrumentation and remote sensing algorithms have advanced tremendously in recent years, the separation of the optical signature into organic and inorganic components has been problematic and has only recently been addressed. The concentration of total suspended solids (TSS) and its partitioning into particulate organic and inorganic matter (POM, PIM) is of interest from both remote sensing and modeling aspects. The concentration and space/time distribution of the inorganic component (including silts, clays, sand, and phytoplankton tests) can be used to trace river plumes and fronts and can indicate regions of particle resuspension from wave and storm-induced turbulence. The distribution of the organic component (including living phytoplankton, zooplankton, and their decay products) impacts the development of anoxic “dead zones” and is required for carbon flux estimates; it does not necessarily mirror the distribution of the inorganic component because they are influenced by different processes (physical vs biological controls). Carbon is the currency used in the exchange processes between the biosphere, hydrosphere, atmosphere, and lithosphere, so its distribution has far-reaching effects on global warming and ocean circulation.

During 2001 and 2002, we collected a suite of optical measurements in Mississippi Bight, in both clear offshore waters and turbid coastal waters (Fig. 6). We used this data set of in situ measurements to develop new algorithms to estimate the



(a) Particulate inorganic matter concentration.



(b) Particulate organic matter concentration.

FIGURE 6

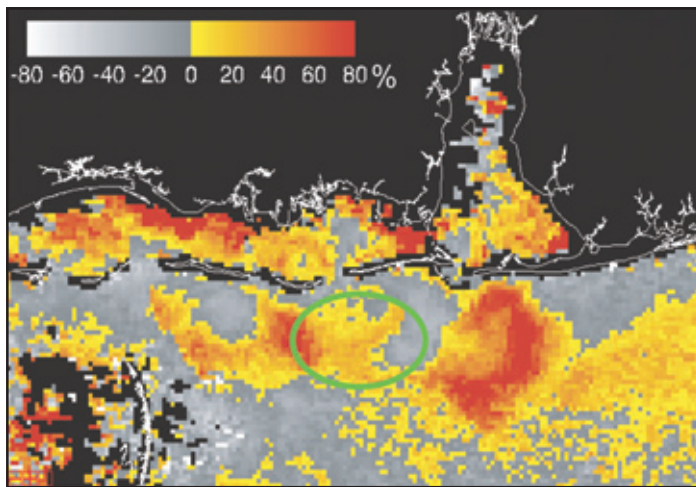
New optical products from SeaWiFS imagery. Northern Gulf of Mexico, May 20, 2002. Color scale indicated on each image with units of mg/l.

concentrations of PIM, POM, and TSS, and we have applied these algorithms to SeaWiFS satellite ocean color imagery.

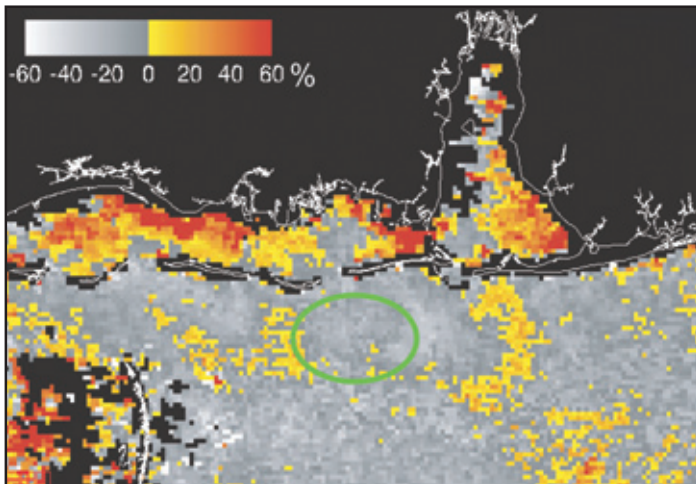
Tracing Water Masses with Optics: We can use these new satellite products to optically characterize and trace water masses. For example, if we take two sequential images of the TSS product and form a “difference” image (i.e., at each pixel in the image, subtract the value on day one from the value on day two), we can follow river plume advection and trace the fate of the associated effluent (Fig. 7(a)). Furthermore, if we create images of the ratio of the PIM and POM products and create another difference image for the same two days, we can assess the relative

changes in the particle composition (Fig. 7(b)). An increase in TSS between the two days could be due to an increase in the organic component of the particulate load, the inorganic component, or both. The PIM/POM difference image helps us determine which case occurred, and even helps us distinguish between competing physical and biological processes (an increase in the inorganic component indicates wave resuspension of bottom sediments or river discharge, whereas an increase in the organic component indicates phytoplankton growth).

Optical Water Mass Classification: The total absorption coefficient can be partitioned into individual components due to phytoplankton a_{ϕ} ,



(a)



(b)

FIGURE 7

(a) Percent difference in concentration of total suspended solids between 12 and 14 June, 2002. (b) Percent difference in the ratio of particulate inorganic matter concentration to particulate organic matter concentration (PIM/POM). Yellow-to-red color scale in each panel indicates pixels where the TSS concentration or PIM/POM ratio increased over the 2-day period; black-to-white color scale indicates pixels where they decreased. The changes in TSS concentration and PIM/POM ratio indicate advection of the Mobile Bay outflow plume as well as changes in the composition of the particulate matter. For example, the pixels in the circled areas (both panels) showed an increase in the TSS load and a decrease in the PIM/POM ratio, indicating an increase in the organic component relative to the inorganic component, possibly due to phytoplankton growth or settling of suspended sediments.

detritus a_{det} and colored dissolved organic matter a_{CDOM} . We have developed new algorithms to estimate each of these components from the satellite ocean color imagery. We can create a combined image of these three parameters to help us visualize the spatial distribution of the components. First we sum the three coefficients together at each pixel in an image, then calculate the percentage of the total due to each component. In Fig. 8(a), the red pixels indicate areas of relatively high detrital and CDOM absorption; the blue pixels correspond to relatively high CDOM absorption and lower phytoplankton and detrital absorption; and the green pixels represent areas of relatively high phytoplankton and CDOM absorption and low detrital absorption. For a more quantitative characterization of the optical characteristics of the water masses, we form ternary diagrams (Fig. 8(b)) to classify each image pixel into

one of 16 classes based on the percentages of each of the absorption components. We can classify and trace the temporal and spatial variability of the water masses in a region by performing these analyses on multiple scenes over time.

Summary: Our research has led to the development of new algorithms to assess water properties from space. Specifically, we estimate partitioned absorption, TSS, POM, and PIM from satellite ocean color imagery. For the first time, we have the capability to monitor geochemical and optical processes and the impact of human activity on our coastal zone. The development of this capability to remotely estimate both the concentrations and the optical characteristics of the organic and inorganic constituents of the water, coupled with the new ocean color sensors coming online, helps us trace and classify

water masses and monitor river discharge, circulation patterns, sediment resuspension, phytoplankton growth, and the carbon cycle.

[Sponsored by ONR]

References:

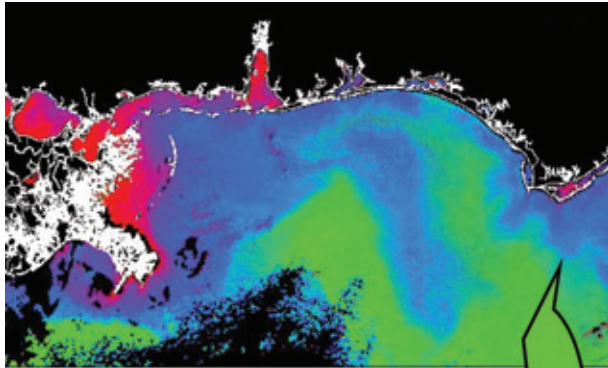
¹ A. Morel and L. Prieur, "Analysis of Variations in Ocean Color," *Limnol. and Oceanog.* **22**, 709-722 (1977).

² S.B. Hooker and C.R. McClain, "The Calibration and Validation of SeaWiFS Data," *Prog. Oceanog.* **45**(1), 427-465 (2000).

³ R.W. Gould, Jr., R.A. Arnone, and M. Sydor, "Absorption, Scattering, and Particle Size Relationships in Coastal Waters: Testing a New Reflectance Algorithm," *J. Coast. Res.* **17**(2), 328-341.



(a)



(b)

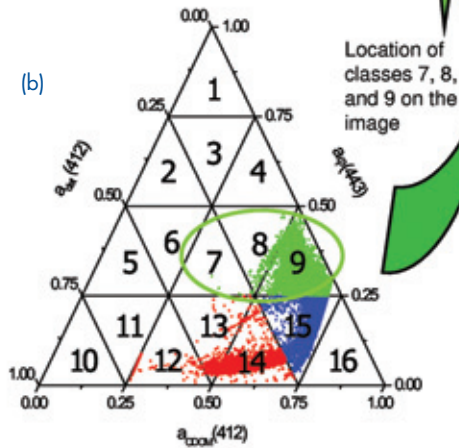


FIGURE 8

(a) SeaWiFS image from 20 May, 2002, representing the contributions of phytoplankton, detritus, and CDOM absorption at each pixel (red pixels are dominated by detrital absorption a_{det} , blue pixels by CDOM absorption a_{CDOM} , and green pixels by phytoplankton absorption a_{ph}). (b) Ternary diagram for Fig. 8(a). Each axis represents the percentage of the total absorption coefficient that is due to the individual component. Colors correspond to pixel colors in Fig. 8(a). We can quantitatively classify each pixel in an image into one of 16 unique water classes based on the percentage of each absorption component. For example, the green pixels in Fig. 8(a) correspond predominately to class 9 in Fig. 8(b); thus, 0-25% of the total absorption coefficient for those pixels is due to detrital absorption, 25-50% is due to phytoplankton absorption, and 50-75% is due to CDOM absorption.



WOMEN IN MILITARY SERVICE FOR AMERICA MEMORIAL.

This memorial was dedicated in 1997 to honor the nearly two million women who have served in the United States Armed Forces.

- 205** NRL's Finder UAV: A Counterproliferation Asset
A. Cross
- 207** Networked Specific Emitter Identification in Fleet Battle Experiment Juliet
I. Terry
- 209** Flapping Flight in Insects and Fish: 3-D Unsteady Computations
W.C. Sandberg and R. Ramamurti
- 212** RAM to Navy Standard Parabolic Equation: Transition from Research to Fleet Acoustic Model
R.A. Zingarelli and D.B. King

[BACK TO CONTENTS](#)

NRL'S FINDER UAV: A COUNTERPROLIFERATION ASSET

A. Cross

Tactical Electronic Warfare Division

Introduction: The Naval Research Laboratory (NRL) has been tasked to develop the Flight Inserted Detector Expendable for Reconnaissance (FINDER) by the Defense Threat Reduction Agency (DTRA). The NRL effort is set to produce a warfighting component within the Chemical Combat Assessment System (CCAS). The goal is to exhibit a capability to determine the presence of chemical agents following an attack on a Weapons of Mass Destruction (WMD) facility. The mission requires pre-strike deployment of an unmanned aerial vehicle (UAV) (Predator). The FINDER UAVs are carried on the wing pylons of a specially modified USAF Predator, and then released to descend to low level and collect air samples. Under human supervision at the Predator Ground Control Station (GCS), the UAV gathers meteorological and chemical data for real-time information reports. After collecting data for up to 2 hours, the FINDER will autonomously fly to a designated recovery site, at which it will autonomously land and be recovered by friendly forces.

During the past two decades, NRL has conducted substantial research and mission demonstrations involving advanced technology, expendable mini-UAVs. Significant technological advances and breakthroughs were made in the areas of low Reynolds number (LRN) aerodynamics, in-flight deployability, advanced composite structures, and micro digital electronics. Utilization of this technology base has enabled rapid development of the fully autonomous FINDER UAV. This vehicle will add a highly capable, small, affordably expendable asset to the military inventory.

The FINDER has a propulsion system that used Predator aviation fuel and is able to sustain flight for 8 to 10 hours at 70 km/h airspeed. For this 26-kg vehicle that translates into an operational range of more than 350 nm. Figure 1 shows the CCAS system.

Timeline: The FINDER project was initiated in June 1999. Full development of the vehicle structure and fabrication of prototype units was completed at NRL. Advance autopilot development, communications, and autonomous flight testing of the prototypes essentially began in August 2000. The full CCAS system is scheduled for a military utility dem-

onstration as a participant in the Counterproliferation Advanced Concept Technology Demonstration (ACTD) in May 2003.

Field Exercises Prove Feasibility of FINDER

Concept: FINDER has participated in multiple field exercises over the past 18 months. Its initial rollout occurred at the Nevada Test Site (NTS) in July 2001. This exercise and a follow-up test in October 2001 demonstrated the capability of the FINDER to search, detect chemical agents, and report detections in real time. After these initial tests, NRL continued the development effort toward full integration with the Predator UAV and its GCS for communications and control. Initial integration efforts culminated in June 2002 with a FINDER deployment from Predator. Subsequent to initial testing, FINDER has continued to participate in CCAS scheduled field exercises. Figure 2 shows FINDER's integration on the Predator and a deployment.

Summary: FINDER supports the European Command requirements for a chemical Battle Damage Assessment tool. The vehicle and current payload provides real time or near real time: local area meteorological data, integration with the existing Predator infrastructure, Predator stand-off capability, critical sample collection, return of sample to a safe area, and extended range egress.

As technology evolves, FINDER possesses the flexibility to accept a wide variety of modular payloads and deployment options. Figure 3 shows a demonstrated deployment alternative that was a fall-out of the normal vehicle development. Future growth capabilities are already being discussed as follow-on options:

- Toxic chemical/precursors sensing
 - IMS detectors reprogrammable to add new signatures;
- Biological detection capability
 - Preliminary study of mature technologies
 - Flexibility for future payload integration options;
- NAVY at-sea base option
 - Rail launch future capability is feasible;
- Radiological hazard sensing
 - Flexibility for future payload integration options.

Acknowledgments: The author acknowledges the support of DTRA and Dr. J. Montgomery for enabling this project. It was the long hours and dedication of NRL Code 5712 and ITT personnel that

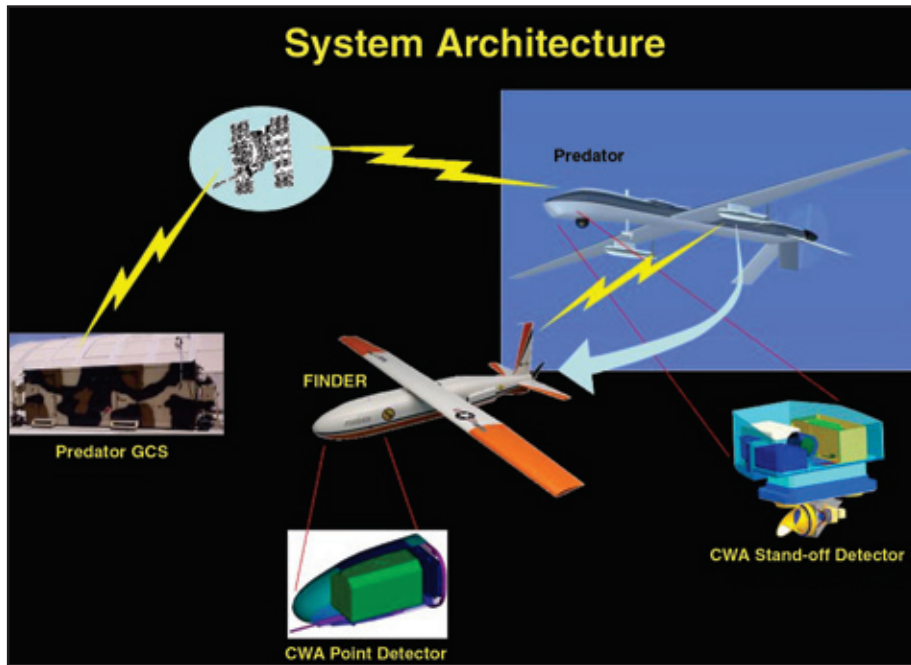


FIGURE 1
Chemical combat assessment system (CCAS) overview.



FIGURE 2
Predator/FINDER integration and initial deployment.



FIGURE 3
FINDER growth options include alternative deployment methods and payload modularity.



made the accomplishments presented in this paper possible.

[Sponsored by DTRA]



NETWORKED SPECIFIC EMITTER IDENTIFICATION IN FLEET BATTLE EXPERIMENT JULIET

I. Terry

Tactical Electronic Warfare Division

Introduction: Specific Emitter Identification (SEI) technology developed by the Tactical Electronic Warfare Division provided a significant capability to participants during Fleet Battle Experiment Juliet/Millennium Challenge 2002 (FBE-Juliet/MC-02), which was held in Fall 2002 in San Diego, California. SEI provides a reliable, long-range, all-weather positive target identification capability against seaborne platforms and land-based systems that emit radar signals. A network of geographically separated SEI-equipped aircraft, ship, and land-based platforms operating in a networked environment provided time-critical, tactically relevant Electronic Intelligence (ELINT) that contributed to early Indications and Warning (I&W) of suspected hostile vessels, enhanced the commander's situational awareness, and assisted him in forming courses-of-action during the exercise.

Details: FBE-Juliet was the tenth in a series of FBEs. It was conducted under the overarching objec-

tives of Millennium Challenge 2002, the Congressionally mandated joint event designed to simulate a realistic 2007 battlefield to assess the interoperability of new methods to plan, organize, and fight. NRL's focus during FBE was to aid in the identification of suspect ships operating close to shore (littorals). Naval operations in the littorals often occur in regions with high shipping densities. Interdiction operations and strikes against seaborne platforms under restrictive rules of engagement (ROE) scenarios require the capability to positively identify surface contacts, thereby reducing the ambiguities in the commander's overall target picture. Traditional surveillance methods fall short in the rapid establishment of the surface tactical picture when operating in such conditions. For FBE-J and MC-02, NRL installed UYX-4 SEI sensor systems onboard the destroyer USS *Benfold*, the command ship USS *Coronado*, a P-3 aircraft, and a mobile and fixed land-base site (Fig. 4). These systems demonstrated the ability for one platform to acquire a target of interest, inject that target's SEI information into a network, and have a different platform miles away receive that contact's information in near real time. Of significance was the ability to identify and consistently re-identify shipboard, land-based, and airborne radars on different days, using SEI systems on different platforms, operated by different operators (Fig. 5).

Highlights of Participation in FBE-J/MC-02

Rapid dissemination of information: In the past, Tactical Electronic Intelligence (TACELINT) messages containing SEI signature data were sent to the-

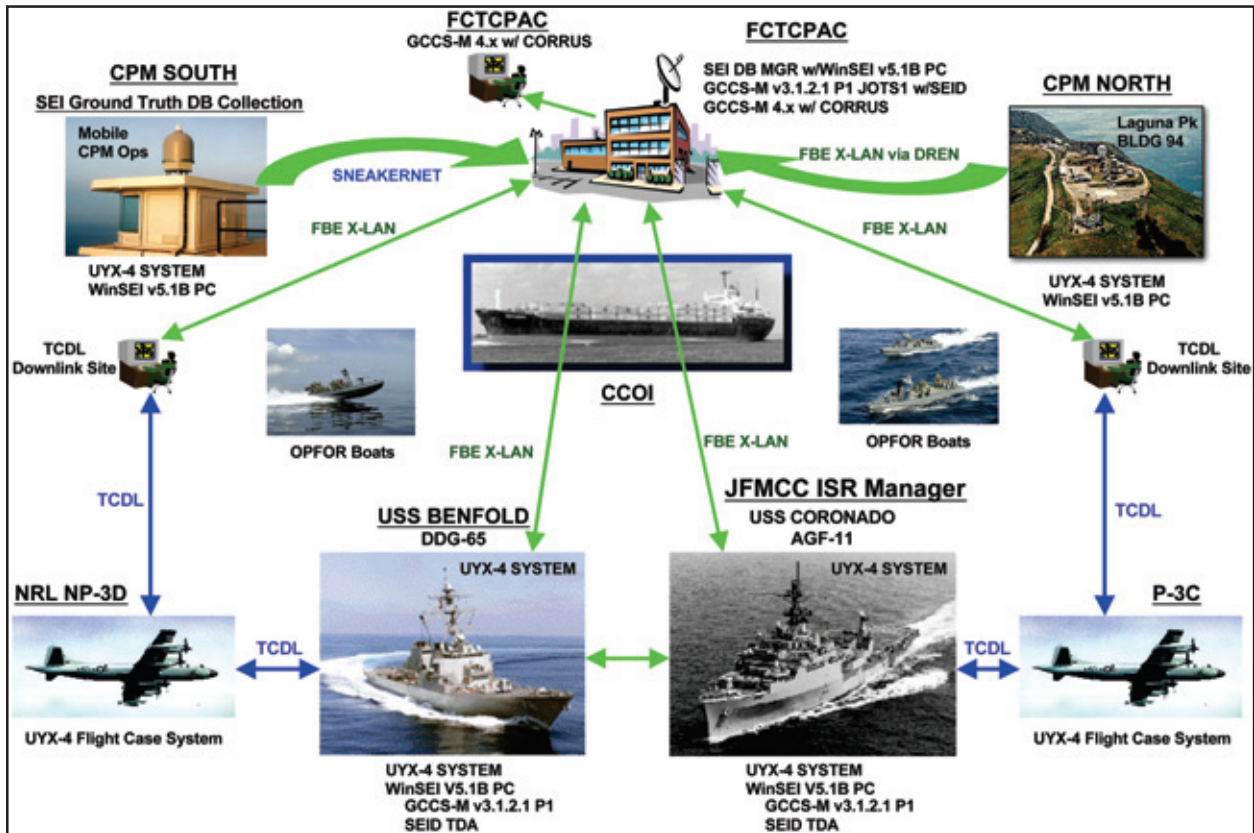


FIGURE 4
FBE-J networked SEI connectivity

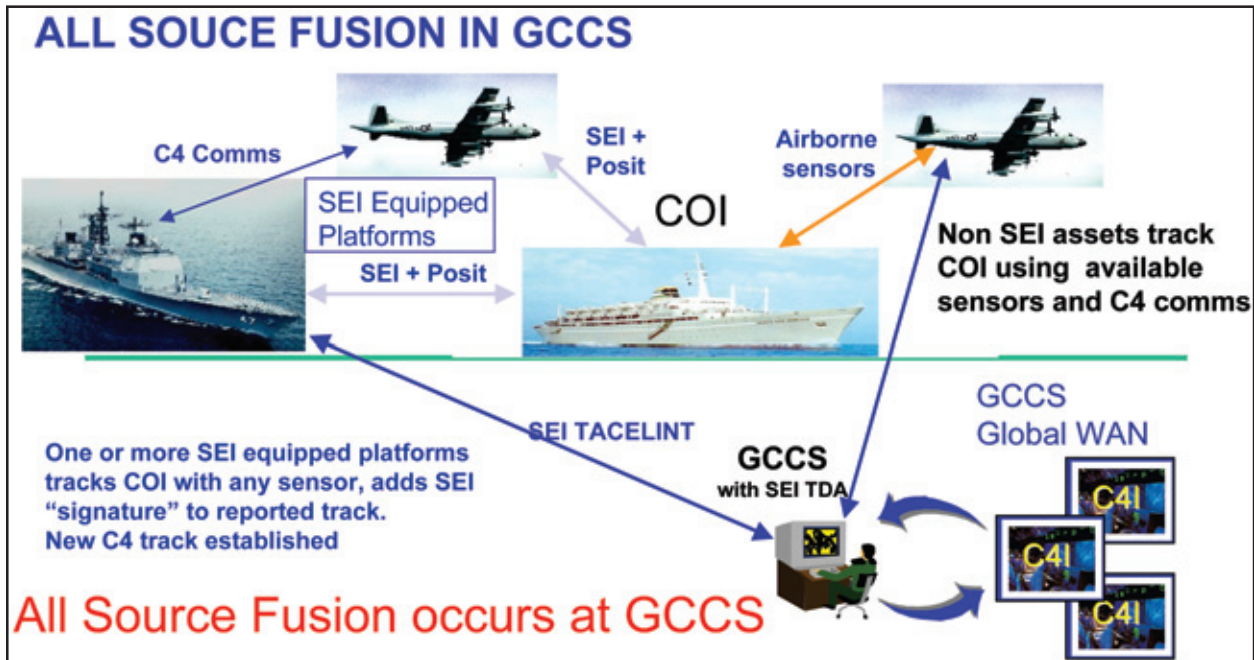


FIGURE 5
SEI TACELINT message carries SEI "signature" appended to track reports from SEI capable units.

ater commanders, national agencies, and other SEI sensor platforms, generally arriving 24-48 hours after the event occurred. During FBE-J, TACELINT messages sent from an SEI sensor over the command network to another SEI sensor or to a command entity, were observed with a latency 10-15 seconds under normal network operating conditions. This ability to rapidly acquire and disseminate target information allowed the commander to make quick decisions in determining courses of action during the exercise.

Development of electronic order of battle: SEI-equipped units developed an SEI Ground Truth Data Base of Opposing Forces (OPFOR), potentially hostile, friendly, and background emitters over a period of 2 months prior to exercise, forming the basis for threat emitter identification/re-identification during FBE-J/MC-02 execution.

Tactical usage of electronic order of battle: Using the ground truth database, the SEI-equipped P-3 aircraft, ships, and coastal site provided vital support in identifying/re-identifying emitters of interest. The information injected into the sensor grid provided real-time situational awareness by amplifying and de-conflicting the naval tactical picture with the SEI signature information.

Networking achievements: NRL demonstrated that TACELINT messages produced and sent by the SEI sensor systems could be introduced into the GCCS-M 3.x command net as ELINT contact reports via a JOTS 1 Master TDBM, and further distributed to other GCCS-M workstations over the network using Common Operational Picture (COP) Sync Tools (CST). This was done using existing network TCP/IP communications, and the capabilities built into a GCCS-M 3.x JOTS 1 workstation, including auto-forward communications, track attribute correlation, track processing, generation, plotting, display and archiving.

Fleet Demand for NRL Technology: Leveraging on the successes and lessons learned from FBE:

1. Commander in Chief, Pacific Fleet made a direct request for the SEI system on USS *Benfold* to be cross-decked to another DDG to support real-world operations.

2. At the request of Commander, Naval Forces Europe, NRL is currently involved in the implementation of a Networked SEI Sensor Grid in the U.S. Sixth Fleet operational theater to support national defense objectives.

3. The Office of Naval Research (ONR) has funded the development and installation of an Integrated Sensor Suite, including an UYX-4 SEI system onboard the Navy's High Speed Vessel *Joint Venture* follow-on, HSV-X2.

4. ONR is also funding the Battle Group Distributed SEI Experiment (BGDSE) to equip an entire deploying carrier battle group with a Networked SEI capability.

Conclusion: Fleet Battle Experiment Juliet demonstrated the value and power of SEI's capability to uniquely identify and consistently re-identify radar signals. SEI provides a significant contribution to solving the deconfliction problem between hostile radars from friendly radars in dense, complex emitter environments. NRL's research in Networked SEI is expected to continue to bring a significant capability to operational commanders for a variety of tactical missions around the world.

[Sponsored by ONR]



FLAPPING FLIGHT IN INSECTS AND FISH: 3-D UNSTEADY COMPUTATIONS

W.C. Sandberg and R. Ramamurti
Laboratory for Computational Physics and Fluid Dynamics

Introduction: Recent computational technology developments have enabled three-dimensional unsteady computations to be successfully completed for flapping wings and deforming shapes. The mathematical description of the performance of flying creatures has been limited, due to the previously insurmountable difficulties associated with flapping wings with changing shape. There are numerous operational advantages if we could successfully incorporate live creature performance characteristics into our vehicles and systems. Before we can proceed with such an undertaking we wish to understand, quantitatively, the fluid dynamics of the observed performance of those creatures. We describe below two recent computations carried out for the *Drosophila* (fruit fly),¹ and the *Gomphosus varius* (bird wrasse—a coral reef fish),² creatures, which might serve as biological inspiration for air and undersea vehicles, respectively.

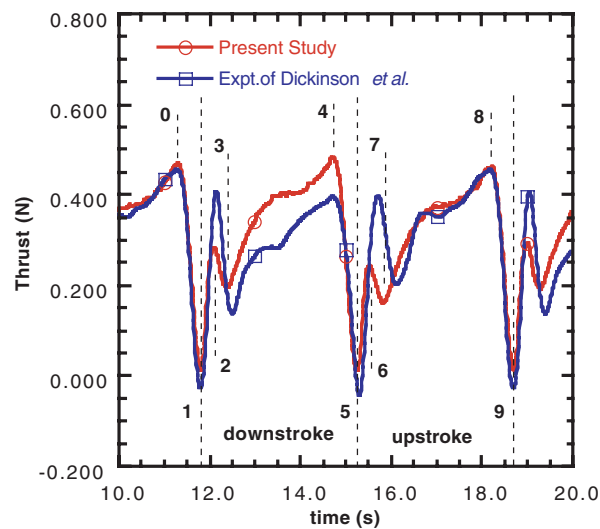
Insect Wing Flapping: The three-dimensional wing strokes of the insects can be divided into two translational phases and two rotational phases. During the translational phases, upstroke and downstroke, the wings move through the air with high angles of attack; during the rotational phases, the wings rotate rapidly and reverse direction. Professor Michael Dickinson and his collaborators at the University of California Berkeley have studied

the effects of the translational and rotational mechanisms of the wing in *Drosophila*.³

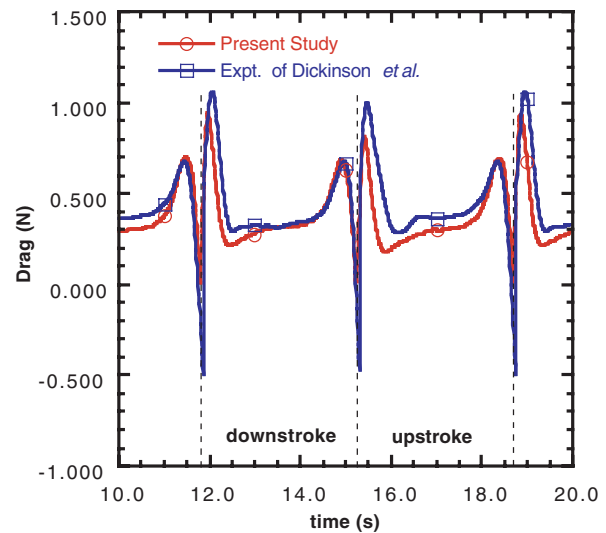
Our insect flapping wing computations were performed for the same conditions as in their experiments. The unsteady computation was carried out for five cycles of oscillation. Figure 6 compares thrust and drag forces, respectively, during one cycle of the wing beat. Professor Dickinson has suggested that the slight differences between our computed results and his experimental measurements may be due to a small asymmetry that was present in the experimental setup.

To gain insight into the flow behavior associated with the wing flapping motion, a considerable amount of flow visualization was computed. Figure 7 is an example of a particular case of the flow about the wing during the downstroke.

Fish Pectoral Fin Flapping with Changing Shape: In the bird wrasse computations, we extended the development to the unsteady flow about a flapping 3-D surface whose shape is changing in time. In this pectoral fin investigation, we are continuing to focus our fish swimming work on oscillat-



(a) Thrust



(b) Drag

FIGURE 6
Comparison of time history of thrust and drag forces (from Ref. 1).

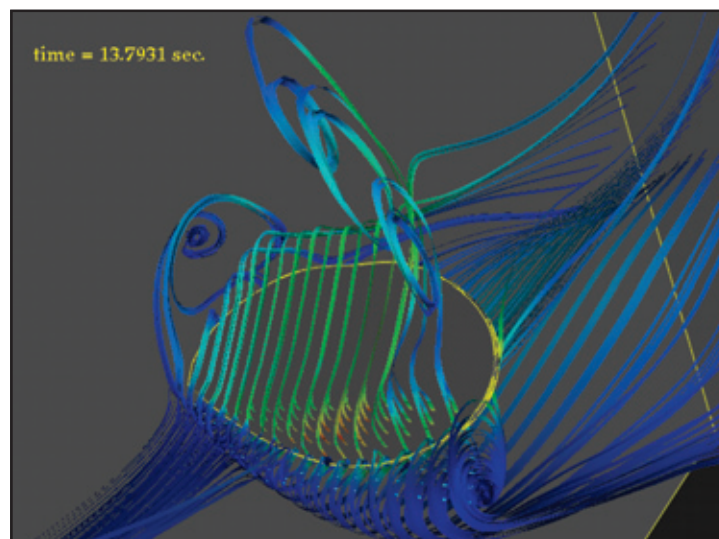


FIGURE 7
Flow field about flapping *Drosophila* wing at $t = 13.79$ s at 50% of the downstroke (from Ref. 1).

ing control surface flows for nonundulating bodies that began on the swimming tuna several years ago. There is a more direct applicability of findings on the unsteady hydrodynamics of flapping fins on a nonundulating fish like the bird wrasse to the oscillating control surfaces on rigid naval vehicles.

The unsteady computations were carried out using a new mesh movement capability developed to accommodate the deforming fin surface. Unsteady simulations were carried out with the bird wrasse swimming at two body lengths per second. The computations were carried out for more than

four cycles of fin oscillation. Figure 8 shows the instantaneous velocity field on the swimming wrasse. The time-varying 3-D lift and thrust forces, shown in Fig. 9, were computed by integrating the surface pressure over the wrasse body and fin at each time step throughout the simulation. These force time histories lead to horizontal and vertical accelerations that are in very good agreement with the experimentally obtained fish center of mass accelerations obtained by Prof. Westneat and Dr. Walker of the Field Museum of Natural History in Chicago.⁴ As in the *Drosophila* computations, we also carried

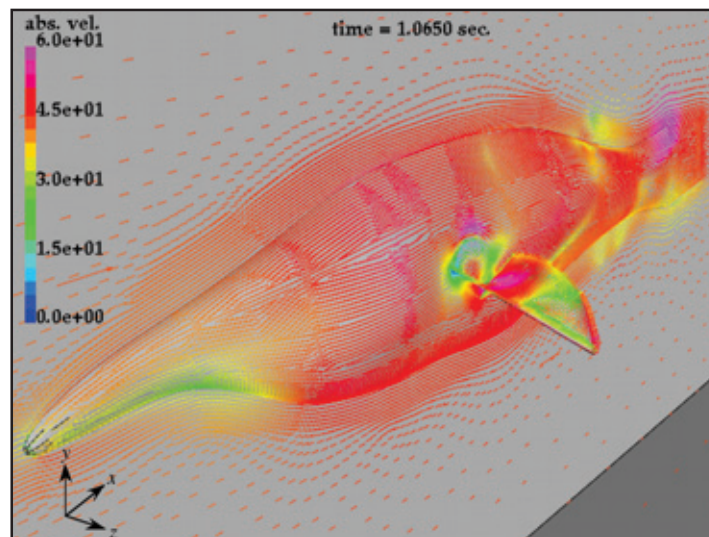


FIGURE 8
Velocity vectors on the surface of the bird wrasse at one instant during the fin oscillation (from Ref. 2).

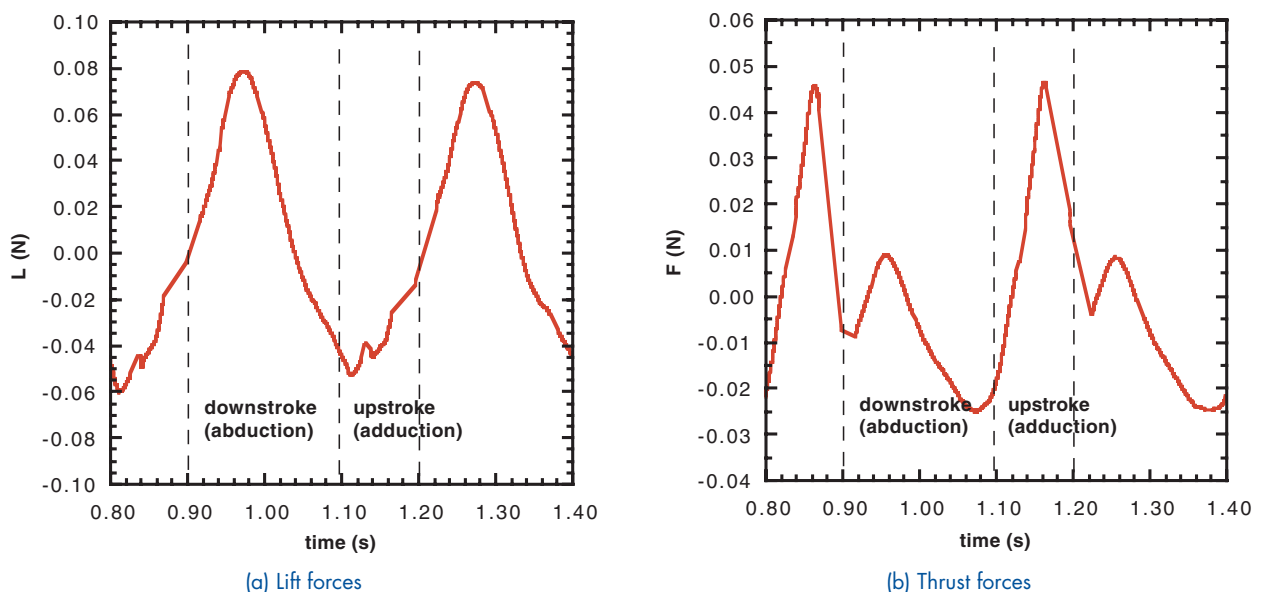


FIGURE 9
Time variation of unsteady (from Ref. 2).

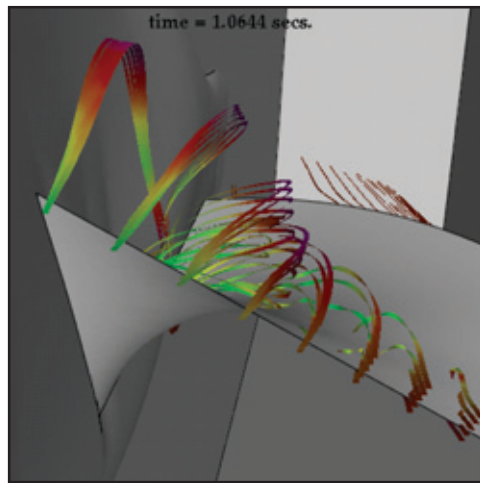


FIGURE 10

Instantaneous traces of particles released from a rake that is parallel to the fin leading edge throughout the stroke cycle. Color indicates the magnitude of the velocity (in cm/s) at each location along the trace.

out extensive visualization to gain insight into the flow dynamics associated with the time history of force generation. The particle traces plotted in Fig. 10 are indicative of the fluid motion past the pectoral fin at the middle of the down stroke.

Summary: We have computed the unsteady dynamics around the rigid wing of a flapping fruit fly and around the deforming pectoral fin of a swimming bird wrasse. The unsteady computations have been compared with experimental data and found to be in excellent agreement. The understanding gained from these computations is useful as we proceed to the design of high-performance air and undersea autonomous vehicles.

Acknowledgments: This work was supported by the Office of Naval Research through the NRL Undersea Warfare Focus Area Swimming Vehicles Project and the NRL Tactical Electronic Warfare Division Micro Air Vehicles Program. The authors thank Prof. M. Dickinson (now of California Institute of Technology), Mr. S. Sane, and Dr. J. Birch from University of California Berkeley for providing experimental *Drosophila* wing kinematics, force data for comparison, and many very useful discussions. We also thank Prof. M.W. Westneat of the Field Museum of Natural History and the University of Chicago and Prof. J. Walker (now of the University of Southern Maine) for experimental kinematics, measured data, close collaboration, and again, many useful discussions throughout the bird wrasse computations. We also thank Prof. R. Löhner and Dr. J. Cebra of the George Mason University for their support with grid generation and flow visualization throughout the course of this work. The computations carried out for this work were supported in part by a grant of HPC time from the

DOD HPC centers, ARL MSRC SGI-O2K, and NRL SGI-O2K.

[Sponsored by ONR]

References

- ¹R. Ramamurti and W.C. Sandberg, "A 3-D Computational Study of Aerodynamic Mechanisms of Insect Flight," *J. Exp. Biol.* **205**, 1507-1518 (2002).
- ²R. Ramamurti, W.C. Sandberg, R. Löhner, J.A. Walker, and M.W. Westneat, "Fluid Dynamics of Flapping Aquatic Flight in the Bird Wrasse: Three-Dimensional Unsteady Computations with Fin Deformation," *J. Exp. Biol.* **205**(19) 2997-3008 (2002).
- ³M.H. Dickinson, F.O. Lehmann, and S. Sane, "Wing Rotation and the Aerodynamic Basis of Insect Flights," *Science* **284**, 1954-1960 (1999).
- ⁴J.A. Walker and M.W. Westneat, "Labriform Propulsion in Fishes: Kinematics of Flapping Aquatic Flight in the Bird Wrasse," *Gomphosus Varius*, *J. Exp. Biol.* **200**, 1549-1568 (1997).

®

RAM TO NAVY STANDARD PARABOLIC EQUATION: TRANSITION FROM RESEARCH TO FLEET ACOUSTIC MODEL

R.A. Zingarelli and D.B. King
Acoustics Division

Introduction: The Navy Standard Parabolic Equation (NSPE) model is an amalgam of research-oriented underwater acoustic propagation algorithms based on the parabolic equation (PE) approach to solving the forward acoustic wave equation, with various features and input/output routines required for operational use. NSPE originated in the 1980s to fill the need for a standardized low-frequency deep-water acoustic model. In early versions, a split-step Fourier¹ solution method (SSF)

was combined with an input routine that allowed use of bottom database parameters. Routines that simulate rough wave or ice-covered surfaces, allow directed sound sources, and emulate broadband and beamforming receiver systems were also added.

An assumption inherent in the SSF approach is that there are no vertical discontinuities in the propagation medium. By the 1990s, the emphasis in Naval research had shifted to shallow waters, where interaction with the ocean bottom is more significant and the SSF's water-sediment boundary and single bottom layer approximations are no longer valid. Fortunately, by this time research efforts had produced several other PE models that could numerically handle these discontinuities and provide reliable predictions in shallow water.

The Research Model: One research and development (R&D) model that showed outstanding promise was the Range-dependent Acoustic Model² (RAM), developed at NRL by Michael Collins. This model is based on a user-selected multiple-term Padé approximation of the PE operator. Because this solution allows range steps much greater than the acoustic wavelength and does not require fine vertical gridding, RAM is a very fast research model.³ Additionally, RAM's grid can be tuned to smoothly trade accuracy and speed as the operational situation requires. Finally, several parallelization methods are applicable, allowing further speed improvements. The odyssey of this model from R&D to operational status represents a first for the Navy because it was done entirely within NRL, with the R&D developer (Collins) playing a key role. The success of this effort establishes a roadmap for future Navy operational models.

Integration and Testing: With RAM's accuracy and speed documented in the peer-reviewed R&D literature, the first step in incorporating it into the operational framework was confirming that the model could work with all necessary features. Some of these required substantial modification; others were simply subroutines that provided specific features.

A major change was in the ocean bottom profile referencing. Originally, bottom layering was indexed relative to the ocean surface within the model; however, Navy databases index relative to the seafloor. Adapting to this convention required shifting the model's internal indexing with bathymetry changes. Collins developed a version of RAM with this capability.

Three items that were easily added were beam sources, seawater volume attenuation, and rough surface losses. Beam sources are accommodated by

including them with the original omnidirectional starter in a conditional statement. Volume attenuation was added by including a small complex absorption value in the seawater wavenumber array. Rough surfaces are treated by subroutine calls at each range step that either reduce the field intensity in a surface layer, or directly simulate using conformal mapping.

Another part of incorporating RAM was developing a routine to read from the existing input format, switch on options, and generate an environmental stream for RAM to use. To accomplish this, the entire input is read, then a profile is built at each range where there is a change in the water, bottom, or bathymetry. Figure 11 depicts these additions.

Testing, Optimization, and Formal Acceptance: New capabilities were continuously tested as they were added during development. The completed model was tested using a set of cases designed to cause each routine to be called and verified. Finally the model was tested using 840 environments extracted at random from a shallow-water database to comprehensively simulate real-world use. Once agreement with reference solutions was reached, the grid parameters were repeatedly relaxed and the cases re-run until the model produced acceptable answers in minimum runtime. Testing completed, the model and documentation were submitted to the Oceanographic and Atmospheric Master Library (OAML) secretary for formal review, chiefly to ensure that the added features were correctly implemented. The total process, culminating in NSPE version 5.0, was completed in 18 months.

Continuing Development: Initial comments from the user community were favorable regarding model capabilities, but mixed regarding input/output formats. Complete file compatibility with previous versions had been retained, but at the price of keeping the old punchcard-based input format. In the succeeding version (5.1), we updated the input to a more readable list-based form, and supplied a conversion program for the older format. Runtime is always of concern, and we were able to reduce runtimes by a factor of 5 through several optimizations. Future versions will have further improvements including environmentally sensitive grid tuning and improved indexing techniques. Capabilities in development include improved surface treatments, faster broadband algorithms, and profile range interpolation.

To summarize, NSPE is now a robust and capable model that incorporates one of the fastest and most accurate underwater acoustic models, viz., RAM. In essence, both the ocean acoustics R&D

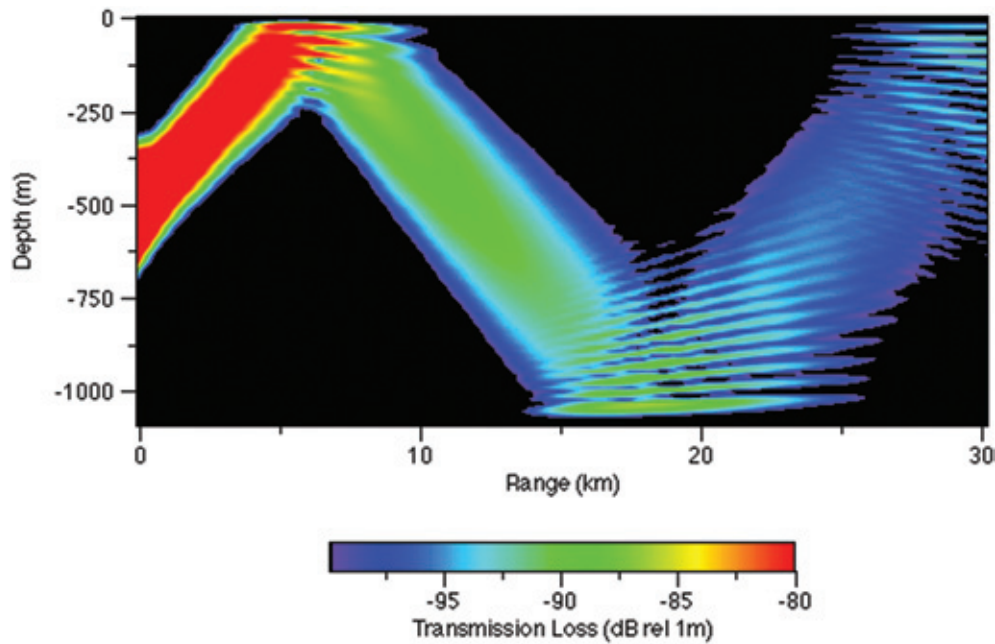


FIGURE 11
Acoustic simulation in a simple ocean environment, depicting several of the features required in a Naval operational model: beam source, wind-driven sea surface losses on the first reflection, and loss-vs-angle ocean bottom treatment. Also present but less evident in the simulation are seawater volume attenuation and spherical Earth corrections. Source frequency, angle, and beamwidth are 250 Hz, 5 degrees, and 1.5 degree respectively; water is isovelocity at 1500 m/s and depth is 1000 meters; windspeed is 20 m/s; ocean bottom parameters approximate soft rock.

community and the Navy operational community are using the same PE model. The overall NSPE program and file structure have been revamped to modern, maintainable standards. Tools and techniques for upgrading, evaluating, and optimizing newer versions have been developed. Work remains to be done, and the foundation provided by RAM and NSPE 5.1 provide a strong starting point.

Acknowledgments: A special acknowledgment is given to the CNO N096 Standing Acquisition and Coordinating Team (SACT) and the Rapid Transition

Process (RTP) program for added support in transitioning the RAM model into NSPE 5.1.
[Sponsored by ONR and SPAWAR]

References

- ¹H.K. Brock, "The AESD Parabolic Equation Model," NORDA Technical Note 12, Naval Research Laboratory, Stennis Space Center, MS, January 1978.
- ²M.D. Collins, "Generalization of the Split-Step Pade," *J. Acoust. Soc. Am.* **96**, 382-385 (1994).
- ³M.D. Collins, R. J. Cederberg, D.B. King, and S.A. Chin-Bing, "Comparison of Algorithms for Solving Parabolic Wave Equations," *J. Acoust. Soc. Am.* **100**, 178-182 (1996).



SPACE RESEARCH AND SATELLITE TECHNOLOGY



SPANISH-AMERICAN WAR NURSES MEMORIAL.
The Spanish-American War was the first war involving the United States in which nurses were organized and assigned as a special, quasi-military unit.

- 217** Inter-Spacecraft Optical Communication and Navigation Using Multiple Quantum Well Modulating Retroreflectors
N.G. Creamer, T.J. Meehan, M.J. Vilcheck, J.A. Vasquez, G.C. Gilbreath, W.S. Rabinovich, and R. Mahon
- 220** Modeling Single-Event Transients in Complex Digital Devices
K.A. Clark
- 222** Full-Sky Astrometric Mapping Explorer Solar Precession
T.W. Lim and P.G. DeLaHunt

[BACK TO CONTENTS](#)

INTER-SPACECRAFT OPTICAL COMMUNICATION AND NAVIGATION USING MULTIPLE QUANTUM WELL MODULATING RETROREFLECTORS

N.G. Creamer,¹ T.J. Meehan,¹ M.J. Vilcheck,¹ J.A. Vasquez,¹ G.C. Gilbreath,² W.S. Rabinovich,³ and R. Mahon⁴

¹Spacecraft Engineering Department

²Remote Sensing Division

³Optical Sciences Division

⁴Jaycor, Inc.

Introduction: Because of the benefits of autonomous spacecraft-to-spacecraft interrogation, communication, and navigation for civilian, commercial, and military space missions, there has been a significant amount of research and development on associated relative sensor systems over the past decade. These systems typically implement radio communication links, GPS sensing for long-range relative positioning, and combinations of visual and laser ranging for short-range proximity operations. In contrast, NRL has developed and tested a multifunctional device that uses solid-state multiple quantum well (MQW) modulating retroreflectors to provide inter-spacecraft laser interrogation, communication, and navigation. The modulating retroreflectors enable compact, low-power, and low-mass optical data transfer on the order of megabits per second, and relative navigation on the order of centimeters in

three-axis position and arcminutes in two-axis orientation. Links over ranges of kilometers down to a few meters are possible.

Multiple Quantum Well Modulating Retroreflectors: An MQW modulating retroreflector (MRR) is an NRL-patented solid-state device that allows optical communication and ranging between two platforms.¹ This device enables fast data rates at very low drive power and can be packaged in a lightweight, compact unit. Implementation requires that only one platform contain an onboard laser, telescope, and tracker; hence, the device is well suited to asymmetric problems in which one platform serves as the interrogator and pursuer and the other platform serves as the target. As depicted in Fig. 1, the pursuer illuminates the target platform carrying the modulating retroreflectors with a laser beam. The laser beam is modulated using an on-off keying mode and reflected back to the pursuer, with no need for precise laser pointing or tracking. Modulation is achieved by placing a moderate voltage (10-20 volts) across the MQW device in reverse bias. This causes an abrupt change in the optical transmissibility of the material, thus providing a controllable high-speed (up to 10 Mbps) solid-state shutter.

Target MRR Array: To achieve relative position and orientation knowledge of the target platform in addition to communication, an MRR array was designed with eight retroreflectors arranged in the configuration shown in Fig. 2. The center retroreflector and three outer retroreflectors lie in the same

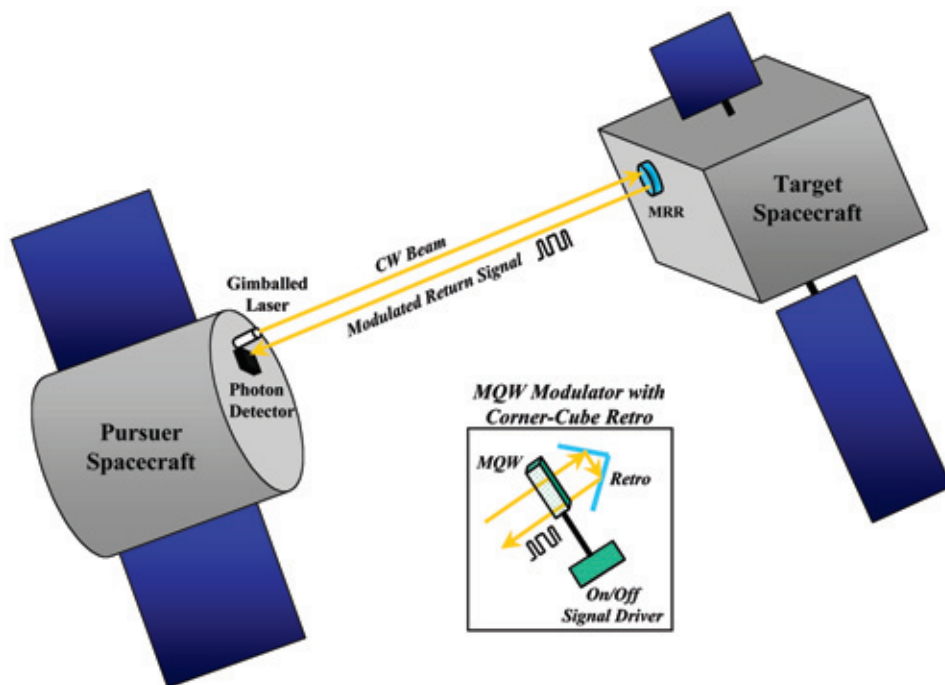


FIGURE 1
Conceptual depiction of inter-spacecraft communication using modulating retroreflectors.

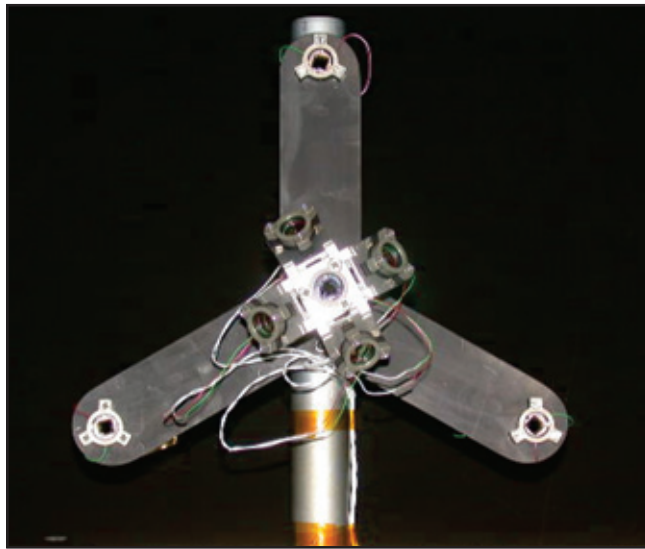


FIGURE 2
Target MRR array.

plane, and four inner retroreflectors are canted 20 degrees from this plane. Upon illumination of the entire array by the pursuer laser beam, the reflected signals from each MRR are uniquely modulated and reflected back to the pursuer. The intensity of each reflected signal is linearly proportional to the angle of the incoming laser beam relative to the MRR boresight direction, allowing discrimination between target translation and rotation.

Pursuer Spacecraft Laser Interrogator, Detector, and Signal Processing Logic: The pursuer spacecraft houses the interrogating gimballed laser, an analog photodetector, an analog-to-digital converter, and the signal processing logic required to transmit the continuous-wave laser beam to the target and receive the modulated signals from the target. As depicted in Fig. 3, upon illumination, the aggregate photon return is captured by the analog photodetector and converted to a digital signal. Isolation of each individual MRR signal is then achieved through a set of matching filters tuned to the unique modulator code sequence associated with each MRR.

Target Tracking and Relative Navigation: Initial target detection is achieved by performing a series of rectangular searches in gimballed azimuth and elevation space until all retroreflectors are illuminated. Subsequent gimballed tracking is achieved by equalizing the signal intensities from the three outer retroreflectors, resulting in a laser beam that is continually centered on the MRR array. Relative navigation is achieved using the eight signal returns from the retroreflectors, the laser gimballed azimuth and elevation angles, and the range from the pursuer to the

target. The range is determined by applying a pulse to the laser beam and measuring the round-trip flight time for the pulse to return to the pursuer.

Experimental Verification: The Naval Research Laboratory's Dual-Platform Motion Simulator (DMS)² was used for validation and performance evaluation of the inter-spacecraft MRR sensor system. The DMS facility consists of a 6 degree-of-freedom pursuer platform and a 4 degree-of-freedom target platform, each driven autonomously and independently using a Pentium III personal computer. The pursuer platform was equipped with a gimballed optical transmitter/receiver system comprised of a 100 mW-laser diode operating at a 980-nm wavelength, a 10 MHz Avalanche photodetector, a signal amplifier, an analog-to-digital converter, and eight digital matched filters. The target platform was equipped with the MRR array, consisting of eight 0.5-mm MQW modulating retroreflectors, each with a mass of 10 grams and a power draw of 75 mW. The devices were driven by a 15-volt modulator, sufficient to achieve a 3:1 optical on/off ratio. Figure 4 shows the pursuer and target platforms with the associated tracking hardware.

A target tracking maneuver was performed to demonstrate the capability of the MRR sensor suite for relative navigation. Using feedback from the MRR sensors, the pursuer platform was commanded to maintain a fixed relative position and orientation as the target rotated and translated along a 30-degree circular arc with a radius of 5 meters. For this simple test, we achieved a steady-state tracking capability of about 15 cm in position and 4.5 degrees in orientation and a static capability (no target motion) of 1 cm in position and 0.3 degrees in orientation.

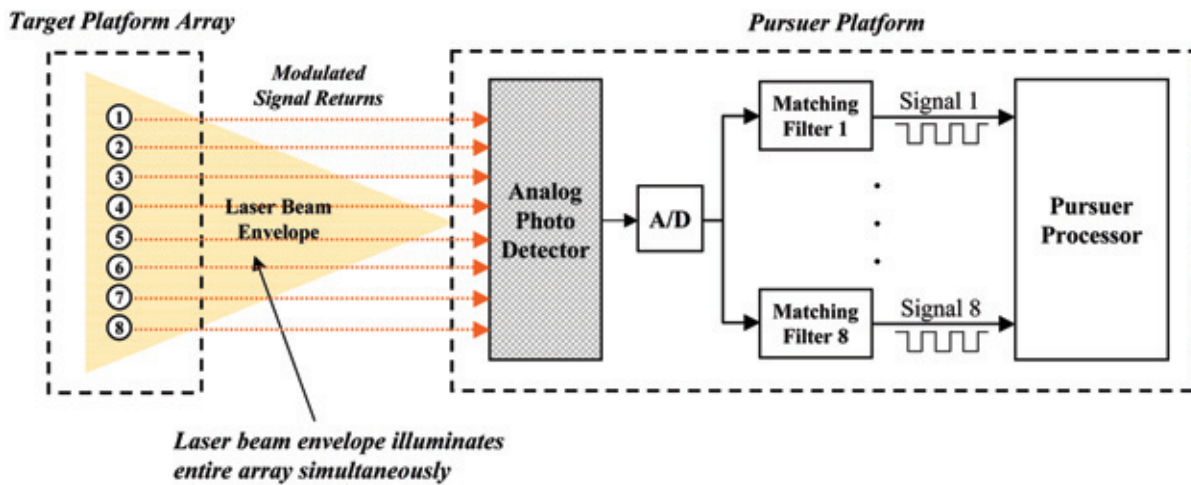


FIGURE 3
Target-to-pursuer communication and MRR discrimination.

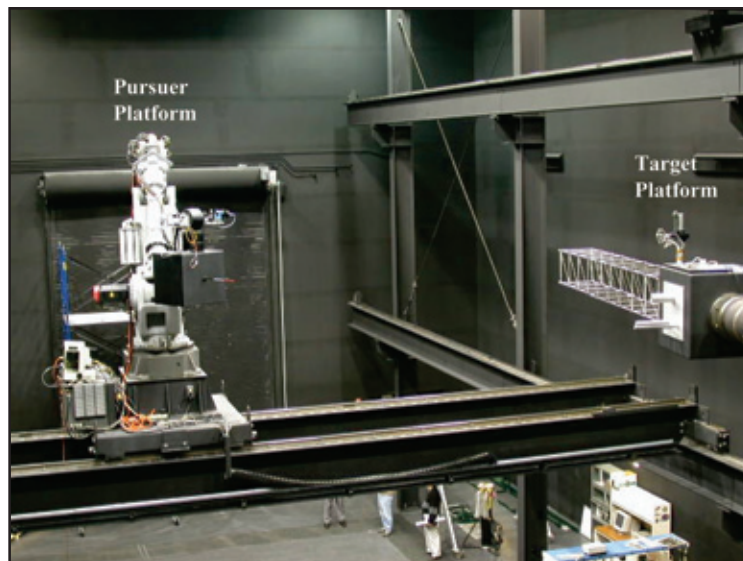


FIGURE 4
DMS laboratory setup of pursuer and target platforms.

Of course, the tracking results are highly dependent on the controller feedback gains and can be reduced by increasing the bandwidth (selected to be 0.02 Hz for this test). More important from a sensor standpoint is the relative navigation knowledge capability, which has been demonstrated to be about 1 centimeter in position and 1 arcminute (0.017 degrees) in orientation.

Summary: We have developed and tested a multifunctional sensor technology for inter-spacecraft communication and navigation using solid-state modulating retroreflectors. This technology has the potential to simplify hardware requirements for

asymmetric applications involving an agile pursuer spacecraft and a docile target spacecraft, such as autonomous rendezvous and capture of orbiting canisters containing fuel, electronic equipment, and supplies.

[Sponsored by NASA]

References

- ¹ G.C. Gilbreath, S.R. Bowman, W.S. Rabinovich, C.H. Merk, and H.E. Senasack, "Modulating Retroreflector Using Multiple Quantum Well Technology," U.S. Patent No. 6,154,299, awarded November 2000.
- ² G. Creamer and S. Hollander, "The Spacecraft Robotics Engineering and Controls Laboratory," 2002 NRL Review, pp. 207-209.

MODELING SINGLE-EVENT TRANSIENTS IN COMPLEX DIGITAL DEVICES

K.A. Clark
Space Systems Development Department

Introduction: Requirements for onboard electronics of many satellites are greatly increasing. One approach to meeting these requirements is to use state-of-the-art commercial electronics. However, to ensure reliable on-orbit operation, effects of the natural space radiation environment must be considered. These effects can be divided into two categories: total dose and single-event transients. Total-dose radiation effects on electronics can result in a slow but steady shift of the threshold voltages of transistors. Eventually, the threshold voltage may have shifted so much that the transistor can no longer function. Characterization of total-dose tolerance is well understood. Single-event transient (SET) effects from radiation are typically the result of a single charged particle, such as a heavy ion, that strikes a sensitive region of a circuit and deposits energy, resulting in an unintended analog pulse. In a digital circuit, this pulse may cause a single-event upset (SEU), in which the logic value of a memory element is changed (i.e., a logic "1" becomes a logic "0" or vice versa). Characterization of single-event transient tolerance for simple digital devices, such as memories, is well understood. However, for a complex digital device, one that contains multiple functional modes and both combinational logic elements and memory elements, this is not the case. For this reason, a methodology to determine the effect of single-event transients in complex digital devices has been developed.

Methodology Development: The SET state-transition model, shown in Fig. 5, defines the framework of the methodology (Ref. 1, pp. 7-9). The model reduces the operation of the complex digital device into four separate fault states. State S1: No SETs or SEUs is the fault-free state; the device is operating correctly. From S1, an SET can occur on a logic gate. This will occur with transitional probability β_2 , causing a transition to S2: Logic Gate Transient. Also from S1, the SET can occur on a memory element with transitional probability β_1 , causing a transition to S3: SEU. From S2, if the logic gate transient is latched into a memory element, which occurs with transitional probability δ_1 , the state becomes S3: SEU. If the transient is not latched into a memory element and stops propagating, the state returns to S1, which occurs with transitional probability α_2 .

From S3, if the SEU is overwritten before it can cause an error to the external system, the present state returns to S1. If, instead, the SEU causes an error to the external system, a transition to state S4: Failure occurs with transitional probability ϵ_1 .

Predicting the effect of single-event transients in a complex digital device involves determining the transitional probabilities in this model. The overall SET tolerance of the device is calculated by combining the transitional probabilities to account for all the possible paths from S1 to S4.

Methodology Validation: To validate this methodology, the SET tolerance of a candidate complex digital device was determined. This device was the KDLX microprocessor, a 16-bit version of the processor described in Ref. 2. Figure 6 shows the processor. It was fabricated using the MOSIS prototyping system on the Agilent (formerly Hewlett-Packard) 0.5 μm CMOS process.

Determining the transitional probabilities involves SET generation modeling, SET analog propagation modeling, clock-edge effects modeling, logic propagation modeling, and SEU propagation modeling. The purpose of SET generation modeling is to determine how an incident ion will generate a transient pulse that can be described electrically. It is accomplished using a dependent current source in SPICE (Simulation Program with Integrated Circuit Emphasis) to create a double exponential pulse. SET analog propagation is modeled using SPICE and determines whether or not this electrical transient pulse is amplified or attenuated as it propagates through the circuit. Clock-edge effects modeling determines the probability that an SET pulse will be latched into a memory element; it is also modeled in SPICE. Logic propagation is modeled by analysis and determines the probability that there is a clear logic path through which the transient can propagate. SEU propagation modeling determines the likelihood that an SEU will propagate to the output and cause a failure to the external system, or alternatively, the likelihood that the SEU will be overwritten and the state can return to the fault-free state, S1. SEU propagation is modeled using a combination of register-usage analysis and VHDL (Very high-speed integrated circuit Hardware Description Language) simulations.

The results of the modeling were combined to predict the overall device cross-section of the KDLX processor for three different test programs. The overall device cross-section is a measure of the device's sensitivity to SETs. The true device cross-section was then measured by performing heavy-ion testing at the Radiation Effects Facility at the Texas A&M University Cyclotron Institute. Figure 7 compares

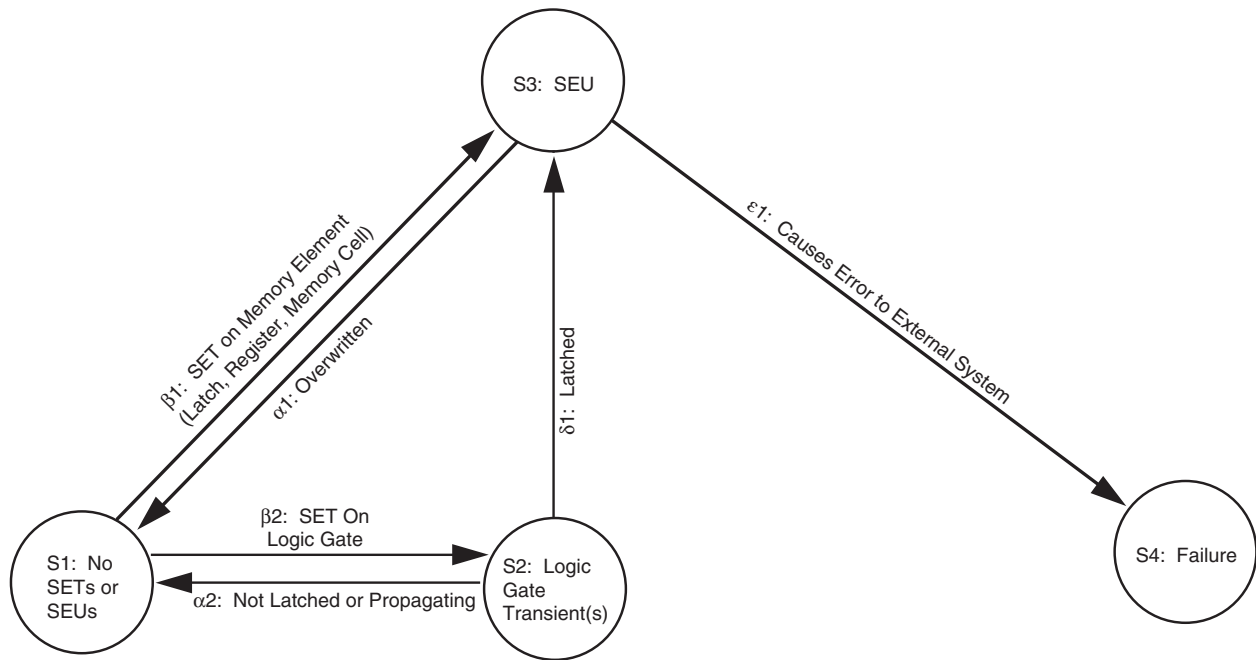


FIGURE 5
SET state-transition model.

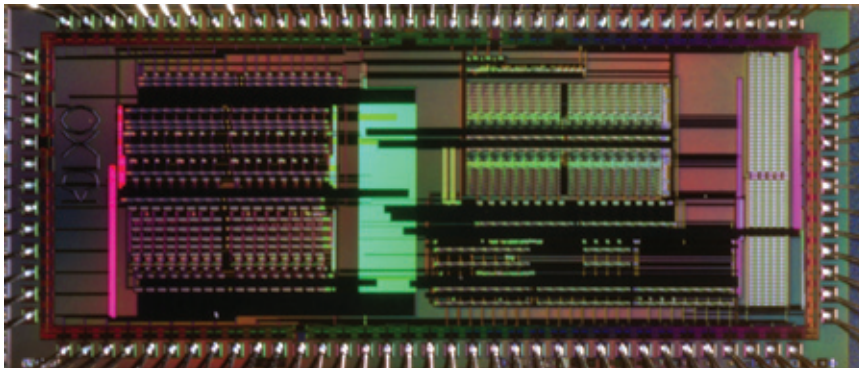


FIGURE 6
Candidate complex digital device: the KDLX.

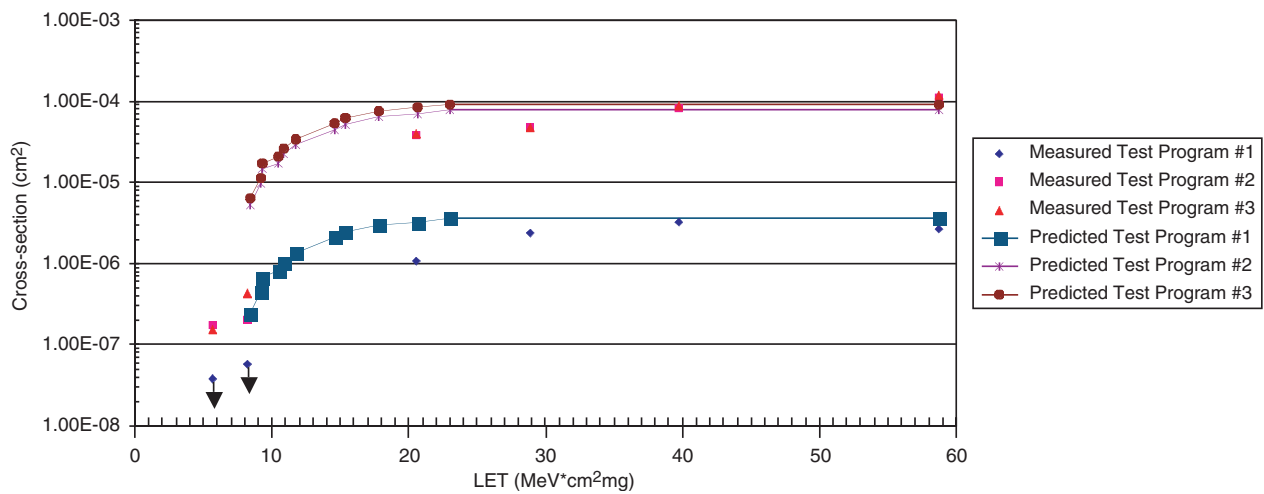


FIGURE 7
Predicted vs measured device cross-sections.

the predicted and measured cross-sections. This comparison shows very good agreement between the predicted and measured cross-sections of the device for each of the three test programs (Ref. 1, p. 79). This validates the described methodology to determine the effects of single-event transients in a complex digital device.

Summary: A methodology to determine the effect of single-event transients on complex digital devices has been developed. The methodology is based on the SET state-transition model and was validated by performing radiation testing on a candidate device, the KDLX microprocessor. This validated methodology is important to the Navy and DOD because it enables the reliable use of state-of-the-art commercial electronics in spacecraft, resulting in enhanced performance while reducing size, weight, power, and cost of the spacecraft's electronics.

[Sponsored by ONR]

References

¹ K.A. Clark, "Modeling Single-Event Transients in Complex Digital Systems," doctoral dissertation, Naval Postgraduate School, June 2002.

² J.L. Hennessy and D.A. Patterson, *Computer Architecture, A Quantitative Approach* (Morgan Kaufman, San Francisco, CA, 1996), pp. 69-163.



FULL-SKY ASTROMETRIC MAPPING EXPLORER SOLAR PRECESSION

T.W. Lim and P.G. DeLaHunt
Spacecraft Engineering Department

Introduction: The Full-Sky Astrometric Mapping Explorer (FAME) mission is designed to collect astrometric and photometric data at a geosynchronous orbit to map the position, parallax, and brightness of over 40 million stars at an unprecedented level of accuracy.¹ To collect the data, the optical FAME instrument requires smooth, stable scanning motion covering the full sky multiple times during the 5-year mission duration. The scanning motion is produced by spinning the vehicle at a nominal 40-min period and precessing the spin axis about the Sun-spacecraft line at a nominal 20-day period (Fig. 8). The spin axis is maintained at a nominal 35-degree angle with respect to the Sun. Required torque to precess the spin axis is obtained from the solar radiation pressure on its Sun shield, which is designed primarily to provide power and shade for the instrument. Solar radiation pressure balancing devices called trim tabs and trim areas have been de-

veloped to accommodate changes in vehicle mass and Sun shield optical properties by updating their positions periodically. During science operation, the trim devices remain passive to ensure high-quality data collection free from jitter.

Solar Radiation Torque Estimation: The FAME Sun shield, shown in Fig. 9, consists mainly of an annular solar array and a truncated cone covered with thermal blankets. When the photons from the Sun strike its surface, a momentum exchange occurs. This produces a reaction force that is determined by the optical property, geometry, and orientation of the surface.² The reaction force has three components corresponding to absorption, specular reflection, and diffuse reflection. Thermal radiation emitted from the surface also contributes to the reaction force. The Sun shield may contain geometric variations stemming from the fabrication, assembly, and launch process. The optical properties are expected to vary gradually for the mission duration due to the exposure of the Sun shield to the space radiation environment. Solar irradiation typically goes through seasonal changes. Furthermore, the vehicle center of mass migrates as onboard propellant is consumed for station keeping. To maintain the required solar precession under these potential error sources, solar radiation torque balancing devices are developed.

Solar Radiation Torque Balancing: As shown in Fig. 9, three rectangular trim tabs are located 120 degrees apart from each other, attached along the circumference of the electronics deck below the solar array. To maximize the effectiveness, trim tabs are coated with silver Teflon (Ag FEP). Trim tabs are sized to accommodate the expected changes in solar radiation torque with sufficient margin. Figure 3(a) shows how the deflection of the trim tabs affects precession rate. Positive deflection moves the trim tabs toward the propulsion deck, and vice versa. At the beginning-of-life, the tabs are deflected +12.5 degrees to increase solar precession torque and -23 degrees at the end-of-life to reduce the increased solar radiation torque of the Sun shield, mainly due to optical property degradation. Three pie-shaped trim areas are also placed under the electronics deck between the trim tabs. The trim areas swing out to control the offset between the vehicle center of mass (CM) and the effective center of pressure (CP) of the Sun shield. The CM-CP offset produces undesirable variations in precession and spin rates.³ Figure 10(b) shows how the 20-mm CM-CP offset along the Y-axis is compensated by rotating out the trim areas 1 and 2 simultaneously.

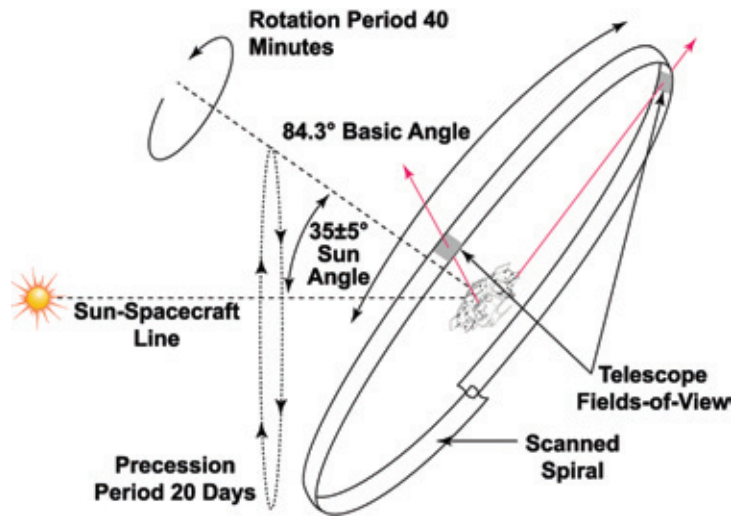


FIGURE 8
FAME observation concept driven by solar precession.

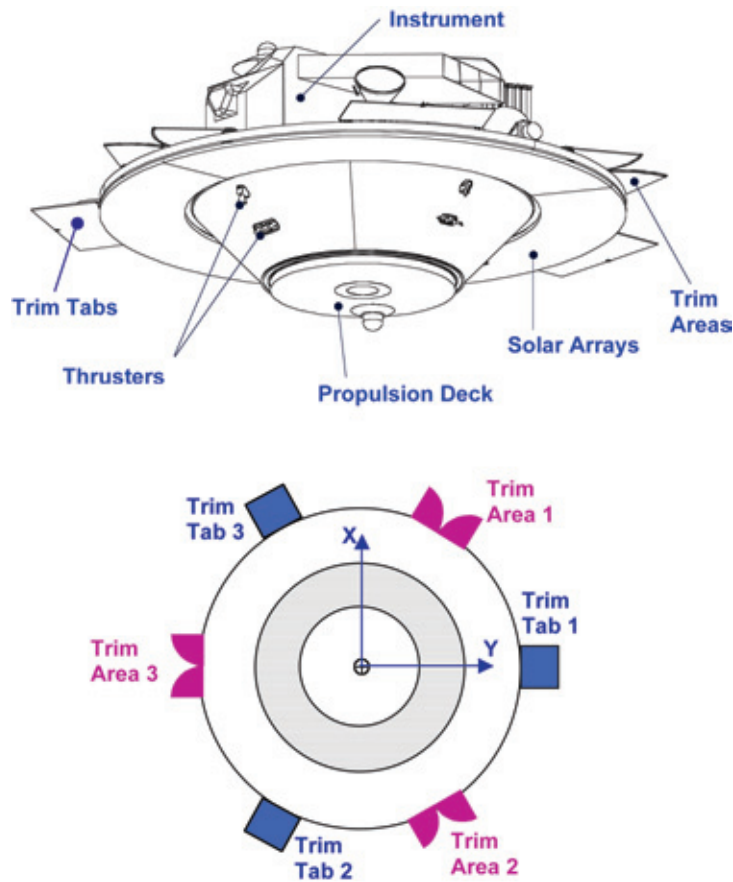
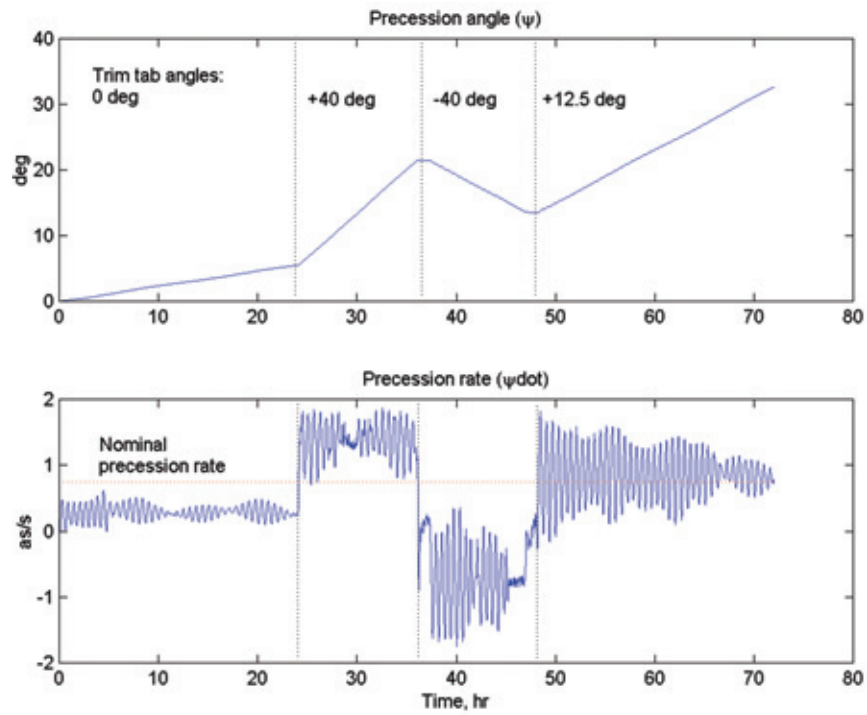
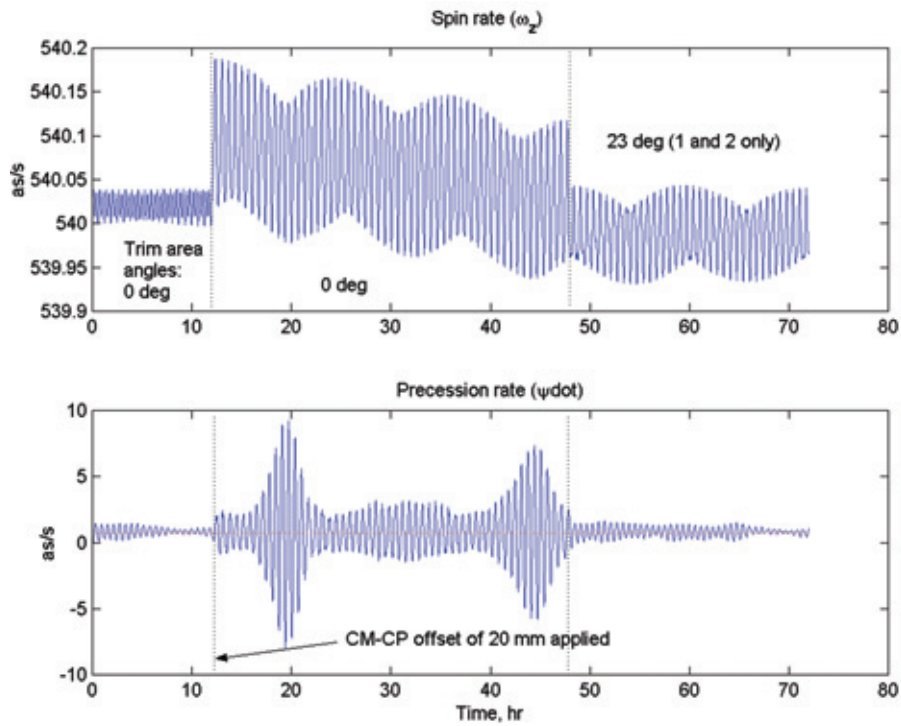


FIGURE 9
Control surfaces for solar precession balancing.



(a) Precession rate control by trim tabs.



(b) Spin and precession rate variation control by trim areas.


FIGURE 10
Solar precession control demonstration.

Summary: Fundamental principles of solar precession for spinning satellites are developed in this research as well as the devices to maintain spin and precession rates, called trim tabs and trim areas, to accommodate changes in surface optical properties, center of mass, and environmental disturbances.

Acknowledgments: The authors acknowledge contributions from the NRL FAME team for the design of trim tabs and areas.

[Sponsored by NASA]

References

- ¹S. Horner et. al., "Full-Sky Astrometric Mapping Explorer: An Optical Astrometric Survey Mission," *Proc. SPIE* Vol. **4013**, UV, Optical, and IR Space Telescopes and Instruments, pp. 473-481 (2000).
- ²"Spacecraft Radiation Torques," NASA Space Vehicle Design Criteria (Guidance and Control), NASA SP-8027 (1969).
- ³T.W. Lim and P.G. DeLaHunt, "Solar Precession Dynamics of a Spinning Spacecraft," AIAA Paper 2002-4782, AIAA Guidance, Navigation and Control Conference, Monterey, CA (2002). 

SPECIAL AWARDS AND RECOGNITION



COMMODORE JOHN BARRY.

In 1776, Commodore Barry became the first American naval officer to capture an enemy ship, and he continued to serve heroically throughout the Revolution.

229 Special Awards and Recognition

242 Alan Berman Research Publication and Edison Patent Awards

[BACK TO CONTENTS](#)

SPECIAL AWARDS & RECOGNITION

NRL is proud of its many distinguished scientists, engineers, and support staff. Here we feature some who have received awards from prestigious institutions, the Department of the Navy, and NRL.

PRESIDENT OF THE OCEANOGRAPHY SOCIETY



Dr. Eric Hartwig

Ocean and Atmospheric Science and Technology Directorate

The Oceanography Society was founded in 1988 and has 1,400 international members representing more than 40 countries. Its goals are to disseminate knowledge of oceanography and its applications through research and education, to promote communication among oceanographers, and to provide a constituency for consensus building across all the disciplines of the field. The society is dedicated to a multidisciplinary view of oceanography through its activities and publications. TOS aims to link and support all the ocean sciences and related technologies. Dr. Hartwig assumed the position of President of The Oceanography Society in August 2002, for a two-year term.



WOMEN IN TECHNOLOGY INTERNATIONAL (WITI) HALL OF FAME



Dr. Elaine Oran

Laboratory for Computational Physics & Fluid Dynamics

Dr. Oran was formally inducted into the Women in Technology International Hall of Fame in late June 2002. She was honored for research that has “contributed significantly to the advancement of the engineering profession by pioneering a computational technology, which has unified engineering, scientific and mathematical disciplines into a methodology for solving complex reactive flow problems.” WITI was established 13 years ago, and their Hall of Fame was launched in 1996 to recognize and honor the outstanding contributions women make to the scientific and technological communities that improve and advance our society.

AMERICAN INSTITUTE OF AERONAUTICS AND ASTRONAUTICS (AIAA) DRYDEN LECTURESHIP IN RESEARCH AWARD

This award was named in honor of Dr. Hugh L. Dryden in 1967. The lecture emphasizes the great importance of basic research to the advancement of aeronautics and astronautics and is a salute to research scientists and engineers. Dr. Oran presented the lecture entitled, “Matchsticks, Scramjets, and Black Holes: Numerical Simulation Faces Reality” at the 40th AIAA Aerospace Sciences Meeting and Exhibit in Reno, Nevada. She is known for her pioneering applications of numerical simulation for solving problems in fluid dynamics and reacting flows. She has made pivotal contributions to a broad range of problems in combustion and propulsion, atmospheric physics, and solar physics and astrophysics. Her work has contributed to both basic science and to advanced engineering applications.

2001 AMERICAN SOCIETY FOR MATERIALS (ASM) DISTINGUISHED LIFE MEMBERSHIP AWARD



Dr. Bhatka Rath

Materials Science and Component Technology Directorate

The ASM established this award in 1954 to recognize those individuals who have devoted their time, knowledge, and abilities for the advancement of materials engineering. The award is among the most prestigious of the society to recognize a truly outstanding scientist or engineer. Dr. Rath was cited for his exceptional leadership and his contributions to the science and application of structural and functional materials. The award is conferred at the society's annual conference banquet following the recommendation of the Award Selection Committee and elected by unanimous, affirmative vote of all members of the Board of Trustees.

FELLOW OF THE INSTITUTE OF MATERIALS OF THE UNITED KINGDOM

The Institute of Materials confers this prestigious recognition to those with an established and enhanced reputation in materials science and technology. The Institute serves the international materials community through its wide range of activities and by acting as the professional body for materials scientists and engineers. It has a membership of over 18,000 throughout the United Kingdom, Europe, and the United States. In addition to recognition as Fellow and as a separate honor, Dr. Rath has also been recognized with an international symposium of "Science and Technology of Interfaces" honoring his seminal contributions in the field of solid state transformations and interface properties for more than four decades. The symposium was dedicated to Dr. Rath for "his pioneering research and for his leadership in the areas of interfaces."

FEDERATION OF MATERIALS SOCIETIES (FMS) NATIONAL MATERIALS ADVANCEMENT AWARD

This award recognizes individuals who have demonstrated their outstanding capabilities in advancing the effective and economic use of materials and the multidisciplinary field of materials science and engineering generally, and who contribute to the application of the materials profession to national problems and policy. Dr. Rath was recognized for being a leading scientist and executive in the materials field for four decades. He has been a formulator and implementer of materials science policy in and for the Department of Defense, the Department of State, and in connection with international bodies in the United Kingdom, Canada, Australia, New Zealand, India, and China.

AMERICAN SOCIETY FOR MATERIALS (ASM) INTERNATIONAL AND THE METALS, MINERALS AND MATERIALS SOCIETY (TMS) TMS/ASM JOINT DISTINGUISHED LECTURESHIP IN MATERIALS AND SOCIETY AWARD

The Distinguished Lectureship in Materials & Society Award was established in 1971 to clarify the role of materials science and engineering in technology and in society in its broadest sense; to present an evaluation of progress made in developing new technologies for the ever-changing needs of society; and to define new frontiers for materials science and engineering. Dr. Rath was cited for his outstanding contributions to materials science and engineering and for his "visionary leadership in guiding leading-edge research for national security."

2002 AUTHOR E. BISSON PRIZE FOR TECHNOLOGY ACHIEVEMENT



Dr. Melvin Kruer
Optical Sciences Division

Dr. Kruer was honored for his outstanding contributions to the development of focal plane arrays and their transitions into Navy missile seekers, missile threat warning systems, and electro-optical reconnaissance cameras. The citation reads, "Dr. Kruer has guided recent development of very large visible and infrared focal plane array capabilities that have placed the Navy in the forefront of reconnaissance camera research and development. These staring cameras have transitioned into the Navy F-14 TARPS-CD and F-18 SHARP programs."



2001 VICE ADMIRAL HAROLD G. BOWEN AWARD FOR PATENTED INVENTIONS



Mr. George Kang and Larry J. Fransen (retired, NRL)
Information Technology Division

The Bowen Award, named in honor of Vice Admiral Harold Gardiner Bowen, the first Chief of Naval Research, recognizes inventions of great benefit to the Navy patented by current or former, civilian or military Navy personnel. The invention must have significant impact upon the operation of the Navy as measured by the extent of its use, cost savings, increased military capability, or increased quality of life. Mr. Kang's and Mr. Fransen's winning NRL invention, the Voice Communication Processing System, improves speech communication at low data rates benefiting Naval tactical voice communications. This new technology has enhanced speech intelligibility on secure telephones and provided direct interoperability between old and new speech parameters, allowing new secure phones and legacy secure phones to work together. This has resulted in a cost savings to date of nearly \$600 million.



SIGMA XI 2002 APPLIED SCIENCE AWARD



Dr. Teddy Keller
Chemistry Division

Dr. Keller was recognized for "research on high temperature resins for composites. Dr. Keller's research over the past 25 years has focused on designing, synthesizing, and understanding polymeric, carbon, and ceramic compositions that exhibit outstanding processability, mechanical, and high temperature properties. In addition to his scientific contributions, his new materials have been patent protected and are under serious consideration for multiple military and civilian applications." The nomination states that Dr. Keller is a "world's leading expert in phthalonitrile resins" and he is responsible for the development of this new class of high temperature material that is currently being evaluated and characterized for numerous aerospace and ship applications.

SIGMA XI 2002 PURE SCIENCE AWARD



Dr. C. Michael Roland
Chemistry Division

Dr. Roland was recognized for his “research in the physics of rubbery materials. His work has had an enormous impact, as evidenced by the 2,304 citations of his work, awards, and consultancies. He has discovered various phenomena, revealing new physics and new applications for these materials.” The award nomination summarizes Dr. Roland’s research contributions in the areas of polymer blends, chemical structure and relaxation behavior, and studies of rubber elasticity in network. To date, Dr. Roland has 12 patents to his name.

AMERICAN CHEMICAL SOCIETY RUBBER DIVISION’S MELVIN MOONEY DISTINGUISHED TECHNOLOGY AWARD

This award is presented for significant, repeated innovative contributions to rubber science and technology. According to the citation, “Dr. Roland’s innovative research led to the discovery of various phenomena, revealing new physics in polymers. Among his outstanding contributions to rubber technologies are rubber for acoustic applications, microgel polymers, double network rubbers, surface modification of elastomers, and microlithography on polymers.”



SIGMA XI 2002 YOUNG INVESTIGATOR AWARD



Dr. Karen Swider-Lyons
Chemistry Division

Dr. Swider-Lyons was noted to be “a leading young investigator in electrochemical power sources for her growing body of creative research on the materials science of batteries and fuel cells. She further contributes to the research and development of power sources through government program management and academic participation.” According to the nomination, Dr. Swider-Lyons’ graduate work at the University of Pennsylvania “focused on the research and development of new electrode materials for solid oxide fuel cells, including yttria-stabilized zirconia with titania.” This work led to patents, which then led to subsequent studies by fuel-cell development teams.



NAVY DISTINGUISHED CIVILIAN SERVICE AWARD



Mr. Richard Foch
Tactical Electronic Warfare Division

Mr. Foch was presented with this award for his accomplishments as a pioneer in the field of small unmanned air vehicles (UAVs). He is recognized for his role in advancing the technologies associated with small UAVs and demonstrating the successful feasibility and applicability of small UAV systems technologies to meet a variety of operational missions. The citation reads “The Navy, Industry, NASA, and the UAV community recognize Mr. Foch as an expert on affordably expendable, autonomous UAVs. His pioneering efforts and extraordinary creativity during his 22 years at the Naval Research Laboratory have been instrumental in creating a new, officially recognized military UAV category; the small UAV...As a direct result of Mr. Foch’s efforts, NRL is a recognized world leader in small UAV technology, design, and development.”

NAVY SUPERIOR CIVILIAN SERVICE AWARD

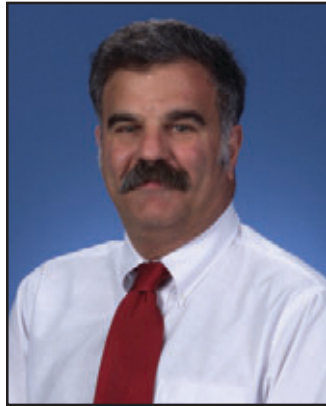


Dr. Richard Hodur
Marine Meteorology Division

Dr. Hodur was recognized for his “superior achievement and service to the United States Navy and the Naval Research Laboratory in the development and validation of the Coupled Ocean/Atmosphere Mesoscale Prediction System (COAMPS). COAMPS is a high-resolution numerical weather prediction system that is used in many locations around the world every day by weather forecasters and Navy operators in carrying out their mission. Over the past decade, Dr. Hodur has provided outstanding personal scientific and technical accomplishments as well as leadership that resulted in the development and validation of COAMPS. COAMPS has had and will continue to have a large positive impact on Navy and other DOD operations.”



AMERICAN PHYSICAL SOCIETY (APS) FELLOWSHIP



Dr. John D. Sethian
Plasma Physics Division

Fellowship in the American Physical Society is limited to no more than one half of one percent of the membership. Election to APS Fellowship is recognition by peers of outstanding contributions to physics. Dr. Sethian was cited “for major contributions to plasma physics and development of associated technologies in the fields of electron beams, Z-pinchs, laser plasma interactions, hydrodynamics, and inertial energy.”

FUSION POWER ASSOCIATES (FPA) LEADERSHIP AWARD

This award is presented annually to individuals who have shown outstanding leadership qualities in accelerating the development of fusion. According to the award citation, “Dr. Sethian was selected in recognition of his leadership of the Electra laser program and especially his leadership in organizing and coordinating a systems approach to the National High Average Power Laser Program.” Dr. Sethian is leading a national program to develop the science and technologies needed to advance this concept into a fusion power plant. The High Average Power Laser Program brings together 24 institutions – national laboratories, universities, and private industry. This integrated approach ensures that laser fusion energy will be developed as a coherent system.



WASHINGTON ACADEMY OF SCIENCES ENGINEERING SCIENCES AWARD



Dr. Christian Rauscher
Electronics Science and Technology Division

Dr. Rauscher was recognized for “his contributions to the understanding and development of miniature, high-performance microwave filters and filter banks.” Dr. Rauscher’s research centers on the pursuit of new high-frequency circuit concepts. His early work dealt with nonlinear signal interaction in microwave field-effect transistors, starting with the derivation of the quasi-static approach to modeling the large-signal behavior of such transistors. The technique later became the cornerstone of all commercial computer-based nonlinear-microwave-circuit analysis tools. This was followed by derivations of novel techniques for designing microwave power amplifiers, frequency multipliers, regenerative frequency dividers, and voltage-controlled oscillators for optimum large-signal performance.

2002 JOSEPH F. KEITHLEY AWARD



Dr. Robert Soulen
Materials Science and Technology Division

This award is sponsored by Keithley Instruments, Inc. and the Instrument and Measurement Science Topical Group. It recognizes physicists who have been instrumental in the development of measurement techniques or equipment that has impact on the physics community by providing better measurements. Dr. Soulen was cited for “developing low-temperature noise thermometry to achieve an absolute thermometer which now defines the year 2000 International Temperature Scale between 1 mK and 1 K to an accuracy of 0.1%, and for other significant contributions to thermometry measurement over a distinguished career.”



2002 FEDERAL LABORATORY CONSORTIUM (FLC) AWARD FOR EXCELLENCE IN TECHNOLOGY TRANSFER



Dr. Joanne Jones-Meehan
Chemistry Division

This award recognizes outstanding work that has led to the successful transfer of technology developed at a federal laboratory. Results of the technology transfers may be commercial products or services or other utilization of the technology for the public benefit. This award recognized Dr. Jones-Meehan for her role in transferring a fouling-release, silicone coating system developed at NRL. The NRL-developed fouling-release coating system reduces the problem of biofouling (i.e., undesired growth of barnacles, mussels, tube worms, etc.) without the use of toxic metals and/or biocides by providing a surface to which organisms find it difficult to adhere. This important technology was transferred for commercialization to Smart Surfaces located in Annapolis, Maryland.



2001 MARCUS A. GROSSMAN YOUNG AUTHOR AWARD



Dr. Richard Fonda

Drs. Richard Fonda and George Spanos
Materials Science and Technology Division

This award was established in 1960, in memory of an eminent metallurgist, research director, and author, who was President of the American Society for Materials in 1944, to honor the author (or authors) under 40 years of age whose paper is selected as the best of those published in a given year (for a specific volume) in *Metallurgical and Materials Transactions*. Drs. Fonda and Spanos were presented this award for their paper entitled “Microstructural Evolution in Ultra-Low-Carbon Steel Weldments—Part I: Controlled Thermal Cycling and Continuous Cooling Transformation Diagram of the Weld Metal,” published in the September 2000 issue of *Metallurgical and Materials Transactions*.



Dr. George Spanos

CHIEF OF INFORMATION (CHINFO) 2001 MERIT AWARD



Mr. Dom Panciarelli, Ms. Donna McKinney, Ms. Janice Schultz, Ms. Denise Stewart, Ms. Kristen Kehres, Ms. Amy Downing, Ms. Jennifer Burke, and Mr. Richard Thompson

Labstracts

NRL Public Affairs Office

Labstracts, the Naval Research Laboratory's twice monthly newspaper has once again been awarded its third consecutive Chief of Information Merit Award for exemplary achievements in internal print media. This award is the U.S. Navy's highest award for internal print and broadcast products by Navy commands and individuals. Competing in the "military-funded (tabloid) newspaper, shore units" category, *Labstracts* placed second overall following a comprehensive review by a distinguished panel of military and civilian judges who evaluated layout and design, content quality, writing, editing, photography, and production quality.



2002 DIGITAL CONSULTING INSTITUTE (DCI) PORTAL EXCELLENCE AWARD



Mr. James King and Mr. Kiriakos Georgiou

Ruth H. Hooker Research Library

Technical Information Division

The Digital Consulting Institute Portal Excellence Awards recognize best practices for implementing and exploiting internal and e-business information portals. The Library was recognized in the category of "Content Management" for its use of Convera's RetrievalWare software to enable researchers from the Naval Research Laboratory and 12 other Naval facilities to access hundreds of journals and thousands of technical reports through TORPEDO *Ultra*. The TORPEDO *Ultra* system combines a custom-designed, intuitive interface with the powerful search capabilities of Convera's RetrievalWare software.



NAVY MERITORIOUS UNIT COMMENDATION



Flight Support Detachment

Patuxent River Naval Air Station

The Meritorious Unit Commendation is awarded to any unit of the Navy or Marine Corps that has distinguished itself by either valorous or meritorious achievement that rendered the unit outstanding compared to other units performing similar service. The Flight Support Detachment (FSD) earned this commendation for meritorious service from

December 1999 to March 2001. According to the citation, "Through meticulous planning, resolute determination, and superior leadership, the FSD provided flawless support of research projects in the fields of electronic countermeasures, electronic warfare, infrared detection systems, synthetic aperture radar development, optical research, gravity measurements, radar and magnetic mapping, and oceanographic environmental surveys."

NAVY-MARINE CORPS COMMENDATION MEDAL



LT Ted Voltz
Flight Support Detachment

The medal was awarded to LT Voltz for his extraordinary performance in the at-sea incident aboard the Navy's deep-diving research submarine USS *Dolphin*. At approximately 11:30 p.m. PDT, May 22, 2002, LT Voltz' aircraft, NRL's Researcher 442 was airborne, conducting communications testing with the aircraft carrier USS *Nimitz* roughly 70 miles southwest of San Diego. An emergency call was received requesting assistance for an SAR operation some 30 miles to the south. The call reported that the USS *Dolphin* was in distress in heavy seas due to a fire and flooding. Researcher 442, with LT Voltz acting as mission commander/combat information center officer, proceeded to the site of the emergency to coordinate the SAR operation. LT Voltz began the critical airspace "deconfliction" required to

ensure safe air operations during the SAR. CDR Munns, commander of Research 442, said that "it is difficult to articulate the importance of LT Voltz's contribution" throughout the operation. He added that LT Voltz's ability to calmly, professionally, and "...quickly assume control of air deconfliction for multiple aircraft flying at night within 100 feet of each other is commendable."



2002 NAVAL DISTRICT WASHINGTON (NDW) REGIONAL COMMUNITY SERVICE PROGRAM OF THE YEAR AWARD



CAPT David M. Schubert and Mr. Dom Panciarelli

NRL Community Outreach Program *NRL Public Affairs Office*

The NDW award is presented to Navy commands in the National Capital Region in recognition of their exemplary voluntary service to American youth and communities. Volunteers from NRL's Community Outreach Program were recognized for their service in support of NRL's annual Holiday Party for Neighborhood Children under the award's Project Good Neighbor Flagship, Large Shore Command category. The party was created to provide holiday festivities and cheer to children who would not normally be able to celebrate the holiday season because of their family's financial situation. Program volunteers are military, civilian, contractor, retired employees, and command partners. This is the second consecutive year that NRL has been selected for this award. It was also awarded in 2001.



LIFETIME ACHIEVEMENT AWARD



Dr. Timothy Coffey
Former Director of Research

Dr. Coffey was presented NRL's Lifetime Achievement Award for a distinguished career devoted to promoting an innovative environment at the Department of Defense's premier laboratory, the U.S. Naval Research Laboratory (NRL). This award is the highest local honor that an NRL Commanding Officer can confer on a civilian employee. According to the citation, "As a "world-class" technical manager, Dr. Coffey's contributions to defense and naval technology policy, and his ability continually to enable world-leading science and technology developments, earned sustained recognition from the Department of the Navy, the Department of Defense, the Federal Government, academia, industry, and the international defense and scientific communities, not only for himself, but for the Laboratory that he served so well and for so long."

E.O. HULBURT SCIENCE AWARD



Dr. Michael Collins
Acoustics Division

This award is NRL's highest civilian honor for scientific achievement. Dr. Collins was recognized for his sustained superior performance in the research of underwater sound propagation and signal processing. Dr. Collins is commended "for substantial contributions to the advancement of theoretical and applied acoustics by his research on parabolic equation techniques for modeling wave propagation in range-dependent media. His models are in wide use throughout the world in applications ranging from mine countermeasures in the ocean to monitoring for explosions in the atmosphere. Dr. Collins has made significant contributions to signal processing including the simulated annealing optimal time-domain beamformer, and focalization, which resolves the problem of mismatch in matched-field processing."



E.O. HULBURT SCIENCE AWARD



Dr. Russell Howard
Space Science Division

This award is NRL's highest civilian honor for scientific achievement. Dr. Howard was cited for "over three decades of scientific contribution and leadership in the design, construction, and operation of solar instrumentation, and in the analysis of their scientific data that has maintained the Naval Research Laboratory as one of the world's premier institutions in solar physics, and for specific contributions to the development of an understanding of coronal mass ejections, the recognition of their role in the interplanetary medium, and the ability to predict the onset of geomagnetic storms following their eruption from the Sun." Dr. Howard designed and implemented some of the first hardware and software solutions for visualizing and analyzing the early coronagraph data that led to many of the initial discoveries about coronal mass ejections.



NAVY MERITORIOUS CIVILIAN SERVICE AWARD



Mr. Stephen Harrison
Research and Development Services Division

The Meritorious Civilian Service Award is the third highest award bestowed by the Navy to its civilian employees. Mr. Harrison's award recognizes his outstanding leadership, management, and transformation of the R&D Services Division over the past six years during a time of significant accomplishment. These accomplishments included the most substantial building renovation effort in the history of NRL; the reduction of the Division workforce and budget, each by more than 20 percent, by implementing various efficiency and cost-saving methods.

NAVY MERITORIOUS CIVILIAN SERVICE AWARD



Mrs. Laurie Stackpole
Ruth H. Hooker Research Library (retired)

Ms. Stackpole is the recipient of this award for her significant contributions to the naval library community and its users. The award citation reads “for meritorious achievement and service to the United States Navy and the Naval Research Laboratory for her pioneering work in developing and applying digital library technologies and her leadership in advancing digital information services in the sciences across the Department of the Navy. As a nationally recognized innovator, Ms. Stackpole has been an inspiration and example for naval librarians, generously sharing her vision for the future and her knowledge of the digital information environment. Ms. Stackpole is especially commended for her role as a founding member of the Consortium of Naval Libraries, in helping to develop an electronic licensing pro-

gram that has saved \$5 million over the past three years and provided critical information resources at the desktops of 90,000 users. This award recognizes Ms. Stackpole for her professionalism, technical expertise, knowledge, and dedication and thanks and commends her for her support and contributions.”



NAVY MERITORIOUS CIVILIAN SERVICE AWARD



Dr. John Harding
Oceanography Division

Dr. Harding was recognized “for his meritorious achievement and dedication to the United States Navy and the Naval Research Laboratory while serving as the Head of the Ocean Dynamics and Prediction Branch since 1995. Because of Dr. Harding’s dedication and vision, the Branch is a world leader in global ocean modeling and prediction, and continues to be at the forefront of important research relevant to the operational missions of the United States Navy.”



NAVY MERITORIOUS CIVILIAN SERVICE AWARD



Ms. Cathy Downing
NRL Human Resources Office

Ms. Downing was recognized for her exemplary service and dedication to the Department of the Navy and NRL as head of the Personnel Operations Branch where she is responsible for administering NRL’s Staffing, Recruitment, Classification, and Compensation Programs. According to the citation, “Ms. Downing exhibited such a high degree of flexibility, adaptability, acceptance of change, and achieved an extraordinary level of knowledge and competence in the areas of staffing, recruitment, classification, compensation, and employee development. Since 1993, the HRO has faced a number of critical requirements including: staff downsizing, assisting the Navy’s HRO regionalization program, implementation of the NRL Personnel Management Demonstration Project, and the transition from

the Legacy Defense Civilian Personnel System (DCPDS) to the Modern DCPDS. All of these requirements were handled with dedication by Ms. Downing, and her leadership provided the highest quality service possible in times of unprecedented change in NRL’s HRO. Her professionalism, technical expertise, knowledge and dedication reflect great credit upon herself, the NRL, and the U.S. Navy.”

NAVY MERITORIOUS CIVILIAN SERVICE AWARD



Mr. Charles J. Stockstill
Office of the General Counsel (deceased)

According to the citation, "During the period from January 1, 2000 to December 31, 2000, Mr. Stockstill expended extraordinary effort toward maintaining the ability of the Office of General Counsel at the Naval Research Laboratory to prepare and prosecute patent applications in the electrical and mechanical arts. During most of this period, Mr. Stockstill was the only patent attorney on staff with experience and expertise in these disciplines. To enable the Office of General Counsel to meet the mission requirements of NRL, Mr. Stockstill drafted and filed thirty-seven patent applications during this period. Completion of this very high volume of effort was an exceptional achievement that was accomplished through his extreme dedication and highly superior skills as a patent attorney. During this same period, despite his daunting workload, Mr. Stockstill also took upon himself the initiative of training and mentoring new patent attorneys, instilling in them a legacy of professionalism and commitment that will long inure to the benefit of the Office of General Counsel and NRL. His accomplishments reflected great credit upon himself and have upheld the highest traditions of the United States Naval Service."



NRL AWARD OF MERIT FOR GROUP ACHIEVEMENT



Ms. Win Jou Cheung, Mr. Michael Rachuba, Dr. Jeffrey Calame, Dr. Bruse Danly, Mr. Ronald Beattie, Mr. Vilhelm Gregers-Hansen, Mr. James Titus, Dr. Baruch Levush, and Mr. George Linde

Radar and Electronics Science and Technology Divisions

NRL researchers received this award for their successful development of a high-power, coherent W-Band Advanced Radar (WARLOC) and its underpinnings of gyro-klystron amplifier technology. This research has been the result of a close collaborative effort between NRL's Radar Division and the Electronics Science and Technology Division. The team was recognized for technical excellence, leadership, and success in the development of the WARLOC radar. The world's highest power coherent 94 GHz radar system first operated on November 21, 2001. They were also noted for their vision, research, and development resulting in the gyro-klystron technology that made this radar feasible, and for the demonstration of the capability of this radar and its benefits to the Navy.



NRL AWARD OF MERIT FOR GROUP ACHIEVEMENT

Chemistry Division (Mr. Xuan Nguyen, Mr. Arthur Durkin, Mr. James Buchanan, Dr. Frederick Williams, Dr. Patricia Tatem, Ms. Jean Bailey, Mr. Thomas Street, Dr. Susan Rose-Pehrsson, Ms. Cheri Schmidt, Mr. David Satterfeld (NAVSEA), and Mr. James Gagorik (ONR))

Over the past five years, the Office of Naval Research (ONR) has sponsored a program, Damage Control-Automation for Reduced Manning (DC-ARM). The object of the DC-ARM program is to demonstrate how damage control tasks can be accomplished with approximately 27 individuals. The citation reads, "A major investment in maintaining a Navy ship over its lifetime is the manning requirement cost. A new class of ships, dubbed the DD21, is being designed for significantly reduced manning. A significant manning requirement is for damage control, which is made up of one third of the crew. Without the automation of damage control tasks, reduced manning is not possible. This team has been responsible for demonstrating Damage Control-Automation Reduced Manning to the Navy, i.e., the architects of modern damage control."

THE 2002 NRL REVIEW ARTICLE AWARDS

Awards for *NRL Review* articles recognize authors who submit outstanding research articles for this publication. The articles are judged on the relevance of the work to the Navy and DOD, readability to the college-graduate level, clearness and conciseness of writing, and the effective use of graphics that are interesting and informative. The following awards were presented for articles that appeared in the *2002 NRL Review*.

FEATURED RESEARCH ARTICLE

"Sensing Macromolecules with Microelectronics," Dr. F. Keith Perkins (Electronics Science and Technology Division), Dr. Marty Peckerar, and Dr. Lenny Tender (Center for Bio/Molecular Science and Engineering)

DIRECTORATE AWARDS FOR SCIENTIFIC ARTICLES

Systems Directorate: *"Technology Demonstration of SHARP, the Navy's Next-Generation Tactical Reconnaissance System,"* Dr. Michael Duncan, Dr. Melvin Kruer, Mr. Dale Linne von Berg, and Dr. John Lee (Optical Sciences Division)

Materials Science and Component Technology Directorate: *"The Electra KrF Laser Program,"* Dr. John Sethian, Mr. Matthew Myers, Dr. Moshe Friedman, Dr. Robert Lehmsberg, Dr. John Giuliani, and Dr. Stephen Obenschain (Plasma Physics Division)

Ocean and Atmospheric Science and Technology Directorate: *"Remote Wind Connections to Strait Transports,"* Dr. Gregg Jacobs, Dr. Henry Perkins, Dr. Ruth Preller, Mr. William Teague, Ms. Shelley Riedlinger, Mr. Dong Ko, and Mr. Jeffrey Book (Oceanography Division)

Naval Center for Space Technology: *"The Spacecraft Robotics Engineering and Controls Laboratory,"* Dr. Glenn Creamer (Spacecraft Engineering Department)



Mr. Keith Perkins of the Electronics Science and Technology Division accepts award for the winning feature article.



Mr. Dale Linne von Berg, Dr. Michael Duncan, Dr. John Lee, and Dr. Melvin Kruer of the Optical Sciences Division accept award for the winning article for the Systems Directorate.



Dr. William Jobst of the Oceanography Division accepts award for the winning article for the Ocean and Atmospheric Science and Technology Directorate.



Dr. Steve Obenschain and Dr. John Sethian of the Plasma Physics Division accept award for the winning article for the Materials Science and Component Technology Directorate.



Mr. Fred Hellrich of the Naval Center for Space Technology accepts award for the winning article for the Center.

AWARD FOR EXCELLENCE IN MISSION SUPPORT



Ms. Linda Owens

Ms. Linda Owens and Ms. Paula Scholten *Human Resources Division*

This award is the highest NRL award given to an NRL employee in recognition of outstanding contributions not involving the sciences or engineering. Ms. Owens and Ms. Scholten are recognized for their positive attitudes and being a pleasure to work with. They were commended for personally visiting division offices to give training and assistance. Much of their assistance is “over and above” their normal responsibilities. The citation reads, “For their support to the NRL administrative community during the implementation of two new automated systems: the Contribution-based Compensation System Data System (CCSDS) and the Modern System. They provided highly effective training, guidance, and problem-solving assistance during the confines of a heavy workload and short period of time. Their responsiveness to the myriad of problems encountered was extraordinary. Their patience with the users’ lack of understanding and general frustration was exceptional and made them a pleasure to work with.”



Ms. Paula Scholten



COMMANDING OFFICER’S AWARD FOR EXCELLENCE IN SECRETARIAL SUPPORT



Ms. Manino Camacho *Marine Meteorology Division*

Ms. Camacho was recognized for “her outstanding achievement and dedication to the United States Navy for her exceptional administrative support of the Marine Meteorology Division. Ms. Camacho continues to provide the highest possible level of customer support to the Division’s managers while working as a part of the overall administrative team and assisting in a number of areas. Her standards of excellence and organizational skills ensure that the products of the Marine Meteorology Division are of the highest quality and are produced in a timely manner. Her personal and professional demeanor is unimpeachable and reflect on her and the Division in the most positive sense. Her ability to plan and execute a variety of functions involving people from outside the Laboratory have added to the Laboratory’s reputation with our national and international colleagues. Ms. Camacho’s professionalism and loyal dedication to duty exemplify, and are in keeping with, the highest traditions of the United States Naval Service.”

ALAN BERMAN RESEARCH PUBLICATION AND EDISON (PATENT) AWARDS

The Annual Research Publications Awards Dinner (ARPAD) was established in 1968 to recognize the authors of the best NRL publications each year. These awards not only honor individuals for superior scientific accomplishments in the field of naval research, but also seek to promote continued excellence in research and in its documentation. In 1982, the name of this award was changed to the Alan Berman Research Publication Awards in honor of its founder.

Of the 259 papers considered for 2002 awards, 30 were selected for recognition. They represent 137 authors. The names of the authors with the titles and abstracts of their publications are listed under their respective research divisions.

NRL also recognizes patents as part of its annual publication awards program. The NRL Edison (Patent) Awards were established in January 1991 to recognize NRL employees for outstanding patents issued to NRL by the U.S. Patent and Trademark Office during the preceding calendar year. The awards recognize significant NRL contributions to science and engineering as demonstrated by the patent process that are perceived to have the greatest potential benefit to the country. Of the 86 patents considered for 2002, 3 were selected representing 3 inventors and 3 patent attorneys. They are listed under the Patent Awards.

PUBLICATION AWARDS

SIGNATURE TECHNOLOGY OFFICE

Ultra-Near Fields of Penetrable Bodies of Translation: ω - κ Representations
Louis N. Medgyesi-Mitschang, Peter G. Moore, Douglas L. Smith, and Samuel G. Lambrakos

RADAR DIVISION

Spiky Sea Clutter at High Range Resolutions and Very Low Grazing Angles
Fred L. Posner

Development of a Digital Array Radar (DAR)
*Ben Cantrell, Jean de Graaf, Lawrence Leibowitz, Frank Willwerth, Glen Meurer,
Christopher Parris, and Ronald Stapleton*

INFORMATION TECHNOLOGY DIVISION

Voice Biometrics for Information Assurance Applications
George S. Kang and Yvette Lee

Energy-Aware Wireless Networking with Directional Antennas:
The Case of Session-Based Broadcasting and Multicasting
Jeffrey E. Wieselthier, Gam D. Nguyen, and Anthony Ephremides

OPTICAL SCIENCES DIVISION

Sensitivity and Stability of a Radiation-Balanced Laser System
Steven R. Bowman, Neil W. Jenkins, Shawn P. O'Connor, and Barry J. Feldman

TACTICAL ELECTRONIC WARFARE DIVISION

Development of New Materials for Laser Countermeasure Ship Applications

Tammie S. Confer

MATERIALS SCIENCE AND TECHNOLOGY DIVISION

Reduction of Spin Injection Efficiency by Interface Defect Spin Scattering in
ZnMnSe/AlGaAs Spin-Polarized Light-Emitting Diodes

*Rhonda M. Stroud, Berend T. Jonker, Aubrey T. Hanbicki, Y. Daniel Park, G. Kioseoglou,
A.G. Petukhov, G. Itskos, and A. Petrou*

Fourth-Order Magnetic Anisotropy and Tunnel Splittings in Mn_{12} from Spin-Orbit-Vibron Interactions

Mark R. Pederson, Noam Berstein, and Jens Kortus

LABORATORY FOR COMPUTATIONAL PHYSICS AND FLUID DYNAMICS

A Three-Dimensional Computational Study of the Aerodynamic Mechanisms of Insect Flight

Ravi Ramamurti and William C. Sandberg

PLASMA PHYSICS DIVISION

Effects of Thin High-Z Layers on the Hydrodynamics of Laser-Accelerated Plastic Targets

*Steve Obenschain, Denis Colombant, Max Karasik, Carl Pawley, Victor Serlin,
Andrew Schmitt, James Weaver, John Gardner, Lee Phillips, Yefim Aglitskiy,
Lop-Yung Chan, Jill Dahlburg, and Marcel Klapisch*

Propagation of Intense Short Laser Pulses in the Atmosphere

Phillip Sprangle, Joseph R. Peñano, and Bahman Hafizi

ELECTRONICS SCIENCE AND TECHNOLOGY DIVISION

Gyrotron Traveling Wave-Tube Circuits Based on Lossy Ceramics

Jeffrey P. Calame, Bruce G. Danly, Baruch Levush, Morag Garven, and Khanh T. Nguyen

Single-Qubit Operations with the Nitrogen-Vacancy Center in Diamond

*Thomas A. Kennedy, John S. Colton, James E. Butler, Forrest T. Charnock,
Robert C. Linares, and Patrick J. Doering*

CENTER FOR BIO/MOLECULAR SCIENCE AND ENGINEERING

Harnessing Microbially Generated Power on the Seafloor

*Leonard M. Tender, Clare E. Reimers, Hilmar A. Stecher III, Dawn E. Holmes, Daniel R. Bond,
Derek R. Lovley, Daniel A. Lowy, Kanoelani Pilobello, and Stephanie J. Fertig*

ACOUSTICS DIVISION

Acoustic Propagation through Anisotropic Internal Wave Fields: Transmission Loss,
Cross-Range Coherence, and Horizontal Refraction

Roger M. Oba and Steven I. Finette

Thermoelastic Loss in Microscale Oscillators

*Brian H. Houston, Douglas M. Photiadis, Martin H. Marcus, Joseph A. Bucaro,
Xiao Liu, and Joseph F. Vignola*

REMOTE SENSING DIVISION

On the Estimation of Radar Polarization Orientation Shifts Induced by Terrain Slopes
*Jong-Sen Lee, Dale L. Schuler, Thomas L. Ainsworth, Ernst Krogager,
Dayalan Kasilingam, and Wolfgang-Martin Boerner*

POAM III Observations of Arctic Ozone Loss for the 1999/2000 Winter
*Karl Hoppel, Richard Bevilacqua, Gerald Nedoluba, Carole Deniel, Frank Lefevre, Jerry Lumpe,
Mike Fromm, Cora Randall, Joan Rosenfield, and Markus Rex*

OCEANOGRAPHY DIVISION

Diffusion Reduction in an Arbitrary Scale Third Generation Wind Wave Model
W. Erick Rogers, James M. Kaihatu, Henri A.H. Petit, Nico Booij, and Leo H. Holthuijsen

Low-Frequency Current Observations in the Korea/Tsushima Strait
William J. Teague, Gregg A. Jacobs, Henry T. Perkins, Jeffrey W. Book, K.-I. Chang, and M.-S. Suk

MARINE GEOSCIENCES DIVISION

Dynamic Measurement of Sediment Grain Compressibility at Atmospheric Pressure:
Acoustic Applications
Michael D. Richardson, Kevin B. Briggs, Kevin L. Williams, and Eric I. Thorsos

Decreased Stability of Methane Hydrates in Marine Sediments Owing to Phase-Boundary Roughness
Warren T. Wood, Joseph F. Gettrust, N. Ross Chapman, George D. Spence, and Roy D. Hyndman

MARINE METEOROLOGY DIVISION

The Dynamics of Mountain-Wave-Induced Rotors
James D. Doyle and Dale R. Durran

Data Assimilation with a Barotropically Unstable Shallow Water System using Representer Algorithms
Liang Xu and Roger Daley

SPACE SCIENCE DIVISION

Strategies for Fault-Tolerant, Space-Based Computing: Lessons Learned from the ARGOS Testbed
*Michael N. Lovellette, Kent S. Wood, Daniel L. Wood, James H. Beall, Philip P. Shirvani,
Nabmsuk Oh, and Edward J. McCluskey*

Characteristics of Coronal Inflows
Neil R. Sheeley, Jr. and Yi-Ming Wang

SPACE SYSTEMS DEVELOPMENT DEPARTMENT

WINDSAT Antenna Testing
Wendy L. Lippincott and Ted Gutwein

Near-Field Calibration for Large Reflectors
Wendy L. Lippincott, Ted Gutwein, Michael Smythers, and Peter J. Souza

SPACECRAFT ENGINEERING DEPARTMENT

Uncorrelated Observations Processing at Naval Space Command
Shannon L. Coffey, Mathew M. Berry, and Harold L. Neal

PATENT AWARDS

INFORMATION TECHNOLOGY DIVISION

Technique for Estimating the Pose of Surface Shapes using Tripod Operators
Frank Pipitone and John Gladstone Mills III

MATERIALS SCIENCE AND TECHNOLOGY DIVISION

Ultra High Density, Non-Volatile Ferromagnetic Random Access Memory
Gary A. Prinz and Barry Edelberg

OPTICAL SCIENCES DIVISION

Microelectronic Stimulator Array
Dean Scribner and John Gladstone Mills III

PROGRAMS FOR PROFESSIONAL DEVELOPMENT



ADMIRAL DAVID G. FARRAGUT.

“Damn the torpedoes, full speed ahead!” Admiral David G. Farragut was the first Admiral of the United States Navy, a title especially created for him by Congress. The statue is a standing figure made of metal taken from Admiral Farragut’s flagship *USS Hartford*.

- 249** Programs for NRL Employees — Graduate Programs, Continuing Education, Professional Development, Equal Employment Opportunity (EEO) Programs, and Other Activities
- 252** Programs for Non-NRL Employees — Recent Ph.D., Faculty Member, and College Graduate Programs, Professional Appointments, College Student Programs, and High School Student Programs

[BACK TO CONTENTS](#)

PROGRAMS FOR NRL EMPLOYEES

The Human Resources Office, Personnel Operations Branch, continues to support and provide traditional and alternative methods of training for employees. During 2002, NRL employees were encouraged to develop their skills by attending training to enhance their job performance in order to continue to meet the future needs of NRL as well as their own goals for growth.

One common study procedure is for employees to work full time at the Laboratory while taking job-related scientific courses at universities and schools in the Washington area. The training ranges from a single course to full graduate and postgraduate programs. Tuition for training is paid by NRL. The formal programs offered by NRL are described here.

GRADUATE PROGRAMS

- The **Advanced Graduate Research Program** (formerly the Sabbatical Study Program, which began in 1964) enables selected professional employees to devote full time to research or pursue work in their own or a related field for one year at an institution or research facility of their choice without the loss of regular salary, leave, or fringe benefits. NRL pays all travel and moving expenses for the employee and dependents. Criteria for eligibility include professional stature consistent with the applicant's opportunities and experience, a satisfactory program of study, and acceptance by the facility selected by the applicant. The program is open to paraprofessional employees (and above) who have completed 6 years of Federal Service, 4 of which have been at NRL.

- The **Edison Memorial Graduate Training Program** enables employees to pursue advanced studies in their fields at local universities. Participants in this program work 24 hours each workweek and pursue their studies during the other 16 hours. The criteria for eligibility include a minimum of one year of service at NRL, a bachelor's or master's degree in an appropriate field, and professional standing in keeping with the candidate's opportunities and experience.

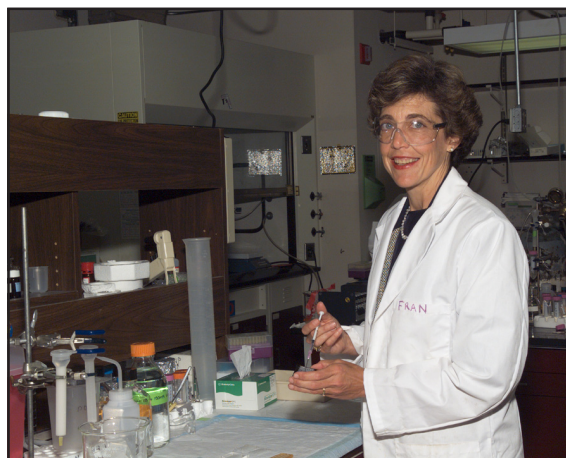
- To be eligible for the **Select Graduate Training Program**, employees must have a college degree in

an appropriate field and must have demonstrated ability and aptitude for advanced training. Students accepted into this program devote a full academic year to graduate study. While attending school, they receive one-half of their salary, and NRL pays for tuition and laboratory expenses.

- The **Naval Postgraduate School (NPS)**, located in Monterey, California, provides graduate programs to enhance the technical preparation of Naval officers and civilian employees who serve the Navy in the fields of science, engineering, operations analysis, and management. It awards a master of arts degree in national security affairs and a master of science degree in many technical disciplines.

NRL employees desiring to pursue graduate studies at NPS may apply for a maximum of six quarters away from NRL, with thesis work accomplished at NRL. Specific programs are described in the NPS catalog. Participants will continue to receive full pay and benefits during the period of study.

- In addition to NRL and university offerings, application may be made to a number of noteworthy programs and fellowships. Examples of such opportunities are the **Capitol Hill Workshops**, the **Legislative Fellowship (LEGIS) program**, the **Federal**



Dr. Fran Ligler, of the Center for Bio/Molecular Science and Engineering, is currently participating in the Advanced Graduate Research Program at Harvard University in Cambridge, Massachusetts.



Mr. James King, of the Ruth H. Hooker Research Library, Technical Information Division, is currently participating in the Edison Memorial Graduate Training Program at Catholic University in Washington, DC.

Executive Institute (FEI), the Fellowship in Congressional Operations, and the Executive Leadership Program for Mid-Level Employees. These and other programs are announced from time to time, as schedules are published.

- Research conducted at NRL may be used as **thesis material for an advanced degree.** This original research is supervised by a qualified employee of NRL who is approved by the graduate school. The candidate should have completed the required course work and should have satisfied the language, residence, and other requirements of the graduate school from which the degree is sought. NRL provides space, research facilities, and supervision but leaves decisions on academic policy to the cooperating schools.

CONTINUING EDUCATION

- **Undergraduate and graduate courses** offered at local colleges and universities are subsidized by NRL for employees interested in improving their skills and keeping abreast of current developments in their fields. These courses are also available at a number of DOD installations in the Washington, DC, area.

- NRL offers **short courses** to all employees in a number of fields of interest including technical subjects, computer operation, supervisory and management techniques. Laboratory employees may attend these courses at nongovernment facilities as well. Interagency courses in management, personnel, fi-

nance, supervisory development, and clerical skills are also available.

For further information on any of the above programs, contact the Employee Relations and Development Branch (Code 1850) at (202) 767-2364.

- The **Scientist-to-Sea Program (STSP)** provides increased opportunities for Navy R&D laboratory/center personnel to go to sea to gain first-hand insight into operational factors affecting system design, performance, and operations on a variety of ships. NRL is a participant of this ONR program.

For participation in the STSP, contact Mary Ann Schmidt, Code 5006A, at (202) 767-3109. For general information on Technology Base Programs, including BMD, SBIR, and critical technology, contact Dr. Stephen Sacks, Code 5006, at (202) 767-3666.

PROFESSIONAL DEVELOPMENT

NRL has several programs, professional society chapters, and informal clubs that enhance the professional growth of employees. Some of these are listed below.

- The **Counseling Referral Service (C/RS)** helps employees to achieve optimal job performance through counseling and resolution of problems such as family, stress and anxiety, behavioral, emotional, and alcohol- or drug-related problems that may adversely impact job performance.

C/RS provides confidential assessments and short-term counseling, training workshops, and referrals to additional resources in the community. (Contact Dr. Ralph Surette at (202) 767-6857.)

- The **NRL Women in Science and Engineering (WISE) Network** was formed in 1997 through the merger of the NRL chapter of WISE and the Women in Science and Technology Network. Luncheon meetings and seminars are held to discuss scientific research areas, career opportunities, and career-building strategies. The group also sponsors projects to promote the professional success of the NRL S&T community and improve the NRL working environment. Membership is open to all S&T professionals. (Contact Dr. Rhonda Stroud at (202) 404-4143 or Dr. Ellen Goldman at (202) 404-6052.)

- **Sigma Xi**, the scientific research society, encourages and acknowledges original investigation in pure and applied science. As an honor society for research scientists, individuals who have demonstrated the ability to perform original research are elected to membership in local chapters. The NRL

Edison Chapter, comprising approximately 400 members, recognizes original research by presenting awards annually in pure and applied science to outstanding NRL staff members. The chapter also sponsors lectures at NRL on a wide range of scientific topics for the entire NRL community. These lectures are delivered by scientists from all over the nation and the world. The highlight of the Sigma Xi lecture series is the Edison Memorial Lecture, traditionally featuring a distinguished scientist. (Contact Dr. Mark Pederson at (202) 767-6577 or Dr. Steve Hellberg at (202) 767-3934.)

- The **NRL Mentor Program** was established to provide an innovative approach to professional and career training and an environment for personal and professional growth. It is open to permanent NRL employees in all job series and at all sites. Mentorees are matched with successful, experienced colleagues with more technical and/or managerial experience who can provide them with the knowledge and skills needed to maximize their contribution to the success of their immediate organization, to NRL, to the Navy, and to their chosen career fields. The ultimate goal of the program is to increase job productivity, creativity, and satisfaction through better communication, understanding, and training. NRL Instruction 12400.1A provides the policy and procedures for the program. (Contact Ms. Dawn Brown at (202) 767-2957.)

- Employees interested in developing effective self-expression, listening, thinking, and leadership potential are invited to join either of two NRL chapters of **Toastmasters International**. Members of these clubs, who possess diverse career backgrounds and talents, meet two to four times a month in an effort to learn to communicate not by rules but by practice in an atmosphere of understanding and helpful fellowship. NRL's Commanding Officer and Director of Research endorse Toastmasters as an official training medium at NRL. (Contact Kathleen Parrish at (202) 404-4963 for more information.)

EQUAL EMPLOYMENT OPPORTUNITY (EEO) PROGRAMS

Equal employment opportunity is a fundamental NRL policy for all employees regardless of race, color, national origin, sex, religion, age, or physical/mental handicap. The NRL EEO Office is a service organization whose major functions include counseling employees in an effort to resolve employee/

management conflicts, processing formal discrimination complaints, providing EEO training, and recruiting for affirmative employment candidates. The NRL EEO Office is also responsible for sponsoring special-emphasis programs to promote awareness and increase sensitivity and appreciation of the issues or the history relating to: females; individuals with disabilities; Hispanic Americans; African Americans; and individuals of American Indian/Alaskan-Native and Asian-American/Pacific Islander descent. (Contact the NRL Deputy EEO Officer at (202) 767-5264 for additional information on any of our programs or services.)

OTHER ACTIVITIES

- The **Community Outreach Program** traditionally has used its extensive resources to foster programs that provide benefits to students and other community citizens. Volunteer employees assist with and judge science fairs, give lectures, tutor, mentor, coach, and serve as classroom resource teachers. The program also sponsors African American History Month art and essay contests for local schools, student tours of NRL, a student Toastmasters Youth Leadership Program, an annual holiday party for neighborhood children, and other programs that support the local community. Also through this program, NRL has active partnerships with four District of Columbia, three Aberdeen, Maryland, and three Calvert County, Maryland, public schools. (Contact Mr. Dom Panciarelli at (202) 767-2541.)

- Other programs that enhance the development of NRL employees include four computer user groups (**IBM PC**, **Mac**, **NeXT**, and **Sun**) and the **Amateur Radio Club**. The **Recreation Club** encourages wide interest in sports for employees with its many facilities and programs, such as a heated indoor pool; basketball and volleyball court; weight room; table tennis; hot tub; five martial arts disciplines; aerobics classes; swimming lessons; water walking and exercise; and sports leagues. Sportswear, NRL paraphernalia, and discount tickets to amusement parks are available at the Rec Club office. The **Showboaters** is a nonprofit drama group that presents live theater for the enjoyment of NRL and the community. Traditionally, the NRL Showboaters perform two major productions each year in addition to occasional performances at Laboratory functions and benefits for local charities. Although based at NRL, membership is not limited to NRL employees. (Contact Barbarajo Cox at (202) 404-4998.)

PROGRAMS FOR NON-NRL EMPLOYEES

Several programs have been established for non-NRL professionals. These programs encourage and support the participation of visiting scientists and engineers in research of interest to the Laboratory. Some of the programs may serve as stepping-stones to federal careers in science and technology. Their objective is to enhance the quality of the Laboratory's research activities through working associations and interchanges with highly capable scientists and engineers and to provide opportunities for outside scientists and engineers to work in the Navy laboratory environment. Along with enhancing the Laboratory's research, these programs acquaint participants with Navy capabilities and concerns.

RECENT PH.D., FACULTY MEMBER, AND COLLEGE GRADUATE PROGRAMS

- The **National Research Council (NRC) Cooperative Research Associateship Program** selects associates who conduct research at NRL in their chosen fields in collaboration with NRL scientists and engineers. The tenure period is two years (renewable for a possible third year).
 - The **NRL/ASEE Postdoctoral Fellowship Program**, administered by the American Society for Engineering Education (ASEE), aims to increase the involvement of highly trained scientists and engineers in disciplines necessary to meet the evolving needs of naval technology. Appointments are for one year (renewable for a second and possible third year).
 - The **Naval Research Enterprise Intern Program (NREIP)** program has been initiated as a two-year demonstration effort involving 69 NROTC colleges and universities. The Office of Naval Research (ONR) is offering summer appointments at Navy laboratories to current sophomores, juniors, seniors, and graduate students from participating schools. Associated Western Universities (AWU) is handling the administration of the application process through a website. Electronic applications are sent for evaluation to the point of contact at the Navy laboratory identified by the applicant. ONR will provide directly to the student a stipend of \$3,000 to undergraduates and \$4,000 to graduate students, plus \$2,000 for travel and living expenses.
- The American Society for Engineering Education also administers the **Navy/ASEE Summer Faculty Research and Sabbatical Leave Program** for university faculty members to work for 10 weeks (or longer, for those eligible for sabbatical leave) with professional peers in participating Navy laboratories on research of mutual interest.
 - The **NRL/United States Naval Academy (USNA) Cooperative Program for Scientific Interchange** allows faculty members of the U.S. Naval Academy to participate in NRL research. This collaboration benefits the Academy by providing the opportunity for USNA faculty members to work on research of a more practical or applied nature. In turn, NRL's research program is strengthened by the available scientific and engineering expertise of the USNA faculty.
 - The **National Defense Science and Engineering Graduate Fellowship Program** helps U.S. citizens obtain advanced training in disciplines of science and engineering critical to the U.S. Navy. The three-year program awards fellowships to recent outstanding graduates to support their study and research leading to doctoral degrees in specified disciplines such as electrical engineering, computer sciences, material sciences, applied physics, and ocean engineering. Award recipients are encouraged to continue their study and research in a Navy laboratory during the summer.
- For further information about the above six programs, contact Ms. Lesley Renfro at (202) 404-7450.

PROFESSIONAL APPOINTMENTS

- **Faculty Member Appointments** use the special skills and abilities of faculty members for short periods to fill positions of a scientific, engineering, professional, or analytical nature.
- **Consultants and experts** are employed because they are outstanding in their fields of specialization or because they possess ability of a rare na-

ture and could not normally be employed as regular civil servants.

- **Intergovernmental Personnel Act Appointments** temporarily assign personnel from state or local governments or educational institutions to the Federal Government (or vice versa) to improve public services rendered by all levels of government.

COLLEGE STUDENT PROGRAMS

The student programs are tailored to the undergraduate and graduate students to provide employment opportunities and work experience in naval research. These programs are designed to attract applicants for student and full professional employment in fields such as engineering, physics, mathematics, and computer sciences. The student employment programs are designed to help students and educational institutions gain a better understanding of NRL's research, its challenges, and its opportunities. Employment programs for college students include the following:

- The **Student Career Experience Program** (formerly known as Cooperative Education Program) employs students in study-related occupations. The program is conducted in accordance with a planned schedule and a working agreement among NRL, the educational institution, and the student. Primary focus is on the pursuit of bachelors degrees in engineering, computer science, or the physical sciences.

- The **Student Temporary Employment Program (STEP)** enables students to earn a salary while

continuing their studies and offers them valuable work experience.

- The **Summer Employment Program** employs students for the summer in paraprofessional and technician positions in engineering, physical sciences, computer sciences, and mathematics.

- The **Student Volunteer Program** helps students gain valuable experience by allowing them to voluntarily perform educationally related work at NRL.

For additional information on these undergraduate and graduate college student programs, contact Code 1810 at (202) 767-8313.

HIGH SCHOOL STUDENT PROGRAMS

- The **DOD Science & Engineering Apprentice Program (SEAP)** employs high school juniors, seniors, and college students to serve for eight weeks as junior research associates. Under the direction of a mentor, students gain a better understanding of research, its challenges, and its opportunities through participation in scientific programs. Criteria for eligibility are based on science and mathematics courses completed and grades achieved; scientific motivation, curiosity, and capacity for sustained hard work; a desire for a technical career; teacher recommendations; and achievement test scores. The NRL Program is the lead program and the largest in DOD.

For additional information, contact Dawn Brown (Code 1850) at (202) 767-2957.

GENERAL INFORMATION



CANADIAN CROSS (CROSS OF SACRIFICE).

Few countries enjoy the bonds of goodwill and friendship that the United States and Canada share. Our common border remains the longest unguarded frontier on Earth, and our nations have shared triumphs and tragedies throughout history. On Armistice Day 1927, this monument was dedicated to reaffirm these bonds.

- 257** Technical Output
- 258** Key Personnel
- 259** Contributions by Divisions, Laboratories, and Departments
- 262** Subject Index
- 265** Author Index
- 266** Employment Opportunities

[BACK TO CONTENTS](#)

TECHNICAL OUTPUT

The Navy continues to be a pioneer in initiating new developments and a leader in applying these advancements to military requirements. The primary method of informing the scientific and engineering community of the advances made at NRL is through the Laboratory's technical output—reports, articles in scientific journals, contributions to books, papers presented to scientific societies and topical conferences, patents, and inventions.

The figures for calendar year 2002 presented below represent the output of NRL facilities in Washington, D.C.; Bay St. Louis, Mississippi; and Monterey, California.

In addition to the output listed, NRL scientists made more than 680 oral presentations during 2002.

Type of Contribution	Unclassified	Classified	Total
Articles in periodicals, chapters in books, and papers in published proceedings	1104	0	1104
NRL Formal Reports	22	4	26
NRL Memorandum Reports	60	2	62
Books	0	0	0
Patents granted			81
Statutory Invention Registrations (SIRs)			3

*This is a provisional total based on information available to the Ruth H. Hooker Research Library and Technical Information Center on January 21, 2003. Additional publications carrying a 2002 publication date are anticipated.

KEY PERSONNEL

Area Code (202) unless otherwise listed
 Personnel Locator - 767-3200
 DSN-297 or 754

Code	Office		Phone Number
EXECUTIVE DIRECTORATE			
1000	Commanding Officer	CAPT D.M. Schubert, USN	767-3403
1000.1	Inspector General	CAPT C.W. Fowler, USN	767-3621
1001	Director of Research	Dr. J.A. Montgomery	767-3301
1001.1	Executive Assistant	Mr. D. DeYoung	767-2445
1002	Chief Staff Officer	CAPT C.W. Fowler, USN	767-3621
1004	Head, Technology Transfer	Dr. C. Cotell	404-8411
1006	Head, Office of Program Administration and Policy Development	Mrs. L. McDonald	767-3091
1008	Office of Counsel	Mr. J. McCutcheon	767-2244
1030	Public Affairs Officer	Mr. R. Thompson	767-2541
1200	Head, Command Support Division	CAPT C.W. Fowler, USN	767-3621
1220	Head, Security	Dr. J.T. Miller	767-0793
1400	Head, Military Support Division	CDR R.B. Grimm, USN	767-2272
1600	Officer-in-Charge, Flight Support Detachment	CDR T.M. Munns, USN	301-342-3751
1800	Director, Human Resources Office	Ms. B.A. Duffield	767-3421
1830	Deputy EEO Officer	Ms. D. Erwin	767-5264
3005	Deputy for Small Business	Ms. M. Nicholl	767-6263
3540	Head, Safety Branch	Mr. K.J. Pawlovich	767-2232
BUSINESS OPERATIONS DIRECTORATE			
3000	Associate Director of Research	Mr. D. Therning	767-2371
3200	Head, Contracting Division	Mr. J.C. Ely	767-5227
3300	Comptroller, Financial Management Division	Mr. S.A. Birk	767-3405
3400	Supply Officer	Ms. C. Hartman	767-3446
3500	Director, Research and Development Services Division	Mr. S. Harrison	767-3697
SYSTEMS DIRECTORATE			
5000	Associate Director of Research	Dr. R.A. LeFande	767-3324
5200	Head, Technical Information Division	Dr. R.A. LeFande (Acting)	767-3324
5300	Superintendent, Radar Division	Dr. P.K. Hughes II	404-2700
5500	Superintendent, Information Technology Division	Dr. J.D. McLean (Acting)	767-2903
5600	Superintendent, Optical Sciences Division	Dr. T.G. Giallorenzi	767-3171
5700	Superintendent, Tactical Electronic Warfare Division	Dr. F. Klemm (Acting)	767-6278
MATERIALS SCIENCE AND COMPONENT TECHNOLOGY DIRECTORATE			
6000	Associate Director of Research	Dr. B.B. Rath	767-3566
6030	Head, Laboratory for Structure of Matter	Dr. J. Karle	767-2665
6100	Superintendent, Chemistry Division	Dr. J.S. Murday	767-3026
6300	Superintendent, Materials Science and Technology Division	Dr. D.U. Gubser	767-2926
6400	Director, Lab. for Computational Physics and Fluid Dynamics	Dr. J.P. Boris	767-3055
6700	Superintendent, Plasma Physics Division	Dr. S. Ossakow	767-2723
6800	Superintendent, Electronics Science and Technology Division	Dr. G.M. Borsuk	767-3525
6900	Director, Center for Bio/Molecular Science and Engineering	Dr. J.M. Schnur	404-6000
OCEAN AND ATMOSPHERIC SCIENCE AND TECHNOLOGY DIRECTORATE			
7000	Associate Director of Research	Dr. E.O. Hartwig	404-8690
7100	Superintendent, Acoustics Division	Dr. E.R. Franchi	767-3482
7200	Superintendent, Remote Sensing Division	Dr. P. Schwartz	767-3391
7300	Superintendent, Oceanography Division	Dr. W.J. Jobst	228-688-4670
7400	Superintendent, Marine Geosciences Division	Dr. H.C. Eppert, Jr.	228-688-4650
7500	Superintendent, Marine Meteorology Division	Ms. P. Phoebus (Acting)	831-656-4721
7600	Superintendent, Space Science Division	Dr. H. Gursky	767-6343
NAVAL CENTER FOR SPACE TECHNOLOGY			
8000	Director	Mr. P.G. Wilhelm	767-6547
8100	Superintendent, Space Systems Development Department	Mr. R.E. Eisenhauer	767-0410
8200	Superintendent, Spacecraft Engineering Department	Mr. H.E. Senasack, Jr.	767-6411

CONTRIBUTIONS BY DIVISIONS, LABORATORIES, AND DEPARTMENTS

Radar Division

- 127 EMI and EM Energy Transport in the Near Field
D.J. Taylor, M.G. Parent, and S. Samaddar
- 128 Detection and Imaging of Buried Objects
K.M. Scheff and J.P. Hansen

Information Technology Division

- 149 Multimodal Interactions with Dynamically Autonomous Robots
D.J. Perzanowski, A.C. Schultz, W.L. Adams, M. Bugajska, M.S. Skubic, G. Trafton, D.P. Brock, E. Marsh, and M. Abramson
- 159 Programmable Embeddable INFOSEC Product
S.J. Chincheck

Optical Sciences Division

- 191 Athermal Solid-State Lasers
S.R. Bowman
- 139 Tactical Aircraft Directed Infrared Countermeasures System Overview
K.A. Sarkady, H.A. Romero, D.M. Cordray, J.G. Lynn, R.M. Mabe, K. Strothers, J.A. Schlupf, and R.C. Cellucci
- 151 Demonstration of a High-Rate Tactical Reconnaissance System with Real-Time Airborne Image Exploitation
J.N. Lee, D.C. Linne von Berg, M.R. Kruer, and M.D. Duncan
- 189 Fiber-Optic Bottom Mounted Array
C.K. Kirkendall and G.A. Cranch
- 195 Synthetic Aperture Ladar
R.L. Lucke, L.J. Rickard, M. Bashkansky, J.F. Reintjes, and E.E. Funk

- 108 Free-Space High-Speed Laser Communication Link Across the Chesapeake Bay
C.I. Moore, H.R. Burris, M.R. Suite, M.F. Stell, M.J. Vilcheck, M.A. Davis, R.T. Smith, R. Mahon, W.S. Rabinovich, J.P. Koplow, S.W. Moore, W.J. Scharpf, and A.E. Reed
- 217 Inter-Spacecraft Optical Communication and Navigation Using Multiple Quantum Well Modulating Retroreflectors
N.G. Creamer, T.J. Meehan, M.J. Vilcheck, J.A. Vasquez, G.C. Gilbreath, W.S. Rabinovich, and R. Mahon

Tactical Electronic Warfare Division

- 205 NRL's Finder UAV: A Counterproliferation Asset
A. Cross
- 207 Networked Specific Emitter Identification in Fleet Battle Experiment Juliet
I. Terry
- 153 Real-Time Tactics Planning Aid for Weapons of Mass Destruction Defense
G.E. Layman

Laboratory for Structure of Matter

- 113 Protein Crystal Surfaces at Molecular Resolution
J.H. Konnert and S. Gorti

Chemistry Division

- 114 Orientation, Manipulation, and Assembly of Carbon Nanotubes
P.E. Pehrsson and J.W. Baldwin
- 117 Creating Chemical and Biological Diamond Interfaces
J.N. Russell, Jr., J.E. Butler, R.J. Hamers, L.M. Smith, and S.F. Bent

Materials Science and Technology Division

- 51 Unified Approach to Fatigue Damage Evaluation
K. Sadananda, R.L. Holtz, and A.K. Vasudevan
- 167 A New Ferromagnetic Semiconductor: Mn_xGe_{1-x}
A.T. Hanbicki, Y.D. Park, B.T. Jonker, S.C. Erwin, J.M. Sullivan, C.S. Hellberg, A. Wilson, and G. Spanos
- 163 Image-based Modeling of Naval Steels
A.B. Geltmacher, G. Spanos, and J.F. Bingert

Laboratory for Computational Physics and Fluid Dynamics

- 209 Flapping Flight in Insects and Fish: 3-D Unsteady Computations
W.C. Sandberg and R. Ramamurti

Plasma Physics Division

- 59 Filamentation and Propagation of Ultra-Short, Intense Laser Pulses in Air
A.C. Ting, D.F. Gordon, C.K. Manka, R.F. Hubbard, J.R. Peñano, and P. Sprangle
- 141 Nested Multi-Wire Array Implosions for KeV X-ray Generation
J. Davis, A.L. Velikovich, and V.I. Oreshkin
- 143 Dusty Plasma Dynamics in the NRL Space Physics Simulation Chamber Laboratory
W.E. Amatucci, D.N. Walker, and G.I. Ganguli

Electronics Science and Technology Division

- 130 Imaging Stacking Fault Growth in SiC Diodes
R.E. Stahlbush, M.E. Twigg, and M. Fatemi
- 165 Molecular Beam Epitaxial Growth of AlGaIn/GaN High Electron Mobility Transistors
S.C. Binari, D.S. Katzer, D.F. Storm, B.V. Shanabrook, E.R. Glaser, and J.A. Roussos

- 133 Long Spin Coherence Lengths for Quantum Devices
M.J. Yang, C.H. Yang, and Y.B. Lyanda-Geller

Center for Bio/Molecular Science and Engineering

- 120 An Improved Method for TNT Analysis in Ground Water, Seawater, and Soil
E.R. Goldman, G.P. Anderson, and J.M. Mauro
- 122 An Automated, Portable Array Biosensor
F.S. Ligler, J.P. Golden, Y.S. Shubin, L.C. Shriver-Lake, J.B. Delehanty, K.E. Sapsford, and C.R. Taitt

Acoustics Division

- 173 Roughness-Induced Ocean Bottom Scattering
R.J. Soukup and R.F. Gragg
- 212 RAM to Navy Standard Parabolic Equation: Transition from Research to Fleet Acoustic Model
R.A. Zingarelli and D.B. King
- 93 Simultaneous Inversion of Bio- and Geo-Acoustic Parameters in the Yellow Sea
O.I. Diachok and S.C. Wales
- 95 Simulations of Low-Frequency Bubble Pulsations Generated by Impacting Cylindrical Water Jets
W.G. Szymczak and S.L. Means

Remote Sensing Division

- 195 Synthetic Aperture Ladar
R.L. Lucke, L.J. Rickard, M. Bashkansky, J.F. Reintjes, and E.E. Funk
- 197 Dynamic Ocean Fronts
A.L. Cooper, R.P. Mied, G.J. Lindemann, and M.A. Sletten
- 217 Inter-Spacecraft Optical Communication and Navigation Using Multiple Quantum Well Modulating Retroreflectors
N.G. Creamer, T.J. Meehan, M.J. Vilcheck, J.A. Vasquez, G.C. Gilbreath, W.S. Rabinovich, and R. Mahon

Oceanography Division

- 199 Coastal Transport of Organic and Inorganic Matter
R.W. Gould, Jr. and R.A. Arnone
- 175 Global Ocean Nowcasts and Forecasts with the Navy Coastal Ocean Model (NCOM)
C.N. Barron, R.C. Rhodes, L.F. Smedstad, C.D. Rowley, P.J. Martin, and A.B. Kara

Marine Geosciences Division

- 91 Through-The-Sensors Concepts to Refresh the Environmental Picture
W.E. Avera, M.M. Harris, D.J. Walter, L.D. Bibee, and D.N. Lambert
- 178 The Influence of Microbial Fe(III) Reduction on Clayey Sediment Flocculation
J.-W. Kim, Y. Furukawa, T. Daulton, S.E. O'Reilly, and S. Newell
- 181 Dissociation of Sub-Seafloor Gas Hydrates and Seafloor Stability: What Thermobaric Models Show
P.R. Vogt and W.-Y. Jung

Marine Meteorology Division

- 69 Satellite Surveillance of Desert Dust Storms
S.D. Miller
- 101 High-Resolution Modeling of Tropical Cyclones Using Moving Grids
C.-S. Liou and T.R. Holt
- 103 A "Satellite Focus" for the War on Terror
S.D. Miller

Space Science Division

- 79 Timing Studies of X-ray Binary Orbits
P.S. Ray, M.T. Wolff, K.S. Wood, and P. Hertz
- 105 NRLMSISE-00: A New Empirical Model of the Atmosphere
J.M. Picone, D.P. Drob, R.R. Meier, and A.E. Hedin

Space Systems Development Department

- 108 Free-space High-speed Laser Communication Link Across the Chesapeake Bay
C.I. Moore, H.R. Burris, M.R. Suite, M.F. Stell, M.J. Vilcheck, M.A. Davis, R.T. Smith, R. Mahon, W.S. Rabinovich, J.P. Koplrow, S.W. Moore, W.J. Scharpf, and A.E. Reed
- 220 Modeling Single-Event Transients in Complex Digital Devices
K.A. Clark
- 156 Better Codes—Better Communication
R.A. Echard and S.C. Chang

Spacecraft Engineering Department

- 217 Inter-Spacecraft Optical Communication and Navigation Using Multiple Quantum Well Modulating Retroreflectors
N.G. Creamer, T.J. Meehan, M.J. Vilcheck, J.A. Vasquez, G.C. Gilbreath, W.S. Rabinovich, and R. Mahon
- 222 Full-Sky Astrometric Mapping Explorer Solar Precession
T.W. Lim and P.G. DeLaHunt

SUBJECT INDEX

- 3 kJ KrF laser facility (Nike), 33
- Absorptivity, 93
- Acoustic Communication
 - Laboratory, 35
- Acoustic Seafloor Characterization System (ASCS), 39
- Acoustics Division, 34
- Acoustics, 46, 173, 189
- Administrative Services Branch, 41
- Advanced Graduate Research Program, 249
- Advanced Research and Global Observation Satellite (ARGOS), 40
- Airborne Geographical Sensor Suite (AGSS), 42
- Airborne Polarimetric Microwave Imaging Radiometer (APMIR), 38
- Airborne processing, 151
- Aircraft 153442, 47
- Aircraft 154587, 47
- Amateur Radio Club, 251
- Array antenna isolation, 127
- Array biosensor, 122
- Assimilation, 175
- Atmosphere, 105
- Atmospheric Science and Technology, 101
- Atomic force microscope, 113
- Autonomous vehicles, 209
- Bergen Data Center, 39, 44
- Bio-acoustic, 93
- Biologically active macromolecules, 113
- Biomaterial development, 34
- Bit error rate, 108
- Bragg Crystal Spectrometer (BCS), 40
- Bubble pulsations, 95
- C4I embedded simulations, 153
- Capitol Hill Workshops, 249
- Carbon nanotubes, 23, 114
- Center for Bio/Molecular Science and Engineering, 34
- Center for Computational Science (CCS), 45
- Charged microparticle, 143
- Chemical analysis facilities, 31
- Chemical/biological warfare defense, 34
- Chemistry Division, 31, 45
- Chesapeake Bay Detachment (CBD), 27, 29, 42
- Class-10 clean room, 47
- Class-1000 clean room, 34
- Climate change, 181
- CMIS, 38
- Coding theory, 156
- Cognitive models, 149
- College Student Programs, 253
- Combating Terrorism Technology Task Force, 22
- Communications data
 - transmission, 156
- Community Outreach Program, 25, 251
- Compact Antenna Range, 26
- Compound Semiconductor
 - Processing Facility (CSPF), 33
- Compound Semiconductor
 - Processing Facility (CSPF), 46
- Computational Electromagnetics (CEM) Facility, 26
- Computing and Modeling, 101
- COMSEC, 159
- Continuing Education, 250
- Cooperative Aircraft Identification system, 27
- Cooperative and collaborative behavior, 149
- Cooperative Engagement Capability (CEC), 42
- Corporate Facilities Investment Plan (CFIP), 44
- Counseling Referral Service (C/RS), 250
- Coupled Ocean/Atmosphere Mesoscale Prediction System-On Scene (COAMPS-OS™), 44
- Crack closure, 51
- Credit Union, 25
- Crystal Face, 42, 47
- CT-Analyst, 14
- Cycloaddition, 117
- Daley Supercomputer, 39, 44
- Damage Control-Automated Reduced Manning system (DC-ARM), 23
- DARKHORSE Project, 22
- dc glow discharge, 143
- Deep-Towed Acoustic Geophysical System (DTAGS), 39
- Defense Research and Engineering Network (DREN), 28
- Deforming fins, 209
- Diamond, 117
- Dielectrophoresis, 114
- Digital acquisition buoy systems (DABS), 35
- Digital Processing Facility, 30
- Directed assembly, 114
- Directed IR countermeasures, 139
- Dislocations, 130
- Distributed Center (DC), 45
- DNA, 117
- DOD Science & Engineering Apprentice Program (SEAP), 253
- Drag, 105
- Dust enhancement, 69
- Dusty plasma, 143
- Dynamic autonomy, 149
- Edison Memorial Graduate Training Program, 249
- Electra Doppler Radar (ELDORA), 47
- Electra, 48
- Electron Backscatter Diffraction (EBSD), 163
- Electron Microscopy Facility, 39, 43
- Electronic intelligence, 207
- Electronics & electromagnetics, 128
- Electronics Science and Technology Division, 33, 46, 48
- EMI, 127
- Empirical model, 105
- Employee Relations and Development Branch, 250
- Environmental cell (EC), 47
- Environmental data, 91
- EPICENTER, 33, 48
- Equal Employment Opportunity (EEO) Program, 251
- Error control coding, 156
- Executive Leadership Program for Mid-Level Employees, 250
- Exhibits Program, 41
- Extreme Ultraviolet Imaging Telescope (EIT), 40
- ex-USS *Shadwell* (LSD-15), 31, 44
- Fatigue, 51
- Federal Executive and Professional Association, 25
- Federal Executive Institute (FEI), 250
- Fellowship in Congressional Operations, 250
- Ferromagnetic semiconductors, 167
- Ferromagnetism, 167
- Fiber optic pulsed laser, 24
- Fiber optics, 189
- Filamentation, 59
- Fire research facilities, 31
- Fire-research chamber (Fire I), 31
- Fish swimming, 209
- Fleet Battle Experience-India (2001), 22
- Fleet Battle Experiment-Juliet (2002), 22
- Fleet Numerical Meteorology and Oceanography Center (FNMOC), 39, 43
- Flight Support Detachment (NRL FSD), 26, 42, 47
- Flocculation, 178
- Focal-Plane Evaluation Facility, 29
- Fouling Release Coating technology, 24
- Free-space lasercomm, 108

Free-Surface Hydrodynamics Laboratory, 38

Frontal propagation, 197

Functionalization, 117

GAMBLE II, 33

GaN, 165

Geo-acoustic parameters, 93

Geospatial Information Data Base (GIDB), 39

Geostationary Satellite Processing Facility, 44

Global circulation, 175

Global Imaging of the Ionosphere (GIMI), 40

Graduate Programs, 249

Head-mounted displays (HMDs), 28

HEMT, 165

High Performance Computing Modernization Program (HPCMP), 45

High power lasers, 191

High School Student Programs, 253

High-definition TV (HDTV), 28

High-Resolution Airglow and Auroral Spectroscopy (HIRAAS), 40

Homeland Defense, 45

Human Resources Office, 249

Human-robot interaction, 149

Hydrophone, 189

Image exploitation, 151

Image-based modeling, 163

Immersive Room, 28

In Situ Sediment Acoustic Measurement System (ISSAMS), 39

Induced discharges, 59

Inertial fusion energy (IFE), 48

InfoNet, 45

Information Security Engineering Laboratory, 28

Information Technology Division, 27, 45, 47

INFOSEC, 159

InfoWeb, 41, 45

InfraLynx, 7, 22

Infrared Test Chamber, 29

Insect flight, 209

INSPEC, 41

Institute for Nanoscience, 10, 26, 45

Integrated Electronic Warfare System (IEWS), 42

Internal stress, 130

International H₂O Project (IHOP), 42, 47

Inverse synthetic aperture radar (ISAR), 27

Inversion, 93

Ion Implantation Facility, 32

Ionosphere, 105

IR Missile-Seeker Evaluation Facility, 29

John B. Hovermale Visualization Laboratory, 39, 44

John C. Stennis Space Center, 43

KG-38, 159

KOV-17, 159

Laboratory for Computational Physics and Fluid Dynamics (LCP & FD), 32

Laboratory for Proximal Probe Nanofabrication (LPPN), 48

Laboratory for Structure of Matter, 30

Large Area Plasma Processing System (LAPPS) facility, 33, 46

Large-Angle Spectrometric Coronagraph (LASCO), 23, 40, 47

Large-Optic, High-Precision Tracker system, 29

Laser communications, 108

Laser Facilities, 32

Laser propagation, 59

Legislative Fellowship (LEGIS) program, 249

Life prediction, 51

Liquid impacts, 95

Low-Frequency Array radio telescope (LOFAR), 23, 46

Map Data Formatting Facility, 43

Marine Corrosion Test Facility, 31

Marine Geosciences Division, 38, 43, 47

Marine Meteorology Division (NRL-MRY), 39, 43

Master Environmental Laboratory, 44

Materials Science and Technology, 31

Materials synthesis/property measurement facility, 31

Mercury pulsed-power generator, 48

Mesoscale, 163

Methane hydrate, 181

Microbial Fe (III), 178

Microwave, 165

Midway Research Center (MRC), 44

Minehunting, 91

Missile warning, 139

Mixed layer depth, 175

Mobile Ad Hoc Networking (MANET), 28

MOCVD Laboratory, 33

MODAS, 175

MODIS, 69

Molecular Beam Epitaxy, 31

Moving Map Composer Facility, 39

Multi-analyte detection, 122

Multibeam bathymetry, 91

Multibeam sonar, 91

Multimedia Center, 41

Multimodal interfaces, 149

Multi-Threaded Architecture (MTA), 28

Nanoelectronics Processing Facility (NPF), 33

Nanoelectronics, 114

Nanometer measurement facility, 31

Nanoprocessing Facility (NPF), 46

Nanostructures, 133

National Defense Science and Engineering Graduate Fellowship Program, 252

National Radio Astronomy Observatory's Very Large Array (VLA), 46

National Research Council (NRC) Cooperative Research Associateship Program, 252

National Weather Service Forecast Office (NWSFO), 43

Naval Center for Space Technology (NCST), 40, 44

Naval Fleet/Force Technology Innovation Officer, 30

Naval Postgraduate School (NPS), 43, 249

Naval Research Enterprise Intern Program (NREIP), 252

NAVOCEANO Oceanographic Surveillance (OS), 42

Navy and Joint Typhoon Warning Center, 39

Navy Integrated Tactical Environmental System (NITES), 44

Navy Prototype Optical Interferometer (NPOI), 37

Navy Technology Center for Safety and Survivability, 43

Navy Ultrawideband Synthetic Aperture Radar (NUSAR), 46

Navy/ASEE Summer Faculty Research and Sabbatical Leave Program, 252

NCOM, 175

Near field, 127

Networking, 207

NEWAVE facility, 29

NICenet, 28

Nonlinear focusing, 59

Nontronite, 178

NP-3D EW flying laboratory, 30

NRL Mentor Program, 251

NRL/ASEE Postdoctoral Fellowship Program, 252

NRL/United States Naval Academy (USNA) Cooperative Program for Scientific Interchange, 252

Ocean color, 199

Ocean fronts, 197

Ocean model, 175

Ocean Research Laboratory, 46

Ocean Science and Technology, 173

Oceanography Division, 38, 43, 46

Operation Enduring Freedom, 69, 103

Optical Calibration Facility, 37

Optical communication, 217

Optical Science Division, 29

Optics, 199

Orbit, 105

Oriented Scintillation Spectrometer Experiment (OSSE), 39

P-3 Orion turboprop aircraft, 27, 44
 Parabolic equation acoustic model, 212
 Pathogen detection, 122
 Pharos III, 32
 Photographic services, 41
 PiN diodes, 130
 Plasma Physics Division, 32, 46
 Plasma Physics, 48
 Plasma radiation sources, 141
 Plasma, 143
 Professional Appointments, 252
 Professional Development, 250
 Profiling Optics Package, 37
 Programmable embeddable INFOSEC product, 159
 Publication services, 41
 Quantum computing, 133
 Radar Division, 26, 47
 Radar imagery, 197
 Radar Imaging Facility, 27
 Radar Signature Calculation Facility, 27
 Radar Test Bed Facility, 27
 Rapid detection, 122
 Real-time targeting, 151
 Reconnaissance, 151
 Recreation Club, 25, 251
 Relative navigation, 217
 Remote Sensing Division, 36, 46
 Remote Sensing, 197, 199
 Resonance frequency, 93
 Responsive Workbench, 28
 Robotics Laboratory, 28
 Ruth H. Hooker Research Library, 41, 45
 Salt Water Tank Facility, 46
 Satellite and Wireless Networking Section, 22
 Satellite Remote Sensing, 69, 103
 Scattering, 173
 Science Citation Index, 41
 Scientists Helping America Conference, 8
 Scientist-to-Sea Program (STSP), 250
 Scintillation, 108
 Sea surface temperature, 175
 Sea WiFS data, 38
 Seafloor stability, 181
 Sediment classification, 91
 Select Graduate Training Program, 249
 Sensing, 189
 SGI Origin2000, 32
 SGI Origin3800, 28, 45, 47
 Shared Reconnaissance Pod system (SHARPS), 42
 Ship Motion Simulator (SMS), 29, 42
 Shock tube theory, 197
 Showboaters, 25, 251
 SiC, 130
 Sigma Xi, 25, 250
 Silicon carbide, 130
 Simulation, 101, 197
 Single-event effects, 220
 Single-event transients, 220
 Single-event upsets, 220
 Solar Coronagraph Optical Test Chamber (SCOTCH), 47
 Solar Heliospheric Observatory satellite, 40
 Solar precession dynamics and control of spinning spacecraft, 222
 Solar radiation torque modeling, 222
 Solar Ultraviolet Spectral Irradiance Monitor (SUSIM), 39
 Space Science Division, 39, 47
 Space Solar Cell Characterization Facility (SSCCF), 33, 48
 Spacecraft rendezvous and capture, 217
 Specific Emitter Identification, 207
 Spin coherence, 133
 Spintronics, 167
 SSMIS, 38
 Stacking faults, 130
 Stennis Space Center (NRL-SSC), 43
 Student Career Experience Program, 25, 253
 Student Temporary Employment Program (STEP), 253
 Student Volunteer Program, 253
 Summer Employment Program, 253
 Sun Ultra, 47
 Surface, 117
 Swim bladder, 93
 Synchrotron Radiation Facility, 31
 Synthetic aperture ladar, 195
 Table-Top Terawatt (T³) laser, 32, 48
 Tactical Electronic Warfare (TEW) Division, 30
 Tactical environmental data, 91
 Tactical missiles, 139
 Tactical Oceanography Simulation Laboratory (TOSL), 36, 43
 Tactical Oceanography Wide Area Network (TOWAN), 36
 Technical Information Services, 41
 Technology transfer, 16, 24
 TEM-EC, 47
 Thin-Film Preparation Facilities, 32
 Through-The-Sensors, 91
 TNT analysis, 120
 Toastmasters International, 25, 251
 Toastmasters Youth Leadership Program, 25
 TORPEDO *Ultra* v.2, 41, 45
 Trace Element Accelerator Mass Spectrometry (TEAMS) – 3 MV Tandem Pelletron Accelerator Facility, 32
 Transient fault propagation, 220
 Transistor, 165
 Transmission electron microscope (TEM), 47
 Transmission loss, 93
 Ultrafast Laser Facility (ULF), 33, 48
 Ultralow-loss, Fiber-Optic Waveguide Facility, 29
 Ultra-short lasers, 59
 Unconventional Stellar Aspect (USA), 40
 Underwater landslides, 181
 Unsteady CFD, 209
 Upper Atmosphere Research Satellite (UARS), 40
 USN Aegis Cruiser system, 42
 Vacuum Electronics Fabrication Facility (VEFF), 33
 Vacuum Ultraviolet Space Instrument Test Facility, 47
 Video services, 41
 Virtual Reality (VR) Laboratory, 28
 Voice Communication Processing system, 24
 WARLOC, 23, 27
 Water mass classification, 199
 Wave propagation, 197
 Weapons of mass destruction defense, 153
 Web design, 103
 WindSat, 12, 38
 Wire arrays, 141
 Women in Science and Engineering (WISE) Network, 25, 250
 X rays, 141
 X-ray astronomy, 79
 Ytterbium lasers, 191
 Z-pinch, 141

AUTHOR INDEX

- Abramson, M., 149
Adams, W.L., 149
Amatucci, W.E., 143
Anderson, G.P., 120
Arnone, R.A., 199
Avera, W.E., 91
Baldwin, J.W., 114
Barron, C.N., 175
Bashkansky, M., 195
Bent, S.F., 117
Bibee, L.D., 91
Binari, S.C., 165
Bingert, J.F., 163
Bowman, S.R., 191
Brock, D.P., 149
Bugajska, M., 149
Burris, H.R., 108
Butler, J.E., 117
Cellucci, R.C., 139
Chang, S.C., 156
Chincheck, S.J., 159
Clark, K.A., 220
Cooper, A.L., 197
Cordray, D.M., 139
Cranch, G.A., 189
Creamer, N.G., 217
Cross, A., 205
Daulton, T., 178
Davis, J., 141
Davis, M.A., 108
DeLaHunt, P.G., 222
Delehanty, J.B., 122
Diachok, O.I., 93
Drob, D.P., 105
Duncan, M.D., 151
Echard, R.A., 156
Erwin, S.C., 167
Fatemi, M., 130
Funk, E.E., 195
Furukawa, Y., 178
Ganguli, G.I., 143
Geltmacher, A.B., 163
Gilbreath, G.C., 217
Glaser, E.R., 165
Golden, J.P., 122
Goldman, E.R., 120
Gordon, D.F., 59
Gorti, S., 113
Gould, Jr., R.W., 199
Gragg, R.F., 173
Hamers, R.J., 117
Hanbicki, A.T., 167
Hansen, J.P., 128
Harris, M.M., 91
Hedin, A.E., 105
Hellberg, C.S., 167
Hertz, P., 79
Holt, T.R., 101
Holtz, R.L., 51
Hubbard, R.F., 59
Jonker, B.T., 167
Jung, W.-Y., 181
Kara, A.B., 175
Katzner, D.S., 165
Kim, J.-W., 178
King, D.B., 212
Kirkendall, C.K., 189
Konnert, J.H., 113
Koplow, J.P., 108
Kruer, M.R., 151
Lambert, D.N., 91
Layman, G.E., 153
Lee, J.N., 151
Ligler, F.S., 122
Lim, T.W., 222
Lindemann, G.L., 197
Linne von Berg, D.C., 151
Liou, C.-S., 101
Lucke, R.L., 195
Lyanda-Geller, Y.B., 133
Lynn, J.G., 139
Mabe, R.M., 139
Mahon, R., 108, 217
Manka, C.K., 59
Marsh, E., 149
Martin, P.J., 175
Mauro, J.M., 120
Means, S.L., 95
Meehan, T.J., 217
Meier, R.R., 105
Mied, R.P., 197
Miller, S.D., 69, 103
Moore, C.I., 108
Moore, S.W., 108
Newell, S., 178
O'Reilly, S.E., 178
Oreshkin, V.I., 141
Parent, M.G., 127
Park, Y.D., 167
Pehrsson, P.E., 114
Penano, J.R., 59
Perzanowski, D.J., 149
Picone, J.M., 105
Rabinovich, W.S., 108, 217
Ramamurti, R., 209
Ray, P.S., 79
Reed, A.E., 108
Reintjes, J.F., 195
Rhodes, R.C., 175
Rickard, L.J., 195
Romero, H.A., 139
Roussos, J.A., 165
Rowley, C.D., 175
Russell, Jr., J.N., 117
Sadananda, K., 51
Samaddar, S., 127
Sandberg, W.C., 209
Sapsford, K.E., 122
Sarkady, K.A., 139
Scharpf, W.J., 108
Scheff, K.M., 128
Schlupf, J.A., 139
Schultz, A.C., 149
Shanabrook, B.V., 165
Shriver-Lake, L.C., 122
Shubin, Y.S., 122
Skubic, M.S., 149
Sletten, M.A., 197
Smedstad, L.F., 175
Smith, L.M., 117
Smith, R.T., 108
Soukup, R.J., 173
Spanos, G., 163, 167
Sprangle, P., 59
Stahlbush, R.E., 130
Stell, M.F., 108
Storm, D.F., 165
Strothers, K., 139
Suite, M.R., 108
Sullivan, J.M., 167
Szymczak, W.G., 95
Taitt, C.R., 122
Taylor, D.J., 127
Terry, I., 207
Ting, A.C., 59
Trafton, G., 149
Twigg, M.E., 130
Vasquez, J.A., 217
Vasudevan, A.K., 51
Velikovich, A.L., 141
Vilcheck, M.J., 108, 217
Vogt, P.R., 181
Wales, S.C., 93
Walker, D.N., 143
Walter, D.J., 91
Wilson, A., 167
Wolff, M.T., 79
Wood, K.S., 79
Yang, C.H., 133
Yang, M.J., 133
Zingarelli, R.A., 212

NRL offers a wide variety of challenging positions that involve the full range of work, from basic and applied research to equipment development. The nature of the research and development conducted at NRL requires professionals with experience. Typically there is a continuing need for electronics, mechanical, aerospace, materials engineers, metallurgists, computer scientists, and oceanographers with bachelor's and/or advanced degrees and physical and computer scientists with Ph.D. degrees.



Chemists. Chemists are recruited to work in the areas of combustion, polymer science, bioengineering and molecular engineering, surface science, materials, synthesis, nanostructures, corrosion, fiber optics, electro-optics, microelectronics, electron-device technology, and laser physics.

Biologists. Biologists conduct research in areas that include biosensor development, tissue engineering, molecular biology, genetic engineering, proteomics and environmental monitoring.

Physicists. Physics graduates may concentrate on such fields as materials, solid-state physics, fiber optics, electro-optics, microelectronics, vacuum science, plasma physics, fluid mechanics, signal processing, ocean acoustics, information processing, artificial intelligence, electron-device technology, radio-wave propagation, laser physics, ultraviolet/X-ray/gamma-ray technology, electronic warfare, electromagnetic interaction, communications systems, radio frequency/microwave/millimeter wave/infrared technology, computational physics, radio and high energy astronomy, solar physics, and space physics.

Oceanographers, Meteorologists, and Marine Geophysicists. These employees work in the areas of ocean and atmospheric dynamics, air-sea interaction, upper-ocean dynamics, oceanographic bio-optical modeling, oceanic and atmospheric numerical modeling and prediction, data assimilation and data fusion, retrieval and application of remote sensing data, benthic processes, aerogeophysics, marine sedimentary processes, advanced mapping techniques, atmospheric physics, and remote sensing. Oceanographers and marine geophysicists are located in Washington, D.C., and the Stennis Space Center, Bay St. Louis, Mississippi. Meteorologists are located in Washington, D.C., and Monterey, California.

for
**Highly Innovative, Motivated,
and Creative Personnel**

Electronics Engineers and Computer Scientists. These employees may work in the areas of communications systems, electromagnetic scattering, electronics instrumentation, electronic warfare systems, radio frequency/microwave/millimeter wave/infrared technology, radar systems, laser physics technology, radio-wave propagation, electron device technology, spacecraft design, artificial intelligence, information processing, signal processing, plasma physics, vacuum science, microelectronics, electro-optics, fiber optics, solid state, software engineering, computer design/architecture, ocean acoustics, stress analysis, and expert systems.



Mechanical and Aerospace Engineers. These employees may work in areas of spacecraft design, remote sensing, propulsion, experimental and computational fluid mechanics, experimental structural mechanics, solid mechanics, elastic/plastic fracture mechanics, materials, finite-element methods, nondestructive evaluation, characterization of fracture resistance of structural alloys, combustion, CAD/CAM, and multi-functional material response.

Materials Scientists/Engineers. These employees are recruited to work on materials, microstructure characterization, electronic ceramics, solid-state physics, fiber optics, electro-optics, microelectronics, fracture mechanics, vacuum science, laser physics and joining technology, and radio frequency/microwave/millimeter wave/infrared technology.

For more information on current vacancy listings,
visit <http://hroffice.nrl.navy.mil>

**EMPLOYMENT
NRL
OPPORTUNITIES**

NAVAL RESEARCH LABORATORY

4555 Overlook Ave., SW • Washington, DC 20375-5320

LOCATION OF NRL IN THE CAPITAL AREA



Quick Reference Telephone Numbers

	NRL Washington	NRL- SSC	NRL- Monterey	NRL CBD
Hotline	(202) 767-6543	(228) 688-5001	(831) 656-4721	(202) 767-6543
Personnel Locator	(202) 767-3200	(228) 688-3390	(831) 656-4731	(410) 257-4000
DSN	297- or 754-	828	878	—
Direct-in-Dialing	767- or 404-	688	656	257
Public Affairs	(202) 767-2541	(228) 688-5328	(831) 656-4708	—

Additional telephone numbers are listed on page 258.

NRL Review Staff

Senior science editor John D. Bultman

TID coordinator Jonna Atkinson

TID consultant Kathy Parrish

Design, layout, and graphic support Jonna Atkinson, Donna Gloystein, Judy Kogok, Jan Morrow, and Suzanne Guilmineau

Editorial assistance Maureen Long

Historical update David van Keuren

Photographic production Gayle Fullerton and Michael Savell

General information on the research described in this *NRL Review* can be obtained from the Public Affairs Office, Code 1030, (202) 767-2541. Information concerning Technology Transfer is available from Dr. Catherine Cotell, head of the Technology Transfer Office, Code 1004, (202) 767-7230. Sources of information on the various educational programs at NRL are listed in the chapter entitled "Programs for Professional Development."

For additional information about NRL, the *Fact Book* lists the organizations and key personnel for each division. It contains information about Laboratory funding, programs, and field sites. The *Fact Book* can be obtained from the Technical Information Division, Publications Services Section, Code 5211, (202) 404-4963. The web-based *NRL Major Facilities* publication, which describes each NRL facility in detail, can be accessed at <http://www.nrl.navy.mil>.

REVIEWED AND APPROVED

NRL/PU/5211-03-457

May 2003



David M. Schubert, Captain, USN
Commanding Officer

www.nrl.navy.mil